THE UNIVERSITY OF HULL

Identification and Functional Characterization of Putative Mitochondrial Iron Transporters from the Human Pathogen *Trypanosoma brucei*

being a Thesis submitted for the Degree of Doctor of Philosophy

In the University of Hull

by

Fuli Zheng,

Bachelor in Biological Science

August 2017

Dedicated

to

my parents

Mrs Pingying Hu and Mr Guocang Zheng

Abstract

Trypanosoma brucei is a medically important protozoan parasite causing African sleeping sickness in humans. Treatment of this disease is possible, but is hindered by the limited availability of effective drugs as well as the rapid emergence of drug resistance. It is therefore of importance to identify novel drug targets for the future development of more effective drugs.

Mitochondrial carrier family (MCF) proteins transport a wide range of different key metabolites across the mitochondrial inner membrane and are important for the maintenance of key metabolic pathways in all eukaryotic cells. In particular, MCF proteins implicated in the *mitochondrial import of iron* are suggested to be essential for cell function and survival by providing iron required for iron-sulfur cluster assembly, mitochondrial electron transport and associated ATP production, and the defence against oxidative stress. Because of these important physiological roles, mitochondrial iron transporters could be considered as potential novel drug targets.

The main aim of this thesis is the identification and functional characterization of putative mitochondrial iron transporters in *T. brucei*. Sequence analysis revealed that the *T. brucei* genome contains 3 MCF proteins, e.g. TbMCP12, TbMCP17 and TbMCP23, for which a potential role in mitochondrial iron transport could be predicted based on their homology to functionally characterized MCF proteins known to transport iron. Of these TbMCPs, TbMCP17 has the highest sequence homology with functionally characterized mitochondrial iron transporters from other eukaryotes, like for example MRS3/4 from *Saccharomyces cerevisiae*. Sequence analysis predicted further that TbMCP12 is more closely related to mitochondrial di/tri-carboxylate transporters, such as DIC1 from *S. cerevisiae*, whilst TbMCP23 is closely related to mitochondrial pyrimidine transporters, such as for example *S. cerevisiae* RIM2. Both mitochondrial di/tri-carboxylate and pyrimidine transporters have been suggested previously to potentially catalyse the mitochondrial co-transport of iron with their main metabolic substrates, here di/tri-carboxylic acids and pyrimidines, respectively.

In addition to the identified TbMCPs, another potential mitochondrial iron transporter, here TbSFNX, was predicted to be potentially involved in mitochondrial iron transport. Sequence analysis revealed significant sequence homology of TbSFNX with members of the mammalian sideroflexin protein family. The exact physiological role of sideroflexins has yet to be determined, but a potential role in the mitochondrial co-transport of iron with citrate has previously been suggested.

Immunofluorescence microscopy experiments using recombinant tagged protein versions of the identified 3 TbMCPs and TbSFNX, and/or polyclonal antibodies raised against these proteins, confirmed that all identified putative iron transporters are exclusively localized in the mitochondrion of *T. brucei*, suggesting that they indeed perform a mitochondrial transport function.

Whether the expression of the 3 TbMCPs and TbSFNX is essential for cell survival, was investigated by the generation of conventional/conditional gene knockout and/or knockdown of expression (RNA interference) *T. brucei* cell lines and the subsequent analysis of cell growth. Results showed that the expression of TbMCP17, TbMCP23 and TbSFNX is essential for trypanosome survival, whereas the knockout/down of TbMCP12 did not show any growth phenotype in *T. brucei*. These results indicate that TbMCP17, TbMCP23 and TbSFNX fulfill key roles in the transport of essential metabolites, while TbMCP12 plays a less important transport role or is redundant in transport function due to the presence of other MCF proteins with similar transport roles.

The putative transport function of the different TbMCPs was investigated by a combination of different experiments, including (1) functional complementation studies using specific *Saccharomyces cerevisiae* deletion strains lacking a specific MCF protein, and (2) mitochondrial ATP production assays using isolated mitochondria from wildtype and knockout/down *T. brucei* cell lines for which the expression of a specific MCF protein has been ablated or down-regulated. In *S. cerevisiae*, DIC is involved in the mitochondrial transport of dicarboxylates such as malate and oxoglutarate. Functional complementation studies using the *S. cerevisiae* deletion strain ΔDIC revealed that TbMCP12 expression was able to restore growth of this strain on the non-fermentable carbon source glycerol. In addition, mitochondrial ATP production assays revealed that TbMCP12-depleted *T.*

brucei mitochondria were not able to produce ATP from dicarboxylic acids, such as malate and oxoglutarate, and the tricarboxylic acid citrate. These results confirmed that TbMCP12 most likely functions as a di/tri-carboxylate transporter in *T. brucei*. Further experimentation revealed that, compared to the wildtype cell line, the TbMCP12-depleted cell line has become sensitive to oxidative stress in the form of the application of hydrogen peroxide to the culture medium. Measurement of the cellular $NADP^+$/NADPH balance in the TbMCP12-depleted cell line revealed a significant shift towards $NADP^+$ accumulation. These results clearly indicate that TbMCP12 also plays an important role in cellular oxidative stress defence in *T. brucei*, which is in agreement with its role as a mitochondrial di/tri-carboxylate transporter and the potential co-transport of iron.

A similar investigative approach was used for TbMCP17. In *S. cerevisiae*, MRS3/4 is essential for the mitochondrial transport of iron across the mitochondrial inner membrane, but only under iron-limiting conditions. Functional complementation studies using the *S. cerevisiae* deletion strain ΔMRS3/4 revealed that TbMCP17 expression was able to restore growth of this strain under iron-limiting conditions. In addition, growth experiments using a TbMCP17-depleted *T. brucei* cell line revealed that this cell line was not able to grow under iron-limiting conditions, however the ectopic over-expression of a recombinant version of TbMCP17 under the same conditions restored *T. brucei* growth. These results confirmed that TbMCP17 most likely functions as a mitochondrial iron transporter in *T. brucei*.

Unfortunately, the same investigative approach could not be followed for TbMCP23 and TbSFNX. This is mainly due to the lack of suitable *S. cerevisiae* deletion strains and an associated detectable phenotype, and the extremely low/non-detectable expression levels of both TbMCPs. Further experiments revealed that not only the knockdown of TbSFNX, but also its overexpression resulted in severe growth defects in *T. brucei*. In addition, measurement of substrate consumption (glucose, proline) and product formation (acetate, succinate) revealed a substantially increased metabolic flux in both the TbSFNX knockdown and overexpression *T. brucei* cell lines. These results clearly suggest that TbSFNX plays a key role in the *T. brucei* energy metabolism. However, a specific transport function cannot be attributed to TbSFNX at this point. For TbMCP23, there was

unfortunately not enough time left to further investigate its potential role in mitochondrial iron transport.

In conclusion, 4 different potential mitochondrial iron transporters have been identified in *T. brucei*, e.g. TbMCP12, TbMCP17, TbMCP23, and TbSFNX. Of the identified transporters, only TbMCP17 was confirmed to function as a mitochondrial iron transporter, while TbMCP12 was shown to function as a mitochondrial di/tri-carboxylate transporter. Further research will be required to determine the specific mitochondrial transport function of the remaining candidates. The findings provide vital information on the mitochondrial metabolites transport of *T. brucei* and provide a solid foundation for future novel drug invention with TbMCP17 as the most suitable target.

Declaration

I declare that this thesis has been composed solely by myself and that it has not been submitted, in whole or in part, in any previous application for a degree. Except where states otherwise by reference or acknowledgment, the work presented is entirely my own.

Fuli Zheng

Signature:

Acknowledgements

Here, I would like to express my biggest ‘thank you’ to my principle supervisor, Dr Frank Voncken. I call him ‘Frank’ under normal conditions, ‘Dear boss’ under ‘chemical/expensive kits-depleted’ conditions, ‘Dr Voncken’ when proudly refer him to others and for formal occasions. In my heart, he is also a kind and friendly (sometimes strict) father who not only cares about experiments and results, but cares more about students (all the PhD students, masters and undergraduates): from study/research to mental and physical health. He is extremely knowledgeable and probably has huge storage space that covers from all the basic knowledge to the latest research findings to all the little tricks to optimize experimental procedures. Every time after discussion with Frank, I feel like boosting by 10 cups of Costa without a heart attack, and so energetic to face all the foreseen and unforeseen challenges. I guess that comes half from his enthusiasm to science and half from immense knowledge. I cannot express my appreciations more, as words failed me. There’s only one thing that I am sure about: without all the dedicated supervision, help, kindness and wisdom, I can never complete my PhD project.

Special thanks goes to my second supervisor, Dr Camille Ettelaie and annual meeting examiners Dr Heather Sealy-Lewis and Dr Jörg Hardege for valuable discussions and encouragements throughout my research.

Lots of thanks goes to my parents for giving birth to me, rising me up, and more importantly, teaching me what the true, the good and beautiful are. I appreciate my motherland China, and the Chinese Scholarship Council and the University of Hull for awarding me the CSC-UoH joint scholarship to financially support my PhD research.

I would like to thank our lab technician Dr Cordula Kemp, for everything she has done: getting all the experimental materials ready ASAP, writing and revising all the COSHH forms, discussion of the experimental results, cheering me up, girl-gossips and being such a FABULOUS friend. And also Dr Fei Gao and Mr Mohammed M Alshegifi, PhD students in our lab, for valuable discussion and accompany throughout my PhD. Thanks also goes

to Dr Rebacca Hill, for sharing the same lab and for her warm encouragements. Appreciates also goes to Mrs Ellie Bibby and Miss Sage Pickwell, for warm shinny smiles and technical helps. I would also like to thank Dr Becky Bibby, Dr Anna Todd, Dr Flore-Anne Poujade, Mrs Hannah Moody and Miss Brittany J Winngham for creating a nice and friendly atmosphere in our office.

I would also like to express my gratitude to the staff from the School of Biological, Biomedical and Environmental Sciences and Graduate School for their support and assistance throughout my studies.

I would also like to thank my friends for all the useful discussions and pleasant memories during the last three years, including marathon joint organization friends Dr Bing Wang and Mr Zhen Yu for sharing my happiness and support my back when I am down; Dr. Moona Ma for sharing her attitude towards life; Miss Yuchen Guo and Miss Lu Wang for delicious desserts; Mr Bingyong Guo for being sensible all the time, Mr Kai Wang and Mr Jianlong Li for biological and experimental ‘complaints’, Miss Yupei Xiao and Mrs Yuehua Dou for the chicken soup and the hairtail, respectively, both of which were cooked with care and love.

Last but not least, I would like to thank 2016 Edingbrough Marathon, body pump and zumba to give me a healthy body. To Costa for tasty Mocca and dark chocolates from various brands to fuel-filled me through writing up stage.

Table of content

Abbreviations

ADP	Adenosine Diphosphate
AMP	Adenosine Monophosphate
ASCT	Acetate: Succinate CoA Transferase
ATP	Adenosine Triphosphate
BLA	Blasticidin
BSF	Bloodstream Form
CATR	Carboxyatractyloside
CIAP	Calf Intestinal Alkaline Phosphate
CP I II III	Contact Points I, II and III
DAPI	4',6-diamidino-2-phenylindole
DIC	Dicarboxylate Carrier
DNA	Deoxyribonucleic Acid
DTC	Dicarboxylate-Tricarboxylate Carrier
ECL	Enhanced Chemiluminiscence
FCS	Foetal Calf Serum
G-3-PDH	Glycerol-3-Phosphate Dehydrogenase
G6PDH	Glycerol-6-Phosphate Dehydrogenase
GPI	Glycosylphosphatidylinositol
HAT	Human African Trypanosomiasis
HYG	Hygromycin
IB	Inclusion Bodies
IFA	Immunofluorescence Microscopy
IgG	Immunoglobulin G
IPTG	Isopropyl-beta-D-thiogalactopyranoside
KO	Knockout
LB	Luria-Bertani Medium
LIP	Labile Iron Pool
MCF	Mitochondrial Carrier Family
MCP	Mitochondrial Carrier Protein

MCS	Multiple cloning site
MEM-Pros	Minimum Essential Medium with Proline
MOPS	3-(N-morpholino)propanesulfonic Acid
mRNA	Messager RNA
MTP	Mitochondrial Transition Pore
mtDNA	Mitochondrial Deoxyribonucleic Acid
mtRNA	Mitochondrial Ribonucleic Acid
NAD^+	Nicotinamide Adenine Dinucleotide Oxidized
NADH	Nicotinamide Adenine Dinucleotide Reduced
$NADP^+$	Nicotinamide Adenine Dinucleotide Phosphate Oxidized
NADPH	Nicotinamide Adenine Dinucleotide Phosphate Reduced
NEO	Neomycin
Ni-NTA	Nickel-Nitriloacetic Acid
O.D.	Optical Density
OGC	Oxoglutarate Carrier
ORF	Open Reading Frame
OXPHOS	Oxidative Phosphorylation
PBS	Phosphate Buffer Saline
PCF	Procyclic Form
PCR	Polymerase Chain Reaction
PEP	Phosphoenolpyruvate
RNA	Ribonucleic Acid
RNAi	Ribonucleic Acid Interference
ROS	Reactive Oxygen Species
SDM-79	Semi-Defined Medium 79
SDS	Sodium Dodecyl Sulphate
SDS-PAGE	Polyacrylamide Gel Electrophoresis in Sodium Dodecyl Sulphate
SoTE	Sorbitol Tris EDTA buffer
TCA	Trycarboxylic Acid
tRNAs	Transference Ribonucleic Acid
TET	Tetracycline
Tf	Transferrin
TfR	Transferrin Receptor

UCP	Uncoupling Protein
UTR	Untranslated Region
VSG	Variant Surface Glycoprotein
WB	Western Blot
WT	Wild Type

Chapter 1 Introduction

1.1 *Trypanosoma brucei* and Sleeping Sickness

1.1.1 African Sleeping Sickness

Trypanosoma brucei is a protista parasite that belongs to class Kinetoplastea, order Trypanosomatida, genus *Trypanosoma* (Moreira et al. 2004). There are three species of *Trypanosoma brucei: Trypanosoma brucei rhodesiense, Trypanosoma brucei gambiense* and *Trypanosoma brucei brucei.* All these are transmitted via insect vector, the tsetse fly, genus *Glossina*. The first two mentioned species are the causative agents of African Sleeping Sickness or Human African Trypanosomiasis (HAT), a prevalent disease in 36 sub-Saharan African countries. HAT can lead to death without necessary treatment (Brun et al. 2010). According to WHO, in 1998, there were approximately 300,000 cases of the disease left undiagnosed and untreated. After continued control efforts, the number of new cases dropped below 10,000 in 2009 and further decreased to 3796 cases in 2014. It was estimated that the disease affected less than 20,000 people worldwide in total (WHO 2017). The third species, *T. b. brucei* causes Nagana, a wasting disease in cattle (Rodgers 2009; Barrett et al. 2003).

HAT presents two forms of disease owing to different species. *T. b. rhodesidense* is predominant in southern and eastern Africa and causes fast onset acute trypanosomiasis, which can be fatal within months or even weeks. In contrast, *T. b. gambiense* causes slow onset chronic trypanosomiasis and is predominant in western and central Africa (Brun et al. 2010). African Sleeping Sickness in humans can be divided into two distinct stages. The first one is called the haemolytic stage where patients get a fever, headache, and lymph nodes enlargements (Rodgers 2009). After that, the disease can turn into a more severe stage where parasites cross the blood-brain barrier and invade the central nervous system (CNS). In this stage, common symptoms of Sleeping Sickness appear, including lethargy, sensory disturbance, confusion, disruption of sleeping patterns and coma (Stich et al. 2002; Kennedy 2006). Meanwhile, disturbances in sleep-wake patterns are developed, which are not caused by hypersomnia, but by nocturnal insomnia and daytime sleep (Lundkvist et al. 2004).

The clinical presentation of HAT is complex and its diagnosis is difficult. Few effective and efficient treatments are available (Hannaert 2010; Gehrig & Efferth 2008). In addition, most of the drugs are associated with adverse reactions. For example, treatment with melarsoprol led to post-treatment reactive encephalopathy (PTRE) (Brun et al. 2010; Rodgers 2009). The resistance to diamidine-based drugs (adenosine-like compounds) developed in *T. brucei* was resulted from the decreased drug import because of the loss of purine transporter P2 (Matovu et al. 2003; Maser et al. 2003). For other drugs used for HAT treatment, the resistance is caused by other unknown mutations or overexpressions. So, it is important and urgent to find new drug targets and drugs to continue the effective treatment of Sleeping Sickness.

In contrast to *T. b. rhodesidense* and *T. b. gambiense, T. b. brucei* cannot infect humans due to their susceptibility to lysis by Trypanosome Lytic Factor-1 (TLF-1) in the human serum (Rodgers 2009; Steverding 2008). The close relationship of *T. b. brucei* with human infective subspecies and the shared major features make it a suitable model to investigate the underlying mechanisms of the African Sleeping Sickness.

1.1.2 The Kinetoplastea parasite: *Trypanosoma brucei*

The order Kinetoplastea contains fatal pathogens in livestock, humans and plants, such as *Trypanosoma, Leishmania* and *Phytomonas* besides free-living species. Being contradictory to the previous concept that kinetoplastids branched very early in evolution (Sogin et al. 1986), *Trypanosoma brucei* belongs to the supergroup Excavata, one of the six supergroups of eukaryotes that exist at the same evolutionary age (Simpson 2003; Adl et al. 2005; Simpson & Roger 2004). Hallmark of Kinetoplastea is the presence of a kinetoplast, which is an intricate network containing the mitochondrial genome (kDNA) (Stuart et al. 2008).

Like other eukaryotes, *T. brucei* contains most of the compartments of eukaryote cells, for example, a nucleus, a golgi apparatus, and the endoplasmic reticulum (ER). In addition, *T. brucei* uses a flagellum attached to the cell body to move in the host environment (Overath & Engstler 2004). Specifically, the trypanosomatids include glycosomes, which are peroxisome-like compartments that are essential for *T. brucei* to complete most of the

glycolytic pathway as well as pentose phosphate pathway, β-oxidation of fatty acids, purine salvage, and biosynthetic pathways for pyrimidines (Parsons 2004; Parsons et al. 2001; Michels et al. 2000).

Furthermore, the mitochondria of trypanosomatids possess extraordinary features (van Hellemond et al. 2005; see Table 1-1). Firstly, despite the fact that classically studied cells have 5 to 10,000 of mitochondria per cell, the trypanosomatids has only one single, large mitochondrion. Secondly, the DNA structure is different because of the presence of kinetoplasts. Moreover, the DNA consisting of kinetoplasts is highly concatenated. Due to the uniqueness of trypanosomatids' mitochondria, the replication of kinetoplast DNA and mitochondrial division are linked to cell division (Gull 2003).

Table 1-1 Special features in trypanosomatids (van Hellemond et al. 2005)

	Classical mammalian mitochondria	**Mitochondria in trypanosomatids**
Number of mitochondria per cell	5-10,000	1
DNA structure	Circular, 16-17 kb mtDNA in total	Many concatenated circular DNAs: 5000-10,000 minicircles and 40-50 maxicircles
RNA editing	No editing	Major editing of transcripts: insertion and deletion of uridylates
Protein translation	tRNAs are mitochondrion encoded	tRNA nuclear encoded and imported from the cytosol
Biogenesis	Division not directly linked to cell division	Division directly linked to cell division

Another feature of *T. brucei* is the presence of variant surface glycoprotein (VSG) on the cell surface, which enables *T. brucei* to protect itself by antigenic variation. *T. brucei* can switch the VSG from one type to another via selective expression of VSG genes and pseudogenes (Hall et al. 2013). The parasites make use of VSG to prolong their circulation in blood and thus increase the possibility of transmission. VSG proteins are anchored by glycosylphophatidylinositol (GPI) to the plasma membrane (Martin & Smith 2006); while in insect vector, the surface coat of *T. brucei* includes procyclin (EP/GPEET) to protect itself against hostile intestinal insect environment (Roditi et al. 1998).

Additionally, the transcription in kinetoplastid prototista (the trans-splicing of mRNA) differs from the paradigms of eukaryotic gene expression. *T. brucei* shows polycistronic transcription, and pre-mRNA molecules are spliced into individual mRNAs (Sather & Agabian 1985). Trans-splicing is a special form of RNA processing which induced the joining of the ends of the two different primary RNA transcripts. Trans-splicing has been discovered by comparing the nucleotide sequences of the 5' ends of VSG mRNAs with the corresponding coding genes (Boothroyd et al. 1982). A 39-bp long spliced leader RNA sequence (SL RNA) has been found at the first exon at the 5' end of mRNA molecules (Liang et al. 2003), which is processed by RNA polymerase II (Das et al. 2006).

1.1.3 Life cycle of *Trypanosoma brucei*

T. brucei has a complex life cycle during which it adapts to different environments in its host and vector with two replicating forms (Matthews et al. 2004; Vickerman 1985). The bloodstream form is found in mammals' blood and tissue fluids, while the procyclic form is discovered in the midgut of the tsetse fly. *T. brucei* first infects the midgut of its vector through a blood meal as a dividing midgut form. Then it migrates via the proventriculus to the salivary glands (See Figure 1-1). This stage is known as the epimastigote life cycle. Some of the parasites differentiate to the infective metacyclic form, ready to be released into the blood stream of mammalian species upon an insect bite. The parasite undergoes a series of adaptations from slender form to stumpy form with an intermediate form in between, resulting in a stumpy form able to re-infect the fly vector after a blood meal (Figure 1-1). The slender form is able to proliferate, while the stumpy form of *T. brucei* cannot (Matthews et al. 2004). The parasite at later stages may infect lymph and cerebrospinal fluids of mammalian hosts. In addition, though uncommon, *T. brucei* can transmit via exchange of body fluids or blood (Rocha et al. 2004). There are some factors like *cis*-aconitase (Czichos et al. 1986; Matthews et al. 2004) that can trigger the differentiation of trypanosomes from BSF into PCF *in vitro*.

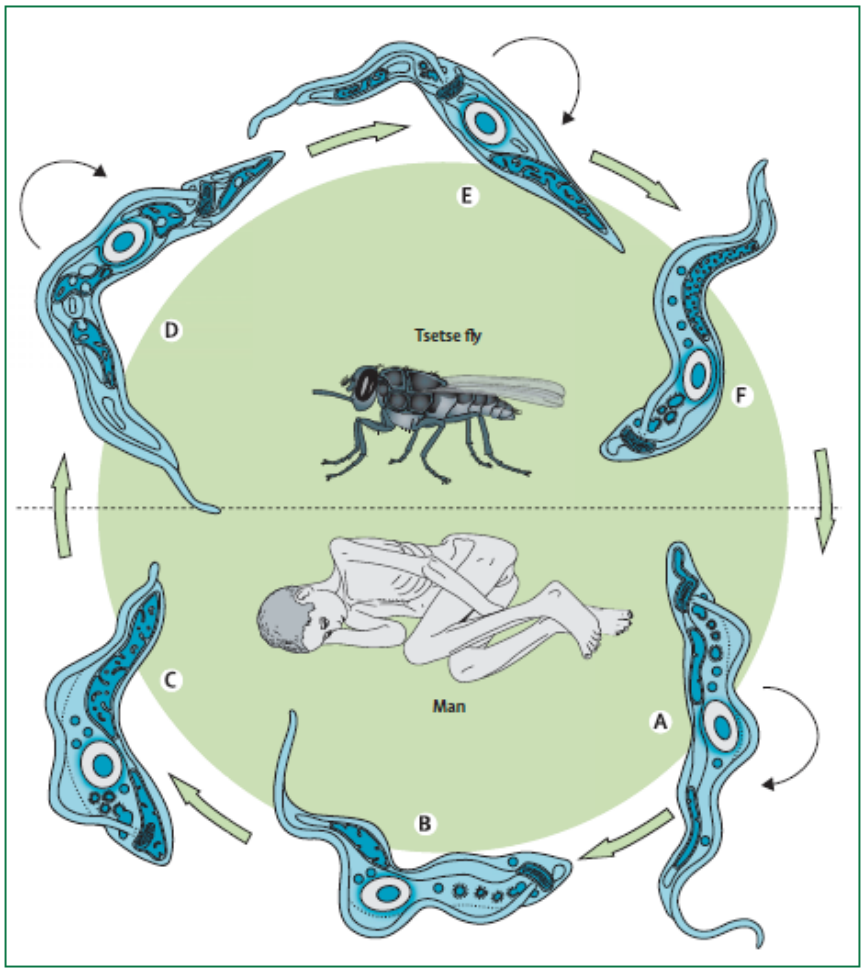

Figure 1-1 Representative life cycle of *T. brucei* (Vickerman 1985)
A. dividing slender form (bloodstream form); B. intermediate form; C. stumpy form; D. dividing midgut form (procyclic form); E. migrating epimastigote form; F. infective metacyclic form.

1.2 Energy metabolism in trypanosomes

The energy metabolism in trypanosomatids involves different subcellular compartments including the glycosome, the mitochondrion and the cytosol.

Glycosomes are found only in Kinetoplastea (Hannaert & Michels 1994) and Diplonemida (Makiuchi et al. 2011). Glycosomes are microbody-like organelles, which contain the majority of enzymes in the glycolytic pathway (Figure 1-2). Glycolysis is a process of ten steps that converts one molecule of glucose into two molecules of pyruvate, two molecules of ATP and two molecules of nicotinamide adenine dinucleotide reduced (NADH) (Bryla & Frackowiak 1968). The compartmentation of glycolysis with glycosomes prevents metabolic interference by separating enzymes and cofactors such as ATP and NADH (Blattner et al. 1998; Helfert et al. 2001). Net ATP is not generated in the glycosome, but in the cytosol when phosphoenolpyruvate is converted into pyruvate. Also, purine salvage occurs in glycosomes.

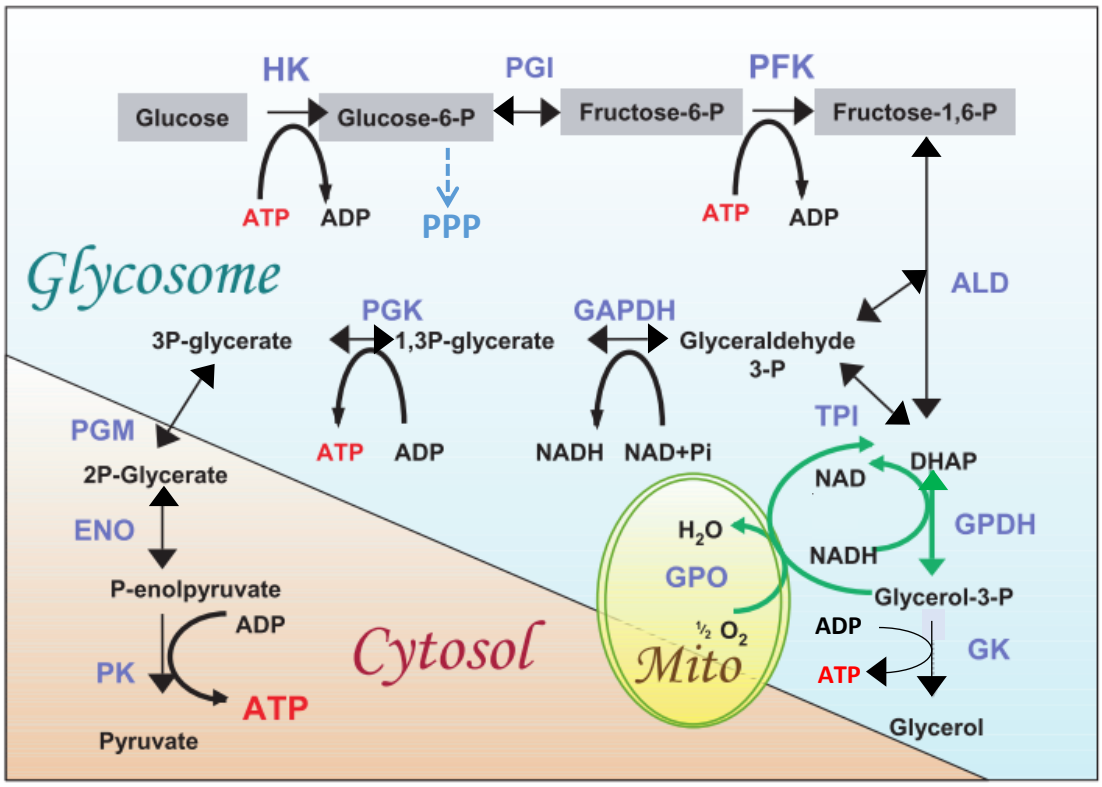

Figure 1-2 Glycolysis in *T. brucei* (Adapted from Parson 2004)
The black arrows show the predominant flow of metabolites of glucose. The six carbon sugars (grey background) are eventually broken into two trioses, and each of them can generate an ATP. A small proportion of trioses is used in the glycerophosphate shunt in collaboration with the mitochondrion. Here, dihydroxyacetone phosphate is cycled to glycerol-3-phosphate and back (green arrows). This allows the glycosome to maintain the NAD/NADH balance. Enzymes are in blue font, and abbreviations are: HK, hexokinase; PGI, glucose phosphate isomerase; PFK, phosphofructokinase; ALD, aldolase; TPI, triose phosphate isomerase; GAPDH, glyceraldehydes-3-phosphate dehydrogenase; PGK, phosphoglycerate kinase; PGM, phosphoglycerate mutase; ENO, enolase; PK, pyruvate kinase; GDH, glycerol-3-phosphate dehydrogenase; GPO, mitochondrial glycerol phosphate oxidase complex composed of glycerol-3-phosphate dehydrogenase (FAD), alternative oxidase and ubiquinone; GK, glycerol kinase.

There are multiple differences in the energy metabolism of the procyclic form (PCF) and the bloodstream form (BSF). The parasite makes adaptations in morphology, surface composition and metabolism (Matthews et al. 2004). In BSF of *T. brucei*, glucose is primarily metabolised to 3-phosphoglycerate inside glycosomes, and further degrades into pyruvate as an end product in the cytosol (Gull 2003). ATP is obtained only by substrate-level phosphorylation, while mitochondria are significantly reduced without key enzymes and components for Krebs cycle in BSF (Opperdoes et al. 1977; Michels et al. 2000; Clayton & Michels 1996).

PCF of *T. brucei* has a more elaborate net-like mitochondrion and ATP can be generated both from substrate level and oxidative phosphorylation (Michels et al. 2000; Tielens & van Hellemond 1998; Coustou et al. 2003; van Weelden et al. 2005). NADH balance is maintained by the pathway turning oxaloacetate into succinate in glycosomes of PCF trypanosomes (Coustou et al. 2005; Besteiro et al. 2002). NADPH, on the other hand, is produced by PCF from both malic enzymes and the pentose phosphate pathway (Allmann et al. 2013). In PCF, pyruvate, the end product of glycolysis, is not excreted but further metabolised inside the mitochondrion, and degrades to acetate or succinate, in which ATP is also generated (van Hellemond et al. 1998; Riviere et al. 2004). It is also proved by testing intracellular levels of glycolytic and Krebs cycle in aconitase-mutated strain that although the Krebs cycle enzymes are present in PCF, they are not used by PCF *T. brucei* as a full cycle for energy generation, but used in part for energy transduction (van Weelden et al. 2003). At the same time, the mitochondrial respiratory chain is essential for survival and growth (Figure 1-3). In addition to carbohydrate degradation, ATP is generated by the oxidation of amino acids, especially proline and threonine (Evans & Brown 1972; Lamour et al. 2005).

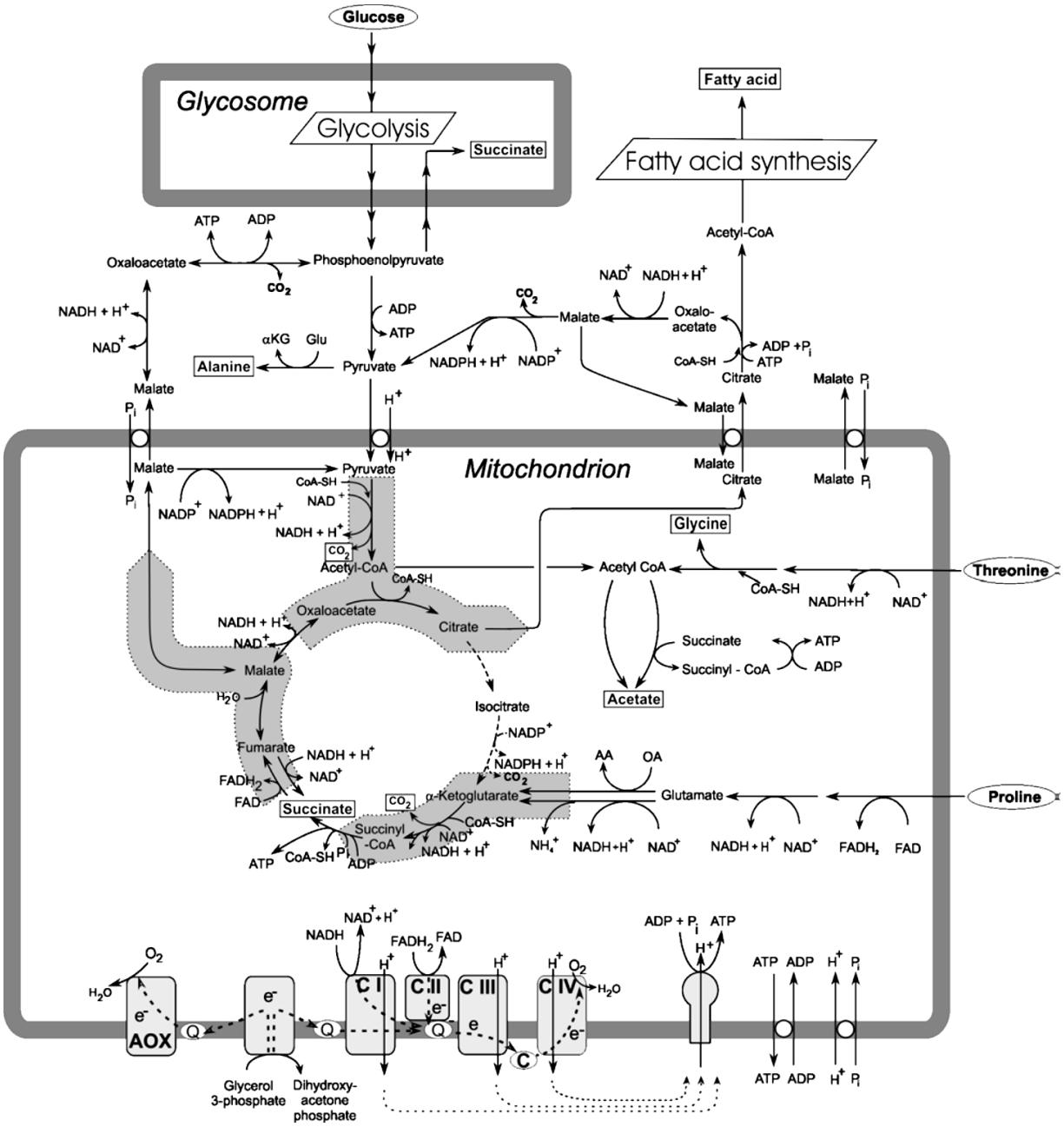

Figure 1-3 Energy metabolism of procyclic *T. brucei* (van Hellemond et al. 2005)

Substrates are shown by ovals and end-products are boxed. The shaded broad arrows in the background of the citric acid cycle are active in PCF. The shaded broad arrow from pyruvate and oxaloacetate to citrate indicates the flux via this part of the citric acid cycle, used in the transport of acetyl-CoA units from the mitochondrion to the cytosol. The shaded broad arrow from α-ketoglutarate to succinate represents the part of the cycle that is used for the degradation of proline and glutamate to succinate. The shaded broad arrow from succinate to malate indicates the part of the cycle that is used during gluconeogenesis. Abbreviations: AA, amino acid; CI, II, III and IV, complex I, II, III and IV of the respiratory chain; c, cytochrome c; Glu, glutamate; α-KG, α-ketoglutarate; OA, oxoacid; Q, ubiquinone.

1.3 Iron metabolism in *Trypanosoma brucei*

Iron is an important redox or structural cofactor of indispensable cellular processes of trypanosomes, such as DNA synthesis, protein translation, oxidant defence and cytochrome respiration (Taylor & Kelly 2010). Iron has two ion forms, ferric iron (Fe^{3+}) and ferrous iron (Fe^{2+}). The amount of iron in the cytosol is regulated at several levels: from absorption to mobilisation and utilisation. Both iron deficiency/ deprivation (Chisi et al. 2004) and iron accumulation (Stijlemans et al. 2008) can cause severe disorders to cells.

In the cytosol, iron is never free as free iron participates in the Fenton reactions (Fenton 1894) which produces highly toxic oxygen species, such as hydroxyl radical (OH·). Only 5% of the total iron is redox active and forms the so-called labile iron pool (LIP). LIP consists of Fe^{2+} and Fe^{3+} associated with a diverse population of low molecular mass such as glutathione (GSH), organic anions (eg. phosphate, citrate and inositol phosphate) and components of membranes.

1.3.1 Iron acquisition in *T. brucei*

As an important cofactor, iron acquisition in *T. brucei* is the first step of iron utilisation. In BSF, iron binds to the host glycoprotein transferrin (Tf). The complex of Tf and iron can be internalised into *T. brucei* cells with the help of transferrin receptor (TfR) which is located on the cell membrane (Grab et al. 1992; Grab et al. 1993). TfR is identified as a heterodimeric complex of proteins encoded by the expression-site-associated-genes ESAG 6 and ESAG 7 (Steverding et al. 1995). TfR is localised in the flagellar pocket, where transferrin-containing iron is internalised and Tf is degraded by a cathepsin B-like protease (CatB) (O'Brien et al. 2008). At the same time, iron is released with the help of a ferric reductase (Fe-RED) and a divalent cation transporter (DCT). Host heme in haptoglobin-hemoglobin (HpHb) is internalised by HpHb receptor. A working model for iron acquisition and utilisation in BSF is shown in Figure 1-4.

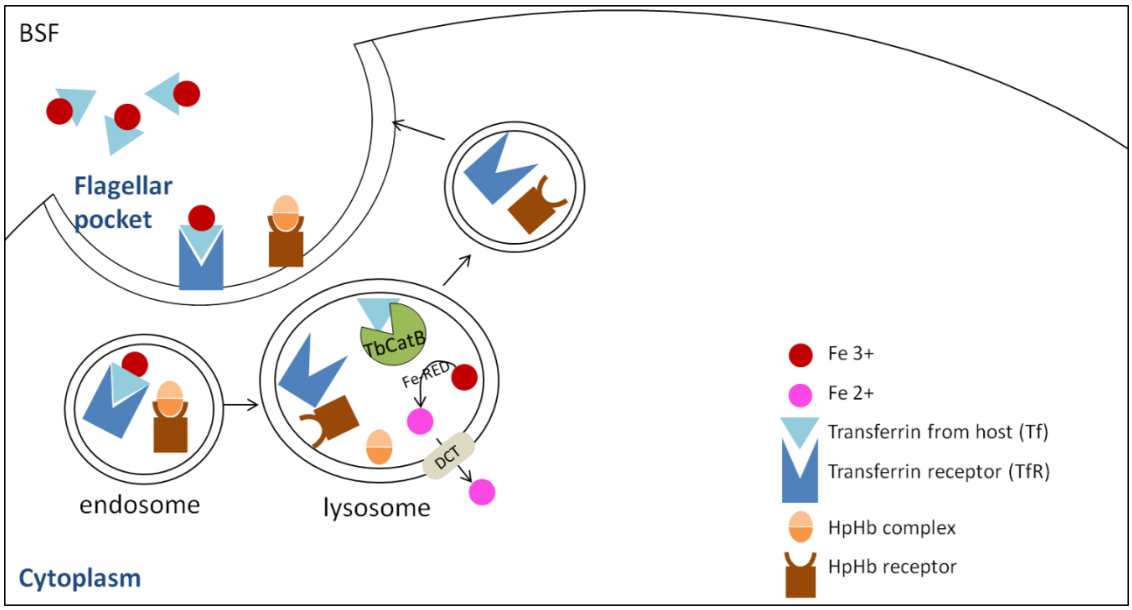

Figure 1-4 Iron and heme acquisition in *Trypanosoma brucei* BSF (Adapted from Taylor 2010, Manta 2011 and Basu 2016)

Transferrin receptors (TfR) are located in the flagellar pocket, which recognise and form a complex with host's transferrin (Tf). Host's haptoglobin-hemoglobin (HpHb) complex is internalised as heme source by the HpHb receptor (HpHbR). Tf-TfR and HpHb-HpHbR are internalised by endocytosis. Subsequently, free iron and HpHb are released from the corresponding receptors in the lysosome, and transferrin is degraded by the protease TbCatB. The released free iron ($Fe3^{+}$) is enzymatically reduced to Fe^{2+} by the ferric reductase (Fe-RED). Fe^{2+} is transported to the cytoplasm via a divalent cation transporter (DCT). TfR and HpHbR are recycled back to the flagellar pocket membrane.

In PCF *T. brucei*, iron is obtained using a reductive mechanism in which ferric complexes are reduced to ferrous complexes followed by endocytosis, while heme from a blood meal is transported into PCF by TbHrg (Huynh et al. 2012), and further transports into mitochondria by the ABC transporter, multidrug resistance like-1 (TbMdl1). In this thesis, TbMCP17 was studied and proposed to function as an iron transporter in mitochondria. The iron-sulfur cluster (ISC) machinery takes place in mitochondria involving cysteine desulfurase TbNfs-TbIsdl (Paris et al. 2010), scaffold unit IscU (Smíd et al. 2006), ferredoxin A (FdxA), ferredoxin reductase (FdR) (Verner et al. 2015), frataxin (TbFxn) (Long et al. 2008), chaperones Hsp70 (Týč et al. 2015), Mge1 and Jac1, Isa1,2 (Long et al. 2011). Afterwards, Fe/S proteins are exported from mitochondrion with the help of the ABC transporter Atm and the inner space protein Erv1, known as ISC export machinery (Hell 2008; Becker et al. 2012). In the cytoplasm, cytosolic iron-sulfur cluster assembly (CIA) machinery (Basu et al. 2014) is composed of complexes of scaffold proteins, targeting complexes, apo-proteins and holo-proteins (Figure 1-5).

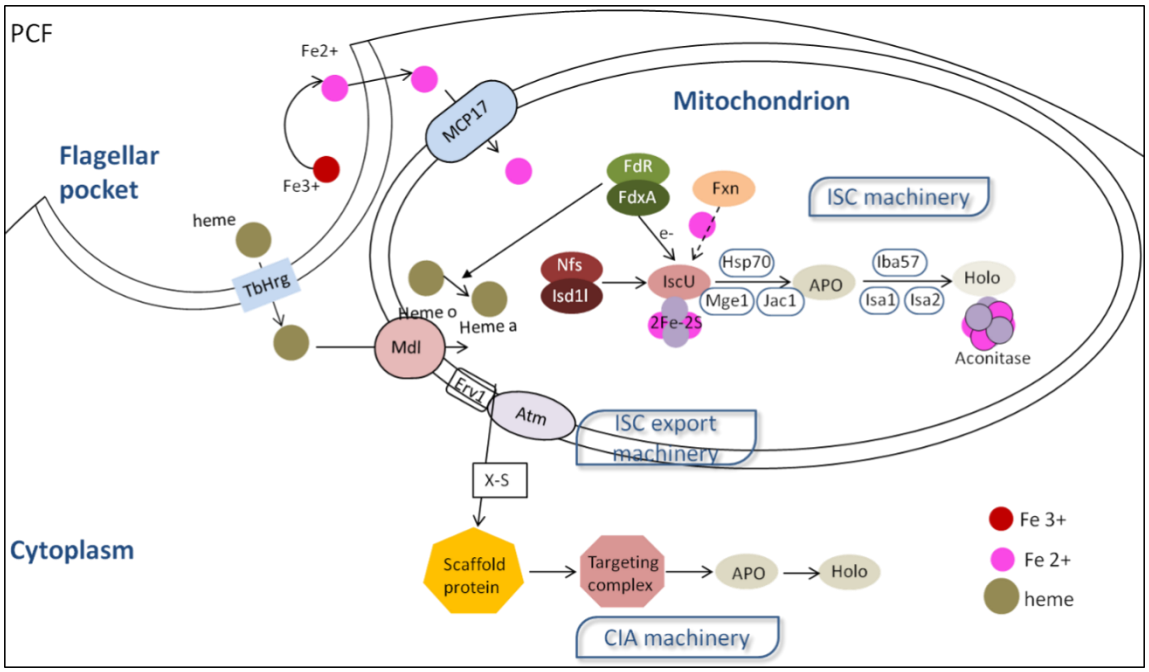

Figure 1-5 Iron and heme acquisition in *Trypanosoma brucei* PCF (Adapted from Basu et al. 2016)

Iron is obtained by a reductive mechanism in PCF *T. brucei*: ferric complexes are reduced to ferrous complexes, then endocytosed into the cytoplasm. Ferric iron is proposed to be transported into mitochondria by mitochondrial inner membrane protein TbMCP17. Heme is imported into the cytoplasm by TbHrg, and then transported into mitochondria by ABC transporter TbMdl. Iron-sulfur cluster (ISC) machinery takes place in mitochondria where cysteine desulfurase TbNfs-TbIsdl and scaffold unit IscU initiate the process and produce [2Fe-2S]. Ferredoxin A (FdxA) and ferredoxin reductase (FdR) form the electron transport chain, providing electron for Fe/S maturation. Frataxin (TbFxn) may involve in transporting ferrous iron to IscU. Subsequently, chaperones Hsp70, Mge1 and Jac1 incorporate Fe/S cluster to apo-proteins. Isa1, Isa2 and Iba57 are involved in holo-protein maturation like aconitase [4Fe-4S]. Afterwards, Fe/S proteins are exported from mitochondrion to cytoplasm with the help of ABC transporter Atm and inner space protein Erv1, known as ISC export machinery. In the cytoplasm, cytosolic iron-sulfur cluster assembly (CIA) machinery is composed of complexes of scaffold proteins, targeting complexes, apo-proteins and holo-proteins.

1.3.2 Iron-dependent proteins in *T. brucei*

So far, four iron-dependent enzymes have been identified in *T.brucei*: aconitase (Overath et al. 1986), alternative oxidase (Fairlamb & Bowman 1977; Clarkson et al. 1989), ribonucleotide reductase (Dormeyer et al. 1997; Hofer et al. 1997) and superoxide dismutase (Le Trant et al. 1983). Aconitase is an enzyme generally known to convert citrate into isocitrate via *cis*-aconitate. Also, aconitase is an iron-responsive element binding protein that functions post-transcriptionally by binding iron to iron responsive

elements on mRNA (Walden et al. 2006; Dupuy et al. 2006). However, aconitase seems to have no vital function for both BSF (Fast et al. 1999) and PCF (van Hellemond et al. 2005) since deletion of both alleles presented no growth phenotype. The other three iron dependent enzymes play essential roles in cellular metabolism, which are discussed as follows.

Iron-dependent proteins help to protect parasites against redox pressure. Firstly, dinitrosyl iron complexes form neutralise nitric oxide (·NO), an important messenger produced in host's endothelial or immune cells (Girard et al. 2005). If nitric oxide is not neutralised rapidly, it can form the highly reactive oxidant peroxynitrite, which is detrimental to the trypanosomes (Lu et al. 2011). Another oxidant defence is associated with iron-dependent superoxide dismutases (Fe-SOD), a family of antioxidant metalloenzymes restricted to protozoans, prokaryotes and chloroplasts (Dufernez et al. 2006; Kabiri & Steverding 2001; Wilkinson et al. 2006; Prathalingham et al. 2007). The anion superoxide ($O_2^{\cdot -}$) produced by aerobic respiration can reduce or oxidise biological targets *in vivo* or dismutate to less reactive but highly diffusible oxidant hydrogen peroxide (H_2O_2). Furthermore, anion superoxide can form the most reactive and harmful radical product hydroxyl radical (OH·) through Fenton reaction if it is not removed (Abreu & Cabelli 2010). Superoxide dismutases catalyse the dismutation of the superoxide ($O_2^{\cdot -}$) radical into either oxygen or hydrogen peroxide. Thus, the SOD family is of great importance owing to the detoxification function of superoxide anions. All of the four isoforms of SODs expressed by trypanosomes are Fe-dependent proteins, with SOD-A and C located in mitochondria (Dufernez et al. 2006).

Iron centred proteins play a role in cell proliferation. The ribonucleotide reductase (RNR) catalyses the reduction of ribonucleotides to deoxyribonucleotides, which is necessary for DNA synthesis. The R2 subunit of class I RNR is composed of two high spin Fe^{3+} atoms which generate a free radical on this catalytic tyrosine radical through electron donation (Cotruvo & Stubbe 2011).

Iron also plays an important role in energy metabolism when it comes to iron centred protein alternative oxidase. It is a plant-like mitochondrial ubiquinol oxidase known as trypanosomal alternative oxidase (TAO). TAO is localised in the inner mitochondrial

membrane and transfers electrons from ubiquinol to oxygen, resulting in the reoxidation of NADH (Clarkson et al. 1989). TAO is expressed about 100 times more in BSF than PCF (Tsuda et al. 2005). Besides NADH reoxidation, TAO also plays an important role in preventing oxidant-induced programmed cell death of long slender bloodstream parasites (Tsuda et al. 2005; Tsuda et al. 2006). TAO might be an important checkpoint connecting metabolic status (NAD^+/NADH ratio) with apoptosis and differentiation. Furthermore, TAO has been shown to compensate for a depletion of complex III or IV activities in the mitochondrial electron transfer chain (Horvath et al. 2005). Iron protein stearoyl-CoA desaturases (TbSCD) participate in lipid biosynthesis. SCD is responsible for monounsaturated fatty acids from saturated fatty acids (Man et al. 2006).

Ribonucleotide reductases and alternative oxidases have been suggested to be targeted by deferoxamine. As an iron chelator, deferoxamine causes the inhibition of DNA synthesis and the decrease of oxygen consumption. Also, growth inhibition of BSF of *T. brucei* caused by deferoxamine has been reported (Breidbach et al. 2002). In this study, deferoxamine was used to create an iron depleted condition.

1.3.3 Iron-sulfur cluster formation and its functions

Iron-sulfur clusters are versatile cofactors for proteins that are involved in many cellular processes, such as electron transport in respiration and photosynthesis, enzymatic catalysis and regulation. The architectural element of the Fe-S cluster is [2Fe-2S], which is formed with two bridging sulphides. Iron cations and sulphide anions can also be assembled to form a cubic [4Fe-4S] cluster (Beinert et al. 1997; Rees 2002). Iron-sulfur clusters are sensitive to H_2O_2 and NO, which allows them to play an important part in the response to oxidative stress. It is believed that a Fe-S protein functions as a sensor for the mitochondrial iron status or aids in the formation of the sensor to regulate the mitochondrial iron homoeostasis (Rouault & Tong 2005).

1.3.4 Sideroflexin family

Iron homoeostasis is essential for aerobic respiration (Aisen et al. 2001). Iron metabolism disorders often lead to anaemia because of its role in heme synthesis and mitochondrial metabolism. The hallmark of mitochondrial iron accumulation is sideroblastic anaemia (Ponka 1999).

A novel gene family, *sideroflexin (SFNX)*, is identified in flexed-tail mice. *SFNX* was initially characterised as a mitochondrial di/tricarboxylate carrier transporting citrate and encoded a mitochondrial transmembrane protein (Azzi et al. 1993). Gene mutation was found to cause siderocytic anaemia in mice (Fleming et al. 2001). *SFNX2* has also been shown to be a candidate gene for human sideroblastic anaemia (Ye et al. 2003). *SFNX5* was identified, and the encoded protein was expressed at a high level in specific human brain regions, which was exclusively related to *PARK3*, a susceptible gene for Parkinson's disease (Lockhart et al. 2002).

1.3.5 Mitochondrial iron metabolism in *S. cerevisiae*

Similar to *T. brucei* or other eukaryotic cells, most of the iron imported into the cytosol is further imported to the mitochondria in *S. cerevisiae*. In yeast, iron in the mitochondria is required for heme synthesis and iron-sulfur cluster assembly. Iron depriving impairs the metabolic and respiratory activity, while the excess of iron causes a toxic effect by the generation of oxidative stress (Lange et al. 1999). In other words, the mitochondrial iron content is tightly regulated in yeast, which involves three proteins: the yeast ABC transporter Atm1p (homologue to Atm in *T. brucei* discussed before) (Kispal et al. 1997; Csere et al. 1998), frataxin Yfh1p (homologue to Tbfxn) (Babcock et al. 1997; Foury & Cazzalini 1997) and Ssq1p (belonging to heat shock protein family, *T.brucei* homologue Hsp70) (Knight et al. 1998). The depletion of any of the three proteins causes a significant increase of mitochondrial iron content.

Iron acquisition into the yeast mitochondria has been first studied in the utilisation of synthesis of heme *in organello*. The requirements for iron import are (i) membrane

potential dependence; (ii) independence of ATP; (iii) the reduced (ferrous) form of iron. Iron import was also suggested to be a rate-limiting step for heme formation (Lange et al. 1999). MRS3 and MRS4, two members of the mitochondrial carrier family with high sequence similarity, were first presented to link with mitochondrial iron homoeostasis, which was supported by the finding that the depletion of both genes suppressed the mitochondrial iron accumulation caused by frataxin-depletion (Foury & Roganti 2002). By *in vivo*, *in organello* (intact mitochondria), and *in vitro* (mitochondrial extracts) assessments of heme formation and iron-sulfur cluster biosynthesis processes, MRS3/4 was suggested to be directly involved in mitochondrial iron uptake. This iron uptake was found to be evident only under iron-limiting conditions (Muhlenhoff et al. 2003). The previous findings were supported by Zhang *et al.* that frataxin (YFH1) and MRS3/4 cooperate in providing iron for heme synthesis (Zhang et al. 2005) as well as for iron-sulfur cluster formation in mitochondria (Zhang et al. 2006). Despite of all the indirect assays applied above, a direct measurement of ferrous iron across mitochondrial inner membrane vesicles (SMPs) using an iron-sensitive fluorophore PhenGreen SK (PGSK) confirmed the role that MRS3/4 played in mitochondrial iron import, and this activity was dependent on the pH gradient (Froschauer et al. 2009).

Table 1-2 Yeast strains used in this study

strain	genotype	phenotype	reference
BY4741	Wild-type strain (*Mat a his3Δ1 leu2Δ0 met15Δ0 ura3Δ0*)	Standard growth	Brachmann et al. 1998
ΔDIC1*	YLR348C (ΔDIC1; *MATa his3Δ1 leu2Δ0 met15Δ0 ura3Δ0*)	Standard growth on glucose Limited growth on acetate or ethanol	Palmieri et al. 1999
ΔMRS3/4	GW403 (mrs3/4Δ; *MATa his3-Δ1 leu2-3 leu2-112 ura3-52 trp1-289 mrs3Δ*::*loxP mrs4Δ*::*loxP*)	Standard growth on glucose Severe growth defect under iron limiting conditions	Froschauer et al. 2009

*DIC is the dicarboxylate carrier in yeast mitochondria, and details are described in Chapter 1.5.

As suggested, there should be alternative mitochondrial iron transport mechanisms in yeast (Muhlenhoff et al. 2003). Indeed, the mitochondrial pyrimidine transporter Rim2 (Van Dyck et al. 1995; Palmieri et al. 2006) was found to complement MRS3/4 mutant

in growth and to promote iron-sulfur cluster assembly and heme synthesis under both mutant and wildtype background of yeast (Yoon et al. 2011). The role of Rim2 in mitochondrial supply was confirmed by the same transport assay into SMPs and was detected by PGSK that Rim2 co-imports pyrimidine nucleotides and iron (Froschauer et al. 2013). This role was not significant under normal physiological conditions, but in the absence of the main iron transporters MRS3/4, Rim2 could supply mitochondria with iron in a pyrimidine-dependent fashion. In this study, the details of the yeast strains used in this study are listed in Table 1-2.

1.4 The mitochondrial carrier family

Metabolites cross the mitochondrial outer membrane through a large diameter voltage-dependent anion channel (VDAC), or mitochondrial porin (Rostovtseva & Bezrukov 1998; Linden et al. 1982), while the inner mitochondrial membrane via mitochondrial carrier family (MCF) proteins (Nury et al. 2006). MCF proteins transport many kinds of metabolic intermediates, including anions such as carboxylates, nucleotides and inorganic phosphate, or cations such as iron, ornithine, carnitine, spermine and glutamine (Aquila et al. 1987; Palmieri 2004). The importance of MCF proteins in many metabolic processes and the maintenance of redox and ATP balance between mitochondria and the cytosol was confirmed by human metabolic diseases caused by MCF gene mutation or aberration (Palmieri et al. 2008). MCF proteins were first and mainly found in the inner membrane of mitochondria, but some were also found in the membranes of other organelles including glycosomes, peroxisomes (van Roermund et al. 2001), hydrogenosomes (Voncken et al. 2002) and chloroplasts (Bouvier et al. 2006; t al. 2002; Bedhomme et al. 2005).

MCF proteins have highly conserved sequence features (Palmieri 2004, Figure 1-6), consisting of six transmembrane helices (H1-6) and the hydrophilic loops to connect the two transmembrane domains (h1-2, h3-4 and h5-6), respectively. Both the N terminal and C terminal end in the mitochondrial intermembrane space, while the hydrophilic loops are facing the mitochondrial matrix. The MCF proteins contain a conserved canonical signature sequence motif, which consists of two parts: the first part Px(D/E)xx(K/R)x(K/R) (x=any amino acid residue) is located at the end of the odd-

numbered transmembrane helices, labelled M1a, M2a, and M3a; and the second part (D/E)Gx4-5(K/R)G is located at the end of each hydrophilic loop, labelled M1b, M2b and M3b. Substrate contact points are localised at the downstream of the second part of the signature sequence and are labelled CPI, CPII and CPIII. CPI and CPII are highly conserved within the same function group, but they differ when transporting different substrates.

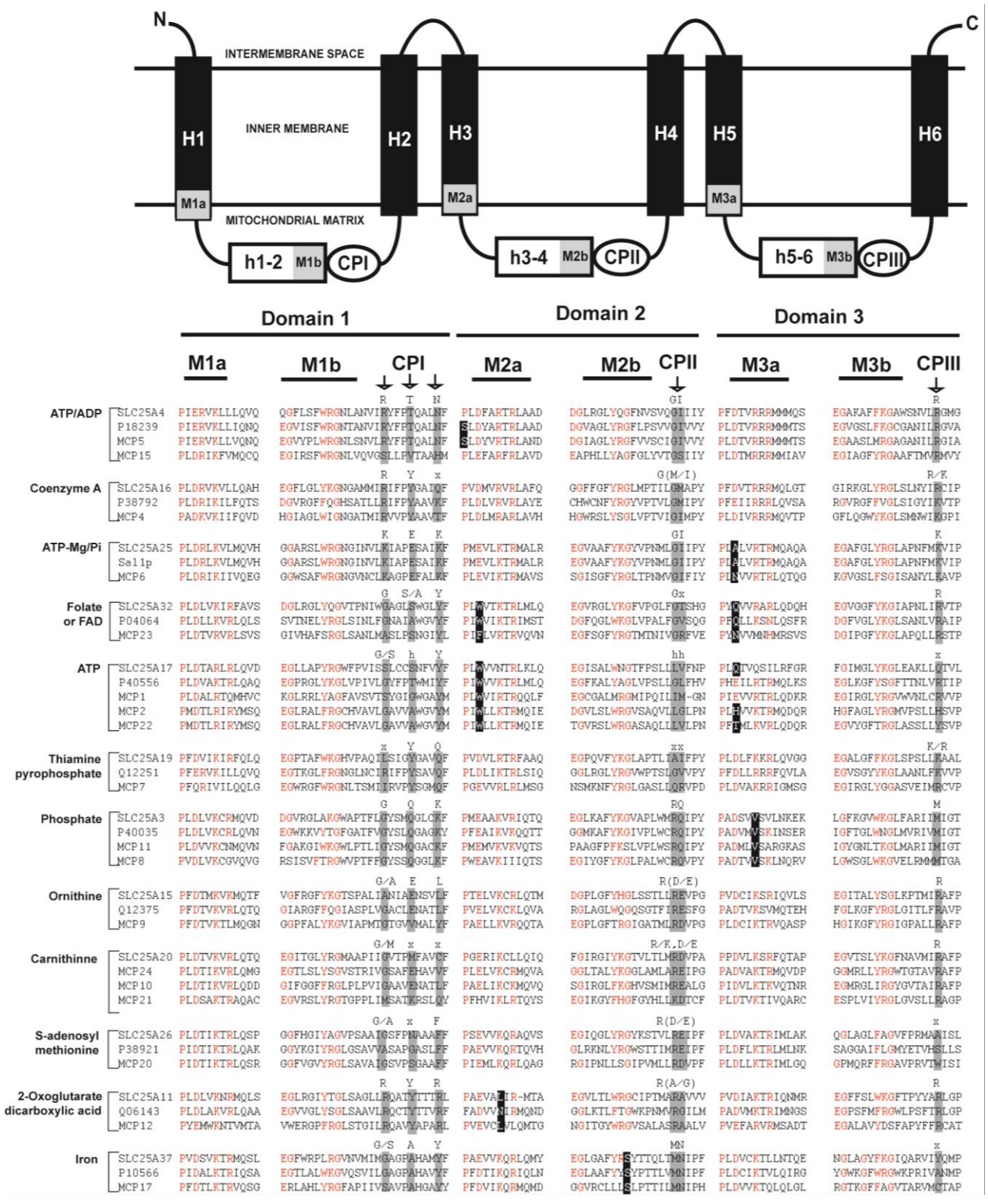

Figure 1-6 Schematic representation of the conserved tripartite MCF protein structure (Colasante et al. 2009)

The six transmembrane helices are labelled H1-6, whereas the hydrophilic loops, connecting the 2 transmembrane domains found in each repeat (1–3), are labelled h1-2, h3-4 and h5-6, respectively. The first part of the canonical signature sequence motif, Px(D/E)xx(K/R)x(K/R), located at the end of the odd-numbered transmembrane helices, is labelled M1a, M2a, and M3a. The second part of the canonical signature sequence

motif, (D/E)Gxn(K/R)G, located at the end of each hydrophilic loop, is labelled M1b, M2b, and M3b. Substrate contact points are located downstream of the second part of the signature sequence and are labelled CPI, CPII and CPIII. TbMCPs and related MCF protein sequences from human (SLC25A) and *S. cerevisiae* are aligned. For each of the different functional transporter subgroups, only those containing the conserved signature sequences (identical signature sequence residues are marked red) and the amino acid residues present in each of the contact points (boxed grey) are shown. Signature sequence residues, deviating from the canonical signature sequence, but found in all members of a specific carrier subgroup, are boxed black. Putative substrates for each of the carrier subgroups are indicated.

24 mitochondrial carrier family proteins were identified and arranged into different groups by potential function(s) according to sequence alignment with human and yeast genomes (Colasante et al. 2009; Figure 1-7). They included nucleotide carriers, amino acids carriers, phosphate carriers, dicarboxylate/oxodicarboxylate carriers and iron carrier. TbMCP12 showed homology to 2-oxoglutarate and dicarboxylic acid transporters. TbMCP17 was the only homologue to human and yeast iron transporters. TbMCP23 was homologous to folate transporters (Figure 1-7).

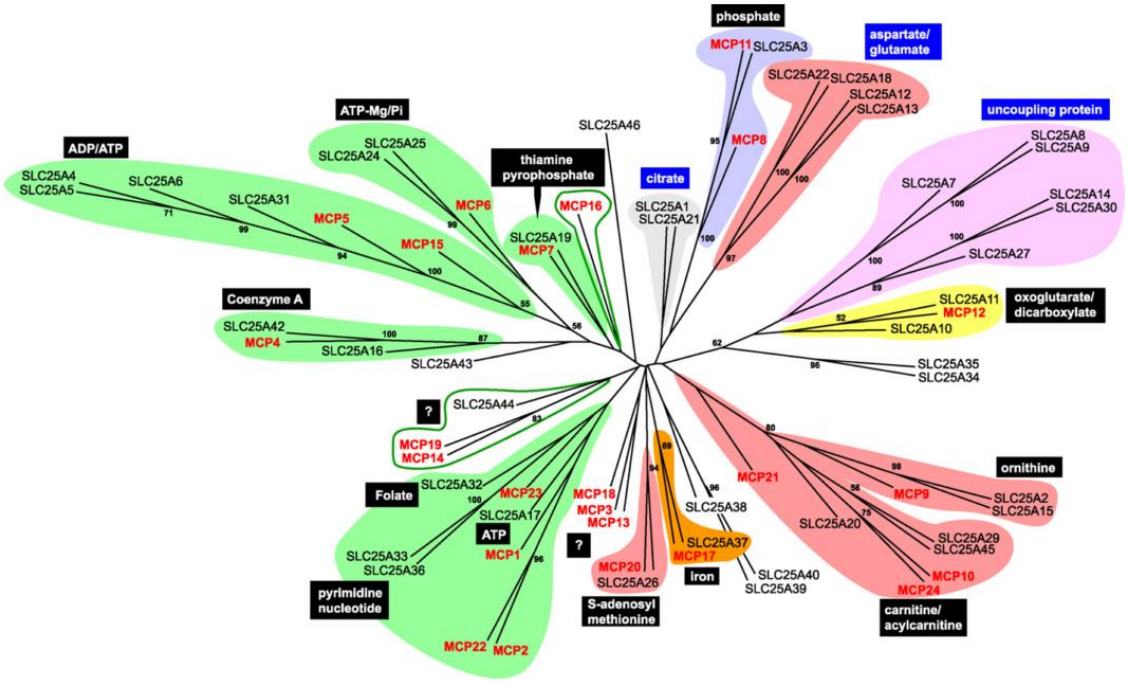

Figure 1-7 The neighbour-joining tree showed the evolutionary relationship between TBMCPs and 43 human MCF proteins

Bootstrap values above 50% are indicated at the relevant nodes. Coloured balloons are used to mark the major functional MCF subgroups: green, nucleotide carriers; pink, amino acid carriers; blue, inorganic phosphate carriers; yellow, dicarboxylate/ oxoglutarate carriers; and orange, iron carriers. Blue text boxes represent MCF subgroups

for which no *T. b. brucei* homologues can be identified. Question marks indicate TbMCPs for which no transport function can be predicted (Colasante et al. 2009).

Mitochondrial carrier family proteins are potential drug targets. The inhibitor of the mitochondrial pyruvate carrier (MPC), lonidamine (LND), is an effective and selective anti-tumour drug. LND causes tumour cells specific MPC inhibition, with additional inhibitory effects on monocarboxylate transporters mediated L-lactic acid efflux and glutamine/glutamate oxidation (Nancolas et al. 2016). TbMCP14 was suggested to be a candidate for drug action or targeting due to the finding that the overexpression of protein increased parasite susceptibility more than 13-fold in PCF; while the down-regulation of TbMCP14 resulted in an increase of resistance towards anti-parasitic choline analogues in both BSF (7-fold) and PCF (3-fold) cells. Moreover, TbMCP14 presented poor similarity to mitochondrial carriers of mammals, suggesting the potential to be an anti-parasitic drug target (de Macêdo et al. 2015).

1.5 Potential iron transporters in *Trypanosoma brucei*

Among the 24 MCF proteins, this thesis is particularly focused on potential iron transporters. The transport of iron into the mitochondrion is of considerable importance because it is essential for heme biosynthesis and Fe-S cluster protein assembly. Three mechanisms of iron transport into the organelle have been proposed. The first one is that iron is taken up by mitochondria as a ferrous ion, using the energy of membrane potential across the inner membrane without ATP consumed (Lange et al. 1999). The second hypothesis is that iron should be transported in the form of chaperone-like partially solvent occluded moieties to avoid being accessed by a chelator (Shvartsman et al. 2007). The third mechanism is called ‘kiss and run’, it is a transient contact of the transferrin-containing endosomal and mitochondrial membranes, followed by the direct transfer of iron from endosomes to mitochondria (Sheftel et al. 2007). MRS3/4, as mentioned before, are the yeast mitochondrial iron importers which uptake ferrous iron driven by the external ferrous iron concentration and stimulated by acidic pH (Froschauer et al. 2009).

TbMCP17 (Tb927.3.2980) is the only homologue in trypanosomes that shows high similarity to mitochondrial iron transporter MRS3 and MRS4 in yeast, and mitoferrin in

mammals. MRS3 and MRS4 have been proposed to mediate iron import in yeast (Foury & Roganti 2002; Felice et al. 2005; Muhlenhoff et al. 2003), while it is suggested that the two are not the only iron carriers that transfer iron into the mitochondrial matrix (Zhang et al. 2005). Mitoferrin (mfrn) is a vertebrate homologue Fe^{2+} transporter to import iron into mitochondria for heme biosynthesis (Shaw et al. 2006). Another paralogous protein coded by gene *mfrn2* is also found in mammals (Li et al. 2002).

Just as iron binds to iron transporter transferrin, Fe^{2+} couples only with an anion (usually carbonate) to serve as a bridging ligand between metal and protein (Aisen & Listowsky 1980; Shongwe et al. 1992). So carboxylates carrier is also very likely to transport iron at the same time.

Sequence analysis and alignment of TbMCP12 (Tb10.389.0690) with various carboxylate carriers of different species from plants to mammals, covering model organisms such as *A. thaliana, S.cerevisiae,* and *H. Sapiens,* revealed the possibility of TbMCP12 belonging to dicarboxylate carriers (DICs, SLC25A10 homologues), dicarboxylate-tricarboxylate carriers in plants (DTCs, AT5G19760 homologues) or oxoglutarate carrier (OGC, SLC25A11 homologues). The detection of TbMCP12 expression level using N-term peptide antibody demonstrated a significant up-regulation of TbMCP12 protein level in PCF life cycle stage compared with BSF. The mitochondrial localisation of TbMCP12 was confirmed by immunofluorescence microscopy and gradient fractionation (Colasante, unpublished data).

DICs catalysed the electroneutral exchange of certain dicarboxylates (malate, succinate, fumarate, 2-oxoglutarate, and oxaloacetate), inorganic phosphate (Pi), inorganic sulfur containing compounds (sulphite, sulphate and thiosulphate) and tricarboxylates (citrate, isocitrate) (Dolce et al. 2014). OGCs facilitated the exchange of both dicarboxylates and oxodicarboxylates across the mitochondrial inner membrane (Monné et al. 2012). DTCs catalysed the exchange of oxodicarboxylates (i.e. α-ketoglutarate), dicarboxylates (i.e. malate, succinate and oxaloacetate) and tricarboxylates (i.e. citrate, isocitrate and cis-aconitate) (Picault et al. 2002). Mitochondrial carrier involved in the shuttling of dicarboxylates and tricarboxylates played a central role in several transport and metabolic mechanisms: (i) the citrate pyruvate shuttle, which played a role in fatty acid biosynthesis;

(ii) the pyruvate malate shuttle involved in the regeneration of cytoplasmic NADPH; (iii) gluconeogenesis from pyruvate which required the export of malate from the mitochondrial matrix to the cytoplasm (Palmieri 2004).

Rim2 was discovered to be related to iron transport by genetic screening using lethal *MRS3/4* mutants in yeast. The growth defect of yeast *MRS3/4* mutants was complemented by Rim2 expression, with the upregulation of heme and iron-sulfur cluster synthesis (Yoon et al. 2011). Previously, *Rim2* was known as a pyrimidine nucleotide exchanger (*Rim2/MRS12*), encoding a 377 aa protein essential for mitochondrial DNA metabolism and proper cell growth (Van Dyck et al. 1995). By reconstituting purified protein into liposomes, its transport function for pyrimidine nucleotides was examined (Marobbio et al. 2006). Drim2, the *Drosophila melanogaster* homolog of rim2, showed the vital function of maintaining normal deoxynucleotide pools, and *Rim2* knockout was lethal at the larval stage (Gull 2003). On the other hand, in a study of high iron toxicity-driven by the deletion of vacuolar iron transporter Ccc1, Rim2 was identified as a suppressor of high iron toxicity besides MRS3/4 (Lin et al. 2011). In trypanosomes, *TbMCP23* was found to be highly similar in gene sequence with *RIM2*.

TbSFNX belongs to the *sideroflexin (SFNX)* family. Previous publications showed that a defect in the sideroflexin gene in mice led to inherited sideroblastic anaemia (Fleming et al. 2001). The best characterised genetic defect causing sideroblastic anaemia was a mutation in the erythroid-specific form of the aminolevulinic acid synthetase (ALAS2) and a mutation in ABC7, a mitochondrial ABC-transporter involved in the maturation of cytoplasmic iron-sulfur proteins (Bekri et al. 2000; Taketani et al. 2003). However, the other genes for the biosynthesis of heme were lacking. These findings exclude a role of TbSFNX in the import of a component involved in the *de novo* heme biosynthesis. It is unclear whether TbSFNX has a role in mitochondrial iron homoeostasis.

1.6 Aim of the thesis

MCF proteins play a crucial role in the energy metabolism of cells. Mitochondrial iron import is essential for oxidative stress defence, energy metabolism and iron-sulfur cluster assembly. *Trypanosoma brucei* is a protista parasite that causes detrimental disease in

mammals. Treatment for Trypanosomosis is limited and new drugs (targets) are needed. Mitochondrial iron transporters in *Trypanosoma brucei* could be promising candidates for potential new drug targets.

The aim of this study is to functionally characterise the mentioned potential mitochondrial iron transporters: TbMCP12 (homologous to DIC), TbMCP17 (homologous to MRS3/4), TbMCP23 (homologous to RIM2) and TbSFNX (homologous to SFNX).

Sequences of the genes were first analysed by sequence alignments with known mitochondrial carriers on DNA and protein level in combination with phylogenetic reconstruction. Protein localisation was studied using immunofluorescence microscopy followed by Western Blot. The generated mutants (knockout) or knockdown (RNAi) and overexpressing cell lines were used to characterise related phenotypes. The functions of the proteins of interest were examined using functional complementation assays in yeast. Physiological roles of proteins mentioned above were measured via iron-dependent enzymes activities assays, iron content and mitochondrial ATP production assays.

Chapter 2 Materials and methods

2.1 Phylogenetic reconstruction and sequence analysis

Multiple sequence alignments were generated using ClustalO (Sievers et al. 2011; Li et al. 2015), and motif structures were added manually using Adobe Illustrator. Phylogenetic trees were constructed using MEGA7 (Molecular Evolutionary Genetics Analysis version 7.0) (Kumar et al. 2016). Blast-Protein (http://blast.ncbi.nlm.nih.gov/Blast.cgi?PAGE=Proteins) was employed to retrieve protein sequences from trypanosomatids, plants, insects, fungi and mammals. The sequences were then imported into MEGA7 and aligned. Using the neighbour-joining (NJ) method (Saitou & Nei 1987), a neighbour-joining tree was drawn with bootstrap set to 1000. Only bootstrap values above 50% were shown. After generation of the phylogenetic tree, different groups were labelled manually with Adobe Illustrator.

The GenBank (gb), EMBL (emb) and Swissprotein (sp) accession numbers for TbMCP17 alignments were as follows: T.b.bruceiMCP17, *Trypanosoma brucei brucei* Tb927.3.2980; T.b.gambiense, *Trypanosoma brucei gambiense* emb_CBH09968.1; T.congolense, *Trypanosoma congolense* emb_CCC89759.1; T.vivax, *Trypanosoma vivax* emb_CCC47046.1; T.cruzi, *Trypanosoma vivax* gb_EKG04497.1; T.rangeli, *Trypanosoma rangeli* gb_ESL10208.1; L.amazonensis, *Leishmania amazonensis* gb_ALP75642.1; L.mexicana, *Leishmania mexicana* emb_CBZ23750.1; L.major, *Leishmania major* emb_CBZ12619.1; L.seymouri, *Leptomonas seymouri* gb_KPI87731.1; L.panamensis, *Leishmania panamensis* gb_AIO00226.1; U.hordei, *Ustilago hordei* emb_CCF54811.1; U.maydis, *Ustilago maydis* gb_KIS71149.1; P.brasiliensis, *Pseudozyma brasiliensis* gb_EST06361.1; R.microspores, *Rhizopus microspores* emb_CEJ04189.1; M.antarcticus, *Moesziomyces antarcticus* gb_ETS61106.1; D.willistoni, *Drosophila willistoni* gb_EDW83029.1; B.cucurbitae, *Bactrocera cucurbitae* XP_011180944.1; D.mojavensis, *Drosophila mojavensis* gb_EDW14539.1; G.raimondii, *Gossypium raimondii* gb|KJB83905.1; F.vesca, *Fragaria vesca* XP_004294768.1; M.mycetomatis, *Madurella mycetomatis* gb_KOP45184.1; P.carnosa, *Phanerochaete carnosa* gb_EKM49983.1; G.arboretum, *Gossypium arboreum* gb_KHG15442.1; R.solani, *Rhizoctonia solani* emb_CUA78164.1; D.virilis, *Drosophila virilis* gb_EDW59237.2; B.cinerea, *Botrytis cinerea* XP_001553628.1; S.indicum, *Sesamum indicum* XP_011080718.1; H.sapiensMFRN1, *Homo sapiens*

gb_EAW63617.1; H.sapiensMFRN2, *Homo sapiens* gb_AAK49519.1; S.cerevisiaeMRS3p, *Saccharomyces cerevisiae* gb_EGA61827.1; S.cerevisiaeMRS4p, *Saccharomyces cerevisiae* gb_AJS43107.1; A.thaliana, *Arabidopsis thaliana* gb_AAP42736.1; Z.maysMRS3, *Zea mays* gb_ACG42379.1; M.musculusMFRN1, *Mus musculus* gb_AAL23859.1; M.musculusMFRN2, *Mus musculus* gb_AAH25908.1; B.taurusMFRN1, *Bos taurus* gb_AAI03256.1; B.taurusMFRN2, *Bos taurus* NP_001192481.1; L.cuprina, *Lucilia cuprina* gb_KNC31521.1; D.busckii, *Drosophila busckii* gb_ALC47563.1; H.saltator, *Harpegnathos saltator* gb_EFN83637.1; A.pisum, *Acyrthosiphon pisum* NP_001280444.1; A.niger, *Aspergillus niger* XP_001390994.2.

The NCBI accession numbers for TbSFNX (Tb09.160.2910) are as follows: dicarboxylate/tricarboxylate carrier, *Arabidopsis thaliana* NP_197477.1; mitochondrial cation transporter, *Aspergillus clavatus NRRL 1* XP_001268595.1; oxoglutarate carrier, *Bos taurus* NP_777096.1; solute carrier family 25 member 1, *Bos Taurus* NP_777081.1; sideroflexin 1, *Bos taurus* NP_001015574.1; sideroflexin 2, *Bos taurus* NP_001029618.1; sideroflexin 4, *Bos taurus* NP_001030232.1; *Candida dubliniensis* Cd_tempid_1_2526; oxoglutarate/malate carrier protein, *Caenorhabditis elegans*, emb_CAA53720.1; Sideroflexin-2, *Canis familiaris* XP_543994.2; Sideroflexin-3, *Canis familiaris*, XP_543977.2; sideroflexin 4, *Canis familiaris* XP_535030.2; sideroflexin 5, *Canis familiaris* XP_855176.1; sideroflexin 1, *Danio rerio* NP_001003537.1; sideroflexin 2, *Danio rerio* NP_997895.1; sideroflexin 5, *Danio rerio* XP_691120.1; sideroflexin 5, *Gallus gallus* XP_420891.2; 2-oxoglutarate carrier, *Homo sapiens* emb_CAA46905.1; dicarboxylate carrier protein, *Homo sapiens* emb_CAB59892.1; citrate transporter SLC25A member 1, *Homo sapiens* NP_005975.1; sideroflexin 1, *Homo sapiens* NP_073591.2; sideroflexin 2, *Homo sapiens* NP_849189.1; sideroflexin 3, *Homo sapiens* gb_EAW49787.1; sideroflexin 4, *Homo sapiens* NP_998814.1; sideroflexin 5, *Homo sapiens* NP_653180.1; tricarboxylate carrier, *Leishmania infantum* emb_CAM65210.; tricarboxylate carrier putative, *Leishmania major* 1XP_001687450.1; sideroflexin 4, *Macaca mulatta* XP_001096920.1; mitochondrial carrier, *Mus musculus* gb_AAH37087.1; dicarboxylate transporter, *Mus musculus* NP_038798.1; sideroflexin 1, *Mus musculus* NP_081600.1; sideroflexin 2, *Mus musculus* NP_444426.3; sideroflexin 3, *Mus musculus* NP_444427.1; sideroflexin 4 *Mus musculus* NP_444428.2; sideroflexin 5, *Mus musculus* NP_848754.1; dicarboxylate/tricarboxylate carrier, *Nicotiana tabacum*

emb_CAC84547.1; 2-oxoglutarate carrier, *Rattus norvegicus* NP_071793.1; dicarboxylate transporter, *Rattus norvegicus* NP_596909.1; sideroflexin 1, *Rattus norvegicus* NP_001012213.1; sideroflexin 3 *Rattus norvegicus* NP_075237.1; Sideroflexin-4, *Rattus norvegicus* XP_342073.2; sideroflexin 5, *Rattus norvegicus* NP_695210.1; Fsf1p, *Saccharomyces cerevisiae* NP_014914.1; mitochondrial citrate transport protein, *Saccharomyces cerevisiae* gb_AAC48984.1; tricarboxylate transporter, *Schizosaccharomyces pombe* emb_CAB16226.1; oxoglutarate malate translocator, *Solanum tuberosum* emb_CAA68164.1; tricarboxylate carrier, *Trypanosoma brucei* genedb_Tb09.160.2910; tricarboxylate carrier, *Trypanosoma brucei congolense* congo1271b09.q1k_0; tricarboxylate carrier, *Trypanosoma brucei gambiense* Tbgamb.22056; tricarboxylate carrier, *Trypanosoma cruzi* gb_EAN84262.1; tricarboxylate carrier, *Trypanosoma vivax* tviv1766e11.p1k_5; sideroflexin 2, *Xenopus tropicalis* NP_001011101.2; sideroflexin 3 *Xenopus tropicalis* NP_001016244.1.

The GenBank (gb), EMBL (emb) and Swissprotein (sp) accession numbers for TbMCP23 (Tb927.5.1550) alignments were as follows: TbMCP23 (gb_AAX70434.1); T.b.gambiense, *Trypanosoma brucei gambiense* XP_011773360.1; T.congolense, *Trypanosoma congolense* emb_CCC90444.1; T.cruzi, *Trypanosoma cruzi* gb_EKG06478.1; Lpanamensis, *Leishmania panamensis* gb_AIN96737.1; L.major, *Leishmania major* emb_CAJ03236.1; Bos taurus SLC25A33, *Bos taurus* XP_010821400.1; Sus scrofa SLC25A33, *Sus scrofa* XP_003127586.4; Homo sapiens PNC1, *Homo sapiens* NP_115691.1; Ailuropoda melanoleuca SLC25A33, *Ailuropoda melanoleuca* XP_015676906.1; Mus musculus SLC25A33, *Mus musculus* NP_081736.2; Rattus norvegicus SLC25A33, *Rattus norvegicus* gb_EDL81173.1; S.cerevisiae Rim2, *Saccharomyces cerevisiae* gb_EGA76005.1; S.cerevisiae Yia6p NAD+ transporter, *Saccharomyces cerevisiae* gb_EGA86348.1; Z.mays YEL006W, *Zea mays* gb_ACN33438.1; A.thaliana folate transporter, *Arabidopsis thaliana* emb_CAH65737.1; H.sapiens folate transporter, *Homo sapiens* gb_AAG37834.1; C.glabrata FAD carrier, *Candida glabrata* gb_KTA96224.1; A.nidulans folate carrier, *Aspergillus nidulans* tpe_CBF70867.1; C.immitis deoxynucleotide carrier, *Coccidioides immitis* gb_KMU78566.1; C.posadasii folate/deoxynucleotide carrier, *Coccidioides posadasii* gb_EER29041.1; M.gypseum FAD carrier, *Microsporum gypseum* XP_003171754.1; T.tonsurans folate carrier, *Trichophyton tonsurans* gb_EGD96496.1; T.rubrum folate

carrier, *Trichophyton rubrum* gb_KMQ42387.1; T.errucosum folate carrier, *Trichophyton verrucosum* gb_OAL68854.1; H.sapiens PNC1, Homo sapiens NP_115691.1; H.sapiens thiamine pyrophosphate carrier, *Homo sapiens* NP_068380.3; A.thaliana ATP-Mg/Pi transporter, *Arabidopsis thaliana* emb_CAB87921.1; H.sapiens graves disease carrier protein, *Homo sapiens* NP_001311242.1; H.sapiens calcium-binding mitochondrial carrier SCaMC-3, *Homo sapiens* NP_077008.2; H.sapiens calcium-binding mitochondrial carrier protein SCaMC-1, *Homo sapiens* NP_037518.3.

2.2 Plasmid construction

Plasmids were constructed using standard molecular biology methods such as polymerase chain reactions, restriction enzyme digestions, ligations and transformations. By cloning the specific gene into different vectors, different aims could be achieved, such as knockdown of gene expression (pHD676, pHD677, pHD678, pLEW100) or gene double knockout (pBluescript), protein expression in different species, i.e. pET28 (*E. coli*, Novagen), pCM190 (*S. cerevisiae*, Euroscarf) and pHD1484, pHD1485 (*T. b. brucei* overexpression).

2.2.1 Polymerase chain reactions (PCR) and primer design

The full sequences of our target genes were obtained from NCBI gene bank (See Appendix A1). And the forward and reverse primers (Table 2-1) were designed according to the target sequence and synthesised by MWG-Eurofins.

A standard 50 µl PCR reaction contained 5 µl of 10×Taq buffer, 5 µl of dNTP mix (2 mM each), 0.1-1 µM of forward primer and reverse primer (details see Table 2-1 below), 1-4 mM of 25 mM $MgCl_2$, 10 pg-1 µg of template DNA, 1.25 units of Taq DNA polymerase (Thermo) and ddH_2O to a total volume of 50 µl. The volume was scaled up or down accordingly to suit different purposes. All the components were assembled on ice. After mixing the reaction, PCR tubes were transferred to a PCR machine (Genetic Research, Biorad and TECHNE) with block preheated to 95 °C. Thermocycling conditions for a routine PCR were the initial denaturation at 95 °C for 5 minutes, followed by 30 to 35

cycles containing 30 seconds of denaturation at 95 ℃; 1 minute of annealing at appropriate annealing temperature (see Table 2-1); and 1 minute of primer extension at 72 ℃. Unfinished PCR reactions were then completed by 10 minutes of extension at 72 ℃, and final hold at 4 ℃. PCR templates used were a dilution of isolated plasmids using a mini-prep kit (Macherey-Nagel). When the PCR was completed, an agarose gel (Sigma) was run for examination or DNA purification.

Table 2-1 Primer pairs used in this thesis

Primer Name	No. oHU	Sequence	Annealing Temp. Used (°C)
MCP12HpaFor	12F	ggacggGTTAACaccatggcgaaagagacaaaggcgccg	68
MCP12BamRev	12R	gcttgcaGGATCCctgctttgcctgaagcttggcg	68
MCP12KO5For	92	gctaGACCTCcgcgacctttgaccgaagtaactgcc	68
MCP12KO5Rev	93	gctaACTAGTtcttcctgtcgttcgatcctcgagtag	68
MCP12KO3For	94	gcatGGATCCtgtgaataaatcactgcgtcacgttatg	68
MCP12KO3Rev	95	cagtGGGCCCtatatatgaagtcaaagtgagaaaaacagag	68
MCP12qPCRfor	461	gtgtacgtatgtccgctgatac	55
MCP12qPCRRev	462	gagtcgtacaccgccaatgc	55
NEOFor	429	atgcggcggctggatacggttg	55
NEORev	105	tcagaagaactcgtcaagaaggcgatagaag	55
NEORev2	430	cgagcccctgatgctcttcgtccagatcatcctgatc	55
BSDFor	82	atggccaagcctttgtctcaagaagaatccac	55
BSDRev	83	ttagccctcccacacataaccagagg	55
MCP17AS5B	291	cGGATCCccatt tgatgttatcaagcagcggatg	68
MCP17AS3XH	293	cAAGCTTtccCTCGAGcattgacagggcaccagcaggagcg	68
MCP17S5H	292	gAAGCTTccaccccatttgatgttatcaagcagc	68
MCP17S3X	294	ggCTCGAGtgactaagacatagcgcaccgcatcgg	68
MCP17KO3ForB	337	gcatGGATCCccgtgttcttgtttcaggtgtgaacc	69
MCP17KO3RevA	338	ctatGGGCCCgtcaaacacattactggagcgg	59
MCP17KO5For Sac	339	gctaGAGCTCcgtgtcgtgaggtggagaggtgatg	68
MCP17KO5Rev Spe	340	gctaACTAGTcacacatcaccgcagccaagcaaaacaacg	59
MCP17NestedFor	347	cacagtgtctataacggtctctgc	67
MCP17HindFor	17F	ggacggAAGCTTaccatggtttccgagggcacttccgctg	68
MCP17BamRev	314	gcttgcaGGATCCccgttcctccatgaacttcttggc	68
MCP17YexFor Bam	349	gaGGATCCatggtttccgagggcacttccgctg	68
MCP17YexStop Hin	350	cgAAGCTTttaccgttcctccatgaacttcttggc	68
MCP17Upstream	427	gatgatcgtatcggctcttgtcgcaatg	55

For			
MCP17DownstreamRev	431	aaggagtgggaacaggggcaaatccac	55
MCP17RevMyc1	375	tgagatgagtttttgttcccgttcctccatgaactt	55
Myc2NotRev	399	cgGCGGCCGCttacagatcctcttctgagatgagtttttgttc	55
Myc2PstRev	400	cgCTGCAGttacagatcctcttctgagatgagtttttgttc	55
MCP17REVStopNot	397	cgGCGGCCGCttaccgttcctccatgaacttcttggc	68
MCP17qRTPCRFor	434	gtggcttctattgtctcgtc	55
MCP17qRTPCRRev	435	cacataactctcgccgtaa	55
MRS3ForBam	377	gaGGATCCatggtagaaaactcgtcgagtaata	61
MRS3RevMyc1	378	tgagatgagtttttgttcatacgtcattaggaaat	55
MRS3RevStoHind	379	cgAAGCTTctaatacgtcattaggaaatgtt	55
MRS3RevStoPst	423	cgCTGCAGctaatacgtcattaggaaatgttttgcacattc	55
SFNXAS5B	306	cgatgtcGGATCCatctaaggcgtacgtcggcgctgttg	68
SFNXAS3A	341	caGGGCCCcgagcccgaacagctgcacagcg	68
SFNXAS3XH	308	atAAGCTTcagCTCGAGcccgaacagctgcacagcggg	68
SFNXS5H	305	cgatgtcggAAGCTTctaaggcgtacgtcgccgctggttg	68
SFNXS3A	342	ctGGGCCCagcggcaacaccatggaaataag	63
SFNXS3X	307	catcCTCGAGagcggcaacaccatggaaataaggttc	68
SFNXNestedFor	348	gtgaattatgcaaatcgctcctc	61
SFNXExpBamFor	62	ggacGGATCCatgcttccatgtccgtcgttctc	68
SFNXExpHinRev	71	gcgcAAGCTTtcacaaacccttgtaatacgtgaata	61
SFNXqPCRFor	476	ttacctttcgtggcggtatc	55
SFNXqPCRRev	477	acctcaccatcctcgtcaac	55
TbBetaTubFor	321	cgactctgtgctcgatgtgt	54
TbBetaTubRev	322	ctgcagcttgcatcatgttt	54
MCP23AS5B	298	accagaaGGATCCacctgccattgcggcttgtg	68
MCP23ASRevApa	323	agGGGCCCgtttccctgtcacgatagctgacg	68
MCP23S5H	297	accagAAGCTTcaacctgccattgcggcttgtg	68
MCP23SRevApa	324	catGGGCCCgttgtaaggataagagacggtg	68
MCP23BamFor	196	ggacggGGATCCaccatggcactcccgacatcgcatgtg	68
MCP23HindRev	195	gcgAAGCTTttatgcgggagcgcaagaaacaacgg	68
MCP23qPCRFor	474	ccaatattgtgggtcggttc	55
MCP23qPCRRev	475	ctaccgcgacagatgtcaga	55
T7 Term	*	ctagttattgctcagcggt	-
T7-pET-Mod	*	cccgcgaaattaatacgactcac	-
TERTqPCRFor	464	gagcgtgtgacttccgaagg	55
TERTqPCRRev	465	aggaactgtcacggagtttgc	55
TUBqPCRFor	436	ctttctccatcatcccatc	55

TUBqPCRrev	437	gttggtgttgtcagtttcag	55
IDHGly qPCRFor	468	gcgagcccattatatgcagt	55
IDHGly qPCRRev	469	aacgcatctcaaatgttccc	55
IDHMito qPCRFor	470	ttgtttcgaatacgccatca	55
IDHMito qPCRRev	471	gtcgctcaaactgttcacga	55
ACOqPCRFor	472	attgcagcaggattattggc	55
ACOqPCRRev	473	ctttgcagcccagagttttc	55

For cloning purposes, restriction enzyme sites were included to enable site-directed cloning. No. oHU was the abbreviation of oligo numbers from the University of Hull, which belonged to the number series used in Dr Voncken's lab. Restriction enzyme sites were indicated with capital letters. Primers labelled with * were commercial primers available from Eurofins for sequencing purposes. Sizes of the amplified fragments were indicated individually in the figure legends of result chapters.

2.3 Restriction enzyme digestion, ligation and transformation of *E. coli*

To make restriction maps, or to create sticky ends for ligation, restriction enzymes (New England Biolabs) and FastDigest enzymes (Thermofisher) were used in digestion. To minimise the self-ligation of the vector during the ligation process, Calf Intestinal Alkaline Phosphatase (CIAP) (Invitrogen) treatment was performed according to manufacturer's instructions when necessary. Afterwards, the digested vector or insert was purified by gel extraction and PCR clean-up kit (Macherey-Nagel).

T4 ligase (Thermofisher) was used for sticky ends ligation, while PCR products were inserted directly into commercial vectors such as pGEM-T- easy (Promega). The ligation product was then transformed to chemical-treated competent cells DH-5α (Thermofisher). A tube of NEB 5-alpha Competent *E. coli* cells (No. C2987I) were put on ice. They were gently mixed and carefully pipetted into a transformation tube on ice.

1-5 µl of plasmid DNA or ligation product of 1 pg-100 ng DNA was added to the competent cell and carefully flicked 4-5 times to mix cells and DNA. The mixture was then incubated on ice for 30 minutes, followed by 90 seconds of heat shock at exactly 42°C. The heat treated mixture was left on ice for 2 minutes, then 450 µl of Lysogeny

broth medium (containing 10 g/L tryptone, 5 g/L yeast extract, and 5 g/L NaCl) (Bertani 2004) was added. After incubated at 37 °C for 30 minutes, the mixture was spread on LB plates with selection antibiotics (concentrations see Table 2-2) and incubated overnight at 37°C.

Table 2-2 Antibiotics concentrations used in this study

Commonly Used Antibiotics	Recommended Concentration (μg/mL)
Ampicillin	100
Chloramphenicol	25
Kanamycin	50
Spectinomycin	50
Tetracycline	10

2.4 Over-expression of a specific gene

The open reading frame of the gene of interest was amplified from *T.brucei* Lister 427 genomic DNA using forward and reverse primers. TbMCP12 open reading frame (ORF) was amplified with oHU 12F and oHU 12R; TbMCP17 ORF with oHU 17F and oHU 17 R; and TbSFNX with oHU 16F and 16R (see Table 2-1 for details). The generated ORF was inserted into pHD676, pHD677, pHD678, pHD1484 or pHD1485 (Appendix A2-1 to A2-5) for the addition of myc tag.

2.5 Down-regulation of the expression of a specific gene

To study the function of target genes, the effects caused by the knocked down of the gene expression were examined. Two methods were used in this study to down-regulate the expression of a specific gene: (i) RNA interference (RNAi) to repress expression, (ii) completely knockout the gene.

2.5.1 Expression knockdown

Gene knockdown was achieved by RNA interference (RNAi). The antisense and sense of the target gene were PCR amplified using the primers listed in Table 2-1 with restriction enzyme sites added at both ends, then cloned into transfection vectors pHD676, pHD677,

pHD678, pLEW100 and pLEW100v5 (Appendix A2-1, A2-2, A2-3, A2-6 and A2-7) in reversed direction.

2.5.2 Conventional double knockout

RNAi cell lines are prone to lose control of tetracycline induction or lose the down-regulation effect. In order to get more stable gene knockdown effect, conventional double knockout of *TbMCP12, TbMCP17* and *TbSFNX* were also generated using the target gene replacement method (Krieger et al. 2000; Voncken et al. 2003) to replace two endogenous copies by antibiotic resistant cassettes. The conventional double knockout constructs were derived from vector pBluScript KS containing neomycin (NEO) or blasticidin (BSD) cassettes (Appendix A2-8), by adding the 5' and 3' UTR of the target gene to the 5' and 3' of the resistant genes, separately. 5' UTR was inserted via restriction sites Sac I and Spe I, while 3' UTR was inserted using restriction sites BamH I and Apa I (Figure 2-1). Related gene sequences were attached in Appendix A1.

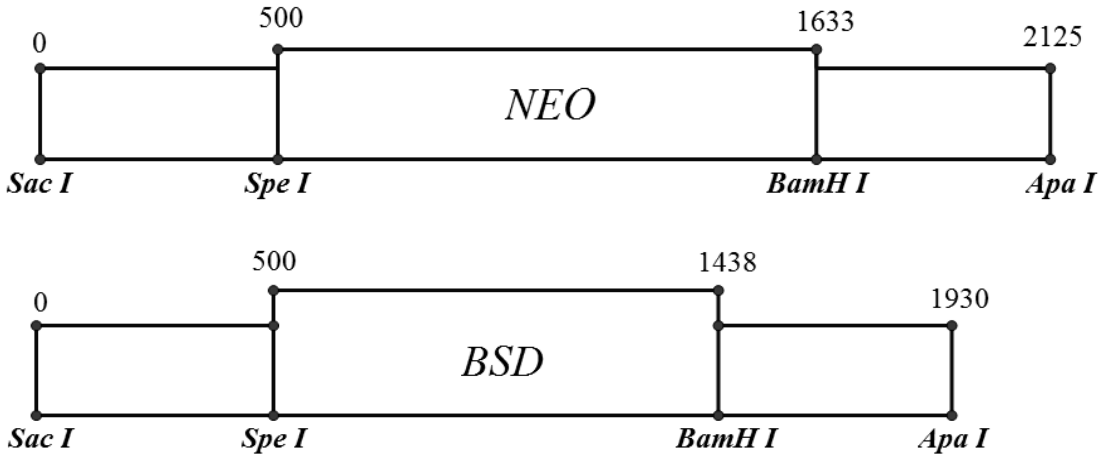

Figure 2-1 NEO and BSD cassettes with restriction enzyme sites for cloning UTR

Numbers show the size of DNA fragments, separated by the restriction enzyme sites for cloning.

2.6 *Trypanosoma brucei* cell culture and growth effect experiments

2.6.1 *Trypanosoma brucei* culture method

Procyclic form EATRO1125T7T was cultured in SDM-79 medium (Appendix A3-1) and PCF449 in MEM-PROS medium (Appendix A3-2), both supplemented with 10% heat-inactivated foetal bovine serum (Lonza), 2.5 mg/ml of heme (in 100 mM NaOH) and 1% of Penicillin/Streptomycin solution containing 10,000 units of penicillin and 10 mg of streptomycin per ml (Sigma). MEM-PROS medium was further supplemented with 5 ml of 0.5 M proline (Sigma). Bloodstream form cell line BSF449 was cultured in HMI-9 medium (Appendix A3-3) supplemented with 10% serum, 1% of Penicillin/Streptomycin solution, 1% 150 mM L-cycteine·HCl·H_2O and 1% 20 mM β-mercapto·ethanol. Different antibiotics were added to maintain different plasmids (Table 2-2). PCF cells were cultured in 27 °C incubator (Scientific Laboratory Supplies and BIDHIT), while BSF ones were cultured under 37 °C with 5.0% of the CO_2 incubator (NUFAIRE). Cells were normally cultured (split) every two days. Antibiotics (Invivogen) were added if applicable with different concentrations: hygromycin of 25 μg/ml, neomycin of 10 μg/ml, phleomycin of 5 μg/ml and blasticidin of 10 μg/ml. Flasks were from Iwaki and pipettes from Sarstedt.

2.6.2 Growth effect experiment

Cell samples of *T. brucei* from different cell lines (overexpression or knockout) were taken from the stock culture during the late exponential growth phase and inoculated into 25 cm^2 culture flasks containing 5 ml of medium supplemented with corresponding antibiotics. Bloodstream cultures were initiated at 2×10^5 cells/ml, while procyclic started at 5×10^5 cells/ml, and diluted to the same concentration daily. Experiments were proceeded in triplicates for more accurate results. The cell density of each flask was measured every 24 hours by haemocytometer (Hawksley) for 3 days or longer. The data collected were then analysed with Microsoft® Excel. The significance between different groups was calculated with SPSS, a software package used for statistical analysis. In some cases, special components such as iron chelator deferoxamine (Sigma) applied at various

concentrations from 10 μM to 100 μM and hydrogen peroxide from 10 μM to 100 μM. Glucose and heme double depletion was achieved by serum dialysis (Thermo). Single compound depletion condition was achieved by adding back the same amount of heme (11.5 μM) as standard condition or glucose (5 mM) to the dialysed serum.

2.7 *Trypanosoma brucei* transfection

Before transfection, the plasmid was linearized by Not I digestion. Then, DNA was purified by precipitation. 2×10^7 cells were centrifuged down at 1700 rpm for 10 minutes. The supernatant of culture was used as the conditional medium (the recovery media which contains 5 ml of conditional medium, 5 ml of fresh medium, 5 mM of glucose, and maintenance antibiotics). After being spun down, the cells were washed by approximately the same amount of filter sterilised ZPFM or Cytomix (both made in the lab, see Appendix A3-4 for protocol), and resuspended in 500 μl of ZPFM/ Cytomix. 20 μl of DNA and 500 μl of the cell were transferred into 4 mm electroporation cuvette (Molecular BioProducts) and mixed briefly. Subsequently, electroporation was performed using electroporator (Biorad). The settings were described as follows. Capacitance: 25 μFD, resistance: 400 OHMS, and voltage: 1.7 kV. Then the mixture was transferred into the culture media prepared before and incubated overnight as normal culture condition.

On the second day of transfection, the selective antibiotic was added and serial dilution was performed to select potential single clones. In the culture flask, selection antibiotic was added, and fresh medium supplemented with selection antibiotics was prepared. 24-well plates (Nunclon) were used for serial dilution. In the first row of each column, 1 ml of transfected cells was added, and 0.5 ml of fresh medium was added to the rest 3 rows. Then, in each column, 0.5 ml of the cells from the first row was added to the second row, and after mixing up, 0.5 ml of cells was taken away from the second row and added to the third row. After mixing, 0.5 ml of cells from the third row was added to the last row of the plate.

After serial dilution, the 24-well plates were incubated for 7 to 10 days and checked every two or three days. Wells containing cells survived from antibiotics after one week were

consided as positive wells, in which cells were taken away and grown in normal flasks for further study.

2.8 Subcellular localisation by Immunofluorescence Microscopy

Coverslips were treated with 0.1 mg/ml of poly-Lysine (SLS Thermo) by adding 0.5 ml of poly-Lysine to each field and incubating them for 30 minutes without shaking. After 3 washes with an excess amount of water, slides were air-dried. An aliquot of culture containing approximately 1×10^7 cells was collected into an Eppendorf tube. For BSF, MitoTracker Red CMXRos (Molecular Probes) was added to a final concentration of 0.05 μM, and then cells were incubated in an open tube at 37 °C in a gassed incubator (5% CO_2) for 10 minutes. For PCF, MitoTracker Red CMXRos was added to a final concentration of 0.5 μM and incubate in a tightly capped tube at 28 °C for 10 minutes. Afterwards, cells were spun down and washed with 10 ml of the appropriate pre-warmed culture medium to remove the residual dye, followed by 20 minutes incubation with 5 ml pre-warmed culture medium (without dye) in order to incorporate a remaining dye in the cytosol to mitochondria. Then cells were pelleted down and washed with PBS (tablets from Sigma), followed by the addition of fresh made 4% (w/v) paraformaldehyde (power from Sigma). After inverting the tube a few times, cells were incubated for exactly 18 minutes without shaking. After fixation with paraformaldehyde, cells were washed three times with PBS to remove paraformaldehyde as much as possible. Then cells were resuspended with PBS and settled onto treated coverslips using a 24-well plate overnight at 4 ^oC. Next day, the supernatant was removed and 0.2% (w/v) Triton X-100 was added and incubated for 20 minutes at room temperature to permeabilize the cell. After 3 washes, 0.5% (w/v) gelatin (PBS/gelatin) was added to each coverslip, and the mixture was incubated for 20 minutes. Afterwards, the primary antibody was added to the coverslips at a dilution of 1:500 for myc antibody, and incubated for 60 minutes on a shaker followed by 2 washes. Then secondary antibody was added (Alexa Fluo488 anti-mouse a 1/500 dilution in PBS/gelatin) for 60-minute incubation in the dark. After delivering one drop of mounting medium with DAPI (Thermo) to each slide, a coverslip containing cells was placed on top and fixed with nail polish. Then the slides were stored in the dark at 4 °C and analysed using a laser scanning confocal microscope (Zeiss) within 2-3 days.

2.9 SDS-PAGE gel and Western Blot

SDS-PAGE was performed following the Laemmli method (Laemmli 1970) in this study. Briefly, samples were prepared in Laemmli sample buffer (0.0625 M Tris-HCl pH 6.8, 0.1% (v/v) β-mercaptoethanol, 0.1% (w/v) EDTA, 0.1% (v/v) glycerol) and heated at 95°C for 5 minutes. 12% denatured polyacrylamide gels (0.375 M Tris-HCl pH 8.0, 0.1% (w/v) SDS, 0.1% (w/v) Ammonium Persulfate (APS) for the Running gel; and 0.125 M Tris-HCl pH 6.8, 0.1% (w/v) SDS, 0.1% (w/v) APS, 4% polyacrylamide for the Stacking gel) were used to run samples. Gels were run at 200 V until the front reached the end of the gel. For Western Blotting (WB), samples were separated by SDS-PAGE and transferred to nitrocellulose (GE Health Care Life Sciences) or PVDF (GE Health Care Life Sciences) membranes at 100 V for 50 minutes in Towbin buffer (48 mM Tris, 39 mM Glycine, 20% (v/v) methanol, pH 8.3). Membranes were blocked with TBST (5% (w/v) skimmed milk in Tris-buffered saline (TBS) buffer containing 0.1% Tween-20) in agitation at room temperature for 1 hour. Subsequently, membranes were incubated with primary antibody (see Table 2-3) in TBST buffer containing 5% milk, for 1 hour at room temperature or 4 ºC overnight for better signals. Membranes were further washed 3 times with excess TBST buffer, 10 minutes each wash. Secondary antibody incubation and washes were performed in similar condition to the procedure of primary antibody. Protein detection was performed using an ECL detection kit (Amersham, GE Healthcare) for further film exposure. Chemicals used for SDS-PAGE and WB were from Sigma.

Table 2-3 Antibodies used for the detection of proteins in WB and IFA experiments

Antibody	Manufacturer	Type	Raised in	Target	Dilution	Technique
Anti-c-myc	Roche	Monoclonal (clone 9E10)	Mouse	c-myc-tag sequence	1:2000	WB, IFA
Anti-rabbit IgG HRP	Abcam	Polyclonal	Goat	Rabbit IgG	1:3000	WB
Anti-mouse IgG HRP	Abcam	Polyclonal	Goat	Mouse IgG	1:2000	WB
Alexa Fluo488 anti mouse	Thermofisher	Polyclonal	Goat	Mouse IgG	1:500	IFA

Anti-His	Santa Cruz	monoclonal	Mouse	His-tagged	1:500	WB
Anti-Xpress	Invitrogen	Monoclonal	Mouse	Xpress epitope	1:5000	WB
Anti-TbMCP12	EZBiolab (USA)	Polyclonal		MCP12 N-term	1:500	WB
Anti-TbMCP17	Thermofisher	Polyclonal	Rabbit	MCP17-His	1:250	WB
Anti-TbSFNX	Thermofisher	Polyclonal	Rabbit	SFNX-His	1:250	WB
Anti-aldolase	C. Clayton's lab	Polyclonal	Rabbit	Aldolase	1:1000	WB
Anti-tubulin	Abcam	Monoclonal	Rat	Tubulin full length	1:5000	WB
Anti-Rat	Abcam	Polyclonal	Goat	Rat IgG	1:2000	WB

In order to obtain optimal SDS-PAGE and WB results for TbMCP17 antisera, approaches below were tested: (i) protein sample preparations: sample loading buffer consisting of either β-mercaptoethanol or Dithiothreitol (DTT) was tested. Various temperature & incubation time combinations were tried at 95 ºC for 5 minutes, 70 ºC for 10 minutes or 37 ºC for 10 minutes. Brief sonication was included to break down genomic DNA. (ii) PVDF and nitrocellulose membrane were tested. (iii) a number of blocking reagents were tested with 5% milk, 5% fish gelatin (Sigma), SuperBlock (Thermo) or 5% BSA (Sigma). (iv) crude serum (Thermo) was purified either with purified protein or with Pierce Protein A/G Magnetic Beads (Thermo). (v) the incubation time of blocking was increased to 6 hours at RT for a clearer background.

2.10 Heterologous protein expression, purification in *E. coli* and antibody generation

An adequate amount of protein (3mg) was heterologously expressed, purified and quantified for antibody generation.

2.10.1 Expression vector

His-tagged TbMCP17 and TbSFNX were expressed in *E.coli* using pET28a vector (Novagen, Appendix A2-9). The heterologously expressed protein was further purified for antibody production. *TbMCP17* ORF or *TbSFNX* ORF was inserted into pET28 using restriction sites: BamH I on 5' and Hind III on 3'. The construct was named as pET28+TbMCP17 (Appendix A2-10) or pET28+TbSFNX (Appendix A2-11). Primers used for cloning were MCP17YexForBam and MCP17YexStopHin. *TbSFNX* ORF was PCR amplified with SFNXExpBamFor and SFNXExpHinRev (see Table 2-1 for more details).

2.10.2 IPTG induction

A specific *E. coli* strain for protein expression, Lemo21 (DE3) (New England Biolabs) was used for inducible expression. The freshly transfected cells were inoculated into LB media with 50 µg/ml kanamycin and 30 µg/ml chloramphenicol, and grown overnight as a preculture. This preculture was used with 1/50 dilution to initiate protein expression culture which was grown with constant shaking at 37 °C in the same media. Once the culture's O.D.600 reached 0.4-0.8, it was induced to express protein with 0.4 mM IPTG. L-rhamnose from 100 to 2000 µM was added when the control of the induction level was necessary. Induction was allowed to last for 4 hours.

2.10.3 Isolation of inclusion bodies (IB)

After 4 hours' induction of the protein expression, the induced culture was harvested by centrifugation at 5000 rpm (4000 g) for 10-20 minutes at 4 °C, then resuspended in the native resuspension buffer (50 mM Na-phosphate pH8.0, 300 mM NaCl, 0.01%Tween-20) supplemented with Protease inhibitor Cocktail without EDTA (Sigma, one tablet in 100 ml buffer), 0.2 mg/ml lysozyme and 5 unit/µl DNase. 5 ml of resuspension buffer was used for each 1 g wet weight of cell pellet. Then the pellet was incubated on ice for 30 minutes. Furthermore, the cell lysate was passed through the French press (University of Hull) twice per portion of protein until the solution turned clear. Inclusion bodies were

pelleted down at 13000 g for 30 minutes. Supernatants and pellets were collected to be SDS-PAGE samples. Inclusion bodies were resuspended in resuspension buffer containing 2% sarkosyl (Sigma).

2.10.4 IB washing

Inclusion bodies were washed with different detergents and denaturants to reduce contaminant levels during preparation steps. 0 M / 1 M/ 2 M/ 4 M/ 5 M / 8 M of urea and 0.2% / 0.5% / 1% of sarkosyl were added to resuspension buffer to form different IB washing buffers. Inclusion body aliquots were resuspended with different IB washing buffers and mixed gently for 5 minutes, followed by 13000 rpm centrifugation for 20 minutes at 4 °C to separate soluble proteins from IB proteins. The wash was repeated twice. SDS-PAGE and WB samples were collected in between for analysis.

2.10.5 Protein purification using Ni-NTA agarose

1 ml of Ni-NTA agarose (Qiagen) was added to 20 ml of solubilised protein, and the mixture was stirred for 60 minutes at room temperature or until the solution had become translucent at 4 °C for protein binding to Ni-NTA column. Afterwards, the supernatant containing unbound proteins or contaminants was removed by 500 g centrifugation for 5 minutes. Then the Ni-NTA agarose was washed twice to remove potential contaminants, using wash buffer containing 8 mM Na_2HPO_4, 286 mM NaCl, 1.4 mM KH_2PO_4, 2.6 mM KCl and 0.1% sarkosyl (w/v) at pH 7.4. Finally, protein was eluted from NiNTA with elusion buffer containing 8 mM Na_2HPO_4, 286 mM NaCl, 1.4 mM KH_2PO_4, 2.6 mM KCl, 500 mM imidazole and 0.1% Sarkosyl (w/v) at pH 7.4. 3 mg of purified protein was loaded onto a prep-gel which was dyed with Coomassie Brilliant Blue R-250 (Sigma), and then the prep-gel was cut out and sent to ThermoFisher Scientific for antibody generation. Antisera was diluted 1:250 in 5% fish gelatin (sigma) so as to be used as a primary antibody for WB.

2.11 Functional complementation experiment using yeast

2.11.1 Yeast strains and media

S. cerevisiae strains used in this study were BY4741 (*Mat a his3Δ1 leu2Δ0 met15Δ0 ura3Δ0*); YLR348C (ΔDIC1; *MATa his3Δ1 leu2Δ0 met15Δ0 ura3Δ0*); DBY747 (ATCC no. 20465; *MATa leu2-3,112 his3-1 trp1-289 ura3-52 trp1-289* [rho^+ mit^+]) (Wiesenberger et al. 1992); GW403 (mrs3/4Δ; *MATa his3-Δ1 leu2-3 leu2-112 ura3-52 trp1-289 mrs3Δ*::*loxP mrs4Δ*::*loxP;* Gerlinde Wiesenberger 2009).

Yeast strains were maintained on standard YPD medium (1% yeast extract, 2% peptone, 2% glucose and 2% agar). In order to test cell growth under different carbon sources, glucose in YPD was replaced by 3% glycerol (known as YPG). Synthetic complete (SC) medium without uracil (0.67% of yeast nitrogen base (w/o amino acids), 1.4% of drop-out medium supplements (w/o histidine, leucine, tryptophan and uracil), supplemented with 60 mg/L of leucine, 20 mg/L of tryptophan, 20 mg/L of histidine, 2% of agar and 2% of dextrose) was applied to clone-selection after transfection. To create iron depriving condition, 100 µM of iron chelator bathophenanthrolinedisulfonic acid (BPS, Sigma) was added to SC medium. All the powers were from Sigma.

Plasmids containing target genes were transformed into the functional corresponding knockout strains (ΔMRS3, ΔDIC), using lithium acetate/single-stranded carrier DNA method described by Gietz and Woods (Daniel Gietz & Woods 2002). Obtained yeast clones were maintained on synthetic complete dextrose (glucose) media without uracil with the presence of tetracycline. Heterologous protein expression in yeast was induced by tetracycline removal.

2.11.2 Growth experiment

Using aseptic technique, a loopful of yeast cells were inoculated to the starter culture of medium specified and grown in a 28–30 °C shaking water-bath overnight. Next day, a small volume of the starter culture was removed into a cuvette, and the absorbance of the

cells at 600 nm (OD600) was measured. Then appropriate volumes of the starter culture were inoculated to the main culture (20 ml of appropriate medium) to reach OD600 0.1 or 0.2 according to different media in triplicate for each experimental group. OD600 of cultures were measured every 3 to 4 hours until the cells grew up to stationary phase (OD600 values over 1.5). Data collected (OD600 values every 4 hours of different cell lines) were analysed using Excel2010. For plate experiment (solid medium), the concentrations of four dots on the plate were OD 1, 0.1, 0.01 and 0.001, respectively. Duplicates were applied to the plate experiments.

2.12 Semi-quantitive PCR

2.12.1 mRNA isolation

5×10^7 cells per sample were collected by centrifugation, and lysed in 1 ml of RNAzol (Sigma). At this time point, cells could be stored at 4 °C for overnight, -20 °C for over a month, -80 °C for longer storage. Then, 0.4 ml of RNase-free water was added and the mixture was shaken vigorously for 15 seconds. After standing at room temperature for 10 minutes, the supernatant containing RNA was separated by 12000 g for 15 minutes and transferred into an RNase-free 2.0 ml Eppendorf tube. Then, 0.4 ml of 75% ethanol (v/v) was added to precipitate the mRNA. Centrifugation at 12000 g for 8 minutes was performed, and the white pellet sat on the side and bottom of the tube was the mRNA. The RNA pellet was washed twice with 0.5 ml 75% ethanol and centrifuged at 8000 g for 3 minutes at room temperature. The alcohol solution was removed completely with a tip. Afterwards, 30 µl RNase-free water was added to solubilize RNA followed by vortexing for 2-5 minutes. Measurement of RNA concentration was done by spectrophotometer (Eppendorf).

2.12.2 1st Strand cDNA synthesis

Before cDNA synthesis, genomic DNA (gDNA) was removed by DNase I (Thermo) treatment. 2 µg RNA was treated with 2 µl of DNase I in 2 µl of 10× reaction buffer with $MgCl_2$, and adequate amount of RNase-free water was added to the total volume of 18 µl.

The DNase treatment was incubated at 37 °C for 30 minutes. Then, the reaction was terminated by adding 2 µl 50 mM EDTA and incubating at 65 °C for 10 minutes. Afterwards, the same amount of $MgCl_2$ was added to inactivate EDTA.

20 µl of 1st strand cDNA synthesis system (10 µl of template RNA from gDNA removal, 1 µg, 1 µl of random primers, 4 µl of 5× reaction buffer, 1 µl of RiboLock RNase Inhibitor, 2 µl of 10 mM dNTP, and 2 µl of M-MuLV Reverse transcriptase) was set up. The chemicals were from 1st strand cDNA synthesis kit (Thermo). The synthesis was performed at 25 °C for 5 minutes, followed by 37 °C for 60 minutes. Then the reaction was terminated by incubation at 70 °C for 5 minutes.

2.12.3 Semi-quantitive PCR

1 µl of cDNA reaction mix was used for per 25 µl system of PCR. Nested primers were used for mRNA existence checking. Those primers were designed outside the RNAi sequence region (see Table 2-1), which avoided the amplification of RNAi sequence and reduce error. The procedure for semi-quantitive PCR was the same as that for normal PCR with reduced cycle number.

2.12.4 One-step real time reverse transcript PCR

In order to acquire a more accurate result of mRNA level, one-step real time qPCR was applied to mRNA samples using QuantiTect SYBR Green RT-PCR kit (QIAGEN). The same RNA isolation and genomic DNA removal steps were preformed followed by qRT-PCR using 0.5 µg RNA per 12.5 µl reaction. Special primers were designed to suit 55 ºC and the resulting PCR product of 150 bp (Table 2-1). C_T values of experimental samples (in triplicates) were compared with wild type C_T after normalising C_T from house-keeping genes (Tubulin or TERT), and the expression fold change was calculated in Table 2-4.

Table 2-4 Calculation of the expression fold change in the target gene

	Exp	Ctrl	ΔCt(Exp)	ΔCt(Ctrl)	ΔΔCt	Expression fold change
WT	E1	C1				1

Sam	E2	C2	E2-E1	C2-C1	(ΔCTExp-ΔCTCont)	2^(-(ΔΔCt)

Exp: experimental; Ctrl: control; Sam: sample; E1&E2: average of experimental group C_T values; C1&C2: average of control group C_T values.

2.13 Aconitase enzyme activity and NADP$^+$/NADPH ratio measurement

Aconitase activity was measured continuously with a spectrophotometer thermostated at 25 °C according to the UV method (Henson & Cleland 1967). 800 µl of the reaction buffer 50 mM Na_2HPO_4/NaH_2PO_4 (pH 7.4) was supplemented with either isolated mitochondrial fraction or supernatant from the digitonin fractionation method (Schneider et al. 2007). The reaction was started by the addition of 150 µl of 50 mM DL-isocitrate as a substrate, and the increase in absorbance at 240 nm was followed for 6 minutes. The specific activity was defined as the formation of nmol product $min^{-1} \cdot mg^{-1}$ protein using an absorption coefficient of 3.4 $mM^{-1} \cdot cm^{-1}$. Protein concentrations were determined using the Pierce BCA protein assay kit (Thermo) and bovine serum albumin (Thermo) as standard. NADP$^+$/NADPH ratios were determined in trypanosome cell lysate at 450 nm, using the NADP$^+$/NADPH Assay Kit (Abcam ab65349) according to the manufacturer's protocol. The enzymes in the system specifically recognise NADP$^+$/NADPH in an enzyme cycling reaction which does not recognise NAD$^+$/NADH.

2.14 Determination of substrate consumption and end product formation

Cells were cultured for 72 hours, and tetracycline was added every 24 hours to maintain continuous expression. The cell density was determined every 24 hours. A 3 mL culture sample was collected for western blot analysis, or for the determination of substrate (proline, glucose) consumption and of metabolic end product (acetate, succinate) formation. Prior to the assays, samples were de-proteinated by mixing 1 mL of culture sample (containing both cells and culture medium) with 100 µl 35% (v/v) perchloric acid. After incubation on ice for 10 minutes, the samples were neutralised by the addition of 134 µl neutralisation solution (5 M KOH, 0.2 M MOPS). The formed protein-precipitate

was removed by centrifugation at 11,000 g for 10 minutes, and the protein-free supernatant was collected for analysis. Glucose was determined by using a glucose oxidase-based method (Bergmeyer & Gawehn 1974): 100 µl precipitated sample and 100 µl glucose standard (91 $mg \cdot L^{-1}$) were mixed with 2.5 mL glucose detection reagent (100 mM phosphate buffer pH 7.0, 1 $mg \cdot mL^{-1}$ horseradish peroxidase, 10 units mL^{-1} glucose oxidase, 1 $mg \cdot mL^{-1}$ 2,2'-azino-bis 3-ethylbenzthiazoline-6-sulphonic acid). The absorbance at 660 nm was determined after 30 minutes incubation at room temperature in the dark. The glucose concentration of the sample was calculated using a corresponding glucose calibration curve. Proline was determined using a standard method (Shabnam et al. 2015). For the proline assay, the following solutions were mixed: 5 µl cell culture sample, 95 µl dH_2O, 100 µl sulfosalicylic acid (3% v/v), 200 µl Ninhydrin reagent (125 mg Ninhydrin, 3 mL 99% acetic acid, 2 mL 6 M phosphoric acid) and 200 µl glacial acetic acid. The reaction was incubated for 1 hour at 95 °C. After 10 minutes incubation on ice, 400 µl toluene was added and the reaction mixture was vortexed vigorously. 300 µl of reaction mixture was diluted with 700 µl toluene and the absorbance read at 520 nm. The proline concentration of the sample was calculated using a corresponding proline calibration curve. The concentrations of the metabolic end products acetate and succinate were measured according to the manufacturer's protocol using acetate and succinate determination kits (Megazyme).

2.15 Mitochondrial ATP production assay

To start with, trypanosomes were prepared and permeabilised. Firstly, Trypanosomes (1×10^8 cells) were collected by centrifugation at 1500 g for 10 minutes (2000 rpm/7 minutes). Secondly, cells were washed once with an equal volume of SoTE-buffer (20 mM Tris-HCl pH 7.5, 2 mM EDTA, 0.6 M Sorbitol), and resuspended in 0.5 mL of the same buffer. After that, cells were transferred to 1.5 ml Eppendorf tube. Thirdly, plasma membrane was permeabilized by adding 0.5 ml of SoTE-buffer with digitonin (0.016%) (pre-warmed to room temperature) to the cell resuspension and inverting once. The mitochondrial fraction was incubated for exactly 5 minutes on ice, (move from containment to lab) followed by immediate centrifugation for 3 minutes at 8000 g (7000 rpm/3 minutes) and 4 °C. Then, the mitochondrial enriched fraction was gathered. After centrifugation, the supernatant was removed and represented in 0.5 mL of assay buffer.

Afterwards, mitochondrial ATP production was measured. Each mitochondrial ATP production assay consisted of 25 µl mitochondria-enriched fraction and 25 µl ATP assay buffer, containing 20 µmol ADP and 2 mM of the different substrates (i.e. succinate, α-ketoglutarate). Negative controls included three groups: (i) CATR group (Carboxyatractyloside was a highly selective inhibitor of cytosolic side-specific mitochondrial ADP/ATP carrier (Henderson & Lardy 1970; Vignais et al. 1973), Sigma, the final concentration of 5.2 µM), which was prepared by the addition of CATR to the mitochondria-enriched fraction and incubation for 5 minutes at 30°C prior to the addition of the different substrates; (ii) ADP group with ADP and without substrate (for verification of non-substrate-producing ATP from the impurity of ADP or from the reaction system); (iii) NC group without ADP or substrate for monitoring background ATP. The mitochondrial ATP-production reaction was initiated by the addition of substrate. After incubation for 30 minutes at 30 °C, the mitochondrial ATP-production was terminated by the addition of 10 µl TE (10 mM Tris-HCl, 1 mM disodium EDTA, pH 8.0) + 0.2% Triton-X100.

ATP concentration was measured using the Luminescent Cell Viability Assay (CellTiter-Glo) by the addition of 60 µl luminescent reagent using fluoskan (Thermo). Meanwhile, ATP standard curve ranging from 0 to 1000 nM was prepared using ATP assay buffer.

2.16 Statistical analysis

To examine the significant differences between the experimental groups, T-tests were conducted with the collected data using SPSS. The calculated probability p-value smaller than 0.05 was considered to be statistically significant with over 95% of confidence presented with *, while p-value smaller than 0.01 was indicated with **, and $p < 0.001$ (statistically highly significant) was denoted with ***.

Chapter 3 Functional characterisation of TbMCP12

3.1 Introduction

The primary study on TbMCP12 has been conducted by Colasante (Colasante, unpublished data) and summaried as follow. The protein sequence of TbMCP12 was analysed by phylogenetic reconstitution, showing that TbMCP12 and sequences from other kinetoplastids formed a separate clade of carriers which linked closely to di/tricarboxylate carriers (DTCs) from plants and fungi and oxoglutarate carriers (OGCs) from a whole range of organisms. This was supported by the highly homologous from protein sequence alignment of TbMCP12 with DTCs and OGCs. The alignment results also confirmed that TbMCP12 belongs to the mitochondrial carrier family (MCF) by exhibiting all conserved sequence and structure features of MCF. The expression level of TbMCP12 presented a significantly different pattern with PCF 29-fold more abundant than BSF. The subcellular localisation of TbMCP12 in mitochondria was verified by immunofluorescence and gradient western blotting.

In this chapter, *Trypanosoma brucei* mitochondrial carrier family protein TbMCP12 was further studied in the following steps in PCF cells. The essentialness of TbMCP12 was examined by growth experiments. Minor growth effect was found with TbMCP12 overexpression (TbMCP12 ORF without myc tag: *TbMCP12-ORF*^{ti}) cells and TbMCP12 knockout (double knockout with inducible rescue copy: *ΔTbMCP12/TbMCP12-cmyc*^{ti}) or knockdown (TbMCP12 RNAi) cells under various glucose conditions. The lack of significant growth difference was contradicted with the failure of the generation of double knockout of both endogenous *TbMCP12* gene copy, signifying special role TbMCP12 plays only under certain stressed conditions. Thus, TbMCP12 mRNA and protein level were monitored under various culturing conditions (heme, glucose and H_2O_2) aiming to reveal the conditions of which TbMCP12 was necessary. These results showed that TbMCP12 protein level was up-regulated by the addition of heme, glucose and hydrogen peroxide. Also, TbMCP12 over-expression (OE: *TbMCP12-cmyc*^{ti}) cells grew better than WT under high concentration of hydrogen peroxide, suggesting a role TbMCP12 played in oxidative defence. Afterwards, the physiological changes caused by TbMCP12 up- or down-regulation were monitored by $NADP^+$/NAPDH ratio, mRNA levels of citrate downstream enzymes (aconitase and isocitrate dehydrogenases), and the metabolic flux. The $NADP^+$/NADPH ratio was observed to be increased in *TbMCP12-cmyc*^{ti} cells under

high glucose condition, while decreased in *ΔTbMCP12/TbMCP12-cmyc*^{ti} cells under low glucose condition. mRNA levels of aconitase, glycosomal and mitochondrial isocitrate dehydrogenases were upregulated in both *TbMCP12RNAi* and *TbMCP12-ORF*^{ti} cells. Metabolic substrate consumption (glucose and proline) and end product content (succinate and acetate) were examined in *TbMCP12-cmyc*^{ti} and *ΔTbMCP12/TbMCP12-cmyc*^{ti} cells, revealing that *TbMCP12-cmyc*^{ti} caused an increase in metabolites flux. These results using metabolic related parameters clearly showed that TbMCP12 was playing physiological roles in PCF of *T. brucei.* As a proposed mitochondrial transporter, the transport function of TbMCP12 was determined by two methods: mitochondrial ATP production assays and yeast functional complementation. In order to determine which carboxylate(s) TbMCP12 transports, a mitochondrial ATP production assay was applied to *TbMCP12-cmyc*^{ti} and *ΔTbMCP12/TbMCP12-cmyc*^{ti} cells. Citrate-, isocitrate- and malate-promoted ATP productions were significantly increased in *TbMCP12-cmyc*^{ti} cells, and TbMCP12 depletion (*ΔTbMCP12/TbMCP12-cmyc*^{ti}) resulted in ablation of ATP production, indicating that TbMCP12 was probably a di/tri-carboxylate carrier. Apart from experiments in *T. brucei,* the transport function of TbMCP12 was also tested by a yeast complementation experiment. TbMCP12 was heterologously expressed in dicarboxylate carrier DIC depleted yeast cells. Introducing TbMCP12 into DIC depleted cells rescued the growth defect in DIC depleted cells. This functional complementation in yeast further confirmed the role of TbMCP12 as a yeast dicarboxylate carrier that exchanges malate and succinate with phosphate. Considering all the results, TbMCP12 is proposed to be a di/tricarboxylate carrier in *Trypanosoma brucei*.

3.2 TbMCP12 over-expression presented no growth effect

TbMCP12 expression levels differed significantly between the two life cycle stages PCF and BSF (Colasante, unpublished data). One of the specific features between the two stages was the usage of carbon source, with BSF mainly relying on glucose and PCF utilising proline. Thus, the effect of TbMCP12 over-expression on cell viability was studied using standard MEM-PROS medium and MEM-PROS medium supplemented with 10 mM glucose (referred to as high-glucose MEM-PROS medium below). Generally, standard MEM-PROS medium (Appendix A3-2) contained low concentrations of glucose (about 0.25 mM) derived from the added 10% (v/v) fetal calf serum (FCS). In tetracycline induction of the *TbMCP12-cmyc*^{ti} cells, a major decrease in growth rate (>80%) was observed in both standard and high-glucose MEM-PROS medium (Figure 3-1).

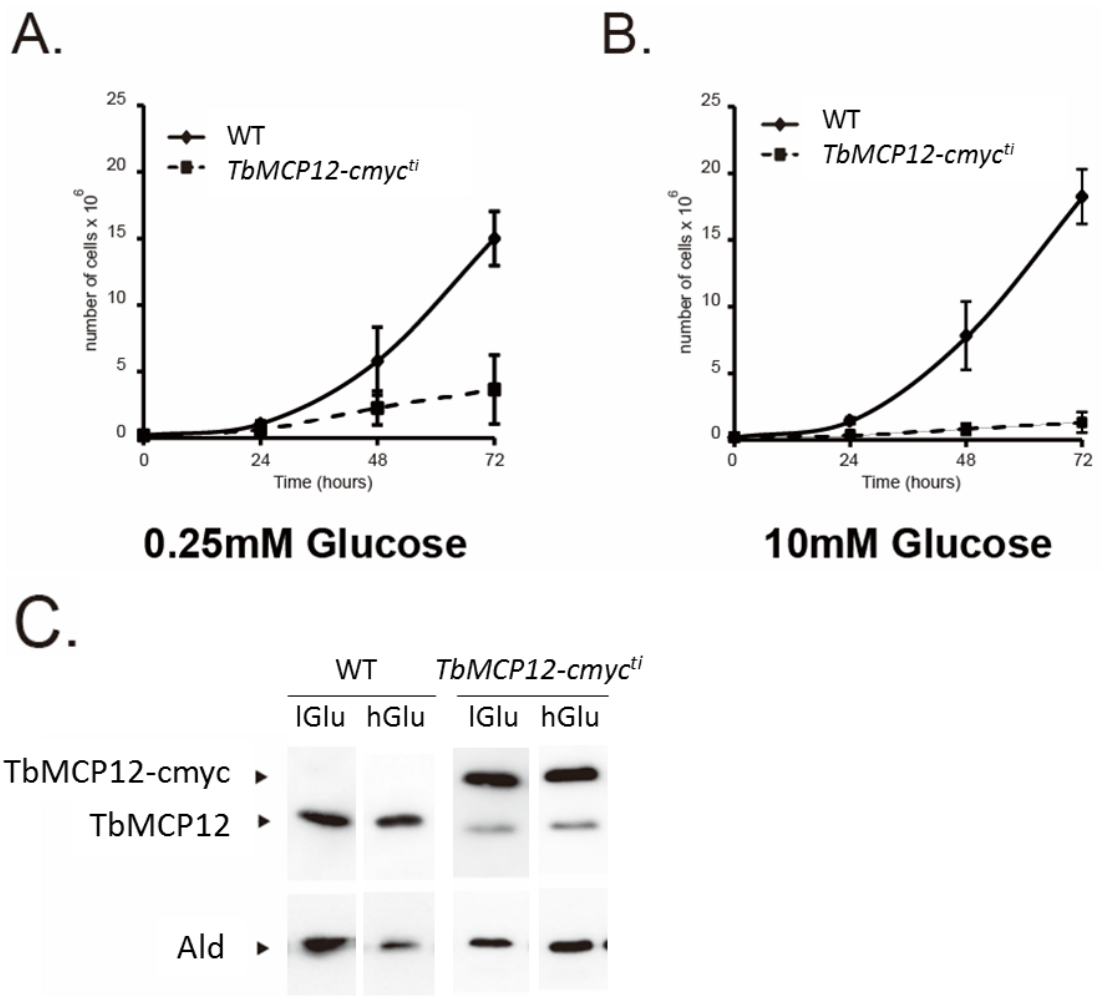

Figure 3-1 Growth curves of TbMCP12 overexpression (*TbMCP12-cmyc^{ti}*) cells compared with WT (PCF449)

Growth curves of the *TbMCP12-cmyc^{ti}* cells (values shown with square dots joined by a broken line) and WT cells (values shown with diamond dots joined by a solid line) are presented by cell concentrations measured every 24 hours in triplicates. A represents the cells cultured in standard MEM-PROS medium with a limited amount of glucose, while B shows cell growth in high glucose (10 mM) medium. C demonstrates the confirmation of TbMCP12 expression level by WB. TbMCP12-cmyc recombinant protein was probed with TbMCP12 N-term peptide antibody, myc antibody and aldolase antibody.

In order to eliminate the possibility that growth defect of *TbMCP12-cmyc^{ti}* cells could have been caused by the addition of myc tags, TbMCP12 ORF containing stop codon at the end of the ORF sequence was cloned into the same vector, and *TbMCP12-ORF^{ti}* cell line was generated accordingly. As shown in Figure 3-2, over-expression of the endogenous TbMCP12 protein was not lethal to cell growth. Thus, the detrimental effect of TbMCP12-cmyc over-expression cell line was caused by the addition of the c-terminal myc tag. As a cross-membrane transporter, C terminal could be involved in cross-talks with neighbour proteins (Clayton 2002), hence, interfering with the communications

between TbMCP12 and other proteins or responsive elements. Noteworthily, at the time when the experiment being conducted, TbMCP12 detection was an issue and only visible when over-expressed by PARP promoter but below the detection limit for WT cells (Figure 3-2 C).

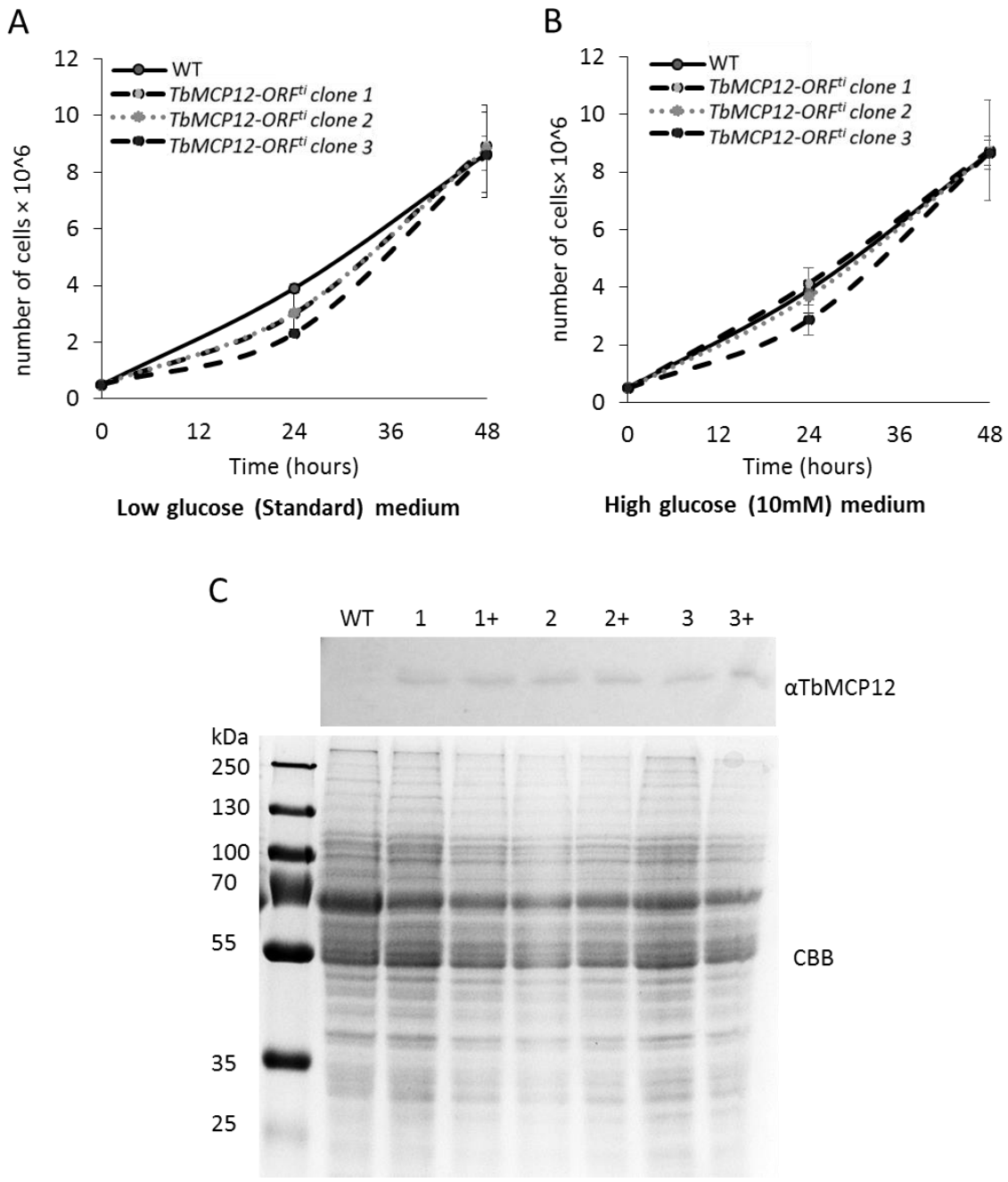

Figure 3-2 Growth curves of TbMCP12 overexpression cells (without myc tag) compared with WT (PCF449) cells

Growth curves of three individually generated *TbMCP12-ORF^{ti}* cell lines (values shown with round dots joined by a broken line) and WT cells (values shown with round dots joined by a solid line) consist of cell densities measured every 24 hours in triplicate. A demonstrates the growth curves of the cells cultured in standard MEM-PROS medium with a limited amount of glucose. B shows the cells in high glucose (10 mM) medium. C illustrates the confirmation of TbMCP12 expression with WB using TbMCP12 N-term peptide antibody, and with Coomassie Brilliant Blue (CBB) as a loading control. Numbers in C indicates three different clones. '+' stands for the addition of tetracycline.

3.3 TbMCP12 down-regulation was not detrimental for cells

To find out whether TbMCP12 was essential for the survival of PCF *T. brucei*, attempts were made to replace both TbMCP12 alleles by using the conventional gene replacement method (see Section 2.5.2 for details). After many attempts however, only half-knockout PCF *T. brucei* cells with the genotype Δ*TbMCP12::BSD/TbMCP12* or Δ*TbMCP12::NEO/TbMCP12* could be obtained. Failing to obtain viable double-knockout clones by using the conventional gene replacement method indicates that TbMCP12 was essential for the growth and survival of PCF *T. brucei*. Alternatively, a conditional double knockout cell line was generated as previously described for the conditional double-knockout of other essential *T. brucei* genes (Colasante et al. 2006).

The *TbMCP12-cmyc*^{ti} cell line was subsequently used for the generation of the conditional double knockout cell line *ΔTbMCP12*::NEO/*ΔTbMCP12*::*BSD*/*TbMCP12-cmyc*^{ti} (referred to as *ΔTbMCP12/TbMCP12-cmyc*^{ti} below) by successive replacement of the two TbMCP12 alleles with neomycin (NEO) and blasticidin (BSD) resistance-encoding gene cassettes, respectively, through homologous recombination. The successive replacement of the two TbMCP12 alleles was performed in the presence of tetracycline in order to maintain the presence of sufficient recombinant TbMCP12-cmyc protein required for trypanosome survival. The successful replacement of both natural TbMCP12 alleles in the obtained *ΔTbMCP12/TbMCP12-cmyc*^{ti} cell line was confirmed by western blot analysis, which showed complete ablation of the natural 32 kDa TbMCP12 protein in the *ΔTbMCP12/TbMCP12-cmyc*^{ti} cell line using the raised TbMCP12 N-term peptide antibody (Figure 3-3).

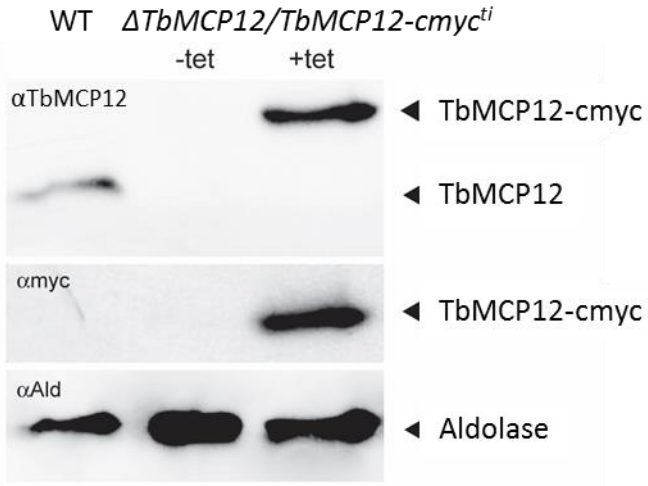

Figure 3-3 Confirmation of conditional double knockout of *TbMCP12* in the generated *ΔTbMCP12/TbMCP12-cmyc^{ti}* cells

The figure shows WB results of WT and knockout cells probed with TbMCP12 N-term peptide antibody (αTbMCP12), myc antibody (αmyc) and aldolase antibody (αAld). The detected protein bands are indicated with triangles.

The viability of the obtained *ΔTbMCP12/TbMCP12-cmyc^{ti}* cell line was assessed by measuring its growth (cell density) in both standard MEM-PROS medium and high glucose medium. The growth of the tetracycline-induced and non-induced *ΔTbMCP12/TbMCP12-cmyc^{ti}* cell line was compared with that of the WT PCF449. The results reveal that growth of both the non-induced and tetracycline-induced *ΔTbMCP12/TbMCP12-cmyc^{ti}* cell lines was similar to that of the wildtype PCF449 cell line if not better (Figure 3-4). Western blot analysis indicated that expression of TbMCP12-cmyc (35 kDa) in the tetracycline-induced *ΔTbMCP12/TbMCP12-cmyc^{ti}* cell line and the expression of natural TbMCP12 (32 kDa) in the wildtype PCF449 cell line were found to be constant throughout the 72-hour experiment (Figure 3-4 C).

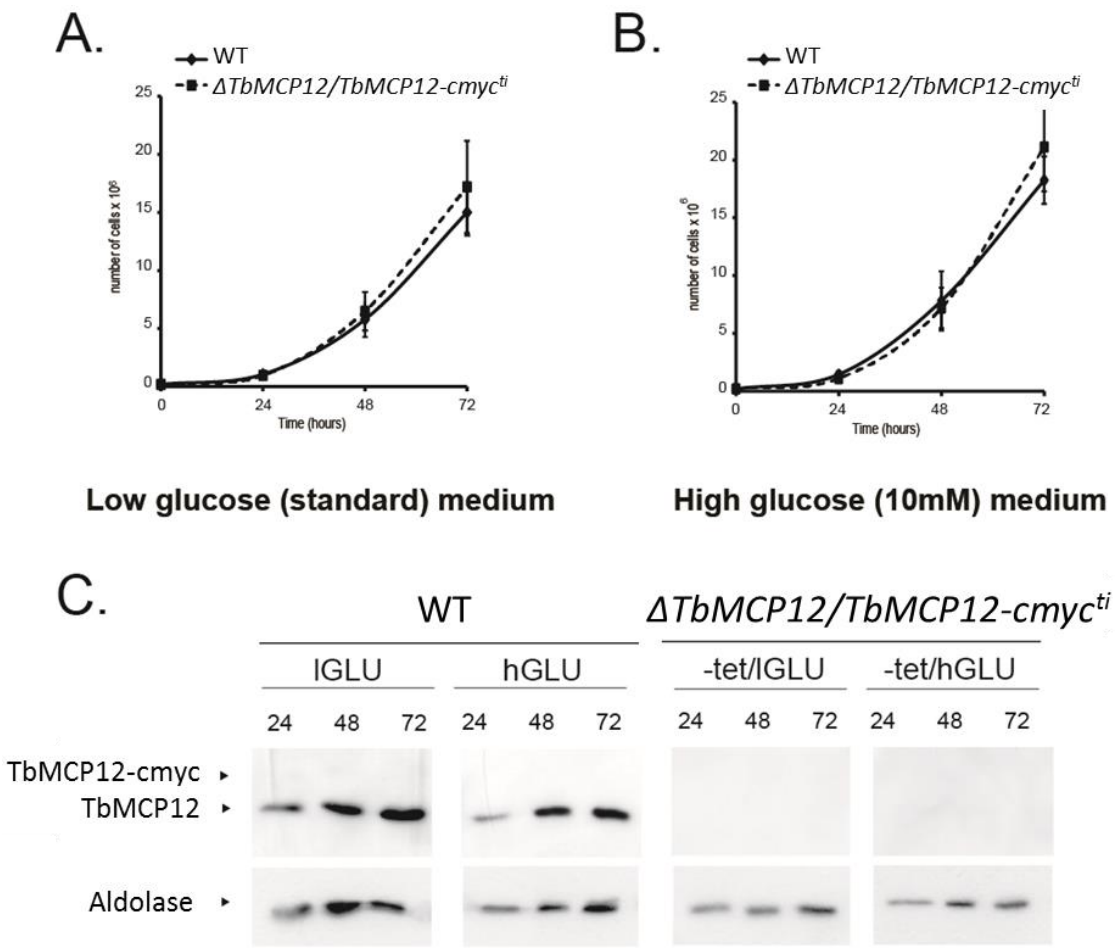

Figure 3-4 TbMCP12 conditional double knockout cells present no growth defect

Growth curves of WT and knockout (*ΔTbMCP12/TbMCP12-cmyc*^{ti}) cells are demonstrated in figure A (standard MEM-PROS medium) and B (MEM-PROS medium containing 10 mM of glucose). Standard deviations of three independent experiments are presented as error bars. The confirmation of expression and depletion of TbMCP12 and/or TbMCP12 recombinant protein with WB is shown in C using TbMCP12 N-term peptide antibody, myc antibody and aldolase antibody. lGLU and hGLU stand for low and high glucose conditions, respectively. –tet represents for *ΔTbMCP12/TbMCP12-cmyc*^{ti} without the induction of rescue copy TbMCP12-cmyc by tetracycline.

This result was unexpected since previous attempts to generate a viable 'conventional' TbMCP12-knockout cell line invariably failed (see above), suggesting that TbMCP12 was essential for trypanosome growth and survival. A possible explanation was that the residual TbMCP12-cmyc remaining in the tet-removal *ΔTbMCP12/TbMCP12-cmyc*^{ti} cell line (below western blot detection limit) restored TbMCP12 function. Additionally, too much of the TbMCP12-myc might be detrimental to cell growth (Figure 3-1). So gene knockdown was performed afterwards by RNA interfere (RNAi) in order to get more effective gene knockdown.

TbMCP12 RNAi cell lines were obtained by transferring pHD678+TbMCP12 antisense plus sense construct (also known as TbMCP12 RNAi construct) in PCF *T. brucei.* PCF449 transformed with an empty pHD678 plasmid was used as a control. Similar growth was observed under 0 and low glucose conditions, while a small growth increase in TbMCP12 depleted cells was found under high glucose (Figure 3-5). This finding was in accordance with the result of conditional double knockout *ΔTbMCP12/TbMCP12-cmyc*^{ti}.

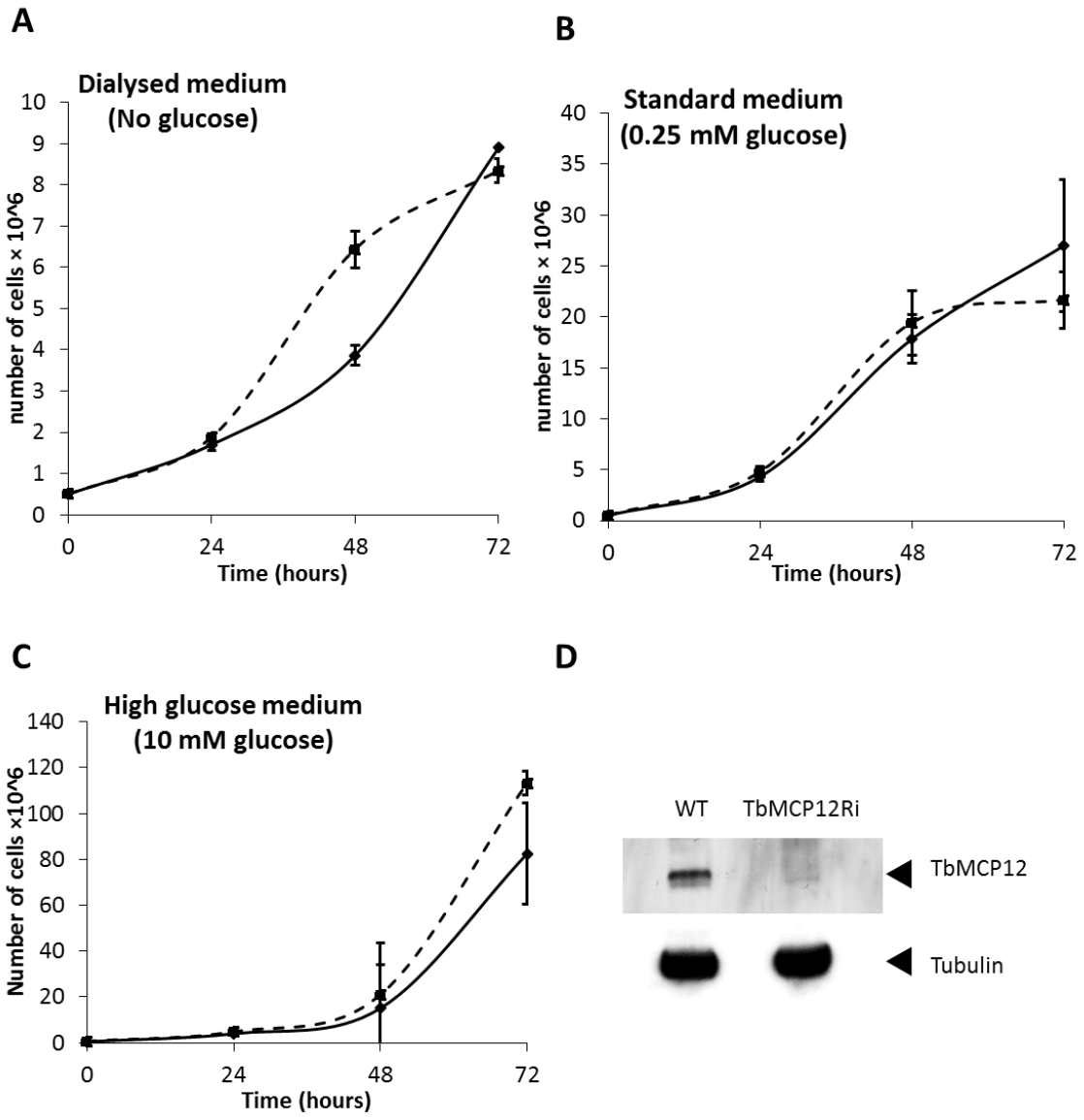

Figure 3-5 TbMCP12 RNAi cells show no growth defect
Growth curves of TbMCP12 RNAi cells (square dots joined with a broken line) and WT cells (diamonds dots joined with a black solid line) are presented under no glucose (A) low glucose (B) and high glucose (C) conditions. Growth curves were repeated for three times and error bars indicating standard deviation are added. For zero glucose medium, serum added was dialysed beforehand to remove glucose. TbMCP12 RNAi efficiency is

shown in D checked by WB. TbMCP12 N-term antibody and tubulin antibody were used. The detected proteins were indicated by triangles.

At the same time, TbMCP12 down-regulation in *T. brucei* BSF cells was measured under normal HMI-9 medium using TbMCP12 RNAi cell line. There was no difference in growth of TbMCP12 mRNA depletion (to 60%, Figure 3-6 C) in BSF using RNAi (Figure 3-6 A). TbMCP12 down-regulation was examined by quantitive PCR, with band density quantified and shown in Figure 3-6 B & C. Thus, whether TbMCP12 was essential for BSF remained a question: decrease of TbMCP12 mRNA level did not necessarily lead to depletion of protein, or reduction to a certain extent. Possibly, the remaining TbMCP12 protein was sufficient for maintaining cell growth.

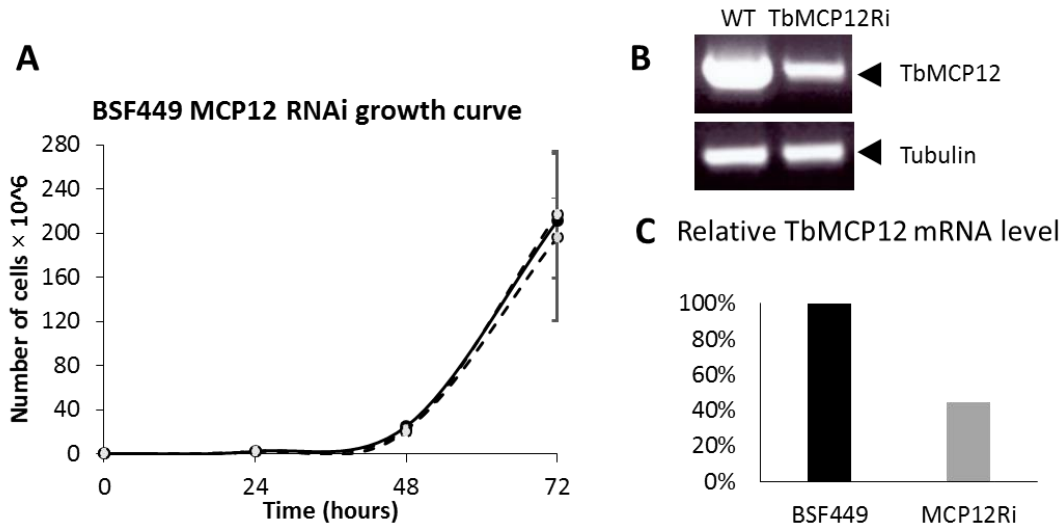

Figure 3-6 TbMCP12 down-regulation in BSF presented no growth difference
A. Growth curves of TbMCP12 RNAi and BSF449 cells. Growth curve of WT cells are presented with a black straight line with dots, and TbMCP12 RNAi cells are labelled with a broken line with dots. Error bars indicate standard deviation of triplicates. The individual experiments were repeated three times. B. TbMCP12 RNAi efficiency is presented checked by semi-quantitive PCR. TbMCP12 and tubulin primers were used in semi-qPCR. C. The normalized TbMCP12 mRNA level by tubulin is presented with WT BSF449 set to 100%.

3.4 TbMCP12 expression was regulated by heme and glucose

It was controversial that no growth defect was found when TbMCP12 was depleted, but the generation of a double copy knockout cell line failed without rescue copy. The contradicting results suggested that TbMCP12 might play a role under certain conditions, thereby it was only essential under certain circumstance. Thus, TbMCP12 expression was examined using variable heme and glucose concentrations in WT PCF449 cells. Apart from roles heme played as cofactors in oxygen transport and storage, mitochondrial electron transport and signal transduction, heme was also known as an iron source in *T. brucei* (Tripodi et al. 2011). Iron must bind with an anion (such as carbonate) to avoid the formation of toxic oxygen species hydroxyl radical (OH·). As a potent di/tri-carboxylate carrier, TbMCP12 was proposed to co-transport iron. Thus potential regulation of TbMCP12 expression by heme availability was also tested.

TbMCP12 mRNA level changed in varying heme and glucose concentrations (Figure 3-7 A). TbMCP12 mRNA level from cells cultured in medium lacking heme and glucose was set to 1. Under glucose depleted condition, the addition of heme resulted in a 40% decrease, while an increase of TbMCP12 mRNA was found in high glucose condition with the addition of heme. If glucose was set as a variable, TbMCP12 mRNA level was upregulated around 90% in the presence of heme but stayed at the similar level in the absence of heme. Overall, glucose caused upregulation of TbMCP12 mRNA was more predominant in the presence of heme.

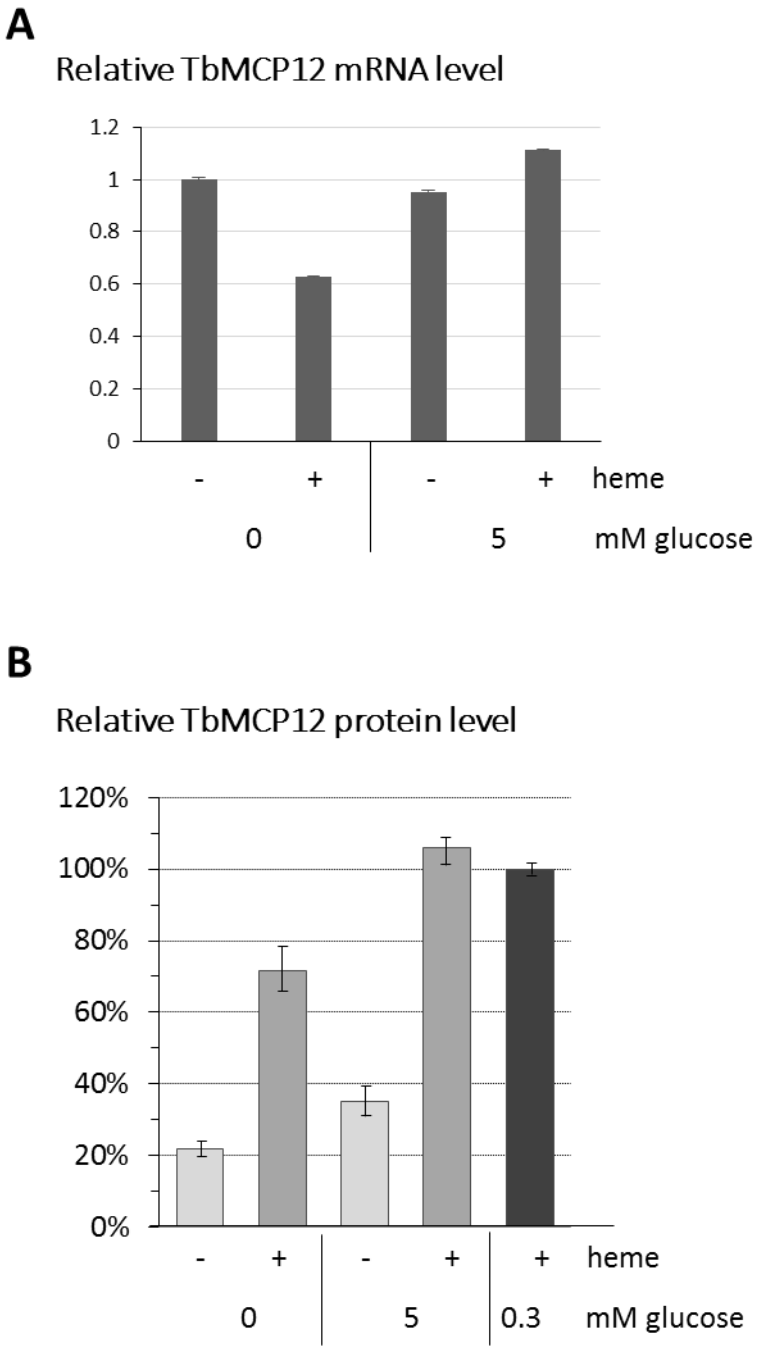

Figure 3-7 Examination of relative TbMCP12 mRNA level and protein level
Using data derived from RT-qPCR and western blot, TbMCP12 mRNA levels are standardised using telomerase reverse transcriptase (TERT, Dreesen et al. 2005), whereas tubulin was used for protein level. PCF WT cells were cultured in the presence of 10 mM proline and varying concentrations of glucose. 0 = no glucose, 0.3 mM = standard (low) glucose, and 5 mM (high) glucose. 11.5 µM of heme, which is equal to standard culture concentration, is presented as '+' or is omitted as '-' during culture. A. The relative TbMCP12 mRNA level is presented with double depletion of heme and glucose set to 1. B. The relative TbMCP12 protein level is demonstrated with expression in PCF on "standard" culture medium (with heme and FCS-containing glucose, black column) set to 100%. The quantification was performed towards one representative WB of three independent experiments.

However, on the protein level, significant differences were unveiled (Figure 3-7 B). Firstly, the addition of heme to culture medium led to a 3-fold increase in TbMCP12 expression. In the case of growth on proline only (without the addition of glucose), TbMCP12 expression was increased 3.3 folds upon the addition of heme. High glucose (5 mM) conditions led to a 3-fold increase of TbMCP12 expression upon the addition of heme. To sum up, the addition of 11.5 µmol of heme, independently of the carbon source used, resulted in a 3-fold up-regulation of TbMCP12 expression. Secondly, the change of carbon source (fermentable versus non-fermentable) resulted in a 1.5-fold up-regulation of TbMCP12. The presence of glucose (0.3-5 mM) led to a 1.6-fold up-regulation (no heme) and 1.5-fold (plus heme) increase, respectively. Furthermore, no significant difference in TbMCP12 expression for 0.3 or 5 mM glucose was found in the presence of heme (Figure 3-7 B). The highest relative TbMCP12 expression was observed on medium containing both glucose and heme. In a word, both the mRNA and protein level of TbMCP12 were increased under high glucose condition.

3.5 TbMCP12 was upregulated by H_2O_2 and helped cell growth in the presence of H_2O_2

Carboxylates were involved in mitochondrial metabolic processes such as electron transport chain and TCA cycle because intermediates were linked to $NAD(P)^+$/NAD(P)H. In this way, carboxylates were connected with oxidative stress. It was tested whether H_2O_2 was a regulator for TbMCP12, in addition to the carbon sources and heme in the media.

TbMCP12 levels of WT PCF449 under various hydrogen peroxide concentrations were first measured at both mRNA and protein level (Figure 3-8 A). A significant increase of protein amount was observed when hydrogen peroxide was present, especially under 100 nM of hydrogen peroxide condition (nearly two-fold increase). Noticeably, TbMCP12 mRNA level was decreased about 10%, despite the fact that approximately twice of TbMCP12 protein was found in 100 nM of hydrogen peroxide, compared with standard condition (Figure 3-8 A). This result indicates that TbMCP12 level was also regulated at the post-transcriptional level. The upregulation of TbMCP12 protein suggests a role TbMCP12 could be playing in oxidative stress.

To confirm the relationship between upregulation of TbMCP12 protein and oxidative stress, WT, TbMCP12 RNAi and overexpression (*TbMCP12-ORF*^{ti}) cells were exposed to oxidative stress in the form of different concentrations of H_2O_2, and their growth was measured, subsequently. The depletion and over-expression of TbMCP12 were detected using an N-term peptide TbMCP12 antibody with tubulin as a loading control. As expected, increased exposure to oxidative stress reduced cell growth. The growth of WT cells decreased to about 87% and 60% of untreated WT cells after exposure to 50 nM and 100 nM hydrogen peroxide for 24 hours, respectively (Figure 3-8 B). Furthermore, the growth of TbMCP12-RNAi cells was more significantly affected by hydrogen peroxide treatment with growth decreased to 68% and 35% after exposure to 50 or 100 nM hydrogen peroxide for 24 hours, respectively, compared with untreated TbMCP12-RNAi cells. The growth of both WT and *TbMCP12-ORF*^{ti} cells decreased to a similar level: 87% and 83% of the respective untreated cell lines, when exposed to 50 nM hydrogen peroxide.

However, when exposed to higher hydrogen peroxide concentrations, here 100 nM, the *TbMCP12-ORF*^{ti} cells clearly grew better than the WT cell line (95% confidence). This finding and the upregulation of TbMCP12 protein level in WT cells under hydrogen peroxide treatment (Figure 3-8 A) indicates that TbMCP12 was upregulated under oxidative stress, and that the over-expression of TbMCP12 helped to rescue the cell growth defect under hydrogen peroxide treatment.

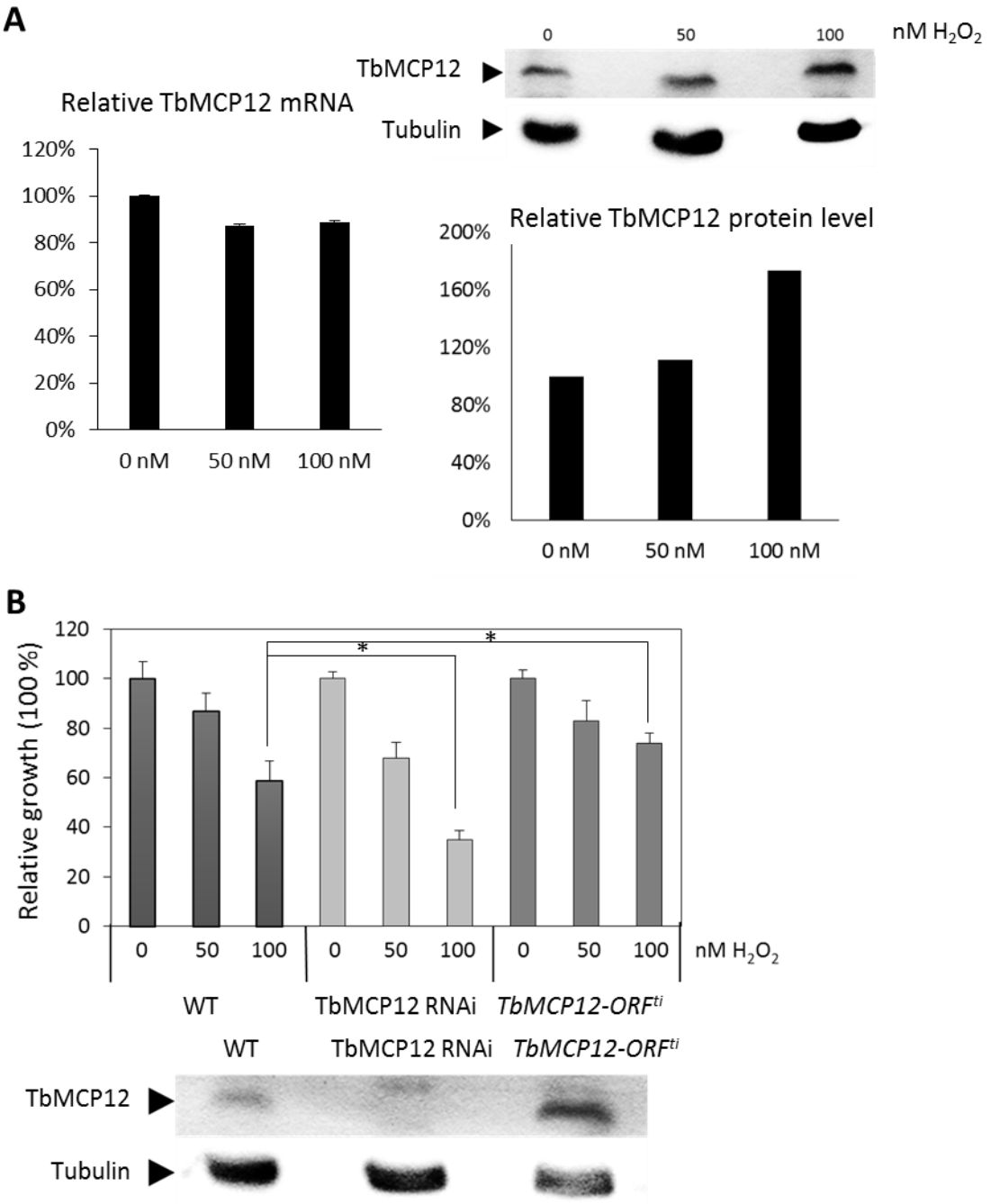

Figure 3-8 TbMCP12 helped with oxidative stress defence

A. TbMCP12 mRNA level and protein level under different H_2O_2 concentrations in WT cells are presented. mRNA and protein levels were measured by quantitive PCR and WB, respectively, followed by the normalisation of mRNA level with TERT (Telomerase reverse transcriptase) or with tubulin on protein levels. B. The growth of PCF *T. brucei* cell lines WT, TbMCP12-RNAi, and *TbMCP12-ORF*^{ti} upon exposure to variable concentrations of hydrogen peroxide (0, 50, 100 nM) is demonstrated. The growth was measured after 24 hours exposure, and the growth of untreated cell lines was set to 100%. Error bars indicating standard deviations of triplicates are shown. Cells were cultured in standard medium containing glucose (low) derived from FCS. Cell lines were checked with WB for TbMCP12 depletion and over-expression using TbMCP12 N-term antibody, whereas using tubulin antibody for a loading control. The significant differences of mRNA level are indicated with '*' confirmed by T-test (p= 0.0332 and 0.017).

3.6 TbMCP12 played a role in oxidative stress defence

As TbMCP12 was proposed to be a di/tricarboxylate carrier (DTC) exporting citrate out of mitochondria. Citrate could be converted to isocitrate by aconitase (ACO), and further to α-ketoglutarate by isocitrate dehydrogenase (IDH) (van Hellemond et al. 2005), in which NADPH was produced. NADPH helped to defence oxidative stress. Accordingly, in this part, mRNA level of the downstream enzymes and cellular $NADP^+$/NADPH ratio were tested.

The *T. brucei* genome contained only one gene coding for aconitase. The gene product was however, found in both the mitochondrion and the cytosol. It was shown that mitochondrial aconitase activity was relatively low (about 30% of the total aconitase activity, Saas et al. 2000). This was in line with the incomplete part of TCA cycle that aconitase was not essential for cell growth in PCF (van Weelden et al. 2003). However, the 90-fold accumulation of citrate in aconitase-knockout cells reported in the same literature suggested the presence of aconitase activity in WT cells. The aconitase, hence, was likely to involve in processes other than energy metabolism, possibly in oxidative stress defence combining with IDH. Isocitrate dehydrogenase was not much studied in *T. brucei*, except for the fact that only NADP-related IDH activity was found (van Weelden et al. 2003). In *T. cruzi*, isocitrate dehydrogenase lay in both mitochondrion and cytosol. *IDHmito* coded for the mitochondrial form, whereas *IDHgly* coded for cytosolic form, which was also found in glycosomes (Leroux et al. 2011).

In WT cells, mRNA level of aconitase, as well as mitochondrial and cytosolic (glycosomal) isocitrate dehydrogenase presented reversed result between 50 nM and 100 nM of hydrogen peroxide treatment (Figure 3-9 A). mRNA levels of aconitase and glycosomal isocitrate dehydrogenase were upregulated slightly (1.16×) under 50 nM of H_2O_2, whereas down-regulated to 0.8× and 0.7×, respectively. Mitochondrial isocitrate dehydrogenase, on the other hand, remained at similar transcription level under hydrogen peroxide treatment, with a slightly increase in 100 nM H_2O_2. Overall, mRNA levels of the three examined enzymes stayed similar.

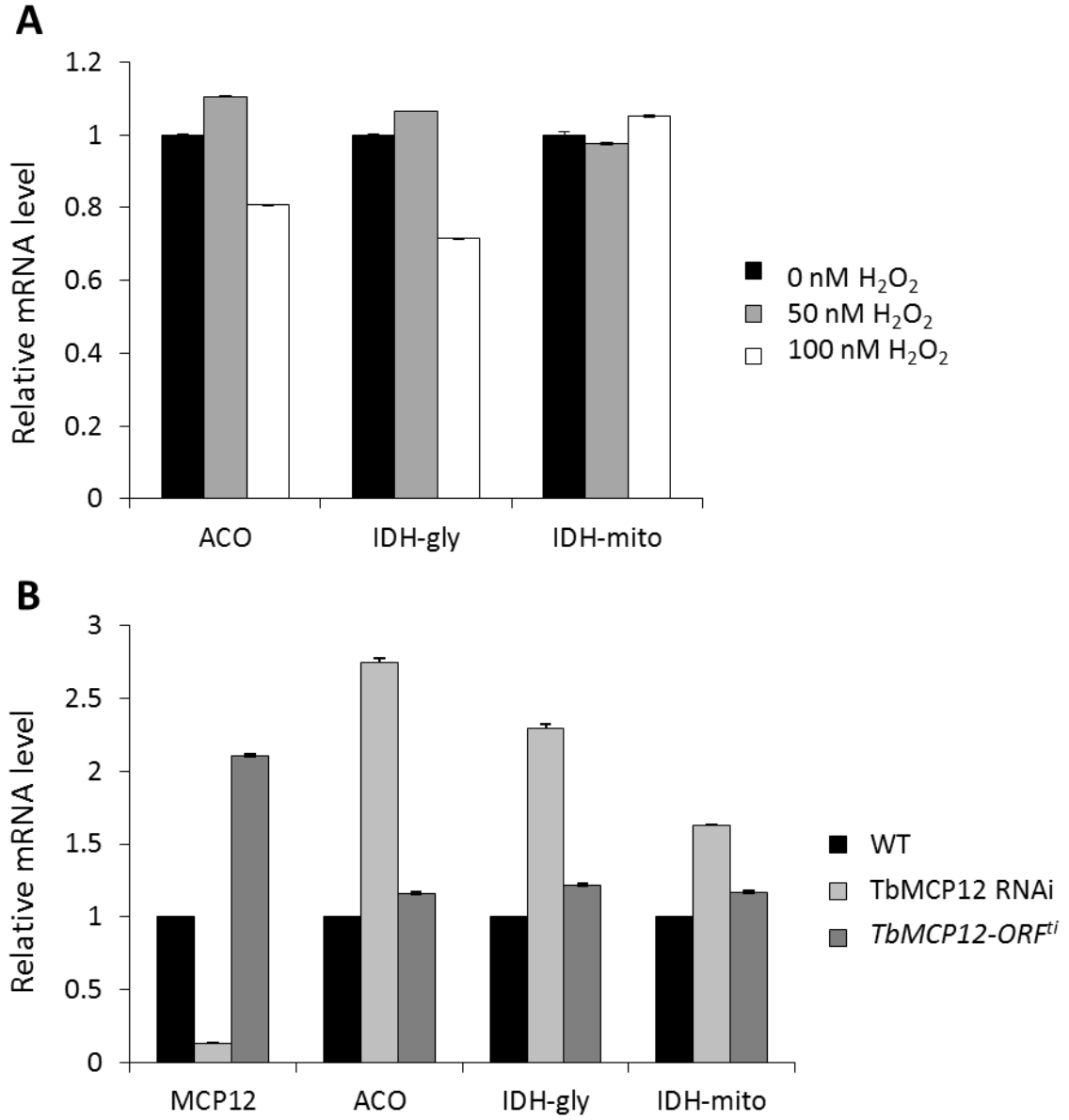

Figure 3-9 mRNA levels of aconitase, cytosolic/glycosomal isocitrate dehydrogenase, mitochondrial isocitrate dehydrogenase and TbMCP12

The relative mRNA levels of aconitase (ACO), mitochondrial isocitrate dehydrogenase (IDH-mito) and glycosomal isocitrate dehydrogenase(IDH-gly) are demonstrated in the graph above with mRNA level of WT cells without hydrogen peroxide set to 1. A presents the mRNA levels of WT cells under varying hydrogen peroxide concentrations (0, 50 and 100 nM). B shows the mRNA levels from three different cells cultured under standard condition.

In order to trigger (potential) maximum regulation of TbMCP12 to these enzymes, TbMCP12 RNAi cells and TbMCP12 over-expression (*TbMCP12-ORF*^{ti}) cells were used to test these enzyme mRNA levels (Figure 3-9 B). First of all, TbMCP12 down-regulation and over-expression efficiency were confirmed: TbMCP12 RNAi demonstrated clear

down-regulation (down to 13% compared to WT) of TbMCP12 mRNA levels, whereas *TbMCP12-ORF*^{ti} showed clear up-regulation (210% or 2.1× compared to WT). TbMCP12 RNAi led to significant increases in mRNA levels of aconitase (2.8× compared to WT), mitochondrial isocitrate dehydrogenase (1.6×), and cytosolic isocitrate dehydrogenase (2.3×). TbMCP12 RNAi was suggested to cause a significant decrease in citrate export, which led to mitochondrial citrate accumulation. To prevent mitochondrial citrate accumulation, mitochondrial aconitase and isocitrate dehydrogenase activity were increased to convert citrate into succinate. Succinate excretion was measured in Section 3.6, and the energy metabolism of TbMCP12 RNAi was discussed in Section 3.11.3. qPCR results supported the expected increased expression of aconitase and mitochondrial isocitrate dehydrogenase (Figure 3-9 B). Interestingly, the cytosolic/glycosomal isocitrate dehydrogenase IDH transcription was also significantly increased. No major effect was observed on *TbMCP12-ORF*^{ti} aconitase, mitochondrial isocitrate dehydrogenases and glycosomal isocitrate dehydrogenase mRNA level (max 1.2×). This result suggested that existing endogenous citrate export activity was sufficient, i.e., not rate limiting for this process. It was also worth pointing out that the enzymes had also been found to be post-transcriptional regulated (Saas et al. 2000).

Due to the fact that the majority of genes are post-transcriptionally and/or post-translationally regulated, cellular $NADP^+$/NADPH ratio was also tested. The total cellular $NADP^+$/NADPH ratio was determined in PCF449, TbMCP12 OE (*TbMCP12-cmyc*^{ti}) and TbMCP12 depletion / conditional knockout (Δ*TbMCP12/ TbMCP12-cmyc*^{ti}) cells. The three cell lines were cultured in either standard or high-glucose MEM-PROS medium. Overall, changes in $NADP^+$/NADPH ratios were observed from the different cells depending on the used culture media. The $NADP^+$/NADPH ratio of WT cells showed no statistical difference (1.2-1.6) between standard and high-glucose medium (Figure 3-10). $NADP^+$/NADPH ratios for the TbMCP12-depletion cells cultured in the standard MEM-PROS medium revealed a significant increase in the $NADP^+$/NADPH ratio to about 2.3, whereas in the high-glucose medium the $NADP^+$/NADPH ratio was found to be similar (about 1.5) to the WT control. On the contrary, as for the TbMCP12-overexpression cell line, a substantial decrease in $NADP^+$/NADPH ratio (about 1.2) was observed in high-glucose MEM-PROS medium, with a minor difference in standard medium. Depletion or overexpression of TbMCP12 apparently resulted in a significant perturbation of the total

cellular $NADP^+$/NADPH balance and NADPH availability, which depended on the available carbon source. These results suggested that TbMCP12 overexpression decreased $NADP^+$/NADPH ratio under high glucose condition, while knockout of the same gene triggered an increase under standard glucose condition.

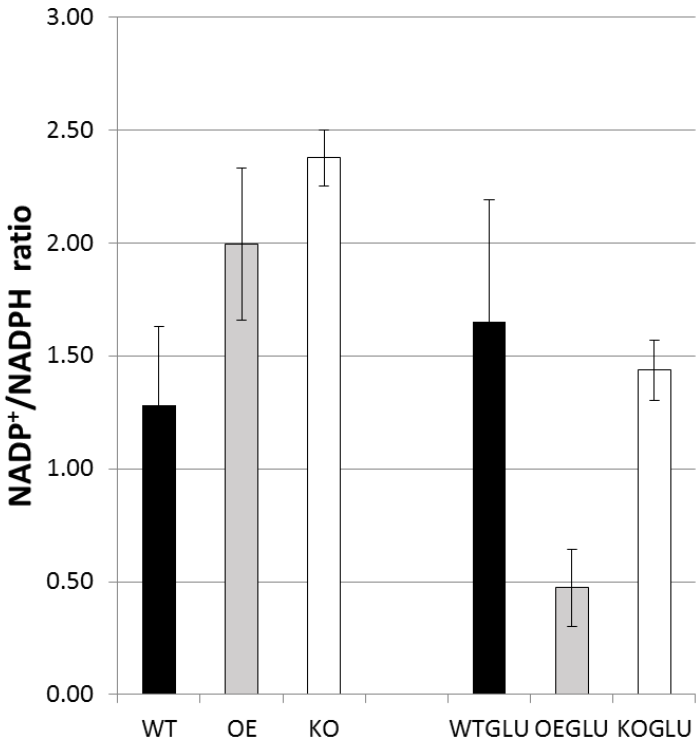

Figure 3-10 Perturbation of the $NADP^+$/NADPH balance in TbMCP12-depletion and overexpression cell lines

$NADP^+$/NADPH ratios in WT (black column), TbMCP12 over-expression (*TbMCP12-cmyc*^{ti}, presented as OE, grey column) and TbMCP12 depletion (conditional knockout Δ*TbMCP12/ TbMCP12-cmyc*^{ti}, presented as KO, white column) cell lines are shown with cells cultured under both low glucose and high glucose (labelled as GLU after cell lines) conditions.

3.7 TbMCP12 over-expression promoted metabolites flux

As discussed before, TbMCP12 is very likely to be a carboxylates transporter on *T. brucei* mitochondrial membrane, and the carboxylates are involved in energy generation. Procyclic trypanosomes use either glucose and/or proline as main substrates for energy (ATP) generation, with succinate and acetate formed as their main metabolic end products (Besteiro et al. 2005). Thus, substrate consumption and end product formation were quantified for the PCF449, the tetracycline-induced *TbMCP12-cmyc*^{ti}, and the non-induced Δ*TbMCP12/TbMCP12-cmyc*^{ti} cells in order to investigate whether the overexpression or depletion of TbMCP12 caused a significant change in the trypanosome metabolism.

Analysis of proline-consumption during growth in standard medium revealed no significant differences between the three analysed cell lines: none of the cells consumed more than 0.4 mM proline per 10^6 cells in the first 72 hours of growth (Figure 3-11 A). Similar proline-consumption values were found in WT and the TbMCP12-depletion cells (Δ*TbMCP12/TbMCP12-cmyc*^{ti}) when grown in high-glucose MEM-PROS medium (Figure 3-11 A). The TbMCP12-overexpression cells *TbMCP12-cmyc*^{ti}, however, revealed a substantially increased consumption of proline in high glucose medium (approximately 6-fold compared to WT). Analysis of glucose consumption during the growth of the cell lines in standard and high-glucose MEM-PROS media suggested a similar substrate consumption pattern as found for proline: slight difference in glucose consumption was found for PCF449 and Δ*TbMCP12/TbMCP12-cmyc*^{ti} cells, whereas *TbMCP12-cmyc*^{ti} showed a substantially increased consumption of glucose (6 folds of WT) when cells were grown in high-glucose MEM-PROS medium (Figure 3-11 B). Notably, growth of *TbMCP12-cmyc*^{ti} was significantly affected in both standard and high-glucose medium (Figure 3-1), even though both media contained sufficient proline (4.7 mM and 4.4 mM proline remaining in standard and high-glucose media respectively after 72 hours) and glucose (8 mM glucose remaining after 72 hours in high-glucose medium) to promote trypanosome growth further as shown for WT.

Analysis of end product formation (Figure 3-11 C-succinate and D-acetate) revealed a substantial increase in the formation of both succinate (about 4-fold compared to WT)

and acetate (about 5-fold compared to WT) after 72 hours of growth of *TbMCP12-cmyc*^{ti} cells in the high glucose medium. An increase in succinate and acetate formation was also observed when the same cell line was grown in standard MEM-PROS medium: succinate formation increased about 8 folds, whereas acetate formation increased only about 1.6 folds in comparison with WT grown in the same medium. In contrast to the TbMCP12-overexpression cells (*TbMCP12-cmyc*^{ti}), TbMCP12-depleted cells (Δ*TbMCP12/TbMCP12-cmyc*^{ti}) produced a similar amount of succinate of the wildtype cell line in high-glucose medium. Compared with WT, succinate formation appeared to be 3 folds less than Δ*TbMCP12/TbMCP12-cmyc*^{ti} cells when grown in standard MEM-PROS medium (Figure 3-11 C). In the same cell line (Δ*TbMCP12/TbMCP12-cmyc*^{ti}), no significant change in acetate formation was observed, compared with WT, when grown in either low- or high-glucose MEM-PROS medium (Figure 3-11 D).

Overall, the results suggested that TbMCP12 over-expression increased proline and glucose consumption in high glucose medium, and that succinate and acetate production were increased regardless of glucose concentration. Also, TbMCP12 depletion resulted in the up-regulation of glucose consumption and acetate production under high glucose condition, while succinate production decreased under low glucose condition.

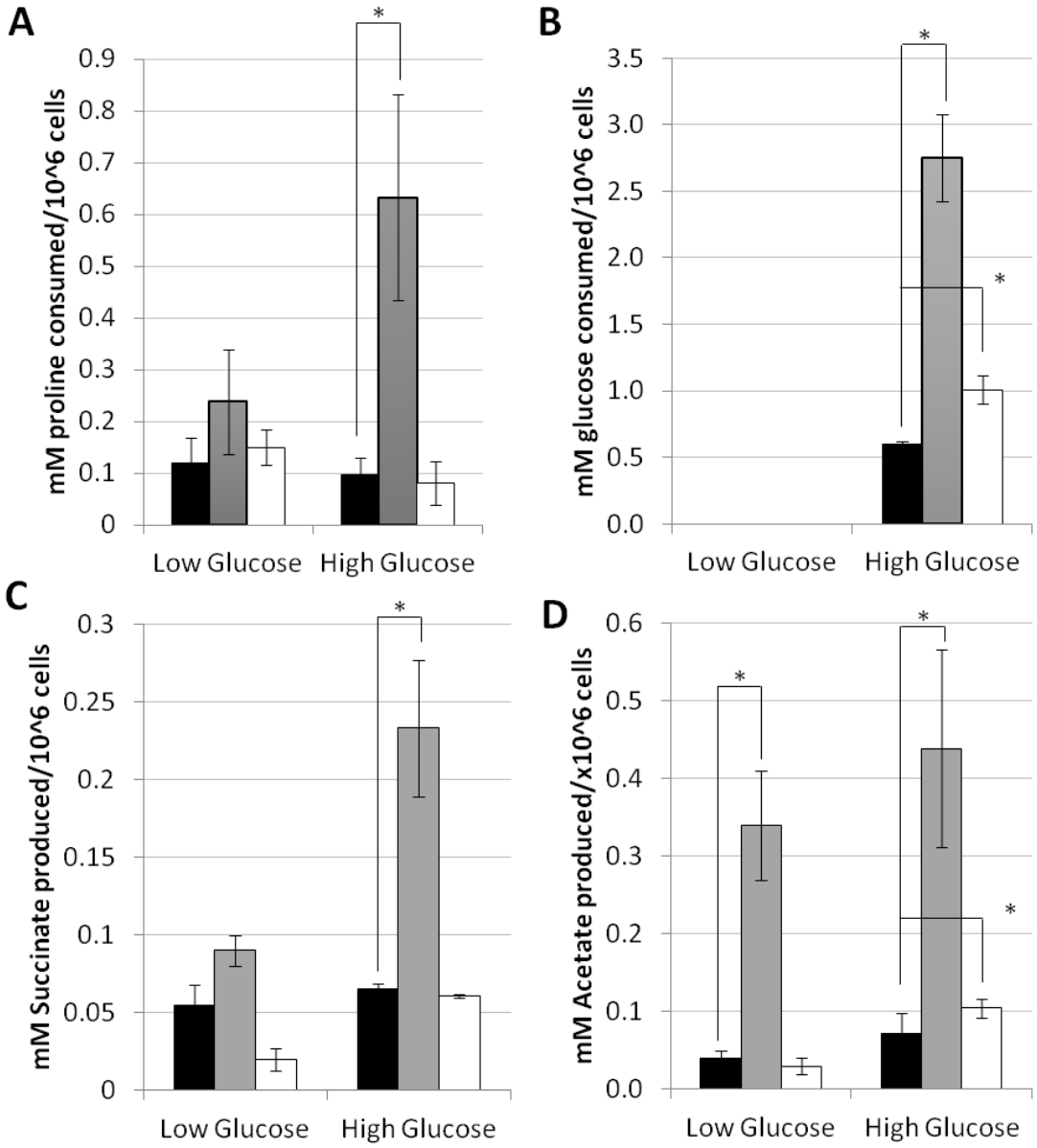

Figure 3-11 Measurement of main end-products and substrates content
Production of succinate and acetate, and consumption of glucose and proline measured in the different cell lines after 72 hours of growth in either standard or high-glucose MEM-PROS medium are presented. As mentioned above, standard medium MEM-PROS contained approximately 0.25 mM glucose (derived from added 10% v/v FCS), whereas the high-glucose MEM-PROS medium was supplemented with 10 mM glucose. Both culture media contained 5 mM proline as substrate. Substrates consumption and end-products formation of WT cell lines are labelled in black, TbMCP12 OE (*TbMCP12-cmyc*^{ti}) in grey and TbMCP12 depletion (Δ*TbMCP12/TbMCP12-cmyc*^{ti}) in white.

3.8 TbMCP12 helped mitochondrial ATP production with the presence of tricarboxylates

As presented before, TbMCP12 up/down-regulation triggered changes in many physiologic parameters, indicating roles played in oxidative stress and energy metabolism. And the exact transport function of TbMCP12 was tested as follows. In order to assess the substrate(s) TbMCP12 transported, a mitochondrial ATP production assay was performed. The classical approach to determine the metabolite exchange function of MCF proteins was the *in vitro* reconstitution of natural or affinity-tag purified carrier proteins into liposomes, followed by transport assays using radiolabeled metabolites. This approach has been successful for functional characterisation of a large number of MCF proteins from mammals, yeasts, and plants (Picault et al. 2004; Palmieri 2004; Palmieri et al. 2011). However, after numerous attempts, this classical approach appeared to be unsuccessful for *T. brucei* MCF proteins (data not shown). We, therefore, decided to use an alternative approach to assessing the putative transport function of TbMCP12. This alternative approach was based on a well-established mitochondrial ATP production assay published previously by Schneider (Schneider et al. 2007; Bochud-Allemann & Schneider 2002). *Trypanosoma brucei* mitochondria-enriched pellets via digitonin-fractionation were metabolically functional and were able to synthesise ATP upon the addition of ADP and metabolic substrates (TCA-cycle intermediates) (Allemann & Schneider 2000). Mitochondrial ATP production depended on the presence of mitochondrial MCF proteins for ADP/ATP exchange (ADP import and ATP export) and the exchange of the different metabolic substrates and end products across the semi-permeable mitochondrial inner membrane (Besteiro et al. 2005). ATP production of digitonin-enriched mitochondria in the presence of different substrates was first assessed in WT (PCF449) cells. WT cells were grown in either standard or high-glucose MEM-PROS medium prior to the enrichment of mitochondria by cellular digitonin-permeabilization. Different TCA-cycle intermediates were used as metabolic substrates, including oxodicarboxylate α-ketoglutarate, dicarboxylates succinate and malate, and tricarboxylates citrate and isocitrate. The results shown in Figure 3-12 reveal that for WT PCF mitochondria the highest ATP production was found on either α-ketoglutarate or succinate as the substrate, followed thereafter by citrate and isocitrate at a lower rate. As expected, the lowest mitochondrial ATP production was found on malate as substrate

(Besteiro et al. 2005). Comparison of mitochondrial ATP production for PCF449 trypanosomes cultured on either standard (low glucose) or high-glucose MEM-PROS medium revealed no significant differences for most of the substrates analysed, with the exception of malate and isocitrate by which about 3 to 4 folds more mitochondrial ATP was produced on standard medium than on high-glucose medium (Figure 3-12).

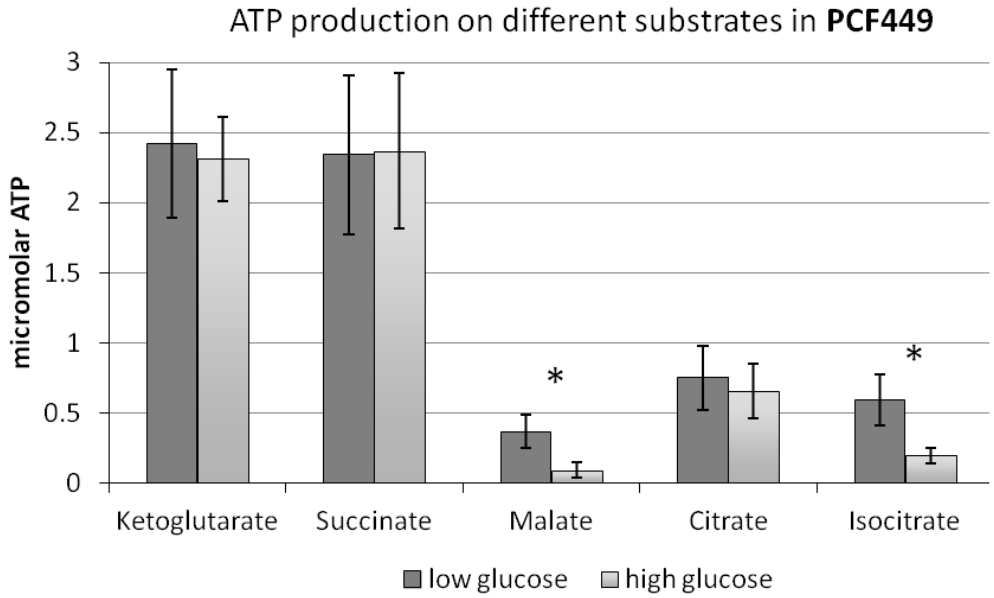

Figure 3-12 Mitochondrial ATP production on different substrates for the medium of 0.25 mM (dark grey) and 10 mM (light grey) glucose towards WT cells

Mitochondrial ATP content is presented as RLU (relative light units). The ATP amount was calculated using an ATP standard curve. Error bars added representes standard deviations in triplicates. '*' indicates the significant difference confirmed by T-test ($p<0.05$).

Mitochondrial ATP production assays were then performed using a tetracycline-induced *TbMCP12-cmyc*^{ti} (TbMCP12-overexpression) cell line cultured in standard MEM-PROS medium. The mitochondrial ATP-production was significantly increased when using tricarboxylates as substrate: on citrate a 2-fold, and on isocitrate, a 1.5-fold increase in ATP-production were observed in comparison with the corresponding ATP-production found in WT mitochondria (Figure 3-13 A). This was in contrast to the decrease of oxodicarboxylates and dicarboxylates with either a moderate decrease (i.e. 29% for succinate and 15% for α-ketoglutarate) or a major decrease (i.e. 96% for malate) in mitochondrial ATP-production. Over-expression of TbMCP12 apparently enhanced the

mitochondrial ATP-production using tricarboxylates as substrates, whereas the mitochondrial ATP-production by α-ketoglutarate or different dicarboxylates was significantly reduced depending on the substrate used.

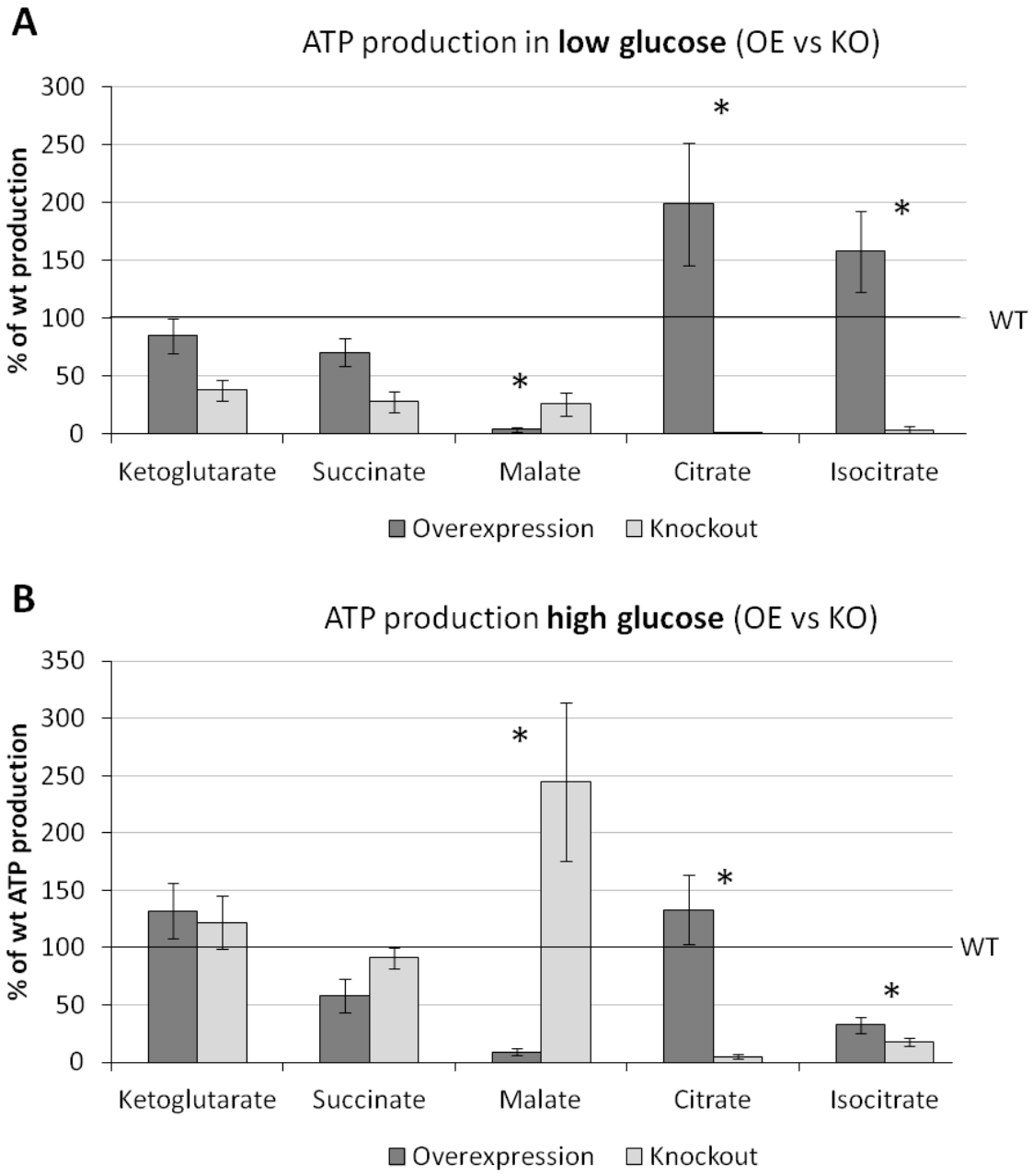

Figure 3-13 Relative mitochondrial ATP production in TbMCP12 knockout and overexpression cells

The relative mitochondrial ATP production in knockout Δ*TbMCP12/TbMCP12-cmyc*^{ti} (light grey) and overexpression *TbMCP12-cmyc*^{ti} (dark grey) cell lines are presented as percentages. WT ATP production using different substrates under low or high glucose concentrations was set to 100% respectively. '*' indicates the significance confirmed by

T test ($p<0.05$). The cells cultured in medium with 0.25 mM (A) or 10 mM of glucose (B) are shown.

Switching to high-glucose culture condition resulted in a number of major changes in mitochondrial ATP production (Figure 3-13 B). The increased mitochondrial ATP production observed earlier in cells cultured in standard (low-glucose) MEM-PROS medium and using different tricarboxylates as a substrate was not found for cells grown in high-glucose MEM-PROS medium, that is, mitochondrial ATP-production on citrate was similar to that of wildtype mitochondria. As for isocitrate however, a significant decrease (>60%) in mitochondrial ATP-production was found. Concerning α-ketoglutarate and the dicarboxylates succinate and malate, only minor or no changes in mitochondrial ATP production was found when comparing TbMCP12-overexpressing cells cultured in standard or high-glucose MEM-PROS medium (Figure 3-13 B).

Similar mitochondrial ATP-production assays were performed with mitochondria-enriched fractions obtained from the non-induced Δ*TbMCP12/TbMCP12-cmyc*^{ti} (TbMCP12-depletion) cell line in standard medium, the result of which revealed substantial changes in the ATP-producing capacity of its mitochondrion. Most strikingly, the >99% ablation of mitochondrial ATP-production was found using either citrate or isocitrate as a substrate (Figure 3-13 A). Additionally, major decreases in mitochondrial ATP-production were found on other analysed carboxylates: on succinate and malate, a major decrease (about 75%) was observed, whereas mitochondrial ATP production decreased by about 60% on α-ketoglutarate (Figure 3-13 A).

Comparison of these results with those obtained from cells cultured in high-glucose MEM-PROS medium also revealed a number of major changes in mitochondrial ATP production when switching between culture media (Figure 3-13 B). The significantly reduced mitochondrial ATP production observed earlier in TbMCP12-depleted cells Δ*TbMCP12/TbMCP12-cmyc*^{ti} cultured in the standard medium using α-ketoglutarate, succinate or malate as a substrate, was not found in high-glucose MEM-PROS medium cultured cells. Instead, mitochondrial ATP-production on α-ketoglutarate or succinate was similar to that of wildtype mitochondria, whereas on malate a significant increase (2.5 folds) in mitochondrial ATP-production was observed. Mitochondrial ATP production on citrate or isocitrate remained minor or non-existing, independent of the

culture medium used. The results were also summarised in Table 3-1 for a clearer view. Also, the values of ATP produced by each substrate and cells (μM) were listed in Table 3-2 as a reference.

Table 3-1 Summary of mitochondrial ATP production of TbMCP12 overexpression and knockout cells under both low glucose and high glucose conditions

Carboxylates		*TbMCP12-cmyc^{ti}*		Δ*TbMCP12/TbMCP12-cmyc^{ti}*	
		Low Glu	High Glu	Low Glu	High Glu
Tri-	citrate	199 ± 53%	133 ± 30%	0.3 ± 0.4%	5 ± 2 %
	isocitrate	158 ± 35%	33 ± 7%	3.7 ± 2.8%	18 ± 4%
Di-	succinate	71± 12%	58 ± 15%	28 ± 9%	91 ± 9%
	malate	4 ± 2%	9 ± 3%	26 ± 10%	245 ± 69%
Oxo-	α-ketoglutarate	85 ± 15%	132 ± 24%	38 ± 9%	122 ± 23%

Percentages of TbMCP12 overexpressing and knockout cells are shown in the table above calculated by comparing experimental data with corresponding WT data. *TbMCP12-cmyc^{ti}*: overexpression cells, Δ*TbMCP12/TbMCP12-cmyc^{ti}*: knockout cells, Low Glu: low glucose condition (standard medium). High Glu: high glucose medium.

Table 3-2 ATP produced on the addition of different substrates by mitochondria from different cells

Carboxylates		*TbMCP12-cmyc^{ti}*		Δ*TbMCP12/TbMCP12-cmyc^{ti}*		**WT**	
		Low Glu	High Glu	Low Glu	High Glu	Low Glu	High Glu
Tri-	citrate	84915 ±22616	51964 ±11721	128 ±188	1954 ±781	42671 ±19845	39071 ±13901
	isocitrate	53720 ±11900	3850 ±1517	1579 ±952	2100 ±467	34000 ±13077	11667 ±3215
Di-	succinate	52398 ±8856	92800 ±24000	20664 ±6642	145600 ±14400	73800 ±21334	160000 ±32026
	malate	530 ±265	489 ±163	3445 ±1325	13299 ±3745	13250 ±11600	5428 ±2765
Oxo-	2-oxoglutarate	70833 ±12500	196680 ±35760	31667 ±7500	181780 ±34270	83333 ±23949	149000 ±27225

Values of mitochondrial ATP production (μM) using different substrates are presented in the table. *TbMCP12-cmyc^{ti}*: overexpression cells, Δ*TbMCP12/TbMCP12-cmyc^{ti}*: knockout cells, Low Glu: low glucose condition (standard medium) and High Glu: high glucose medium.

The citrate analogue 1,2,3-benzenetricarboxylic acid (BTA) was a semi-competitive inhibitor of mitochondrial citrate transport, and was previously shown to specifically

inhibit mammalian and yeast mitochondrial citrate carriers (Infantino et al. 2011; Kajimoto et al. 2005) as well as di/tricarboxylate carriers from plants (Day et al. 2013). Mitochondrial ATP production assays were conducted with mitochondria-enriched fractions derived from PCF449, which were cultured in standard MEM-PROS medium, and in the presence of different concentrations of BTA. The results illustrated that mitochondrial ATP production with citrate as substrate was completely ablated in the presence of 7 mM BTA (Figure 3-14). Regarding isocitrate and malate, significant decreased (around 50%) mitochondrial ATP production was also observed upon the addition of BTA. This was in contrast to succinate, on which no inhibition was found, and to 2-oxoglutarate, on which a remarkable increase in mitochondrial ATP production instead of the expected decrease was observed in the presence of 6.4 mM BTA. Assays performed in the presence of higher BTA concentrations (up to 15 mM) resulted not only in a further decrease in mitochondrial ATP production on isocitrate and malate but also in a decreased mitochondrial ATP production on succinate (data not shown). The BTA experiment indicates that malate, citrate, isocitrate and aconitate were imported into mitochondria with the same transporter as citrate. In other words, TbMCP12 is very likely to transport tricarboxylates citrate, isocitrate and aconitate, as well as malate.

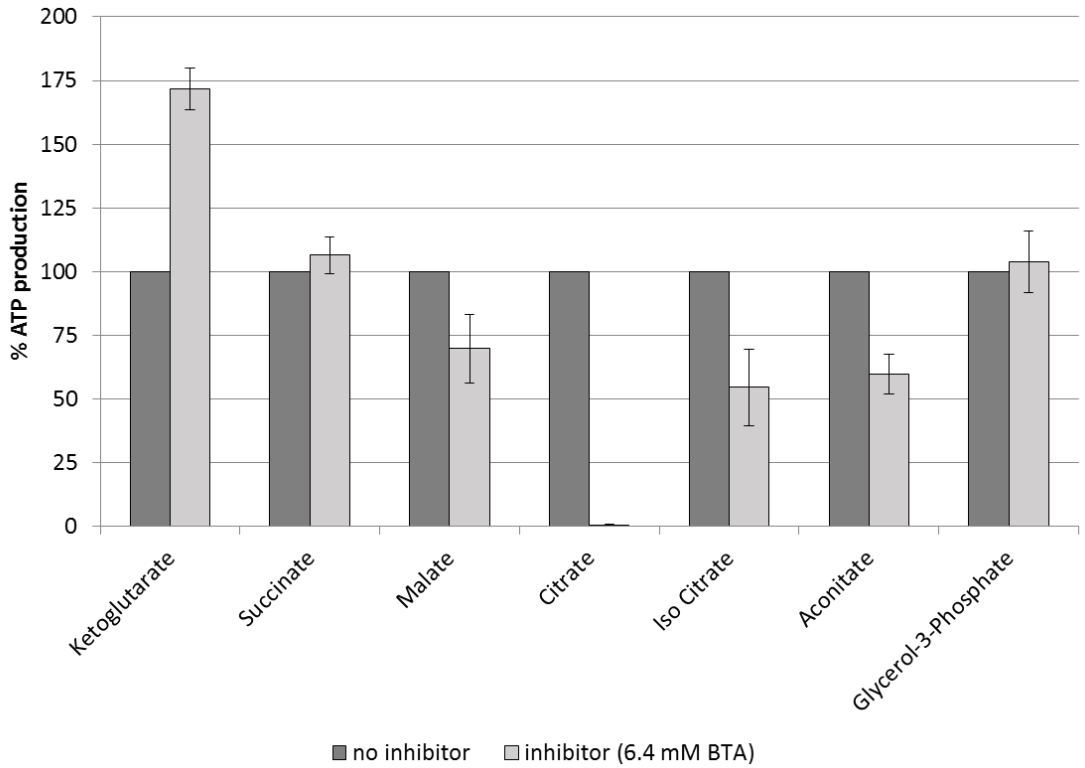

Figure 3-14 Inhibition of mitochondrial ATP production with the citrate carrier specific inhibitor 1,2,3-benzenetricarboxylic acid (BTA)

The bar chart demonstrates percentages of mitochondrial ATP production on different substrates measured with (dark grey) or without (light grey) the citrate analogue BTA. ATP produced on different substrates without BTA is presented as 100%. ATP produced with BTA is shown after adjustment to percentages using the same scale.

In conclusion, the mitochondrion from WT cells produced a similar amount of ATP under both low and high glucose conditions, with the exception of malate and isocitrate by which a significant decrease of ATP production was observed in high glucose medium. TbMCP12 overexpression helped to increase mitochondrial ATP production with the presence of tricarboxylates, especially citrate. Also, significant decreases of ATP production on citrate and isocitrate were observed in TbMCP12 KO Δ*TbMCP12/TbMCP12-cmyc*^{ti} cells. The addition of citrate inhibitor BTA led to a complete ablation of mitochondrial ATP production with the presence of citrate, indicating the expression of ATP totally relied on citrate transport. These results strongly suggest that TbMCP12 transported tricarboxylates citrate and isocitrate.

3.9 TbMCP12 rescued yeast ΔDIC cell growth

In order to obtain direct evidence for TbMCP12 as a carboxylate carrier, yeast dicarboxylate carrier DIC depleted strain ΔDIC was used to heterologously express TbMCP12, and the growth phenotype was measured. According to Palmieri et al, DIC transported malate and succinate with phosphate, and DIC depleted strain could grow on glucose medium but not on acetate (Palmieri et al. 1999). From the result gathered in this study (Figure 3-15 A&B), the same phenotype as described in the above literature was observed: ΔDIC presented no growth difference, compared with WT strain (the parental strain of ΔDIC) on glucose medium (Figure 3-15 A). Whereas, on acetate medium, DIC depleted yeast strain showed a decreased (about 31%) growth (Figure 3-15 B), and the remaining growth was most likely to be driven by succinate-fumarate carrier SFC. SFC was found in yeast mitochondrial membrane to transport cytosolic succinate into yeast mitochondria in exchange for fumarate, and it could also transport α-ketoglutarate and tricarboxylates such as citrate, isocitrate and cis-aconitate (Fernandez et al. 1993; Palmieri et al. 1997; Palmieri et al. 1999). When TbMCP12 was introduced into ΔDIC cell line (ΔDIC+TbMCP12), growth on glucose medium remained the same as WT or

ΔDIC, while recombinant expression of TbMCP12 in the ΔDIC yeast strain restored growth to 73% of WT levels on acetate as a carbon source (Figure 3-15 B). The restoration of growth was not 100%, which was possibly due to lower efficiency of mitochondrial targeting of heterologous TbMCP12, lower expression levels or decreased transport efficiency. At the same time, PCR with total DNA from the mentioned three yeast strains was performed as a control (Figure 3-15 C). No *DIC* genomic DNA was found in ΔDIC strain, with *DIC* present in WT strain. TbMCP12 presented in ΔDIC+TbMCP12 strain but no other strains.

This heterologous TbMCP12 expression and rescue of growth defect caused by DIC depletion in the yeast strain revealed that TbMCP12 could complement the transport function DIC.

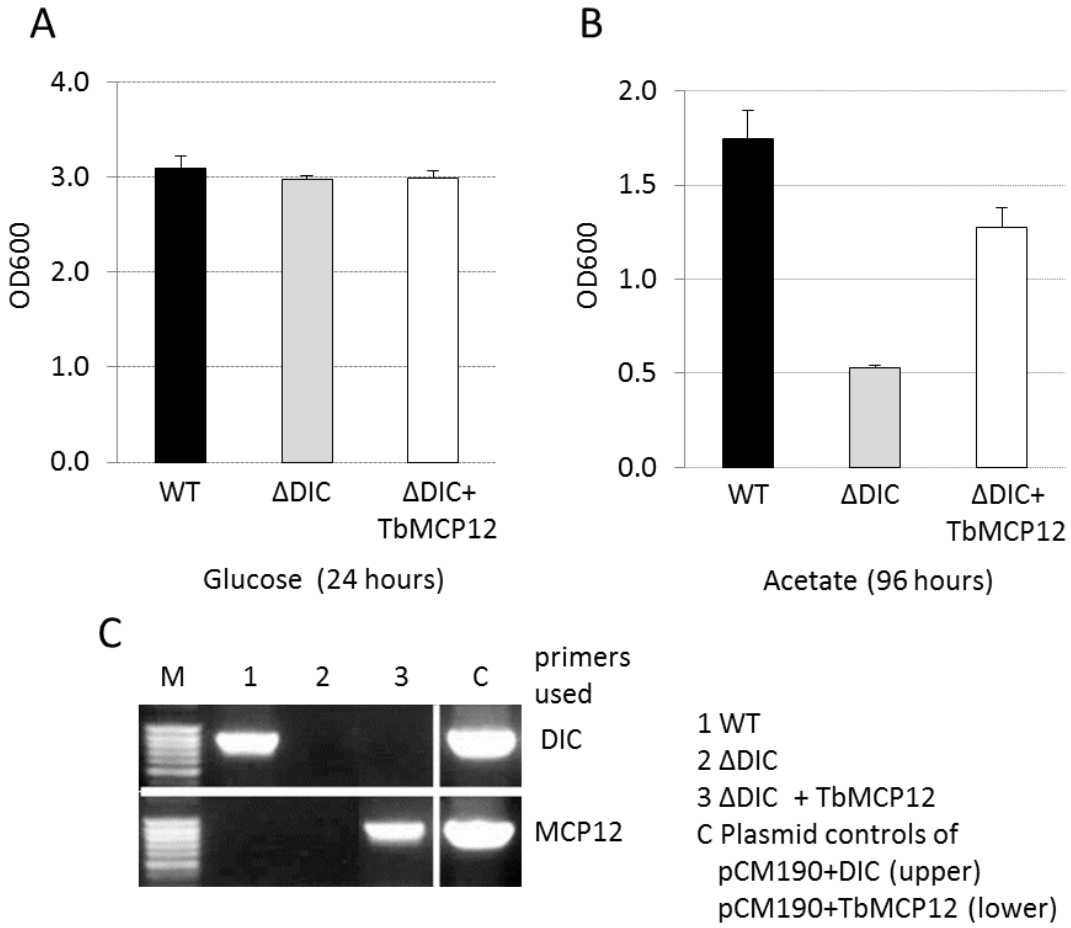

Figure 3-15 TbMCP12 rescued cell growth of DIC depleted cell line
WT *S. cerevisiae* strain BY4741 contained empty pCM190 (URA) yeast expression vector. DIC deficient (ΔDIC) yeast strain contained either empty pCM190 vector or pCM190 vector with the TbMCP12 open reading frame. Protein expression was induced by withdrawal of tetracycline. The growth of three described cell lines is presented above as OD600 in glucose medium (A) or acetate medium (B) cultured for 24 hours or 96 hours, respectively. The correctness of mentioned plasmids is demonstrated in C.Control PCR of total DNA (genomic and plasmid DNA) isolation from yeast using TbMCP12 and DIC primers were performed. M stands for the DNA marker (MassRuler), 1 to 4 are DNA isolated from 4 yeast strains, C refers to controls using corresponding plasmids.

3.10 Discussion

In the discussion part, the main findings of TbMCP12 were summarised. The relation between TbMCP12 and redox balance, and physiological role(s) TbMCP12 might play were discussed.

3.10.1 TbMCP12 is a mitochondrial di/tricarboxylate carrier

In this chapter, TbMCP12 characterisation was performed in order to answer four questions: (i) whether the gene is indispensable; (ii) how TbMCP12 is regulated; (iii) what physiological roles TbMCP12 play; (iv) what TbMCP12 transports.

First of all, the essentiality of TbMCP12 in cell growth was tested in both knockout cells (conditional double knockout Δ*TbMCP12/TbMCP12-cmyc*^{ti} and TbMCP12 RNAi) and overexpression cells (with and without myc tag). *TbMCP12-cmyc*^{ti} over-expression cells resulted in growth defect, especially in high glucose condition. However, TbMCP12 over-expression with open reading frame only (*TbMCP12-ORF*^{ti}) did not affect cell growth. Δ*TbMCP12/TbMCP12-cmyc*^{ti} cells (without the addition of tetracycline) and the *TbMCP12-cmyc*^{ti} cells presented no growth defect under varying glucose conditions, and a similar result was found using TbMCP12 RNAi cells. This was unexpected since TbMCP12 conventional double knockout was not achievable without the inducible rescue copy. Apart from this, similar levels of TbMCP12 ORF proteins were detected in the presence and absence of tetracycline in all three over-expressing *TbMCP12-ORF*^{ti} clones, indicating the possibility of the loss of control with the tet-operon system. This loss of control is not exclusive, but quite common in *Trypanosoma brucei,* especially when a gene plays a critical role or a regulatory role. The similar phenomenon was found in TbMCP17, TbSFNX and TbMCP23 RNAi cell line using the same plasmid (see following chapters). This loss of control could explain the Δ*TbMCP12/TbMCP12-cmyc*^{ti} results: the background level of TbMCP12-cmyc proteins in tetracycline-removal cells helped to maintain cell growth, and in TbMCP12 RNAi cells, the remaining endogenous TbMCP12 was enough too. The overexpression of TbMCP12-cmyc was detrimental to cell growth which was probably because c-terminal myc interfered with protein-protein

cross-talk (Clayton 2002) or because the overload of TbMCP12-cmyc proteins was detrimental to the cells. This defect was compromised in Δ*TbMCP12/TbMCP12-cmyc*^{ti} cells because the endogenous TbMCP12 was completely removed. Taken together, the growth phenotype experiments indicates that TbMCP12 level is tightly controlled.

Secondly, the regulators of TbMCP12 were tested. Up-regulation of TbMCP12 protein level was found when heme was re-introduced to the medium compared with heme depleted medium. This upregulation was possibly a response to oxidative stress caused by iron through Fenton reactions (Ponka 1999; Ryter & Tyrrell 2000; Bresgen & Eckl 2015). Also, the switch from low to high glucose medium resulted in an upregulation of TbMCP12, which was related to the switch of metabolic pathways. The protein level of TbMCP12 was also upregulated by oxidative stress caused by H_2O_2 treatment. This upregulation of TbMCP12 protein level was further associated with a decreased $NADP^+$/NADPH ratio under high glucose condition, indicating that under oxidative stress, TbMCP12 is upregulated and NADPH production is increased to fight against ROS. Also, cellular aconitase and NADPH-isocitrate dehydrogenases mRNA levels were upregulated refering the involvement of those enzymes. The cytosolic NADPH is predominately and redundantly produced by pentose phosphate pathway (PPP) as well as malic enzymes in PCF under low glucose condition (Allmann et al. 2013). As discussed later in Section 3.10.3, TbMCP12 OE (*TbMCP12-cmyc*^{ti}) under low glucose condition promoted the export of malate, providing the substrate for malic enzymes and PPP, thus increased NADPH production. On the other hand, in the *TbMCP12 RNAi* cell line, less malate was imported to the cytosol, leading to less generation of cytosolic NADPH besides the NADPH generated in PPP and malic enzyme reactions required for the oxidative stress response.

The results of mRNA and protein being compared, differences were found, suggesting that TbMCP12 is post-transcriptionally regulated in addition to mRNA level regulation. Post-transcriptional regulation is fairly common in trypanosomatids (De Gaudenzi et al. 2011) due to the polycistronic transcription, which is followed by *trans*-splicing and polyadenylation reactions to generate individual mRNA (Martínez-Calvillo et al. 2003; Liang et al. 2003). Moreover, mRNA stabilisation and turnover mechanisms have been found in life cycle specific gene regulation (Haile & Papadopoulou 2007). In addition,

mRNA of TbMCP12 was suggested to be regulated by post-transcriptional operons to cope with oxidative stress (Ouellette & Papadopoulou 2009) with the help of RNA binding proteins (RBPs) (Fernández-Moya & Estévez 2010; Kramer et al. 2012). The evidence supports the possibility of post-transcriptional regulation of TbMCP12.

Thirdly, the transport function of TbMCP12 was examined using both mitochondrial ATP production assay and yeast functional complementation. In order to interpret ATP production results, the criteria for ATP production using this assay are discussed below. First of all, ATP/ADP carrier is essential for importing ADP into the mitochondria and exporting produced ATP. Next, substrate transporter needs to be functional to import the added metabolites into the mitochondria. Furthermore, if the carrier is functional as a co-transporter or counter-transporter, the cofactors or counter-transport metabolite has to be available (generated in the mitochondrial pathways starting with the added substrate). Also, the activities of enzymes for generating ATP are required. Additionally, if ATP is produced by oxidative phosphorylation through electron transport chain, the mitochondrial membrane potential is required. On the other hand, ATP generated through substrate level phosphorylation which is catalysed by either succinyl-CoA synthetase (SCoAS) or acetate:succinate CoA transferase (ASCT cycle). Finally, if ATP is generated through ASCT cycle, succinate has to be provided in addition to the testing substrate.

Mitochondrial ATP production with different substrates using mitochondria isolated from WT cells, TbMCP12 OE (*TbMCP12-cmyc*^{ti}) cells and TbMCP12 KO (Δ*TbMCP12/TbMCP12-cmyc*^{ti}) cells are summarised in Figure 3-16.

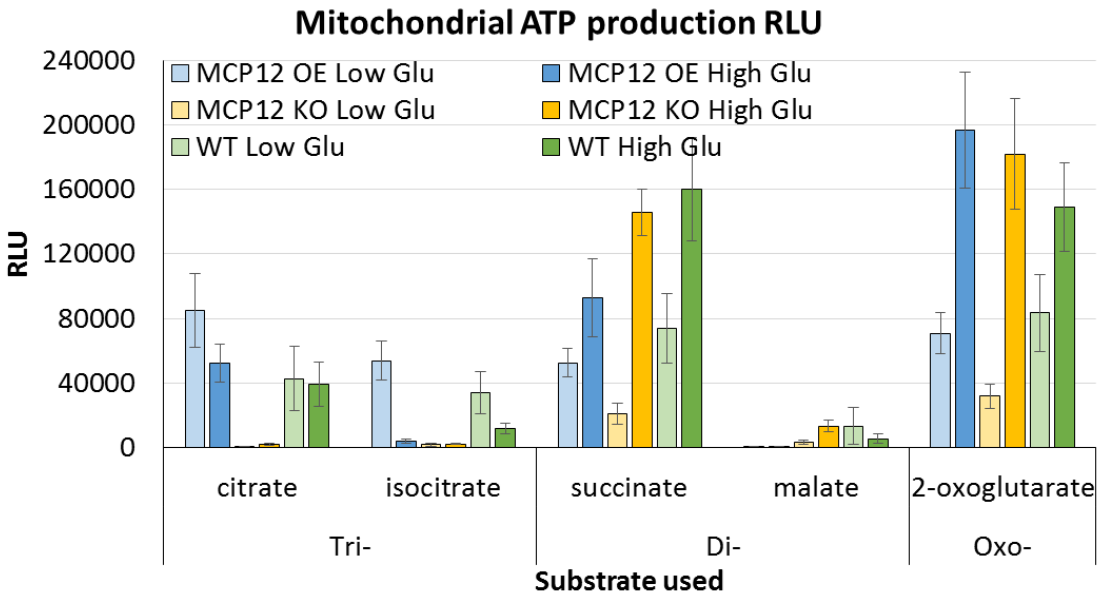

Figure 3-16 Summary bar chart of mitochondrial ATP production shown in RLU

The same amount of mitochondria (25µl of prepared fractions per reaction) was used in various substrates with cells cultured under both low and high glucose conditions. TbMCP12 OE (*TbMCP12-cmyc*^{ti}, blue), TbMCP12 KO (Δ*TbMCP12/TbMCP12-cmyc*^{ti}, yellow) and WT (green), with low glucose are shown in light color and high glucose in dark color. RLU stands for relative light unit.

As for the addition of α-ketoglutarate to mitochondria fractions, the majority of ATP production was substrate phosphorylation converting succinyl- CoA to succinate (Figure 3-17, Schneider et al. 2007). When comparing the ATP produced from low and high glucose conditions, high glucose presented an increase of ATP production around 2-3 folds, suggesting an increase in enzyme activities (α-ketoglutarate dehydrogenase and succinyl-CoA synthetase) or an upregulated transporter activity. Under high glucose condition, all three strains presented similar ATP productions. Mitochondria from parasites cultured in low glucose, however, produced the same amount of ATP by WT and *TbMCP12-cmyc*^{ti} cells, but Δ*TbMCP12/TbMCP12-cmyc*^{ti} halved. The decrease of ATP from Δ*TbMCP12/TbMCP12-cmyc*^{ti} could be interpreted by (i) one of the transporters TbMCP12 for α-ketoglutarate was depleted; (ii) the activities of enzymes mentioned above were down-regulated by TbMCP12 knockout. Furthermore, no difference of ATP produced from *TbMCP12-cmyc*^{ti} and WT unveiled that TbMCP12 transport function was not the rate-limiting step of ATP production. Thus, it can be concluded that TbMCP12 is at least one of the transporters for α-ketoglutarate.

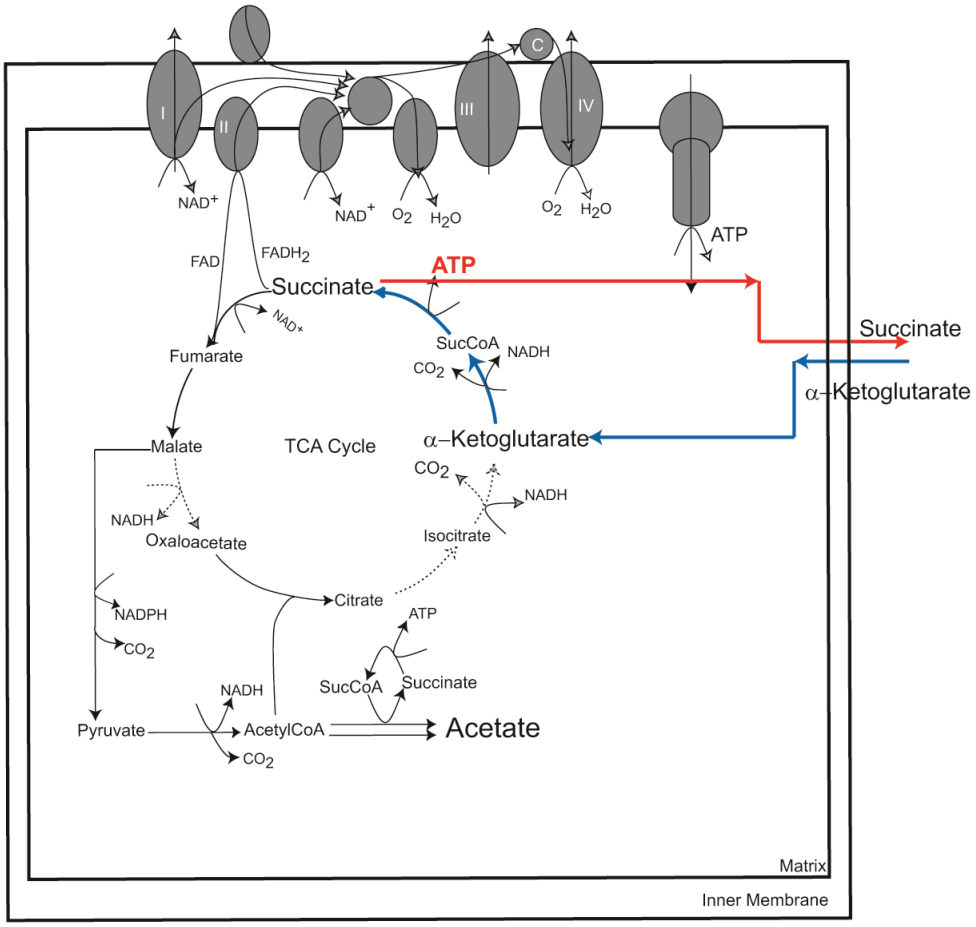

Figure 3-17 Scheme of α-ketoglutarate promoted ATP production in isolated mitochondria

Blue lines indicate the imported flow of substrate generate ATP, red lines represent the 'end/export' product flow. ATP generated by the provided substrate are highlighted in red. NB. Only the related reactions are shown and simplified as ATP, NADPH, NADP and CO_2.

When using the two tested tricarboxylates citrate and isocitrate as substrates, the ATP produced is most likely derived from 'citrate-isocitrate-α-ketoglutarate' that leads to succinyl-CoA and succinate. The ATP produced on citrate and isocitrate is the same as the substrate-level ATP produced by the addition of α-ketoglutarate (Figure 3-18). First of all, results under low glucose condition were analysed. In WT cells, ATP produced on citrate or isocitrate was 50% of WT α-ketoglutarate data, suggesting the route from citrate/isocitrate to α-ketoglutarate is at a limited speed, which is consistent with literature (van Hellemond et al. 2005; van Weelden et al. 2005; Tielens & van Hellemond 2009). In Δ*TbMCP12/TbMCP12-cmyc*^{ti} cells, the citrate and isocitrate ATP production was completely ablated, strongly indicating that TbMCP12 depletion removed the only citrate/ isocitrate transporter. Similarly, in *TbMCP12-cmyc*^{ti} cells, ATP production

doubled compared with WT, and the value was the same as α-ketoglutarate, suggesting TbMCP12 over-expression compensated the low activity from citrate/isocitrate to α-ketoglutarate which boosted ATP production on citrate to the level on α-ketoglutarate. This compensation of ATP production potentially came from (i) the enhancement of related enzyme activities by TbMCP12 over-expression; (ii) more citrate/isocitrate in mitochondria imported by *TbMCP12-cmyc*^{ti}. When it moved to high glucose condition, complete inhibition of ATP production of Δ*TbMCP12/TbMCP12-cmyc*^{ti} cells was observed, confirming the indispensable role TbMCP12 played in citrate and isocitrate transport. *TbMCP12-cmyc*^{ti}, on the other hand, failed to demonstrate a significant increase in ATP production on citrate, and a decrease of ATP production on isocitrate was observed. This suggests that under high glucose condition, the metabolic flow from citrate to isocitrate and further to α-ketoglutarate is downregulated, especially the isocitrate dehydrogenase activity is repressed.

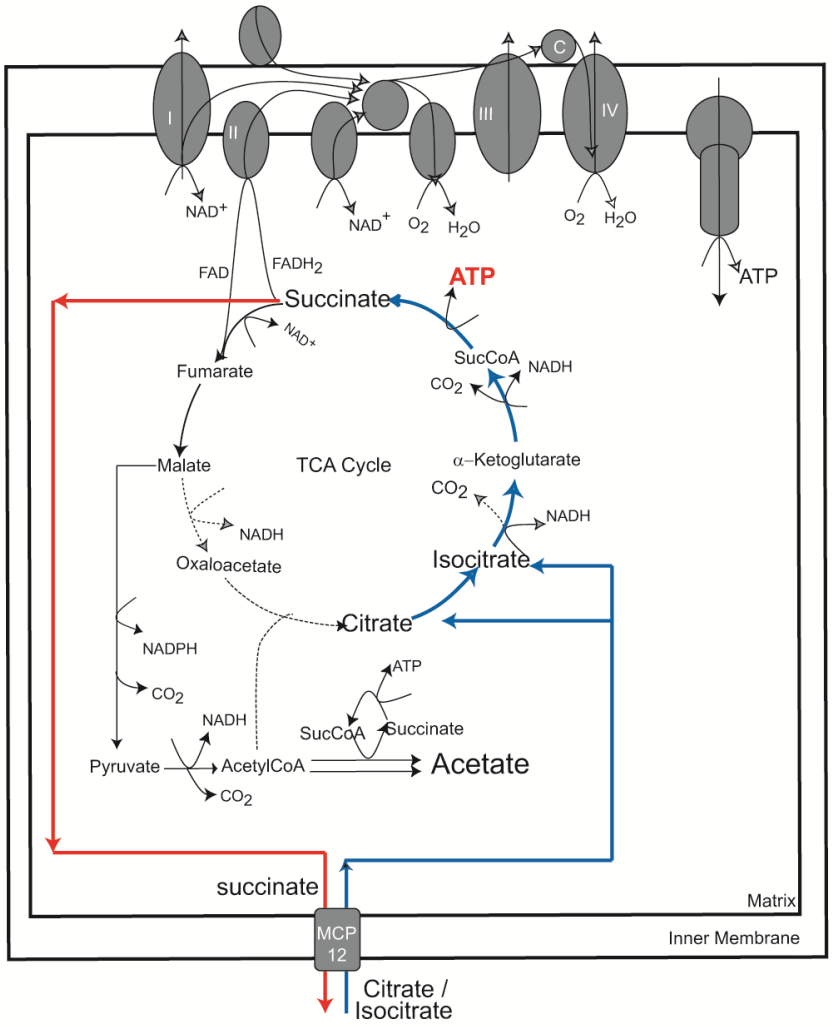

Figure 3-18 Scheme of citrate or isocitrate promoted ATP production in isolated mitochondria (legends see Figure 3-17)

When it came to succinate, TbMCP12 was likely involved in ATP production indirectly. Basically, during the process of succinate converting to fumarate, an ATP is produced by oxidative phosphorylation through electron transport chain. And here fumarate or malate can be counter-transported (if necessary). In high glucose media, *TbMCP12-cmyc*^{ti}, Δ*TbMCP12/TbMCP12-cmyc*^{ti} and WT all presented a relatively high ATP production (Figure 3-19), suggesting that TbMCP12 is not involved in succinate transport, or at least not the only transporter for succinate. Under low glucose condition, on the other hand, Δ*TbMCP12/TbMCP12-cmyc*^{ti} presented a 2/3 decrease in ATP production. Combining the high and low glucose results together, TbMCP12 is suggested to be involved in the change of redox balance. Hence it associates with the electron transport chain activity to regulate succinate-related ATP production, but not the transport function directly.

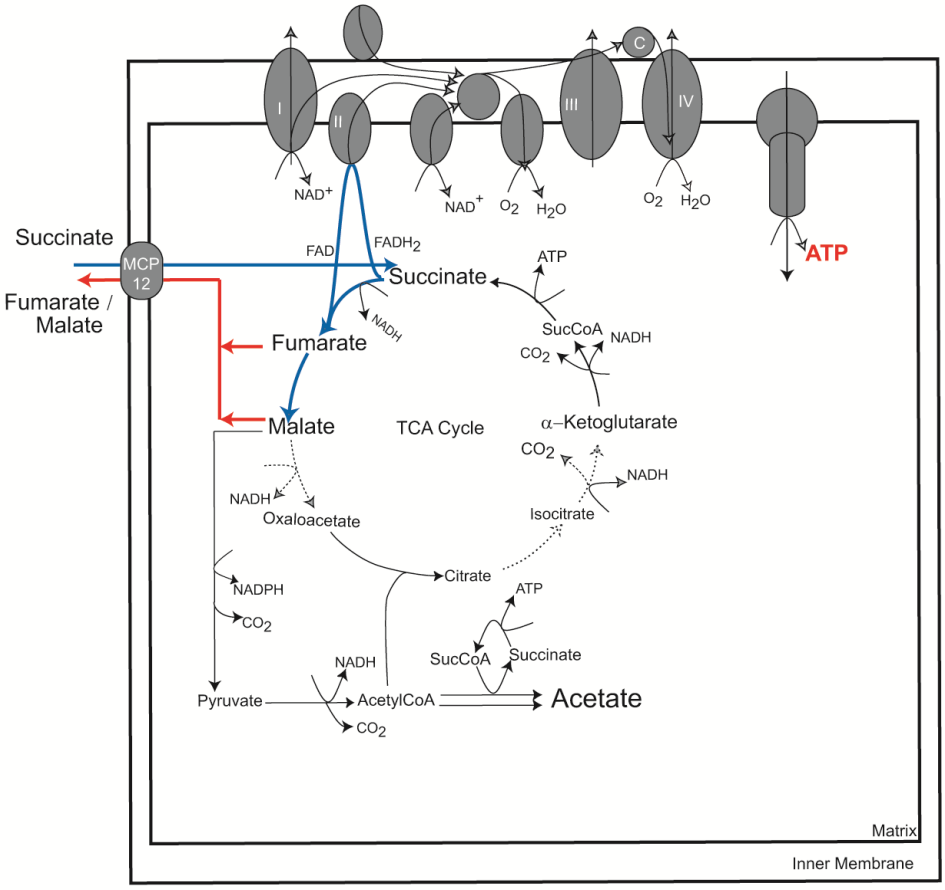

Figure 3-19 Scheme of succinate promoted ATP production in isolated mitochondria (legends see Figure 3-17)

When another dicarboxylate malate was added to the isolated mitochondria, minor ATP was detected for all three cell lines under both high and low glucose conditions. As presented in the metabolic pathways (Figure 3-20), the only way that malate can produce ATP is to convert to pyruvate, further to acetyl-CoA, followed by the ASCT cycle that produces acetate with the recycle of succinate and succinyl-CoA. However, as no succinate was supplemented, the reaction could not go on, thus no ATP was produced. Subsequently, whether TbMCP12 can transport fumarate is in doubt.

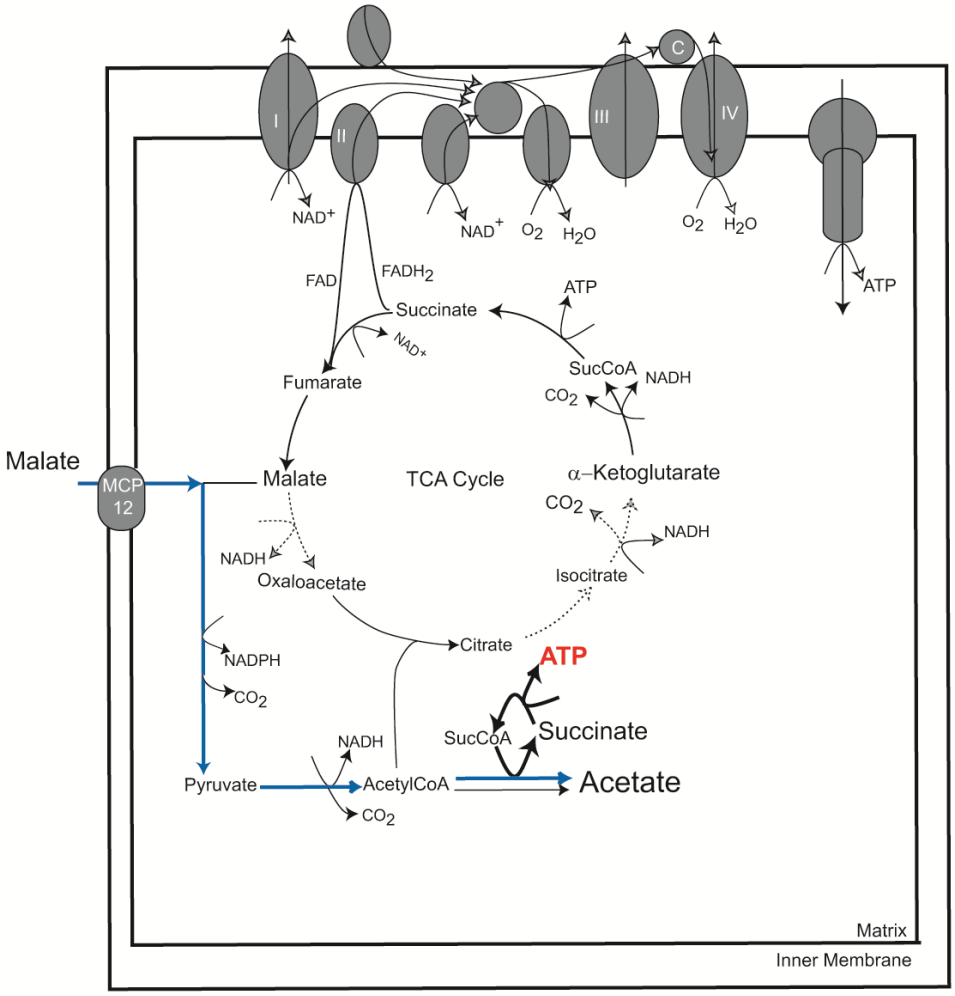

Figure 3-20 Scheme of malate promoted ATP production in isolated mitochondria (legends see Figure 3-17)

In summary, mitochondrial ATP production assay clearly showed that TbMCP12 transports tricarboxylates citrate and isocitrate. α-ketoglularate and succinate related ATP production is also regulated by TbMCP12 level, but TbMCP12 is not the sole transporter

for these two. Also, whether the transport mechanism for TbMCP12 is an exchanger, uni-direction or co-importer remains to be tested.

Apart from work done in *Trypanosoma brucei,* yeast dicarboxylate carrier DIC depleted cell line (ΔDIC) was induced to express heterologous TbMCP12, and a growth restore on acetate medium was found. This successful complementation of yeast growth defect caused by DIC in non-fermentable medium (Palmieri et al. 1999) added strong evidence to TbMCP12 as a yeast dicarboxylate carrier. In other words, TbMCP12 can restore the function of DIC to exchange dicarboxylates (malate and succinate) with phosphate.

Some plant di/tricarboxylate (DTC) carriers are shown to transport all of these substrates. Like maize CiC, the DTCs are capable of transporting both dicarboxylates (such as oxoglutarate, oxaloacetate, malate, succinate, maleate, malonate, and oxoadipate) and tricarboxylates (such as citrate, isocitrate, cis-aconitate, and trans-aconitate) (see Dolce et al. 2014 for review). Furthermore, genome analysis (Colasante, unpublished data) suggests that TbMCP12 is most probably the only *T. brucei* dicarboxylate and/or tricarboxylate carrier. No other CIC, SFC or DIC homologues are found in *T. brucei* genome database (unless very divergent in sequence). Therefore, it's very likely that TbMCP12 is a DTC.

3.10.2 TbMCP12 and oxidative stress

Under glucose-depleted condition, NADPH homoeostasis relies on the malic enzyme and pentose phosphate pathway fed by gluconeogenic flux (Allmann et al. 2013). Under high glucose condition, energy is mainly produced at glycolysis level, and NADPH was generated via an alternative route: cytosolic aconitase/ isocitrate dehydrogenase (IDH) reaction. The upregulation of TbMCP12 expression increased the citrate exported and led to the upregulation of cytosolic aconitase and cyto-IDH (Chapter 3.6). So far, nothing is known about IDHs in *T. brucei*. However, this was studied in *T. cruzi*, which carried 2 IDHs, one processing a mitochondrial targeting signal, the other a glycosomal targeting signal. Importantly, the *T. cruzi* study showed that glycosomal IDH could also be found in cytosol (dual location of glycosomal IDH). *Trypanosoma cruzi* contains two different aconitases: cytosolic c-aconitase and mitochondrial m-aconitase. *T. brucei* genome also

contains two IDH genes, the protein sequence and targeting signal of which are similar to those of *T. cruzi* IDHs. Because the targeting signals are similar, a similar glycosomal and cytosolic location for the "glycosomal" IDH in *T. brucei* is assumed. The overall majority of trypanosomal aconitase activity was cytosolic, whereas limited role was found of mitochondrial aconitase. Knockout of mitochondrial aconitase had no effect on growth and cellular metabolism with a significant accumulation (90-fold) of citrate (van Weelden et al. 2003). More importantly, it was presented that the export of mitochondrial citrate was not used for lipid biosynthesis (usually requiring citrate and NADPH) in *Trypanosoma brucei*, but alternative acetate pathway was used instead (Rivière et al. 2009). Therefore, citrate and aconitase are suggested to play a role in cytosolic NADPH synthesis. Accordingly, TbMCP12-dependent mitochondrial citrate export may play a role in cellular oxidative stress response.

3.10.3 TbMCP12 and energy metabolism

In this chapter, four metabolic conditions were tested: TbMCP12 OE (*TbMCP12-cmyc*^{ti}) and KO (Δ*TbMCP12/TbMCP12-cmyc*^{ti}) under both high and low glucose culture conditions. The functional evidence of TbMCP12 was used to discuss the roles it plays under certain conditions one by one.

Under low glucose condition, Δ*TbMCP12/TbMCP12-cmyc*^{ti} consumed a similar amount of proline, and the content of two products succinate and acetate were the same. However, TbMCP12 depletion stopped malate derived from proline which was exported from mitochondria, therefore, no NADPH was produced in the cytosol (Figure 3-21). This finding was consistent with the increase of $NADP^+$/NADPH ratio. On the other hand, when Δ*TbMCP12/TbMCP12-cmyc*^{ti} was cultured under high glucose condition, the same amount of proline was consumed, with a minor increase of glucose consumption compared with WT (Figure 3-22). The introduction of glucose into Δ*TbMCP12/TbMCP12-cmyc*^{ti} cells helped to retain the $NADP^+$/NADPH ratio using mainly pentose phosphate pathway or mitochondrial malic enzyme converting glucose-derived malate to pyruvate so as to generate NADPH. As for the slight increase in glucose consumption, the similar production of succinate and acetate was acceptable as experimental errors.

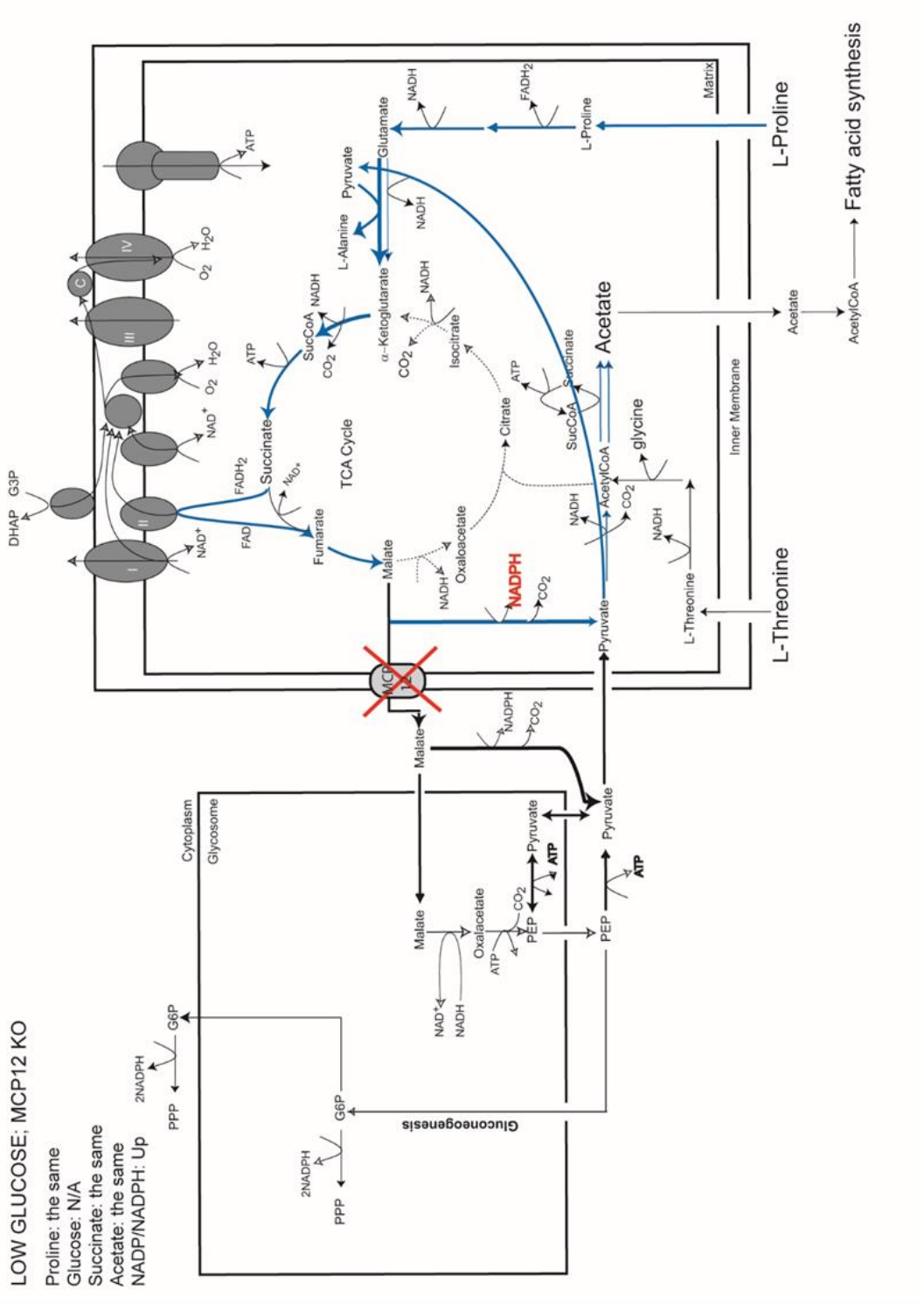

Figure 3-21 Simplified schematic representation of the carbon flux in TbMCP12 knockout cells under low glucose condition

Proline metabolism pathways are coloured in blue. Available NADPH production is highlighted in red. TbMCP12 is labelled and the red cross represents for depletion. Experimental results of metabolic contents (proline, glucose, succinate and acetate) were compared with WT cells of the same condition. 'The same' means that the same amount of content or value was found as WT. 'N/A' stands for not applicable, here glucose measurement not applicable under low glucose conditions. 'Up' indicates values higher than WT and 'down' suggestes that the examined value was lower than WT. Unrelated

substrates for gluconeogenesis (glycerol and glyceraldehyde 3-phosphate) were not shown.

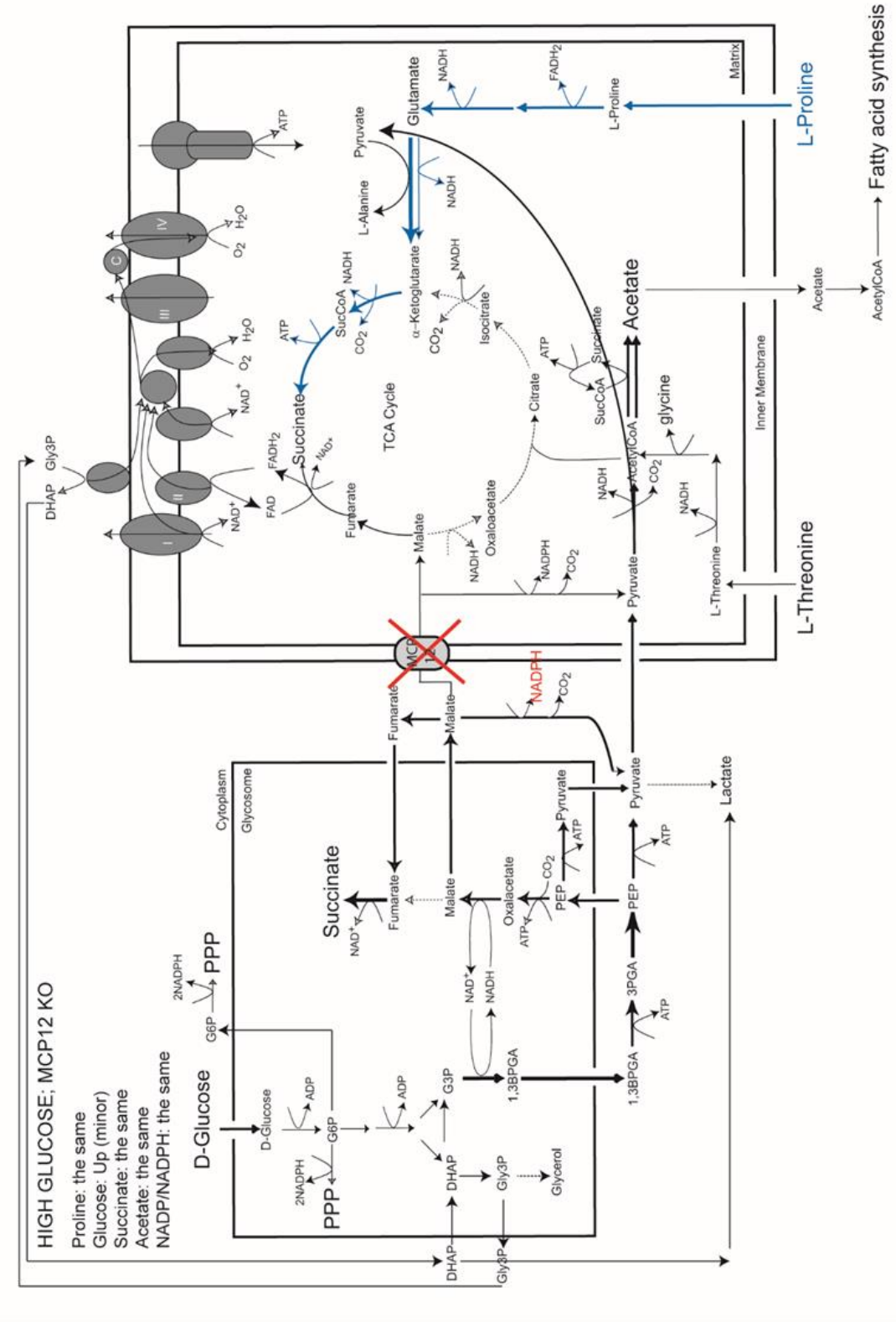

Figure 3-22 Simplified schematic representation of the carbon flux in TbMCP12 knockout cells under high glucose conditions

Figure legends are shown in Figure 3-21. 'Minor' in the brackets means the change of the contents was relatively small.

When it came to TbMCP12 over-expression cells (*ΔTbMCP12/TbMCP12-cmyc*^{ti}), the energy metabolism was shifted. Under low glucose condition (Figure 3-23), proline consumption and succinate production stayed the same as WT, suggesting a similar energy metabolism on TbMCP12 over-expression and WT. This finding was in consistent with the results of similar $NADP^+$/NADPH ratio and baseline TbMCP12 protein level under low glucose condition.

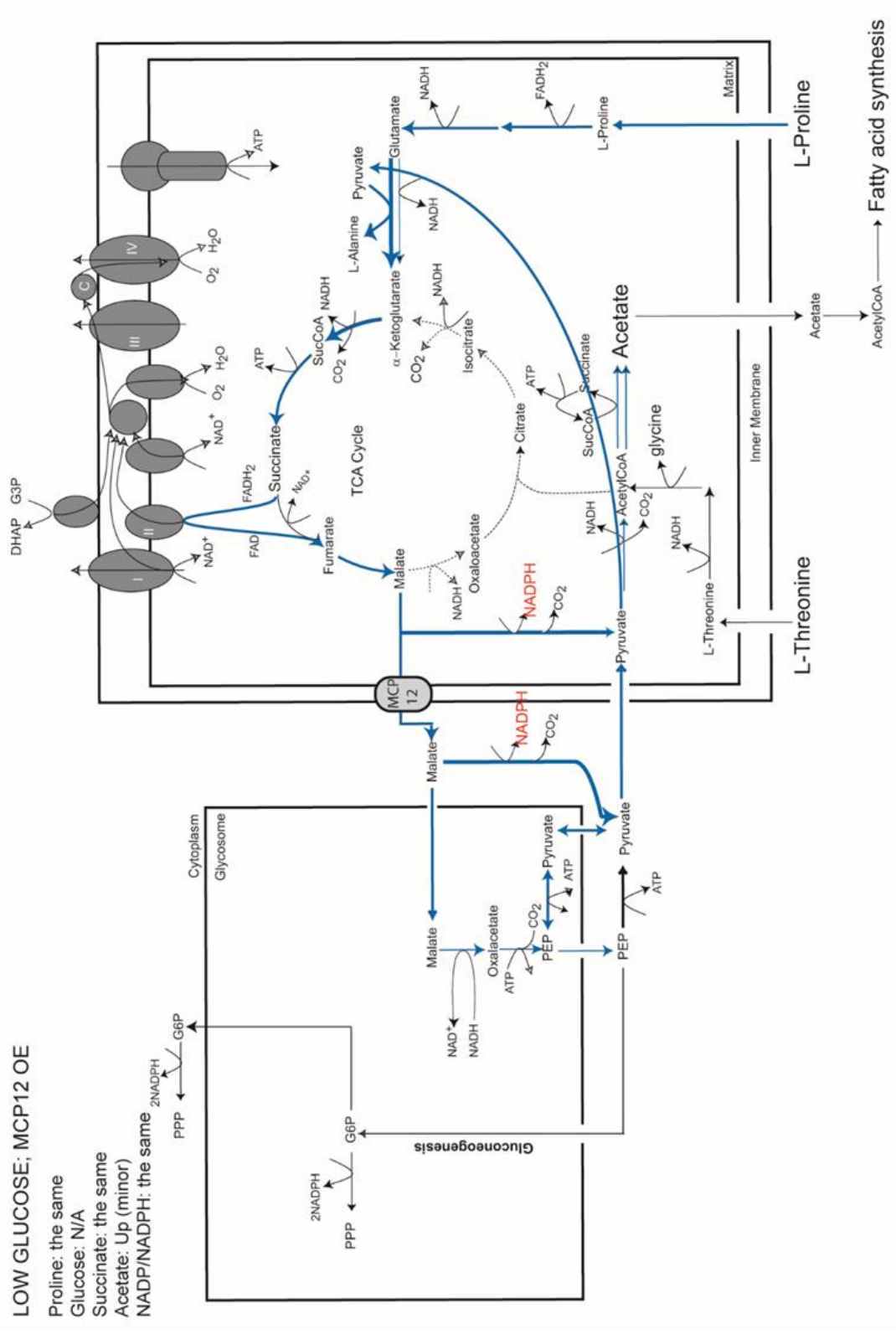

Figure 3-23 Simplified schematic representation of the carbon flux in TbMCP12 over-expression cells under low glucose conditions

Figure legends are shown in Figure 3-21. 'Minor' in the brackets means the change of the contents was relatively small.

Under high glucose condition, overexpression of TbMCP12 resulted in the most significant changes that all the substrates consumption (proline and glucose) and products generation (acetate and succinate) were upregulated (Figure 3-24). An increase of proline consumption accounted for the increase of succinate generation, and thus more malate was produced in the mitochondria. As malate transporter (TbMCP12) was upregulated, mitochondrial malate was transported into the cytosol, and further produced NADPH by either malate enzyme or pentose phosphate pathway. This was presented as a significant decrease of $NADP^+$/NADPH ratio observed in the experiments.

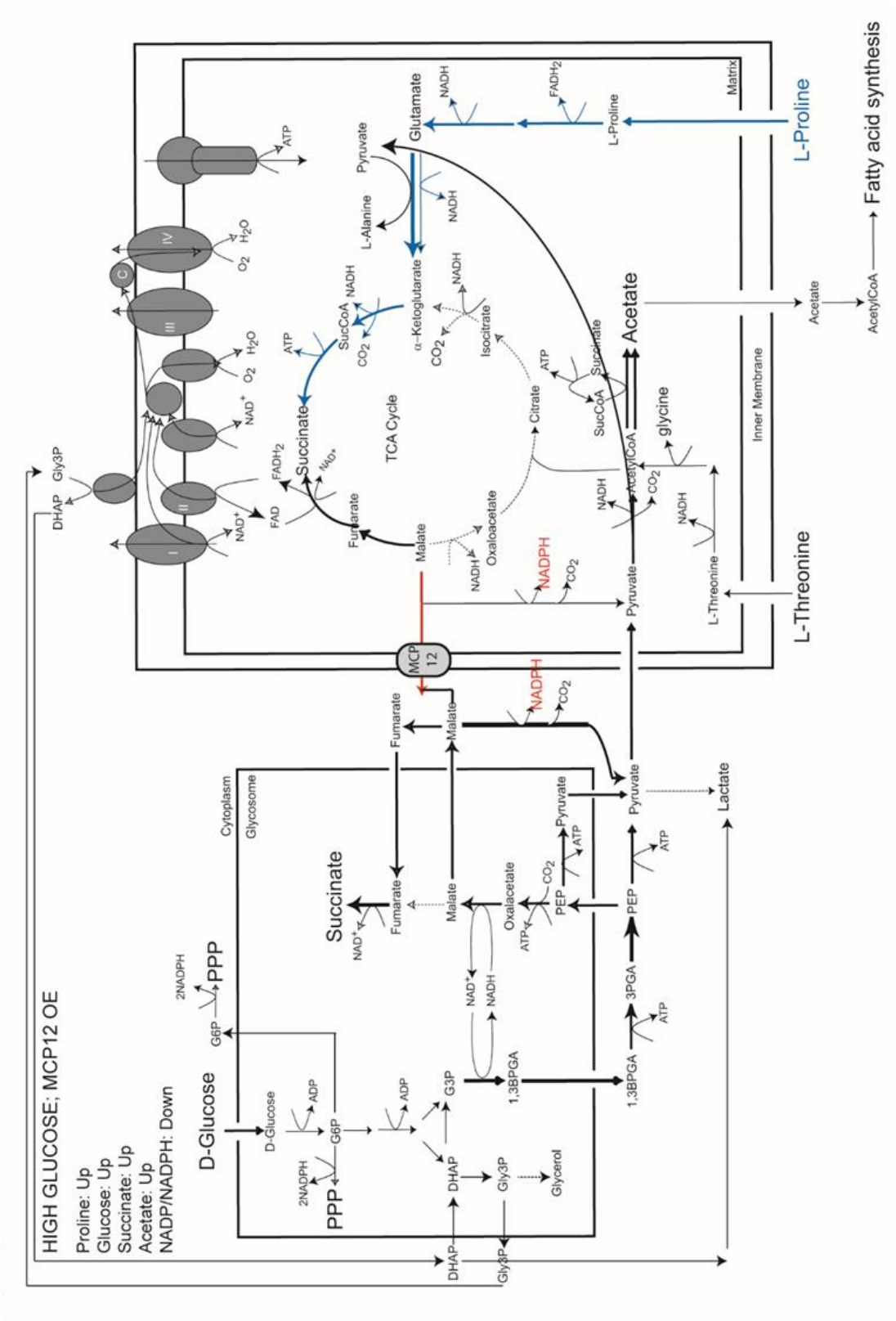

Figure 3-24 Simplified schematic representation of the carbon flux in TbMCP12 over-expression cells under high glucose condition

Figure legends are shown in Figure 3-21.

It is possible that an ancestral trypanosome transporter could transport citrate without showing similarities to the citrate carrier of the developed organisms. The transporter could be a mixture of an oxoglutarate, citrate and dicarboxylate carrier, like the di/tricarboxylate carrier (DTC) from plants (Picault et al. 2002). The di/tricarboxylate carrier could exchange oxoglutarate not only for oxoglutarate, malate, maleate, oxaloacetate, succinate and malonate, but also for citrate and isocitrate. The substrate specificity of di/tricarboxylate carrier was different from the nearest homologue OGC which did not transport tricarboxylates (Runswick et al. 1990). It also differed from tricarboxylate carriers which only transported tricarboxylates (Azzi et al. 1993). In plants, the DTC level was increased in expression under the same condition as photosynthetic enzymes (Taniguchi & Sugiyama 1997). In plants, DTC seemed to have a major switching role. TbMCP12 and homologues from *Leishmania* and *T.cruzi* displayed highest sequence similarity to DTCs. Most probably TbMCP12 is a di/tricarboxylate carrier similar to those found in plants.

In conclusion, TbMCP12 is essential for the growth and survival of the procyclic form of *Trypanosoma brucei* under stress and is involved in the exchange of both dicarboxylates and tricarboxylates across the mitochondrial membrane. It also plays an important role in the provision of the cell with NADPH.

3.10.4 Future research

Due to the failure of reconstitution TbMCP12 into liposomes to study the substrate specificity of the transporter, more metabolomics work in yeast is suggested. Swelling assays using different substrates on isolated mitochondria can be performed to further confirm that TbMCP12 can functionally complement the role DIC plays by transporting the same (or more) substrates/metabolites as DIC does. Yeast functional complementation in succinate-fumarate carrier SFC depleted cell line (ΔSFC) of *S.cerevisiae* by introducing TbMCP12 is also highly recommended. SFC is suggested to shuttle cytosolic succinate from the glycolysis cycle into the mitochondria in exchange for fumarate, an activity that is essential during gluconeogenic growth on C2 compounds (Palmieri et al. 1997). In addition, SFC (also known as Acr1p) was identified as an element which is involved in gluconeogenesis linking glycolic cycle to TCA cycle

(Bojunga et al. 1998). As predicted, TbMCP12, as a di/tri/oxo-carboxylate 'all-in-one' carrier, should be able to functionally complement or at least compromise the growth defect on ethanol or acetate as sole carbon sources (Fernandez et al. 1993). The similar swelling assay can be performed on the ΔSFC+TbMCP12 cell line.

In order to gain more conclusive results for physiological role TbMCP12 plays in oxidative stress and glucose availability (discussed above), a systematic approach should be employed by (i) measuring the changes of various enzymes (malic enzyme, aconitase, isocitrate dehydrogenase and gluconeogenesis related enzymes); (ii) studying the metabolome in *TbMCP12-cmyc*^{ti} and *ΔTbMCP12/TbMCP12-cmyc*^{ti} cells.

Also, due to time limit, not much experiment examining the potential function of TbMCP12 in mitochondrial iron metabolism was performed. As a toxic metal on its own, iron has to couple with other compounds, and carboxylates are potential targets to bind iron. Iron content measurements, iron transport assays and growth phenotype detection under iron deprived conditions are suggested.

A brief summary of investigations on TbMCP12:

- TbMCP12 is essential for cell growth.
- The protein level of TbMCP12 is upregulated by the presence of heme, glucose and hydrogen peroxide.
- TbMCP12 helps to defence the oxidative stress.
- Changes of TbMCP12 protein level cause perturbance in the $NADP^+$/NADPH ratio, the metabolic flux, and the activities of citrate related enzymes.
- TbMCP12 transports citrate and isocitrate, and may transport dicarboxylates (succinate and malate) in yeast.
- Further experiments such as transport assays and metabolomics in yeast are needed to obtain direct evidence of TbMCP12 function.

Chapter 4 Functional characterisation of TbMCP17

4.1 Introduction

The transport of iron into the mitochondrion is of considerable importance. Iron is an important redox or structural cofactor of indispensable cellular processes of trypanosomes (Taylor & Kelly 2010). Both iron deficiency/ deprivation (Chisi et al. 2004) and iron accumulation (Stijlemans et al. 2008) can cause severe disorders to cells. TbMCP17 (Tb927.3.2980) is the only homologue in trypanosomes that shows high similarity to mitochondrial iron transporter MRS3 and MRS4 in yeast, and mitoferrin in mammals. MRS3 and MRS4 have been proposed to mediate iron import in yeast (Foury & Roganti 2002; Felice et al. 2005; Muhlenhoff et al. 2003). Mitoferrin is a vertebrate homologue Fe^{2+} transporter to import iron into mitochondria for heme biosynthesis (Shaw et al. 2006). Another paralogous protein coded by gene mfrn2 is also found in mammals (Li et al. 2002). Therefore, TbMCP17 is identified and analysed in this chapter regarding the predicted function as a mitochondrial iron carrier.

In this chapter, TbMCP17 was functionally characterised. First of all, TbMCP17 was identified as the only homologue in *T. brucei* for mitochondrial iron transport. Further sequence alignments with other characterised mitochondrial iron transporters revealed conserved signature motifs and transport-function-specific contact points in TbMCP17, which confirmed TbMCP17 as a mitochondrial iron transporter in protein sequence level. Subsequently, TbMCP17 localisation was tested by immunofluorescence microscopy and confirmed to be localised in mitochondria.

Function analysis was conducted after generation of *TbMCP17* knockout and overexpression cell lines. First of all, the growth phenotypes of knockout (conventional gene deletion with an inducible rescue copy of TbMCP17-myc: *ΔTbMCP17/TbMCP17-cmyc*^{ti}), knockdown (RNAi: *TbMCP17 RNAi*) and overexpression (*TbMCP17-cmyc*^{ti}) were tested under standard medium conditions. Then, the growth examination was performed with the same cells under iron-depleted conditions (achieved by iron chelator deferoxamine). *TbMCP17-cmyc*^{ti} helped rescue cell growth under iron-limiting conditions. *ΔTbMCP17/TbMCP17-cmyc*^{ti} and *TbMCP17 RNAi*, on the other hand, presented a significant growth defect (40% of WT) and were more sensitive to iron deprived culture with 20% more reduction in cell growth. This growth phenotype strongly

suggested that TbMCP17 played a role in iron metabolism and helped in the defence of iron-limiting conditions. Thus, iron content was measured in both cell lysate and mitochondria fractions from WT, *TbMCP17 RNAi* and *TbMCP17-cmyc*^{ti} cells to find out a potential role that TbMCP17 played in iron metabolism. The results showed that *TbMCP17 RNAi* caused a decrease in mitochondrial iron content despite the increase of the iron level from the cell extract, indicating that TbMCP17 functioned as a mitochondrial iron importer. To confirm the role that TbMCP17 played, yeast functional complementation experiments were performed using a yeast mitochondrial iron carrier (MRS3/4) depleted strain. The introduction of TbMCP17 into MRS3/4-depleted cells rescued the growth defect under fermentable carbon source, proving that TbMCP17 was able to function as a yeast mitochondrial iron transporter.

At the same time, TbMCP17 was heterologously expressed in *E. coli* and purified for antibody generation. After optimisation, TbMCP17 was successfully expressed and purified. The generated antibody successfully detected TbMCP17-His and TbMCP17-myc proteins. But endogenous TbMCP17 in *T. brucei* WT cells could not be detected regardless of all the optimisations, indicating a low abundance of TbMCP17 in procyclic life cycle stage. Hence, *T. brucei* was cultured in challenging conditions, trying to find out the regulation of TbMCP17 expression. Under all the conditions tested (various heme, glucose, deferoxamine), TbMCP17 protein level regulation could not be detected by WB analysis. On mRNA level, TbMCP17 was upregulated by the addition of heme, and repressed by the presence of glucose. Also, the increased hydrogen peroxide conditions resulted in the decrease of TbMCP17 mRNA, and this decrease was more significant when hydrogen peroxide concentration was increased.

4.2 Sequence analysis suggested TbMCP17 as a potential mitochondrial iron transporter

Conserved sequence and structural features of mitochondrial carrier family proteins can be used for the identification of MCF proteins in other eukaryotes and for the prediction of their putative transport function (Millar & Heazlewood 2003; Picault et al. 2004; Cappello et al. 2007). Our group previously reported the identification and molecular analysis of 24 different MCF protein-encoding genes (*TbMCP1-24*) in *Trypanosoma brucei* (Colasante et al. 2009). Extensive genome database searches using deduced amino acid sequences of functionally characterised iron transporters (MRS3p and MRS4p from yeast) identified one sequence homologue in *Trypanosoma brucei*, i.e. *TbMCP17* (accession number Tb927.3.2.2980; Colasante et al. 2009). Reciprocal BLASTP analysis of eukaryotic protein databases (http://www.ncbi.nlm.nih.gov) with TbMCP17 as sequence query resulted in the retrieval of potential mitochondrial iron transporters from different species, such as MRS3 and MRS4 from *Saccharomyces cerevisiae*, mitoferrin from plants like *Gossypium arboretum*, mitoferrin-1 and mitoferrin-2 from mammals such as *Mus musculus* and *Bos taurus*, and mfrn from *Drosophila melanogaster*. The BLASTP-predicted function of TbMCP17 as a mitochondrial iron transporter was further assessed by phylogenetic reconstruction (Saitou & Nei 1987; see Figure 4-1). The resulting neighbour-joining (NJ) tree revealed that TbMCP17 and homologous sequences from trypanosomatids *T. cruzi* and *L. major* formed a separate clade, which was supported by high bootstrap values (Felsenstein 1985). No sequence belonging to phytomonas, trypanosomatids infecting plants, showed up after BLASTP.

The TbMCP17-containing clade branched close to the plant clade, which was consistent with other trypanosomal proteins (Hannaert et al. 2003). Mammals have two mitoferrrins, MFRN1 and MFRN2, and they form two sub-groups of MFRN1 and MFRN2 from different species (Li et al. 2002; Shaw et al. 2006). Mitochondrial iron transporters from insects and mammals are closely related, which was supported by a bootstrap value of 99. Yeasts formed a separate clade far away from trypanosomatids, indicating the high divergence between MRS3/4 and TbMCP17.

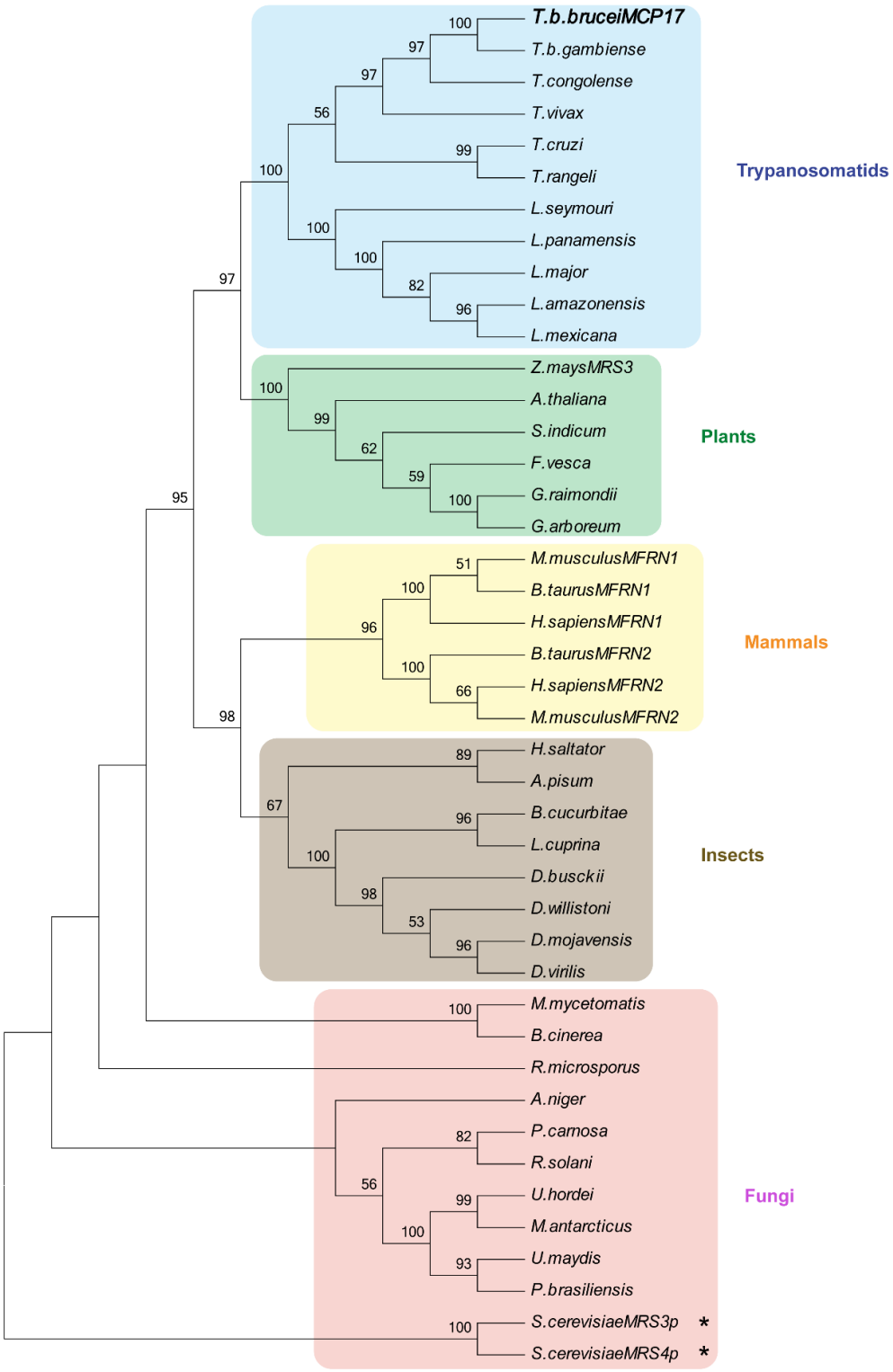

Figure 4-1 TbMCP17 was evolutionarily related to mitochondrial iron transporters as shown by phylogenetic reconstruction

The evolutionary history was inferred using the Neighbor-Joining method with MEGA7. The bootstrap consensus tree inferred from 1000 replicates was taken to represent the evolutionary history, and the percentage of replicate trees are shown next to the branches. Branches corresponding to partitions reproduced in less than 50% bootstraps are collapsed. TbMCP17 is highlighted by bold face. Functionally characterised

mitochondrial iron transporters are labelled with '*'. Accession numbers are listed in Section 2.1.

The deduced amino acid sequence of TbMCP17 consists of 289 amino acid residues, which corresponds to a predicted molecular weight of 31.1 kDa (GeneDB). TbMCP17 exhibits all the conserved sequence and structural features characteristic of MCF proteins (Figure 4-2): its sequence consisted of three conserved repetitive domains of about 100 amino acids, with each domain containing two transmembrane (TM) alpha-helices and a canonical MCF protein signature sequence (Palmieri 2004; Colasante et al. 2009). The MCF protein signature sequence is the hallmark of all MCF proteins and is represented by the amino acid motif 'Px[D/E]x2[K/R]x[K/R]x20-30[D/E]Gx4-5[W/F/Y][K/R]G', with 'x' representing any amino acid residue (Aquila et al. 1987; Saraste & Walker 1982). The first part of the motif 'Px[D/E]x2[K/R]x[K/R]' is located at the carboxy-terminal end of the odd numbered TM helices H1, H3 and H5, whereas the second part '[D/E]Gx4-5[W/F/Y][K/R]G' is located after the amphipathic helices h1-2, h3-4 and h5-6 (Figure 4-2). The conservation of the signature sequence in TbMCP17 was analysed by comparison with corresponding signature sequences from *S. cerevisiae* MRS3, MRS4, *D. melanogaster* mitoferrin, *C. elegans* mitoferrin, and *H. sapiens* mitoferrin 1 and 2 (Figure 4-2). The first part of the signature sequence, namely, M1a, M2a, and M3a, appeared to be conserved for most of the amino acid residues, including (i) the highly conserved proline (P) found at the start of the M1a, M2a and M3a motifs, (ii) the conserved acidic amino acid residue, either an aspartic acid (D) or glutamic acid (E), at position 3 of the same motifs, and (iii) the positively charged amino acid, either a lysine (K) or an arginine (R), at position 6 of the same motifs (see Figure 4-2). In contrast to the first part of the sequence signature, the second part of the signature sequence, [D/E]Gx4-5[W/F/Y][K/R]G', was less conserved (Figure 4-2: M1b, M2b, and M3b). The first two amino acids of the motif, i.e. '(D/E)G', were not well conserved and the number of amino acids (x) between the '(D/E)G' and the '(W/F/Y)(K/R)G' part of the motif also varied. The final glycine (G) of the motif, which allowed flexibility of the loop linking the two helices, was however highly conserved in M1b and M3b.

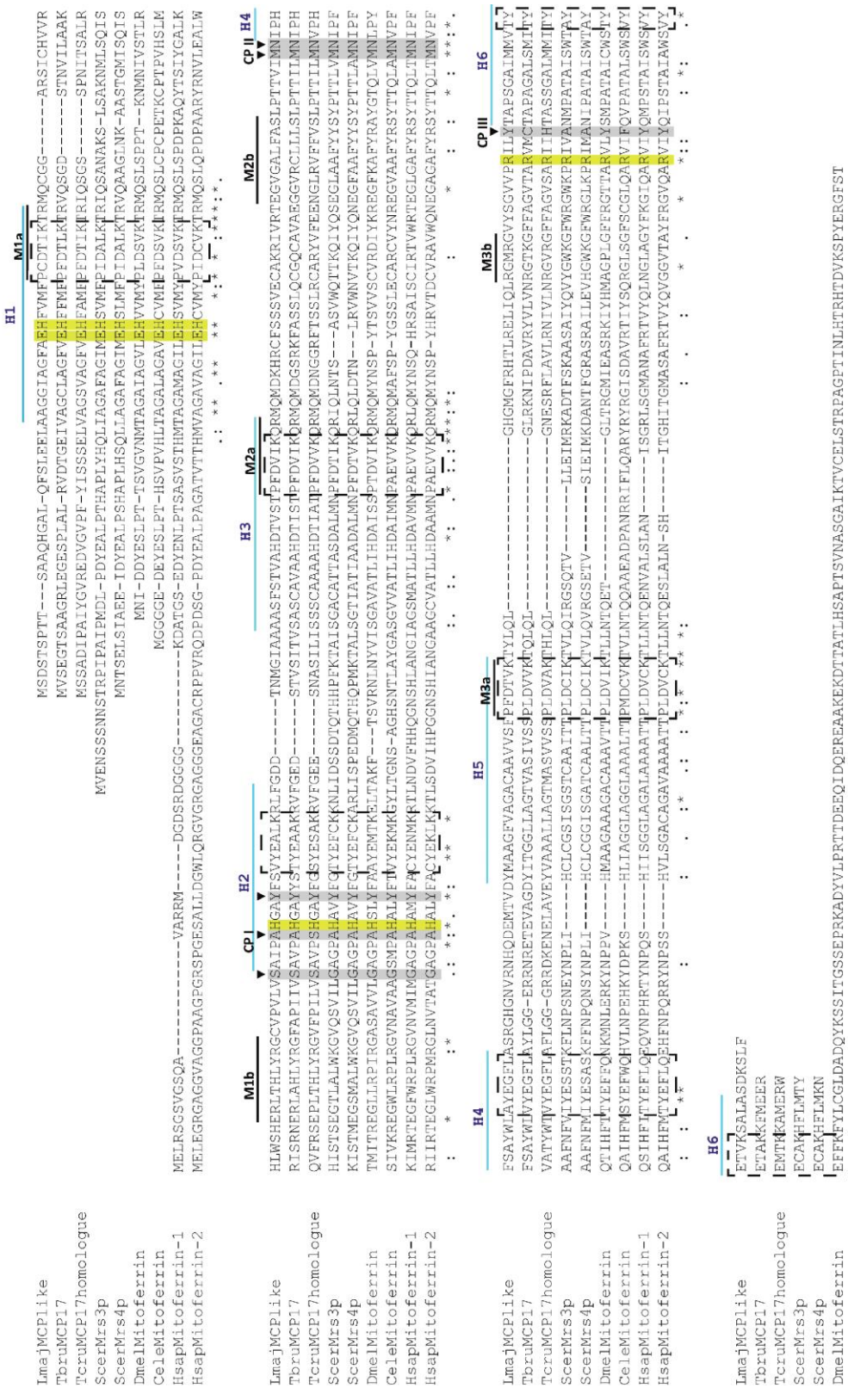

Figure 4-2 Sequence alignment of TbMCP17 with corresponding sequences from *T.cruzi*, *L.major*, *S. cerevisiae* MRS3p, MRS4p, *D. melanogaster* mitoferrin, *C. elegans* mitoferrin, and *H. sapiens* mitoferrin 1 and 2

Accession numbers are listed in Section 2.1. The six transmembrane helices are labelled from H1 to H6 with a blue line. The first part of the canonical signature sequence motifs

located at the end of H1, H3 and H5 are labelled with M1a, M2a and M3a, and the second part motifs are labelled with M1b, M2b and M3b. Substrate contact points (CP I, CP II, and CP III) are located downstream of M1b, M2b, and M3b. The amino acid residues presented in each of the contact points (box grey) are shown. The salt bridge networks are boxed with dash lines. Asterisks (*) shows positions displaying a single, fully conserved residue. Colon (:) indicates conservation between groups of strongly similar properties - scoring > 0.5 in the Gonnet PAM 250 matrix. Period (.) refers to conservation between groups of weakly similar properties - scoring =< 0.5 in the Gonnet PAM 250 matrix.

In MCF proteins, groups of conserved amino acids located downstream of each signature motif participate in substrate discrimination, recognition and binding. Three well-conserved substrate-contact points called CP I, CP II and CP III were extrapolated for all MCF proteins transporting similar substrates (Kunji & Robinson 2006). As shown, the protein sequence alignments of mitochondrial iron carriers CP I (S, A, Y) and CP II (M, N) were conserved (Figure 4-2). In 2008, Robinson group identified two clusters of conserved and highly symmetric residues, which formed salt bridge networks. The first clusters were found on H1, H3 and H5 by the matrix side of the transporter, consisting of PX[DE]XX[RK] motif, while the second clusters consisting of [FY][DE]XX[RK] motif located on the cytoplasmic side of H2, H4 and H6. The matrix and cytoplasmic networks could either open or close the passage to mediate substrate transport. These salt bridge networks were highly conserved among all the sequence aligned (Figure 4-2). Apart from the identified signature features above, more amino acids were found to be conserved, such as glutamic acid (E) and histidine (H) located at helix 1 before M1a, as well as the histidine (H) at CP I region. Also, the arginine right before CP III was conserved among all species tested.

Apart from these similarities, sequences from trypanosomes present the following dissimilarities. First of all, the N-terminal lengths of different species were different (human proteins presented the longest N-terminal sequence), indicating that the more developed the species were, the longer the N-terminal length was. This result was also confirmed by Mittra et al (Mittra et al. 2016). This could be related to protein targeting (Vidilaseris et al. 2014; Liniger et al. 2004). In addition, trypanosomes had six fewer amino acids between H1 and H2, and between H2 and H3, but five more amino acids between H4 and H5 compared with other sequences, indicating modifications on loop lengths during evolution (Kuhn et al. 2001).

4.3 TbMCP17 was localised in the mitochondria of *T. brucei*

Results of sequence analysis and phylogenetic tree strongly suggested that TbMCP17 is the only mitochondrial iron transporter. Thus, the localisation of TbMCP17 was determined. Over-expression plasmids of TbMCP17 were constructed with myc tags for detection and localisation by immunofluorescence microscopy.

4.3.1 Plasmid construction

Plasmids over-expressing TbMCP17-myc were constructed. pHD1484 contained 2*myc at C-terminal of multiple cloning sites (MCS), and pHD1485 harboured 2*myc at N-terminal (see Figure 4-3 A). As shown in Figure 4-3 B, BamH I and Hind III digestion towards the two plasmids generated a band at around 900 bp, respectively. The observed size of the bands was in accordance with that of TbMCP17 ORF (870 bp), confirming that TbMCP17 ORF had been inserted into vectors with restriction enzymes BamH I and Hind III. In addition, plasmids were digested with either Hind III and Pac I (pHD1484+TbMCP17) or BamH I and Pac I (pHD1485+TbMCP17) to determine that TbMCP17 ORF had been inserted into the right position. The only Pac I site located in between two myc genes, hence pHD1484+TbMCP17 was digested with Hind III and Pac I. As a result, a band of TbMCP17 and one myc gene at the end dropped out (870+30 bp), while pHD1485+TbMCP17 was digested with BamH I and Pac I, and a band of one myc gene at the front plus TbMCP17 ORF was observed (30+870 bp).

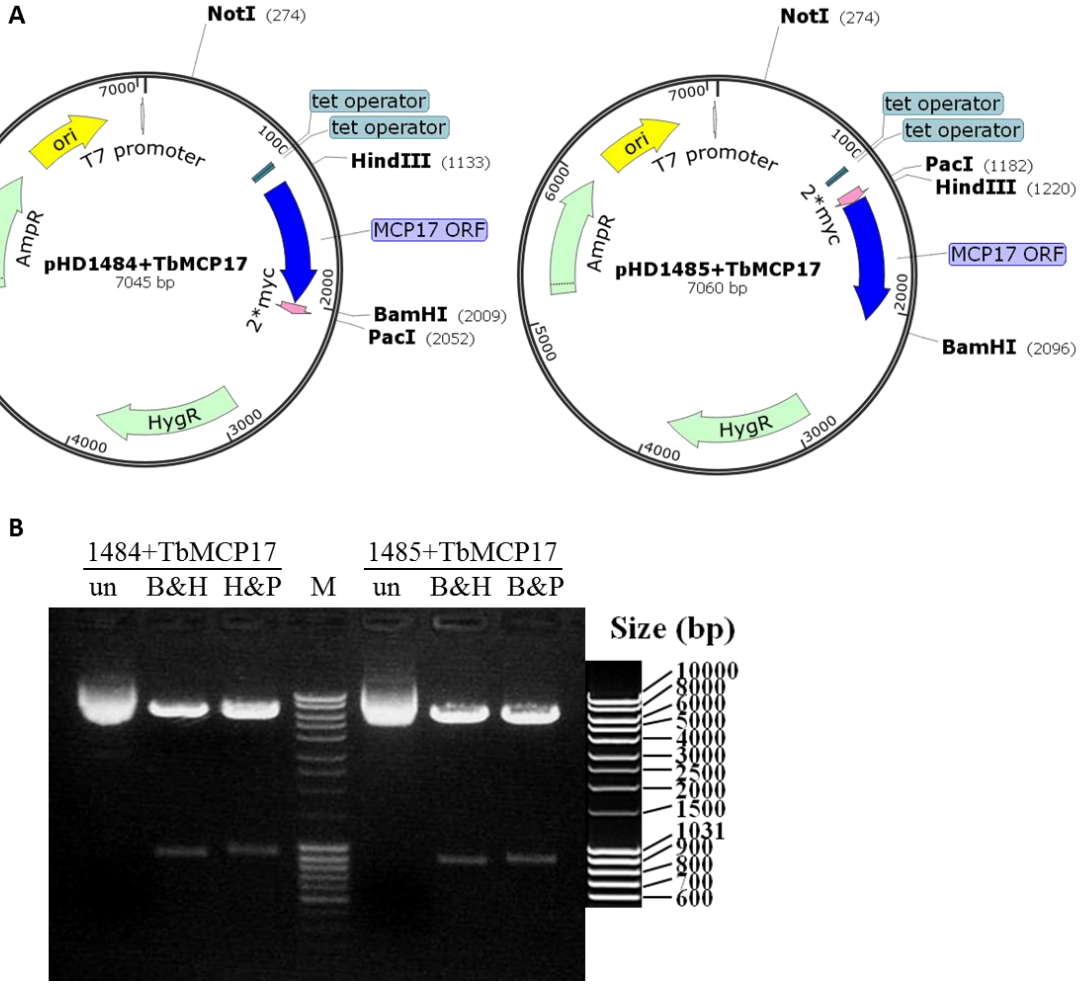

Figure 4-3 TbMCP17 over-expression plasmid checking
A presents plasmid maps of two over-expressing constructs pHD1484+TbMCP17 and pHD1485+TbMCP17, and related restriction enzymes are labelled. Abbreviations: Ori: Origin of Replication; HygR: hygromycin resistance gene, a selectable marker for *Trypanosoma brucei*; AmpR: ampicillin resistance gene used for selection of plasmid-containing bacteria. B displays isolated plasmids digested with BamH I and Hind III (B&H) or Hind III and Pac I (H&P) or BamH I and Pac I (B&P). Undigested plasmids (un) were loaded on the same agarose gel next to the digested ones as a control.

4.3.2 Sub-cellular localisation

The generated plasmids were transfected into *Trypanosoma brucei* wild type cell line (PCF449) and over-expression of TbMCP17-c/nmyc was induced. Immunofluorescence was performed towards *TbMCP17-cmyc*^{ti} and *TbMCP17-nmyc*^{ti} overexpression cells. TbMCP17-myc proteins (detected with anti-myc antibody) presented co-localisation with trypanosomal mitochondria dyed with MitoTracker (Figure 4-4).

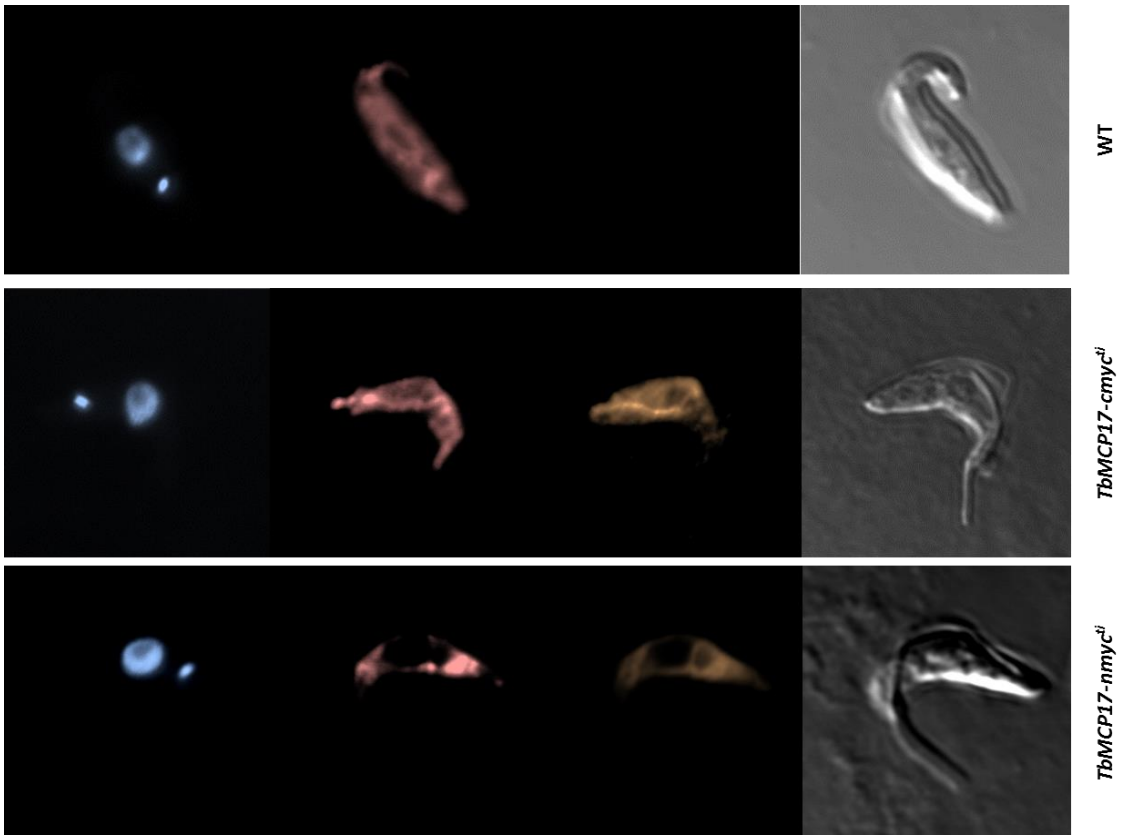

Figure 4-4 TbMCP17 was exclusively localised in the *T. brucei* mitochondrion
The figure displays fluorescent immunomicroscopy result of WT (wild type), TbMCP17 over-expression cell lines with either C-term (*TbMCP17-cmyc*^{ti}) or N-term myc (*TbMCP17-nmyc*^{ti}) detected with MitoTracker (red), myc antibody (green) and DAPI (blue). Bright fields are also presented to indicate intact cells.

4.4 Over-expression of TbMCP17 rescued growth under iron-limiting condition

As a potential mitochondrial iron transporter, TbMCP17 was suggested to play a role in iron-related growth. The same TbMCP17 overexpression cell lines (*TbMCP17-cmyc*^{ti} and *TbMCP17-nmyc*^{ti}) were used to monitor potential growth phenotype under standard and iron limiting conditions created by iron chelator deferoxamine (Merschjohann & Steverding 2006).

The results showed that under the standard growth condition, WT and over-expression cells presented no significant difference in growth (Figure 4-5). The growth phenotypes were presented in histograms to convey information more straightforward and growth curves could be found in Appendix A5-1. A reduction of free iron in the cell culture medium negatively affected the growth of WT cells. This inhibition correlated with the dose of deferoxamine added (50% and 25% corresponded to 50 μM and 100 μM, respectively). Furthermore, overexpression of TbMCP17 was able to rescue the deferoxamine-induced growth phenotype to 90% (50 μM of deferoxamine) or 50% (100 μM of deferoxamine). And *TbMCP17-cmyc* cells rescued growth defect better than *TbMCP17-nmyc* cells (10% more under 100 μM of deferoxamine, Figure 4-5). The results suggested that TbMCP17 over-expression helped recover cell growth under iron-limiting conditions.

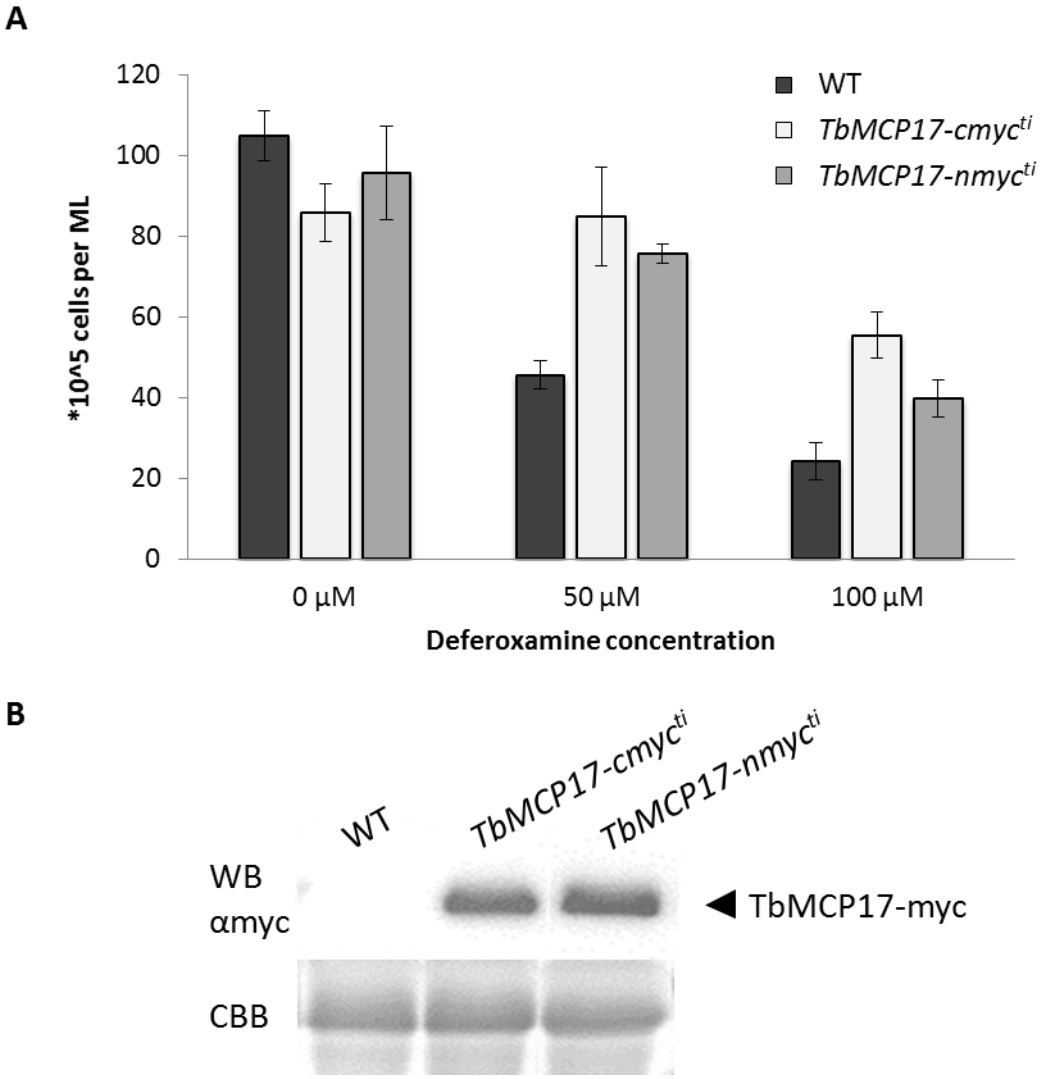

Figure 4-5 Over-expressing TbMCP17 helped cells defence iron limiting conditions

Cell densities of wild-type (WT) cells (black, first lane), TbMCP17-cmyc expression cells (white in the middle) and TbMCP17-nmyc expression cells (gray, last lane) treated with different concentrations of iron chelator deferoxamine measured after 48 hours of subculture are presented in the bar chart A. Error bars correspond to standard deviation of triplicates. The similar pattern was observed for 24 hours, with growth curves shown in Appendix A5-1. B displays WB checking results of the cell lines using myc antibody, and CBB is presented as a loading control.

4.5 TbMCP17 Knockout and knockdown both caused growth defect

From Section 4.3, over-expressing of TbMCP17 was capable of restoring cell growth under low iron conditions, it was very likely that *TbMCP17* depletion would cause growth defect. Gene depletion was achieved by two approaches, gene knockout and gene knockdown. By replacing the two copies of *TbMCP17* in *Trypanosoma brucei* genome with two antibiotic resistant cassettes NEO and BSD individually, the gene was depleted in the same way as TbMCP12 depletion. Gene knockdown was also done by RNA interference (RNAi) via introducing a double-stranded DNA containing part of TbMCP17 to the target cell and disrupting *TbMCP17* mRNA synthesis.

4.5.1 Knockout and knockdown related plasmid construction

Gene knockout was achieved by replacing *TbMCP17* on both DNA strands with two antibiotic resistant genes *BSD* and *NEO* simultaneously by homologous recombination (see Section 2.5.2 for details). First of all, constructs containing the *NEO/BSD* resistance cassettes between 5' and 3' UTR of *TbMCP17* were made. Initially, 5' and 3' UTR of TbMCP17 were amplified by PCR with 5% of DMSO to lower the annealing temperature and facilitate the PCR process (Figure 4-6).

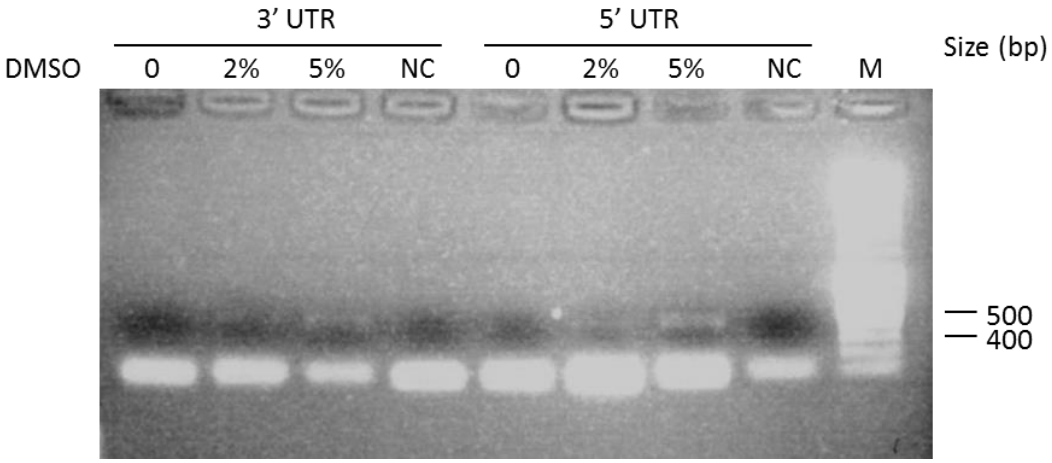

Figure 4-6 3'UTR and 5'UTR of TbMCP17 amplification with 5% DMSO addition

2% and 5% of DMSO labels the lanes in which DMSO of displayed concentration was added to PCR mixture to help with PCR process. Primer sets used are described in Chapter 2. Abbreviations: M: DNA marker; NC: negative control which contains all the components except template. A single band around 450 bp is of the right size for 3'UTR and 5' UTR.

Subsequently, PCR products of 3'UTR and 5'UTR were ligated into the pGEM T easy vector. Potential clones containing 3'UTR (clones 1 to 6) or 5'UTR (clones 7 to 10) were digested with enzyme pairs Apa I & BamH I and Sac I & Spe I (Figure 4-7 A) to check whether the ligation was successful. Because the pGEM T-easy vector contained Apa I site before MCS, Spe I and Sac I sit right after MCS, two bands (500 bp and 100 bp) dropped out after double digestion (Figure 4-7 A). In order to determine the direction of the insert, single digestion with Apa I towards 3' UTR (clone 1 and 4) and Sac I towards 5' UTR (clone 7 and 8) were performed. As shown in Figure 4-7 B, only one band at approximately 100 bp dropped out after digestion, suggesting that the direction of two 3' UTR clones (clone 1 & 4) was from Apa I to BamH I. Similarly, 5' UTR in clone 8 was under Spe I to Sac I direction.

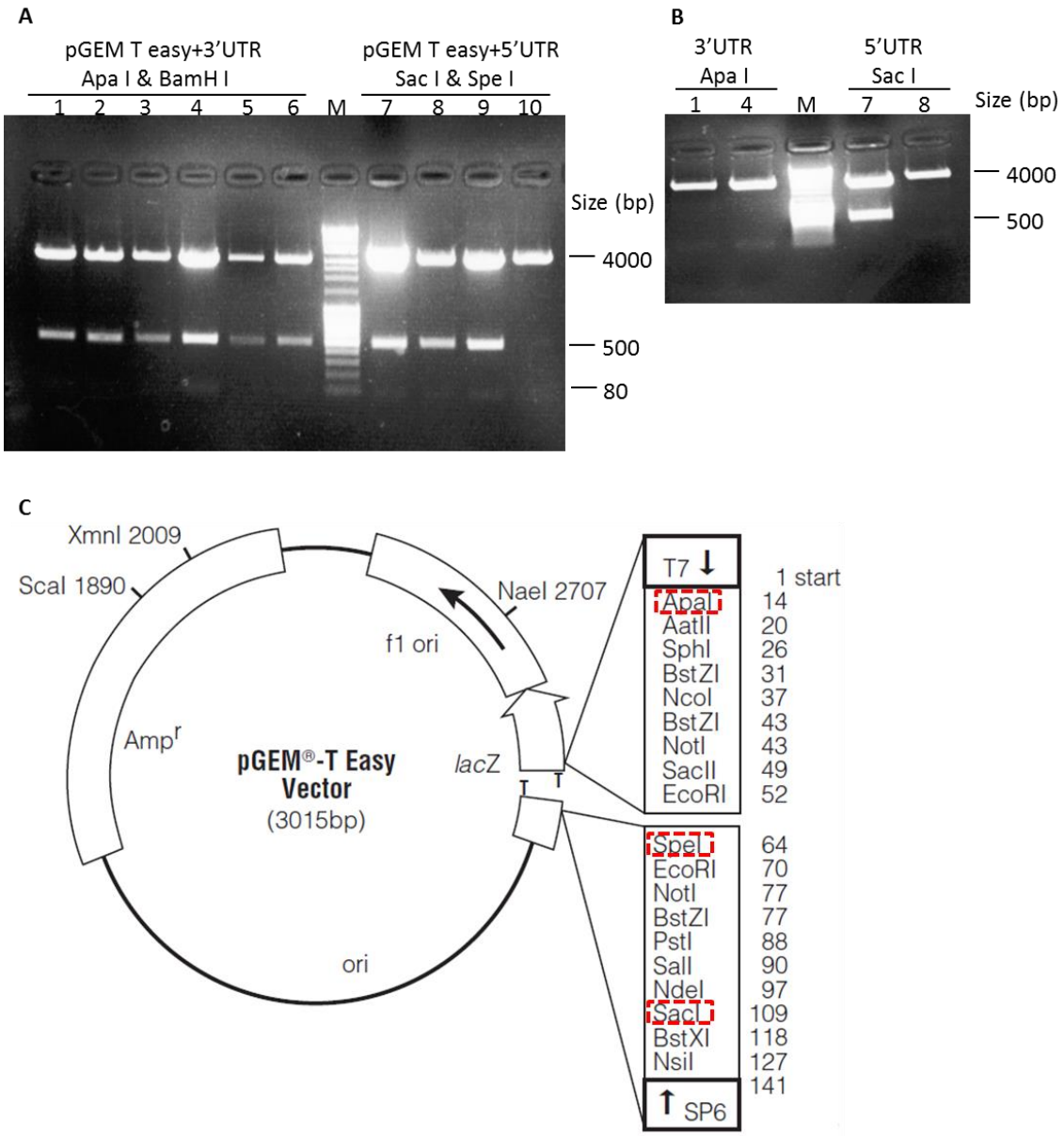

Figure 4-7 Various digestions to examine pGEM T easy + 3' UTR and pGEM T easy + 5' UTR plasmids

A and B show the digestion result of plasmids isolated from various clones with multiple restriction enzymes. C illustrates pGEM T easy plasmid map (Promega) with red dash squares to point out the mentioned restriction sites.

Sequencing results confirmed that clone 1 and 8 contained the right sequences of TbMCP17, 5'UTR and 3'UTR, respectively (Appendix A4-1). The confirmed sequences were inserted into pBlueScript SK +NEO/BSD vectors (approximately 4000 bp) using enzyme sets Sac I and Spe I (5'UTR) and Spe I and BamH I (3'UTR) (see Figure 4-8 B for a schematic representation of TbMCP17 5'UTR+BSD / NEO+TbMCP17 3'UTR). The predicted sizes of Sac I & Apa I digestion were 1897 bp for BSD and 2092 bp for NEO, and the size of the pBlueScript vector was 2958 bp. The predicted size for BamH I

& Spe I digestion for NEO was 795 bp and BSD 938 bp. Figure 4-8 B was the plasmid restriction enzyme mappings towards potential pBlueScript+*TbMCP17* 5'UTR+NEO+3'UTR of the *TbMCP17* construct (clone 1) and pBlueScript+*TbMCP17* 5'UTR+BSD+3'UTR of the *TbMCP17* construct (clone 2), which shown the same size as predicted. The resulting plasmids were sequenced from both ends (Appendix A4-1), and the result proved that the constructs were correct.

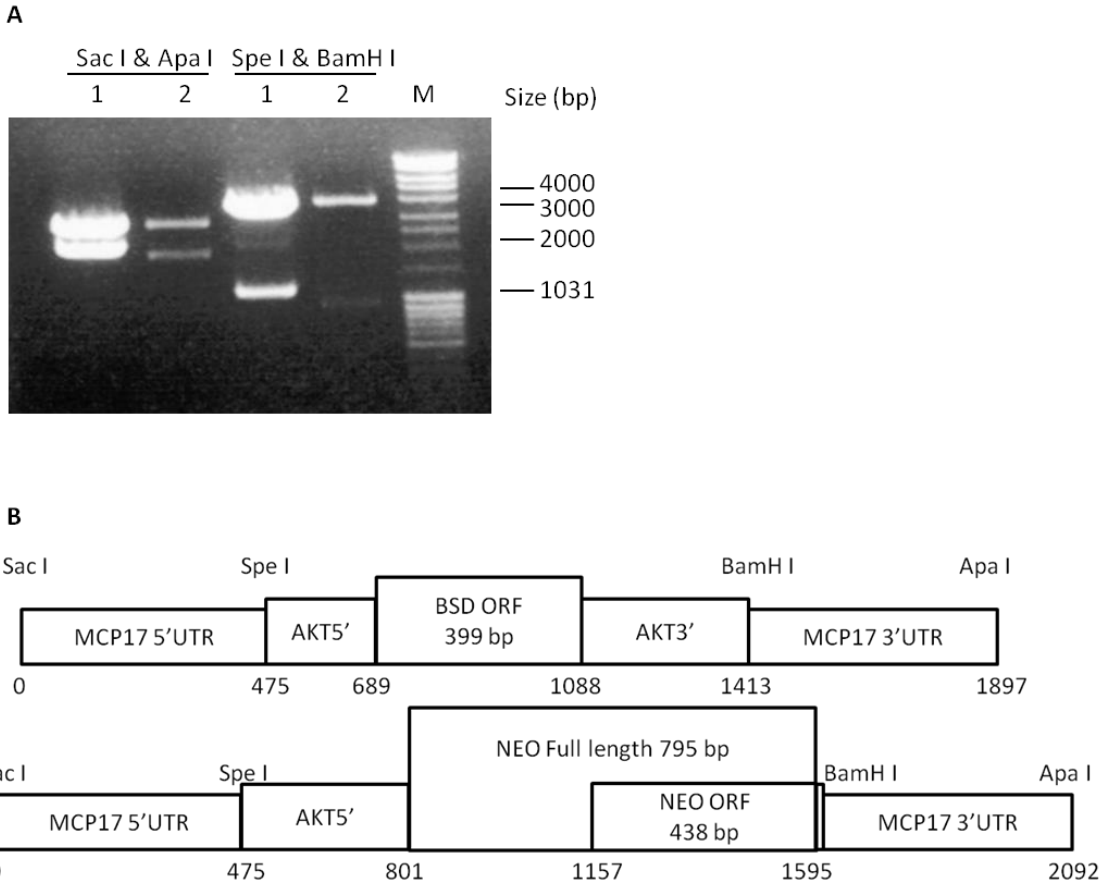

Figure 4-8 Restriction enzyme examination of pBlueScript containing TbMCP17 5'UTR+NEO+TbMCP17 3'UTR or 5'UTR+BSD+TbMCP17 3'UTR

Sac I & Apa I digestion separates plasmid into the pBlueScript backbone and designed fragment of TbMCP17 5' and 3' UTR with resistance gene NEO (plasmid labelled as 1) or BSD (plasmid labelled as 2). Spe I & BamH I digestion results in fragments containing BSD or NEO. B displays the schematic representation of TbMCP17 5'UTR+BSD+TbMCP17 3'UTR and TbMCP17 5'UTR+NEO+TbMCP17 3'UTR. Different fragments are boxed and labelled. ORF stands for the open reading frame. Used restriction enzyme sites are labelled above.

TbMCP17 RNAi plasmids contained the TbMCP17 RNAi fragment, which consisted of two identical copies of half *TbMCP17* gene in reversed orientation. The hairpin structure

formed by self-complementation made it more stable than single-stranded RNA (Ngô et al. 1998). After PCR amplification, TbMCP17 RNAi fragment was inserted into alternative vectors (pHD676/677/678) bearing restriction sites BamH I and Hind III. The resulting clones were tested using both double digest (Figure 4-9 A) and PCR (Figure 4-9 B). As shown in A, clone 1,2,4,5 and 6 were clones containing TbMCP17 RNAi size fragments (836 bp) with the two restriction sites located at the two ends of the AS+S fragment. B indicated that clone 1-6 contained sense or antisense fragment. After combining the two results, clone 1, 2, 4, 5, and 6 were considered as positive clones and used for further study.

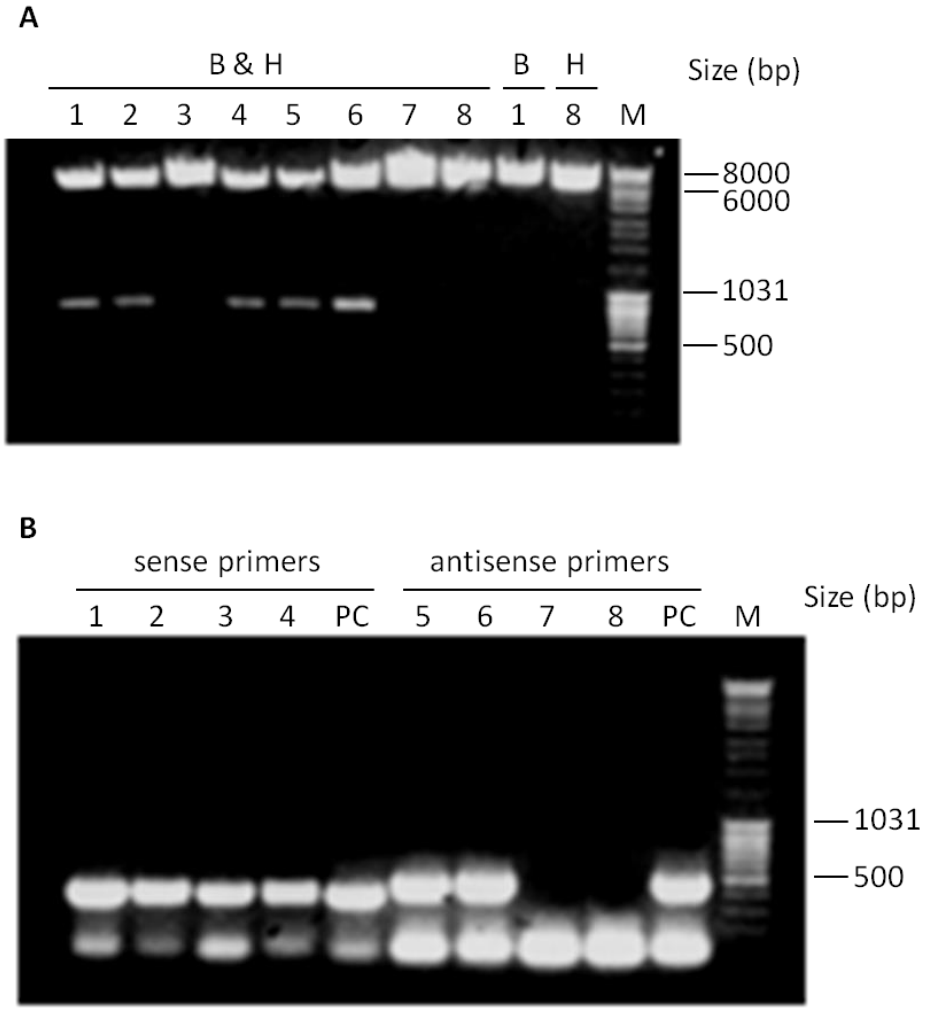

Figure 4-9 Examination of *TbMCP17* RNAi-containing pHD676, pHD677, pHD678 and pHU1

TbMCP17 RNAi fragment was inserted into pHD676 (1&2), pHD677 (3&4), pHD678 (5&6) and pHU1 (7&8). Examinations of different clones by restriction enzymes mappings using BamHI and Hind III, accompanied by single enzyme digestion controls are shown in A to exclude the fake construct with only one restriction enzyme site. B

displays the PCR checking of clone 1-4 amplified with *TbMCP17* sense primers and clone 5-8 with antisense primers, both groups were followed by a positive control.

4.5.2 TbMCP17 conditional double knockout and RNAi cell line confirmation

TbMCP17 double knockout cell line (*ΔTbMCP17/TbMCP17cmyc*^{ti}) was generated stepwise according to previous descriptions (Krieger et al. 2000; Voncken et al. 2003): plasmid pBlueScript containing TbMCP17 5'UTR+NEO+TbMCP17 3'UTR was first transfected into PCF449 WT cell line, but many attempts to transfect pBlueScript containing TbMCP17 5'UTR+BSD+TbMCP17 3'UTR failed, indicating that TbMCP17 was essential in this cell line. Thus, tetracycline inducible TbMCP17-cmyc over-expression cell line was used for generating TbMCP17 conditional double knockout *ΔTbMCP17/TbMCP17cmyc*^{ti} in the presence of tetracycline. Genomic DNA of the resulting conditional double knockout cell line was examined by PCR. The results of PCR using corresponding primers demonstrated that TbMCP17 5'UTR+NEO+TbMCP17 3'UTR and TbMCP17 5'UTR+BSD+TbMCP17 3'UTR fragments were in the *ΔTbMCP17/TbMCP17cmyc*^{ti} cell line (Figure 4-10). In order to determine whether the fragments were homologously recombined to the same sites where TbMCP17 genes localised, a primer located in the upstream of TbMCP17 5'UTR and one in the downstream of TbMCP17 3'UTR were used in combination with primers in the cassettes for PCR (Figure 4-11). The PCR results shown bands of predicted sizes meant that the generated clone *ΔTbMCP17/TbMCP17cmyc*^{ti} indeed had replaced two TbMCP17 gene copies with BSD and NEO.

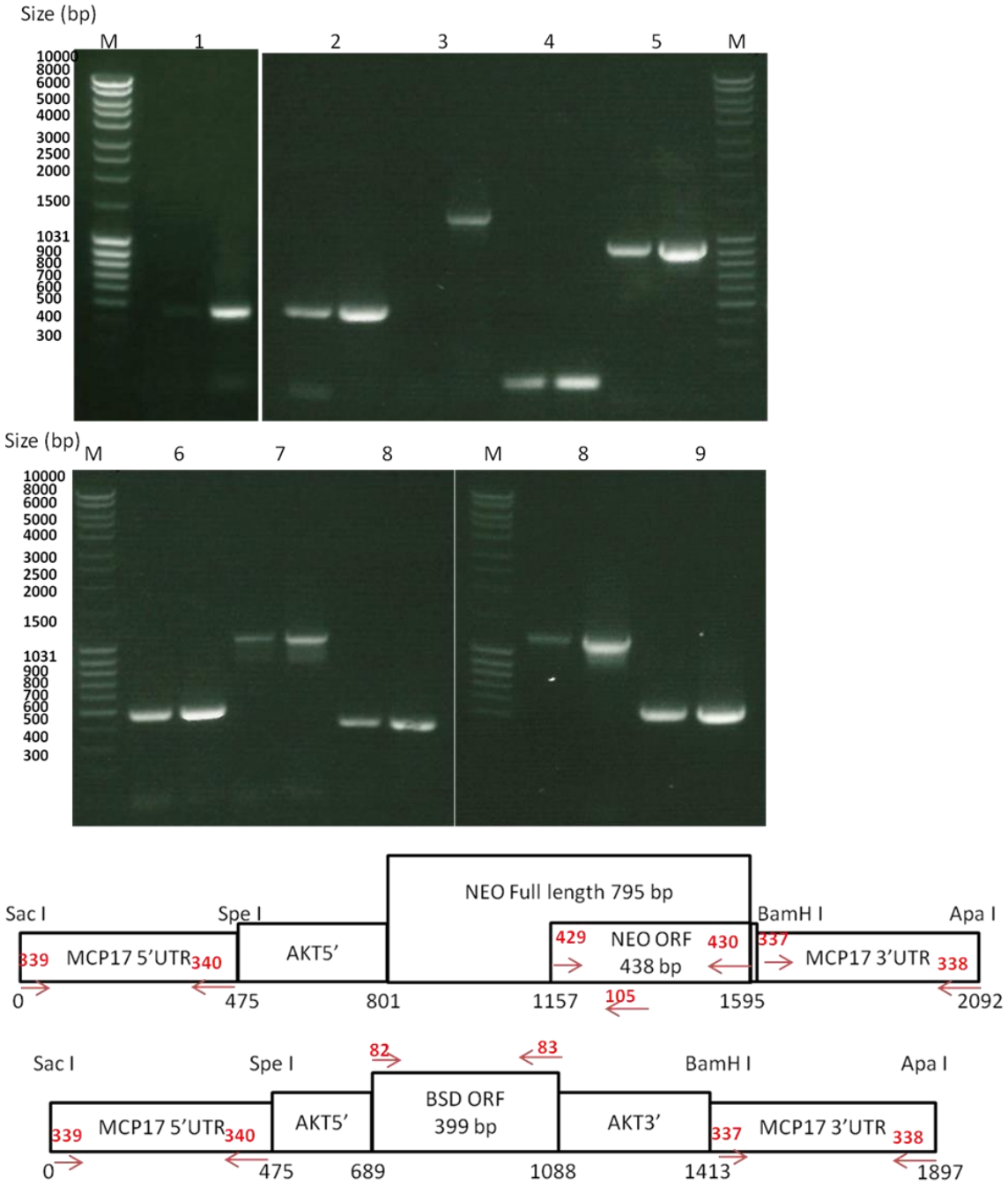

Figure 4-10 PCR on gDNA of *ΔTbMCP17/TbMCP17cmyc^{ti}* using primer sets of each fragment, respectively

PCR results and schematic representation map containing primer numbers are demonstrated. Primer sets used and predicted size(s) are listed: 1: 429&430 for NEO ORF (438 bp); 2: 339&340 for 5'UTR (475 bp); 3: 339&105 for 5'UTR and part of NEO (1296 bp); 4: 429&105 for part of NEO (139 bp); 5: 429&338 for NEO ORF+3'UTR (935 bp); 6: 337&338 for 3'UTR (484 bp); 7: 339&83 for 5'UTR+BSD (1088 bp); 8: 82&338 for BSD+3'UTR (1208 bp); 9: 321&322 for tubulin (572 bp). The first lane of each primer sets used gDNA isolated from *ΔTbMCP17/TbMCP17cmyc^{ti}* samples as the template, and plasmids containing 5'UTR+NEO/BSD+3'UTR were used for the template as a positive control (shown in the second lane). Primers positions are indicated in red colour number

with an arrow for direction. Numbers in black at the bottom of each cassette are fragment sizes in bp.

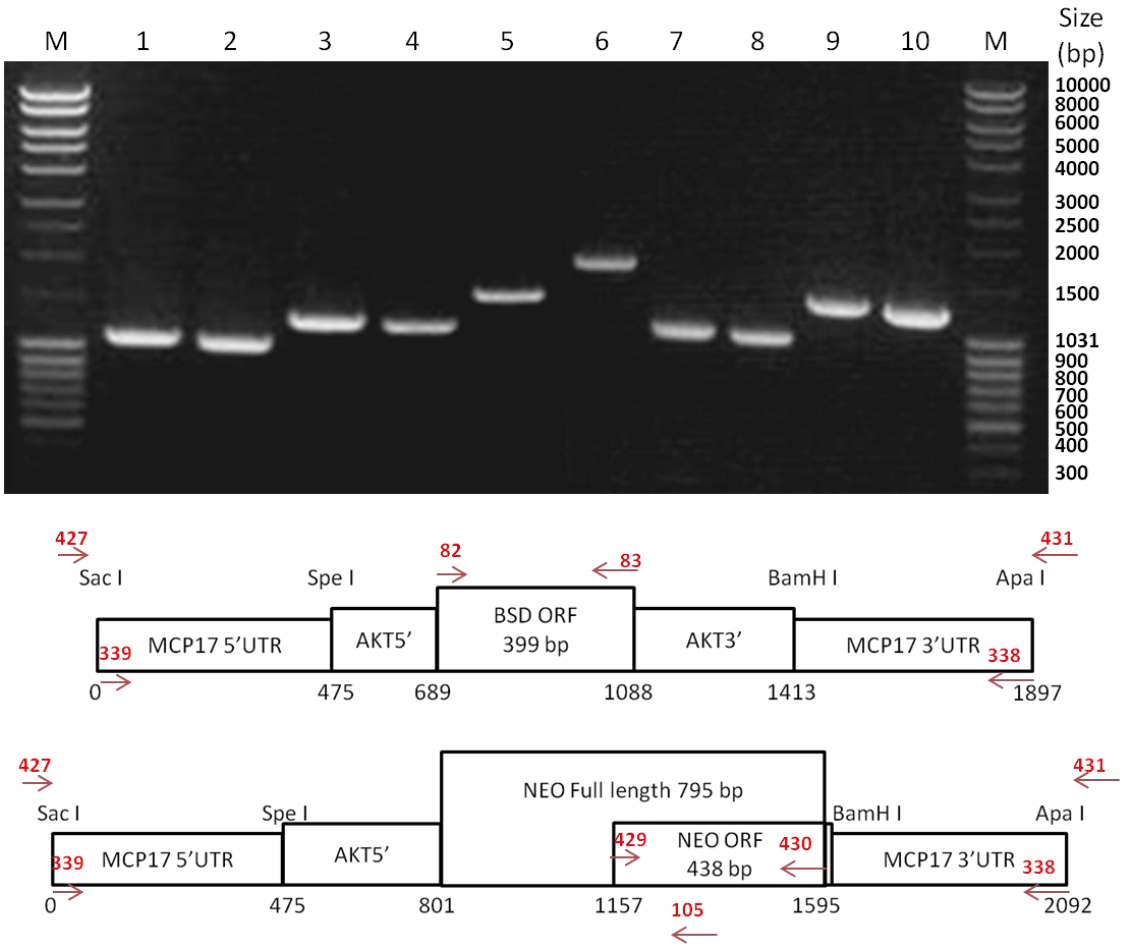

Figure 4-11 PCR on gDNA of *ΔTbMCP17/TbMCP17cmyc*^{ti} using upstream and downstream primers of the replaced cassette

Upstream and downstream primers of TbMCP17 5'UTR (427) and TbMCP17 3'UTR (431) were used in combination with BSD/NEO primers to localise the recombined antibiotic restriction cassettes. PCR results and schematic representation map containing primer numbers are demonstrated. In detail, primer sets and the corresponding sizes used were listed: 1: 427&83 (1116 bp), 2: 339&83 (1088 bp), 3: 427&105 (1324 bp), 4: 339&105 (1296 bp), 5: 427&430 (1623 bp), 6: 339&431 (1924 bp), 7: 429&431 (962 bp), 8: 429&338 (935 bp), 9: 82&431 (1235 bp), 10: 82&338 (1208 bp). Primers positions are indicated in red colour number and arrow for direction. Numbers in black at the bottom of each cassette are fragment sizes in bp.

TbMCP17 RNAi plasmid was transfected into PCF449 cell line, and 6 clones were obtained. Due to the low expression level of TbMCP17 protein, mRNA levels of TbMCP17 in both WT and 6 clones were measured by reverse transcript quantitative PCR (RT-qPCR), using tubulin as a loading control (Figure 4-12). *TbMCP17 RNAi* clone 3, 5

and 6 showed a down-regulation of TbMCP17 mRNA about 50% and thus clone 3 and 5 were used in future experiments.

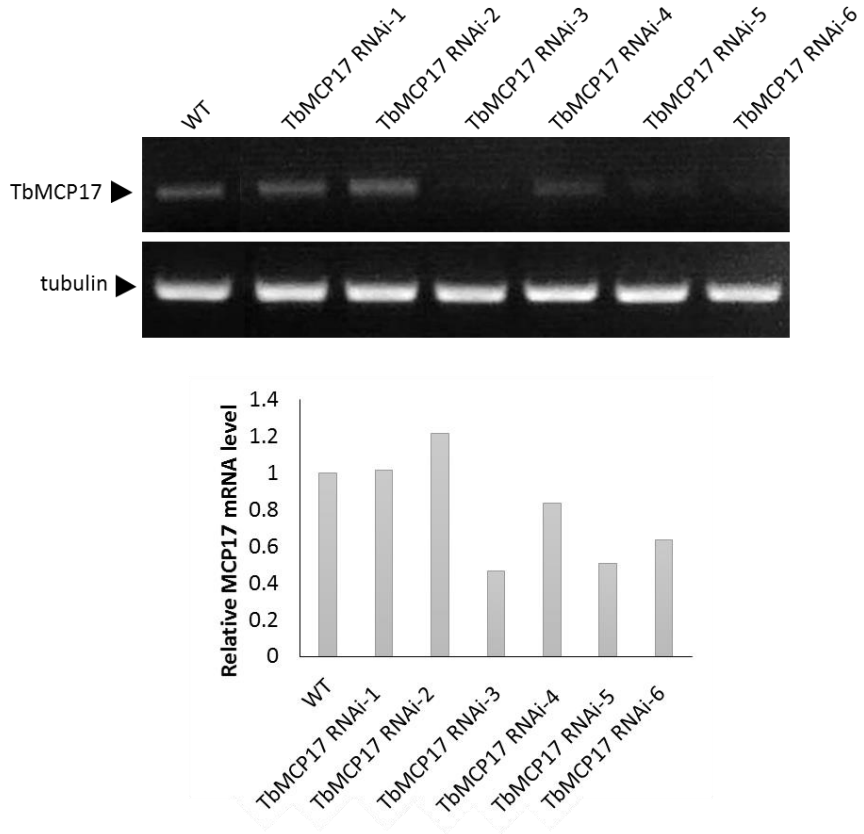

Figure 4-12 RT-qPCR of mRNA from TbMCP17 RNAi induced clones and WT cell line using TbMCP17 and tubulin primers

PCR results of TbMCP17 and tubulin level from seven samples are shown in gel picture. The relative TbMCP17 mRNA level is presented after normalised with loading control tubulin (WT was set as 1).

4.5.3 TbMCP17 KO and RNAi caused growth defect

Growth effects of *ΔTbMCP17/TbMCP17cmyc*^{ti} or *TbMCP17 RNAi* were determined. *ΔTbMCP17/TbMCP17cmyc*^{ti} presented significantly reduced growth to 17.4% of WT under normal media (Figure 4-13, 0 μM), and this growth defect was rescued to 52.4% of WT by TbMCP17-cmyc (*ΔTbMCP17+TbMCP17cmyc*^{ti}). When iron chelator deferoxamine was added to media of different concentrations (50 μM and 100 μM in Figure 4-13), WT cells struggled to grow: 43.5% of standard media under 50 μM of deferoxamine and 23.1% of standard media under 100 μM of deferoxamine. Also, *ΔTbMCP17/TbMCP17cmyc*^{ti} cell line presented a decrease in growth speed. When

TbMCP17cmyc rescue copy was induced (*ΔTbMCP17+TbMCP17cmyc*^{ti}), cell defect of *ΔTbMCP17/TbMCP17cmyc*^{ti} under iron-limiting conditions (50 µM and 100 µM of deferoxamine) was rescued to WT level (Figure 4-13, Appendix A5-2 for growth curves). In total, the results showed that TbMCP17 was essential for cell growth, and the depletion caused a growth defect. Furthermore, re-introduction of TbMCP17cmyc into *ΔTbMCP17/TbMCP17cmyc*^{ti} cells partially rescued the growth defect under standard conditions and fully rescued under reduced iron concentrations.

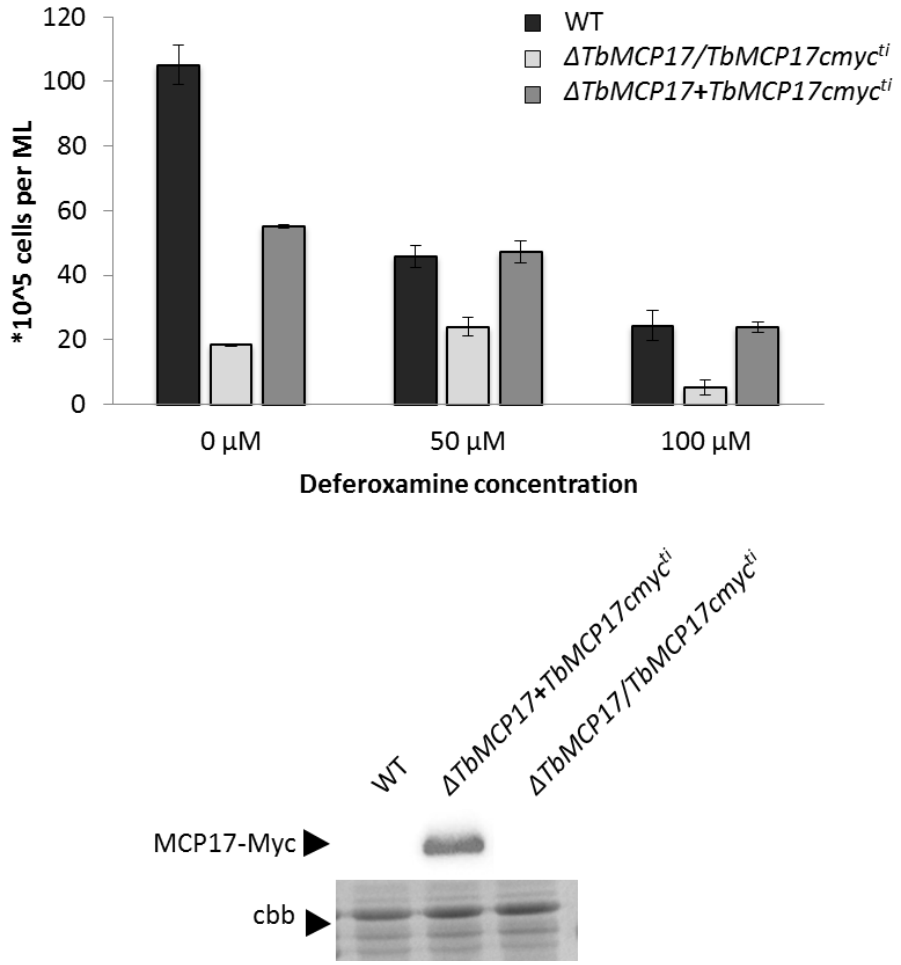

Figure 4-13 TbMCP17 over-expression rescued cell defect of *ΔTbMCP17/TbMCP17cmyc*^{ti} under different iron concentrations

The bar chart above displays cell densities of wild type (WT) cells (black, first lane), *ΔTbMCP17/TbMCP17cmyc*^{ti} (without tetracycline; light grey, in the middle) and *ΔTbMCP17+TbMCP17cmyc*^{ti} (with tetracycline induction; dark grey, last lane) treated with different concentrations of iron chelator deferoxamine after 48 hours of subculture. Error bars corresponds to the standard deviation of triplicates. Confirmation of TbMCP17-myc protein expression is presented in the WB using myc antibody and in Coomassie Brilliant Blue (CBB) as a loading control. Growth curves can be found in Appendix A5-2.

The growth defect caused by TbMCP17 depletion was also confirmed using RNAi cell line clone 3. RNAi cell line presented a significant decrease of cell density compared to WT under various iron conditions (Figure 4-14). Under normal media condition, RNAi cell line showed approximately 40% growth of WT, which was higher than that of *ΔTbMCP17/TbMCP17cmyc*^{ti} (17.4%). This was very likely due to the incomplete depletion of TbMCP17: 40% of mRNA level of TbMCP17 in RNAi cell line was detected (Figure 4-12). When deferoxamine was applied, growth defect of TbMCP17 RNAi was more severe with a growth ratio reduced to 20% (Figure 4-14, Appendix A5-3 for growth curves).

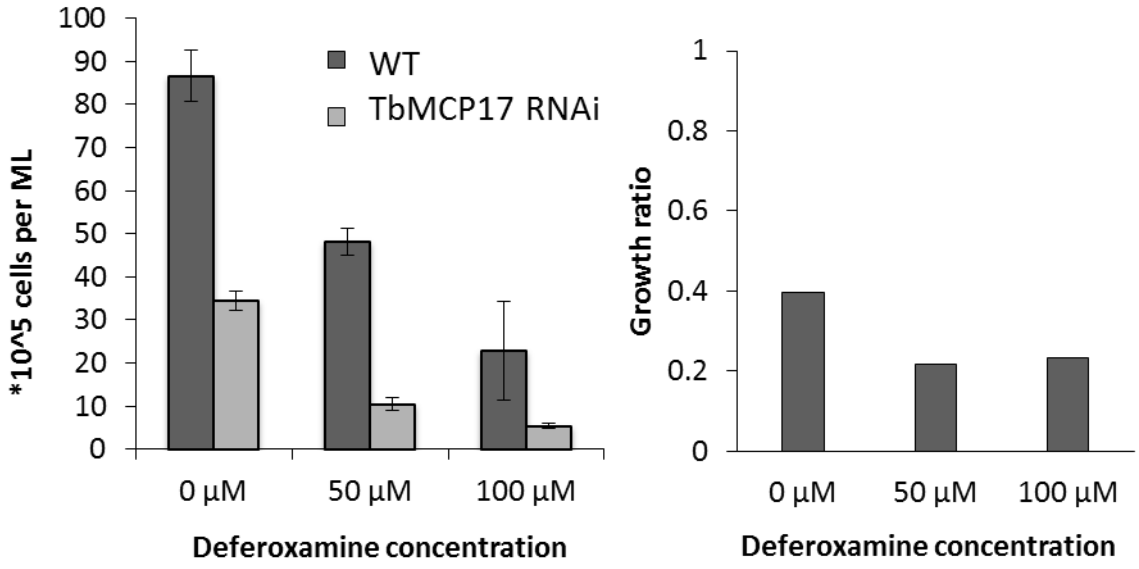

Figure 4-14 TbMCP17 RNAi caused growth defect
The left panel shows cell densities of wild type (WT) cells (dark grey, first lane) and TbMCP17 RNAi clone 3 (light grey, second lane) treated with different concentrations of iron chelator deferoxamine after 48 hours of subculture. Error bars corresponds to the standard deviation of triplicates. Furthermore, the growth ratio is calculated by dividing TbMCP17 RNAi growth by WT growth under each deferoxamine concentration. RT-qPCR of TbMCP17 RNAi clones is showed in Figure 4-12 confirming that RNAi was working at mRNA level. Growth curves can be found in Appendix A5-3.

4.6 Mitochondrial iron content is decreased in TbMCP17 knockout cells

The gathered growth phenotypes suggested that TbMCP17 imported iron into the mitochondria and the depletion of TbMCP17 caused severe growth defect under standard medium and a further growth reduction under iron-limiting condition. This indicated that mitochondrial iron content in TbMCP17 knockout cells might be decreased. Thus, the iron content of total cell lysate and mitochondria were measured for WT, *TbMCP17cmyc*^{ti} and *TbMCP17 RNAi* cells.

In the standard medium, WT and *TbMCP17cmyc*^{ti} cells presented similar Fe content: the total cell contained around 0.8 nM per 10^8 cells, and the mitochondria contained 0.6 nM of iron (Figure 4-15 A). Despite that *TbMCP17 RNAi* cells contained more iron in the total cell (0.99 nM), mitochondria possessed lower iron than WT and *TbMCP17cmyc*^{ti} (0.55 nM). Low iron in mitochondria of TbMCP17-depleted cells indicated that TbMCP17 was strongly related to mitochondrial iron transport, supporting that TbMCP17 was very likely to be a mitochondrial iron transporter. Since the knockdown of TbMCP17 caused a deficiency in iron importing, more iron was imported into cells to boost mitochondrial iron import, which led to a higher iron content of the total cell. The iron distribution percentage (Fe_{mito}:Fe_{total}) showed the same pattern as mitochondrial iron content. Mitochondria of WT and *TbMCP17cmyc*^{ti} contained approximately 75% of total cellular iron, with the exception of *TbMCP17 RNAi* cell line of only 56% (Figure 4-15 B).

As shown in Sections 4.3 & 4.4, TbMCP17 played a more important role under iron depleted conditions. Therefore, the same iron content measurement experiment was conducted on cells grown on heme-depleted medium. Under this condition, the iron content of each of the three cell lines was lower than that under the standard medium condition, supporting that PCF *T. brucei* indeed used heme as an iron source. *TbMCP17cmyc*^{ti} seemed to acquire more iron in both mitochondria and total cell (Figure 4-15 C) than WT with the same iron distribution percentage (Figure 4-15 D). Consistent with the previous results, *TbMCP17 RNAi* cell line presented a more severe decrease in

mitochondrial iron content in heme-depleted condition (0.3 nM) and a decrease of total cell iron content around 0.6 nM. In addition, a lower iron distribution percentage (52%) was found in Figure 4-15 D. Noticeably, the iron distribution percentage stayed at a similar level within each cell line under both standard and heme-depleted conditions. This indicated a tight regulation towards iron content *T. brucei* had.

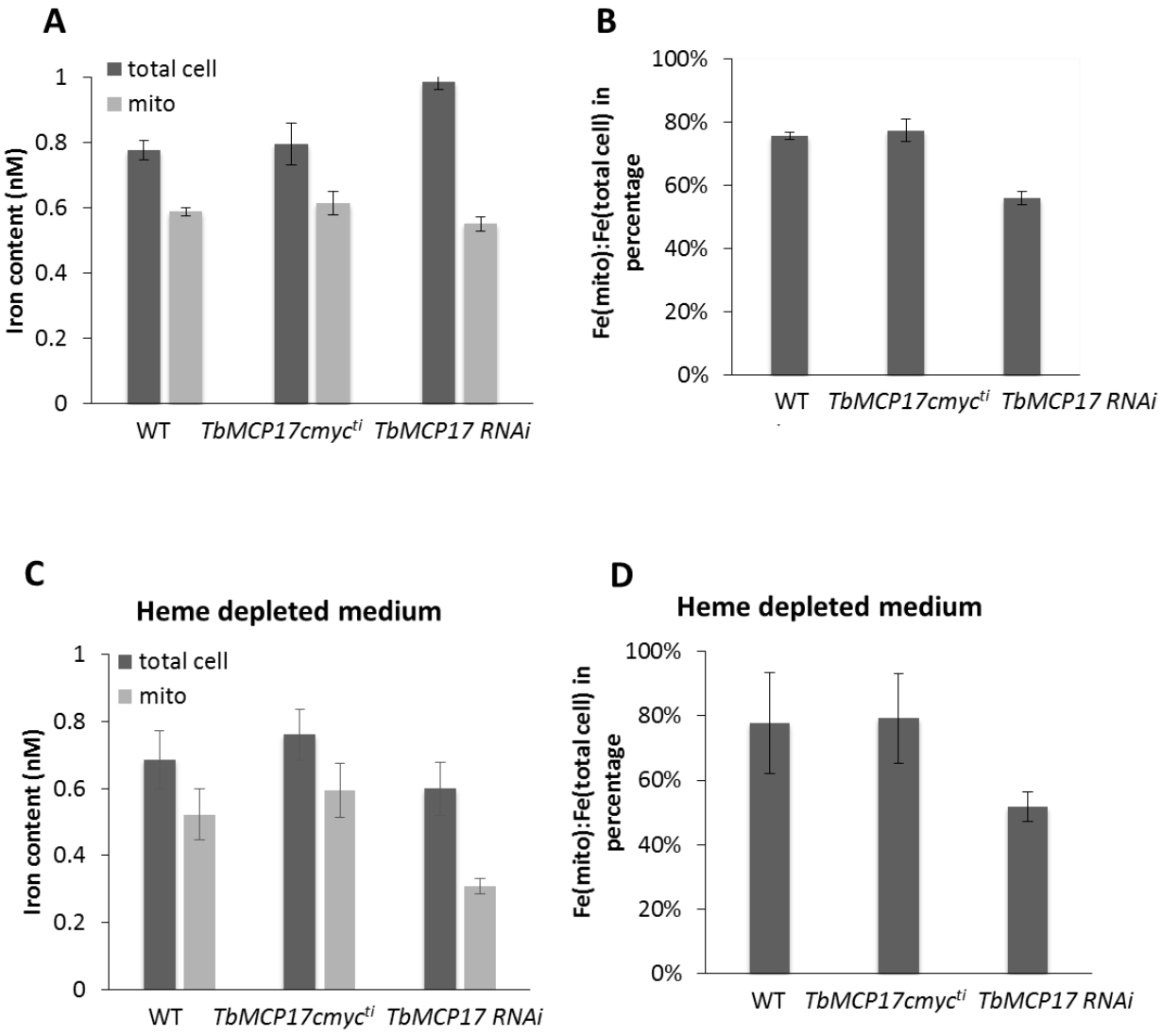

Figure 4-15 Iron content of WT (PCF449), TbMCP17 over-expression cells (*TbMCP17cmyc^{ti}*) and *TbMCP17 RNAi* cells in total cell and mitochondria

Values generated from cells cultured in the standard medium are displayed in A and B, while C and D present results from heme-depleted medium (using the dialysed serum). Bar charts A and C are iron content (nM) per 10^8 cells from the total cell (dark blue) and mitochondria (light blue). Bar charts B and D demonstrate the iron distribution in percentage (Fe_{mito}:Fe_{total}). Error bars calculated from triplicates are added.

4.7 TbMCP17 rescued growth defect caused by mitochondrial iron transporters in yeast

To confirm that TbMCP17 was indeed a mitochondrial iron importer, yeast functional complementation was performed by using yeast strains wild type DBY747, BY4741 (strain genotypes listed in Section 2.11.1) and mitochondrial iron transporters MRS3 & MRS4 knockout strain GW403 (presented as ΔMRS3/4 below). The complementation effect was examined by introducing TbMCP17 into the ΔMRS3/4 cell line to check whether the growth defect was rescued. Also, MRS3 was transfected to ΔMRS3/4 as a positive control.

4.7.1 Plasmid construction

Yeast transfection construct pCM190 was used in this study. The ORF of TbMCP17 and MRS3 were amplified and inserted into the vector using restriction sites BamH I & Not I and BamH I & Pst I, respectively, with the myc tag added via two-step sequential PCR. The resulting plasmids were tested using PCR (Figure 4-16 A). The fragment size of TbMCP17 (approximately 900 bp) was amplified for all clones. Furthermore, restriction enzyme digestion (Figure 4-16 B&C) was performed using the respective cloning enzyme sites, and fragments of predicted size were dropped out (900 bp for TbMCP17, 950 bp for TbMCP17-myc and MRS3). The potential clones were further sequenced (Appendix A4-3 & A4-4) and verified to be the right plasmids of pCM190+TbMCP17, pCM190+TbMCP17-myc and pCM190+MRS3.

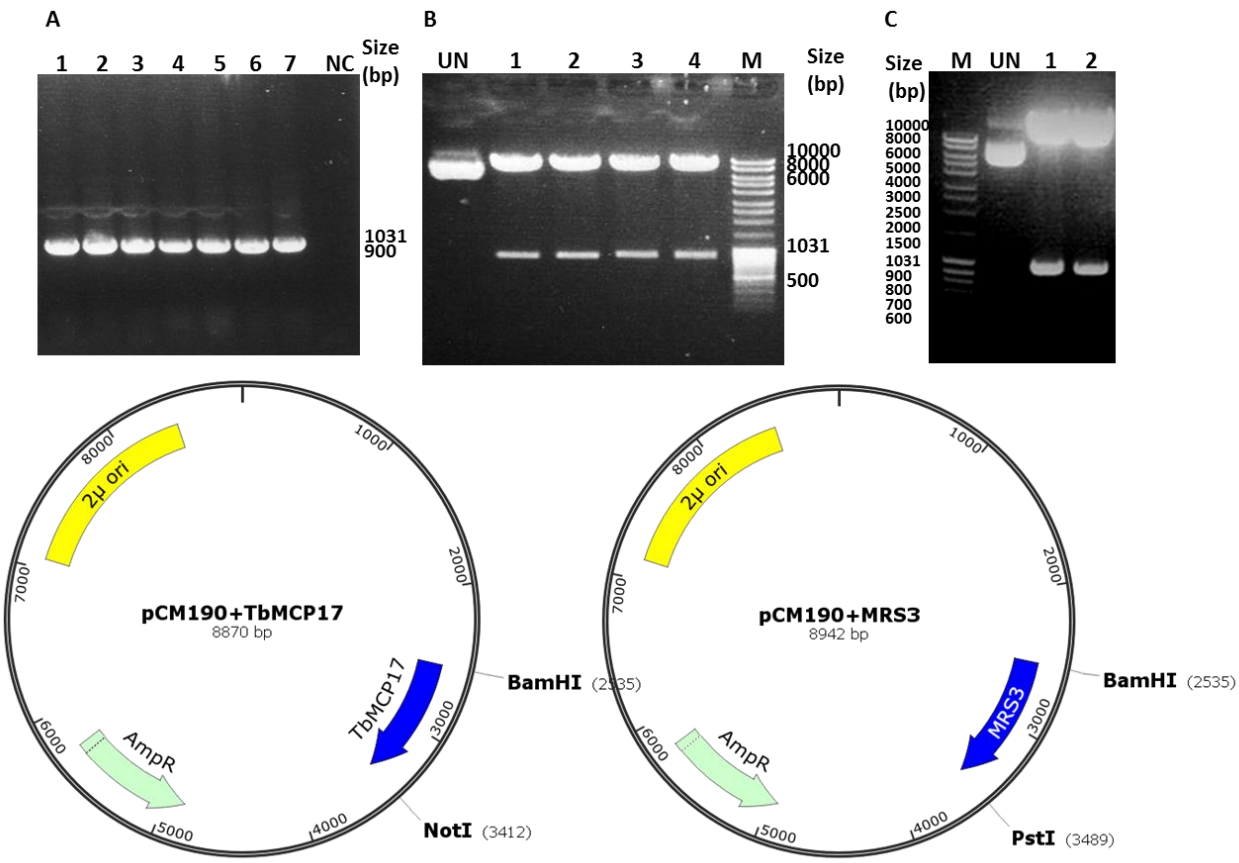

Figure 4-16 Plasmid construction of TbMCP17 yeast complementation
PCR confirmation is shown in A using TbMCP17 forward and reverse primers with clones containing pCM190+TbMCP17 (lane 1-7) or pCM190+TbMCP17-myc (lane 5-7), respectively. B demonstrated the restriction enzyme digestion results using BamH I & Not I on pCM190 inserted with TbMCP17 or TbMCP17-myc. UN stands for undigested plasmids. Digestion results of pCM190+TbMCP17 are shown in lane 1 & 2 and those of pCM190+TbMCP17-myc in lane 3 & 4. C shows the confirmation of two pCM190+MRS3 constructs from two separate clones by digesting with BamH I & Pst I. Plasmid maps of pCM190+TbMCP17 and pCM190+MRS3 are attached with indications of restriction enzyme sites used.

4.7.2 Growth complementation

pCM190 containing TbMCP17 and MRS3 were transfected to ΔMRS3/4 cell line, and empty plasmid pCM190 was transfected to wild type cell line BY4741 and ΔMRS3/4 as a control. Obtained yeast cell lines were grown on different carbon sources to examine the growth effect. The plate results showed that GW403 (ΔMRS3/4+pCM190) grew a bit slower than the rest cell lines WT (BY4741+pCM190), ΔMRS3/4+TbMCP17 and ΔMRS3/4+MRS3 (Figure 4-17). While in glycerol medium, where cell growth is more reliant on mitochondrial function, a more significant growth defect was observed in

GW403, which was consistent with Froschauer's finding (Froschauer et al. 2009). Furthermore, recombinant expression of TbMCP17 in the ΔMRS3/4 strain (ΔMRS3/4+TbMCP17) restored growth to WT levels. The introduction of MRS3 rescued ΔMRS3/4 growth to some extent, but the growth was not as good as that of WT and ΔMRS3/4+TbMCP17. The possible reason was that the expression level of MRS3 (promoted by the plasmid) was different from the expression level of endogenous MRS3.

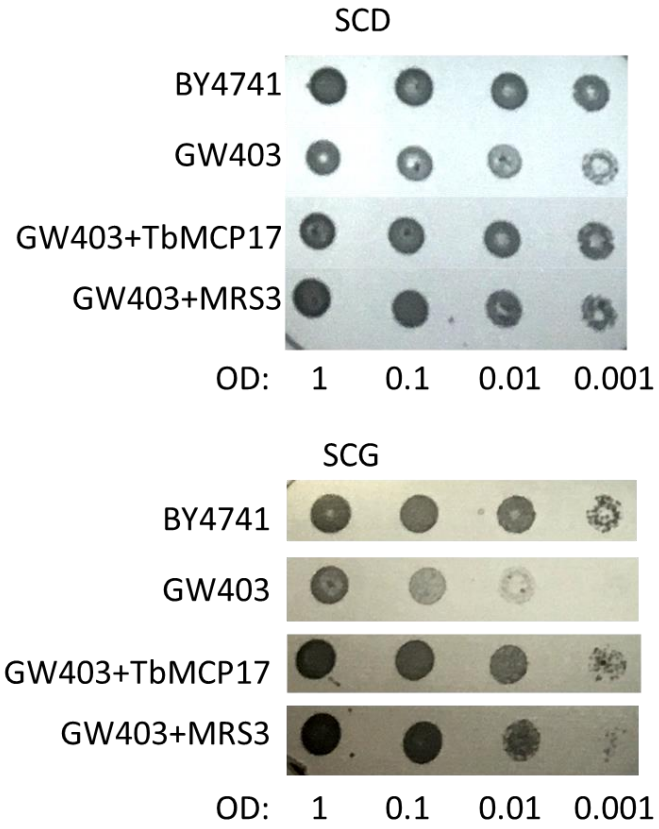

Figure 4-17 Plate results of TbMCP17 complementing ΔMRS3/4 cell line
Wildtype *S. cerevisiae* BY4741 contains the empty pCM190 expression vector. MRS3/4 deficient yeast strain (GW403) contains empty pCM190 or TbMCP17 open reading frame or MRS3 (as a control). The four dots in one line are the ten-fold dilution of each cell line from OD 1 to OD 0.001. The results are representative of two individual experiments. Synthetic complete media minus uracil was supplemented with dextrose (SCD) or glycerol (SCG) to trigger mitochondrial metabolism.

At the same time, four cell lines were inoculated to YPD (with glucose), YPG (with glycerol), YPD+BPS (iron chelator) and YPG+BPS media, and their growth was monitored up to 35 hours. As presented in Figure 4-18, on YPD medium, WT grew fastest and the rest grew at approximately the same speed. In YPG media, ΔMRS3/4+TbMCP17 managed to rescue cell growth to some extent (faster than ΔMRS3/4 but slower than BY4741), while ΔMRS3/4+MRS3 presented similar growth phenotype of knockout strain. Furthermore, as iron depletion was conducted using iron chelator BPS, recombinant expression of TbMCP17 managed to rescue cell growth under dextrose medium and over-restore growth under glycerol medium, indicating that TbMCP17 was sensitive to iron concentration in the media and played a more important role under iron limiting condition. This result itself was consistent with the finding in *T. brucei* presented earlier in this chapter.

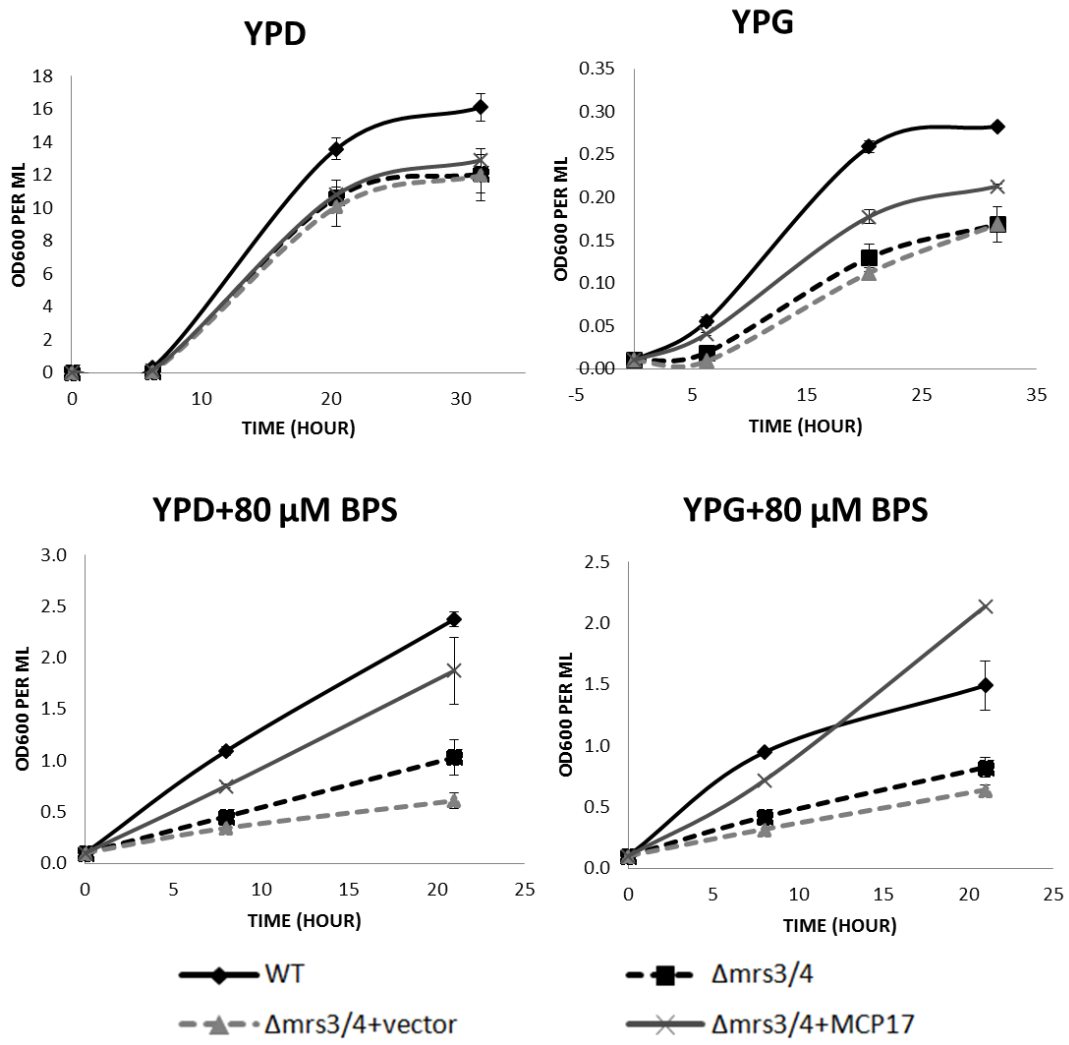

Figure 4-18 Liquid culture results of TbMCP17 complementing ΔMRS3/4 cell line under standard or iron depriving conditions

Wildtype *S. cerevisiae* BY4741 containing empty pCM190 expression vector (black solid line with diamonds), MRS3/4 deficient yeast strain (GW403) (black square lined up with a broken line), GW403 containing empty plasmid pCM190 (grey broken line with triangles) and GW403 containing TbMCP17 open reading frame (grey solid line with crosses) are presented. Error bars are standard deviations of triplicates. The figures are representatives of three single experiments. BPS is an iron chelator bathophenanthrolinedisulfonic acid.

4.8 Protein expression and antibody testing

In order to better characterise function(s) of TbMCP17, the protein expression level was determined by Western Blot analysis using a specific antibody. Thus TbMCP17 protein was heterologously expressed, purified and used for antibody generation. The efficiency of TbMCP17 antisera was further determined.

4.8.1 Plasmid construction

TbMCP17 open reading frame (ORF, 870 bp) was amplified using oHU349 and oHU350 primers (see Table 2-1) and inserted into the pET28 vector via restriction sites BamH I and Hind III. Potential clones were checked with PCR and restriction enzyme digestions. Colony PCR was performed towards eleven potential clones with oHU349 and oHU350 primers, and templates from clone 1, 3, 4, 5, 6, 8, 9, 10 and 11 did show the expected DNA product of 900 bp (Figure 4-19 A). Clones 1, 3, 4, 5, 6, and 8 were then digested with BamH I & Apa I or Hind III & Apa I (Figure 4-19 B). Double digestion of pET28+TbMCP17 using BamH I & Apa I should result in two fragments of 1136 bp and 5084 bp in size, while Hind III &Apa I digestion should create two fragments sized 2012 bp and 4208 bp, respectively (Figure 4-19 C). Figure 4-19 B suggested that plasmids 1, 3, 4, 5, 6 and 8 were all positive. Plasmid 1 was then chosen for sequencing with specific primers of the pET28 plasmid (T7-pET-Mod and T7 term, see Table 2-1). Sequencing results were aligned with TbMCP17 ORF DNA sequence (Figure 4-20). Five mutations were revealed, four of which coded for the same amino acid as before (ATC and ATT coding for isoleucine, GCT and GCC coding for alanine, CCC and CCT coding for proline, GGA and GGG coding for glycine), whilst the last mutation, codon ACT (Thr), mutated to AGT (Ser) and resulted in a mutation from a polar to an uncharged R group. It was worth noticing that sequence alignment of pET28 +TbMCP17 isolated from the sequence used for sequencing was derived from genome sequence derived from strain 927, while strain 427 was used in the lab. Thus, the resulting protein was assumed to be similar in terms of structure and function. Hence, the correct position and sequence of plasmid pET28+TbMCP17 were confirmed and used for protein expression.

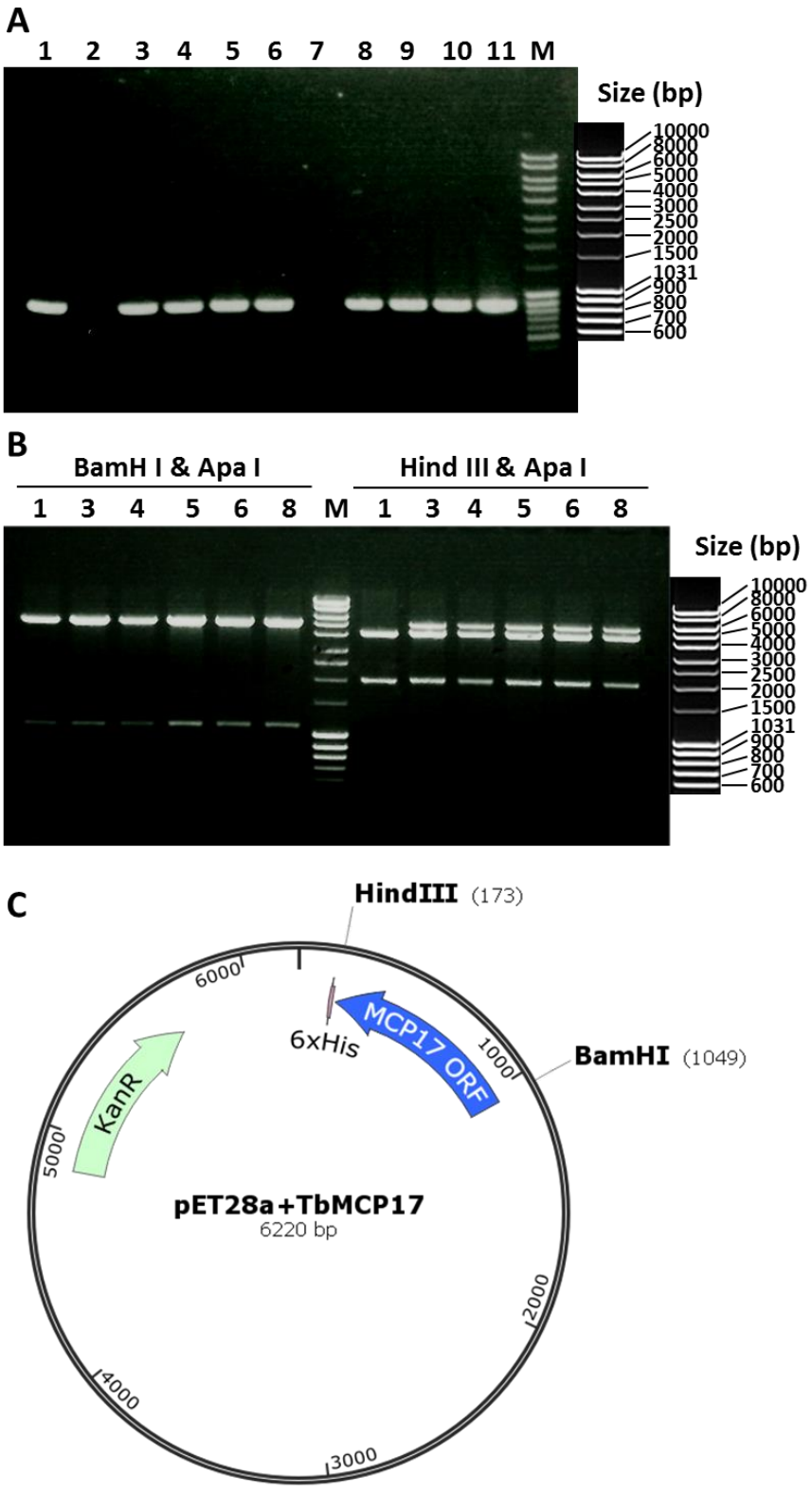

Figure 4-19 pET28+TbMCP17 plasmid examination with PCR and enzyme digestion

A displays colony PCR result of potential 11 clones with cloning primers (oHU349 and oHU350, see Table 2-1). B demonstrates digestion results using BamH I, Apa I and Hind III towards potential positive plasmids. C presents a simplified plasmid map of pET28+TbMCP17 indicating TbMCP17 ORF and related restriction enzyme sites.

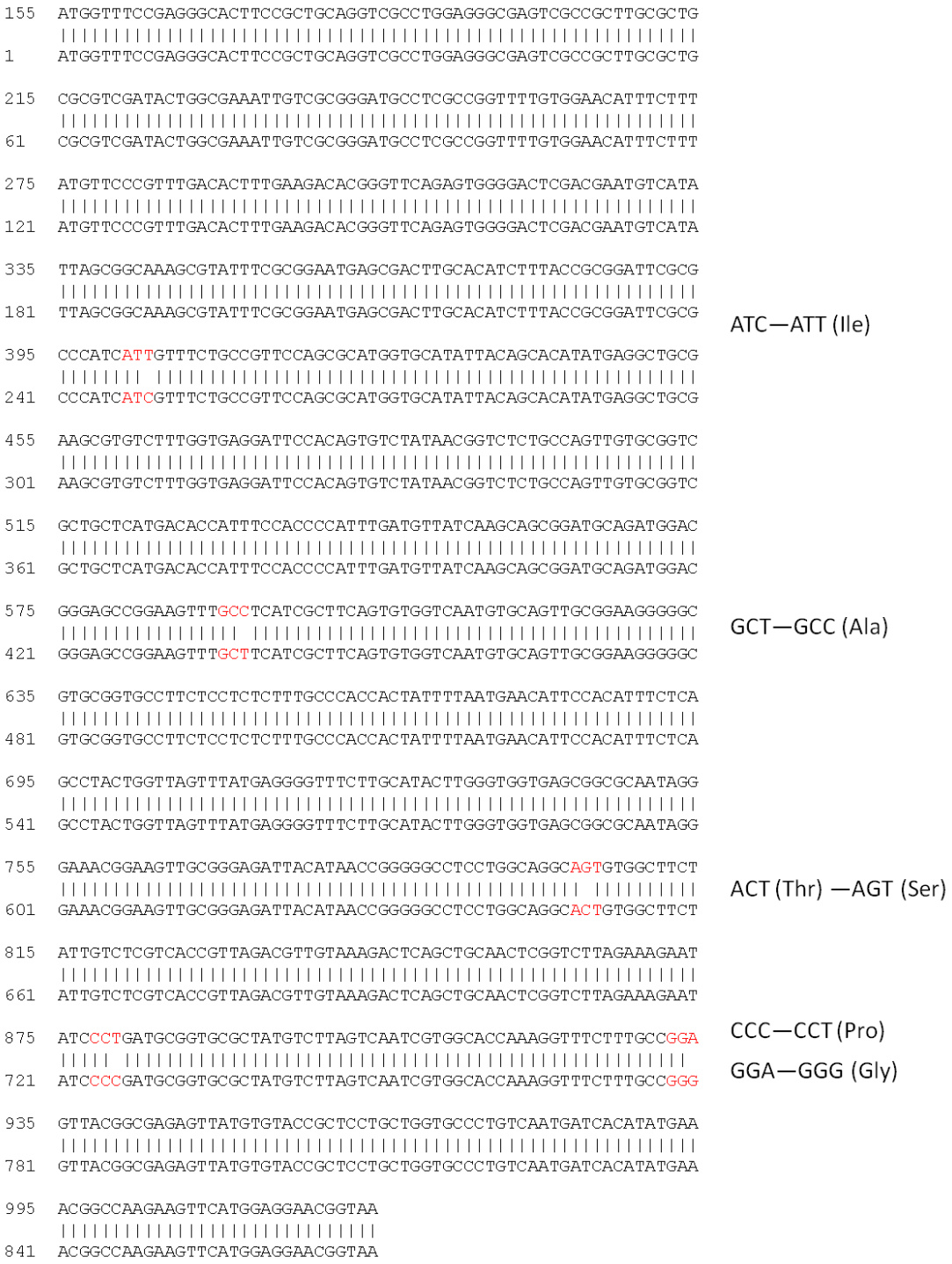

Figure 4-20 DNA alignment of pET28+TbMCP17 sequence result and TbMCP17-full transcript

The sequence of pET28+TbMCP17 amplified by T7-pET-mod and T7 term primers (see Table 2-1) are shown. The upper line represents pET28+TbMCP17 sequence result, while the lower line displays TbMCP17-full transcript. Mutations are coloured red and related coding amino acids are presented on the right in the brackets.

4.8.2 Protein expression

In order to produce a significant amount of protein, a special inducible strain Lemo21 (DE3) was transformed with the generated plasmid pET28+TbMCP17 for protein expression. Protein expression was induced by the addition of 0.4 mM IPTG and the expression level was negatively controlled by the addition of L-rhamnose (Figure 4-21). As L-rhamnose concentration increased, the protein expression level was down-regulated. A corresponding CBB gel was used as a loading control, and TbMCP17 was visible at 32 kDa and indicated with a triangle.

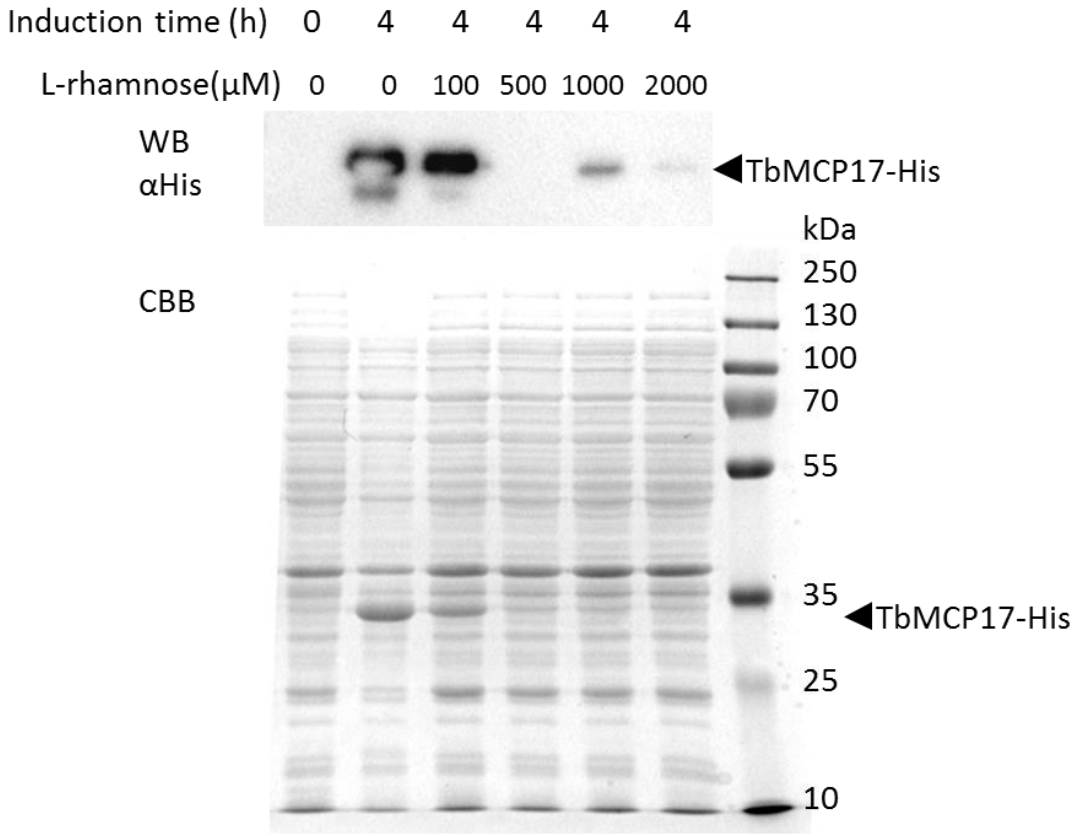

Figure 4-21 TbMCP17 protein expression induced with IPTG and controlled by L-rhamnose in Lemo21 (DE3) strain

WB and CBB display samples collected from cells which were induced for 4 h under different concentrations of L-rhamnose (0, 100, 500, 1000, and 2000 μM), with the first lane contains non-induced cells. TbMCP17-His expression is detected with His antibody. CBB staining is used as a loading control. For each lane, *E.coli* cells of OD600=0.02 are loaded.

Heterologously expressed protein has been found to end up in insoluble and inactive protein aggregates called inclusion bodies (Rosano & Ceccarelli 2014; Wingfield et al. 2001). In order to get the maximum amount of purest protein, induction of TbMCP17 without L-rhamnose was applied to further experiments. Thus, purification of inclusion bodies and solubilisation were performed.

As shown in Figure 4-22, TbMCP17-His expression was successfully induced and purified. Cell lysis using the French press did not affect protein amounts (Figure 4-22 A). In the following steps, samples of supernatant and pellet from each step were collected to determine where the protein rested. When compared S1 with TC (Figure 4-22 A), only a small amount of protein was detected in S1, which indicated that the majority of TbMCP17 protein was localised in inclusion bodies. The inclusion bodies were then washed with native resuspension buffer with/without 0.1% Triton X-100. These washes were essential for removing contaminants from inclusion bodies but were unable to solubilise TbMCP17. Then, inclusion bodies were washed twice with 0.1% sarkosyl or 5M urea. S4 and S5 presented approximately the same amount of protein, indicating that 0.1% of sarkosyl was enough to solubilise TbMCP17. On the other hand, less protein was detected in lane S7 than in S6, suggesting that 5M urea could only dissolve inclusion bodies to some extent. See Figure 4-22 B for a clear overview of protein expression and purification steps.

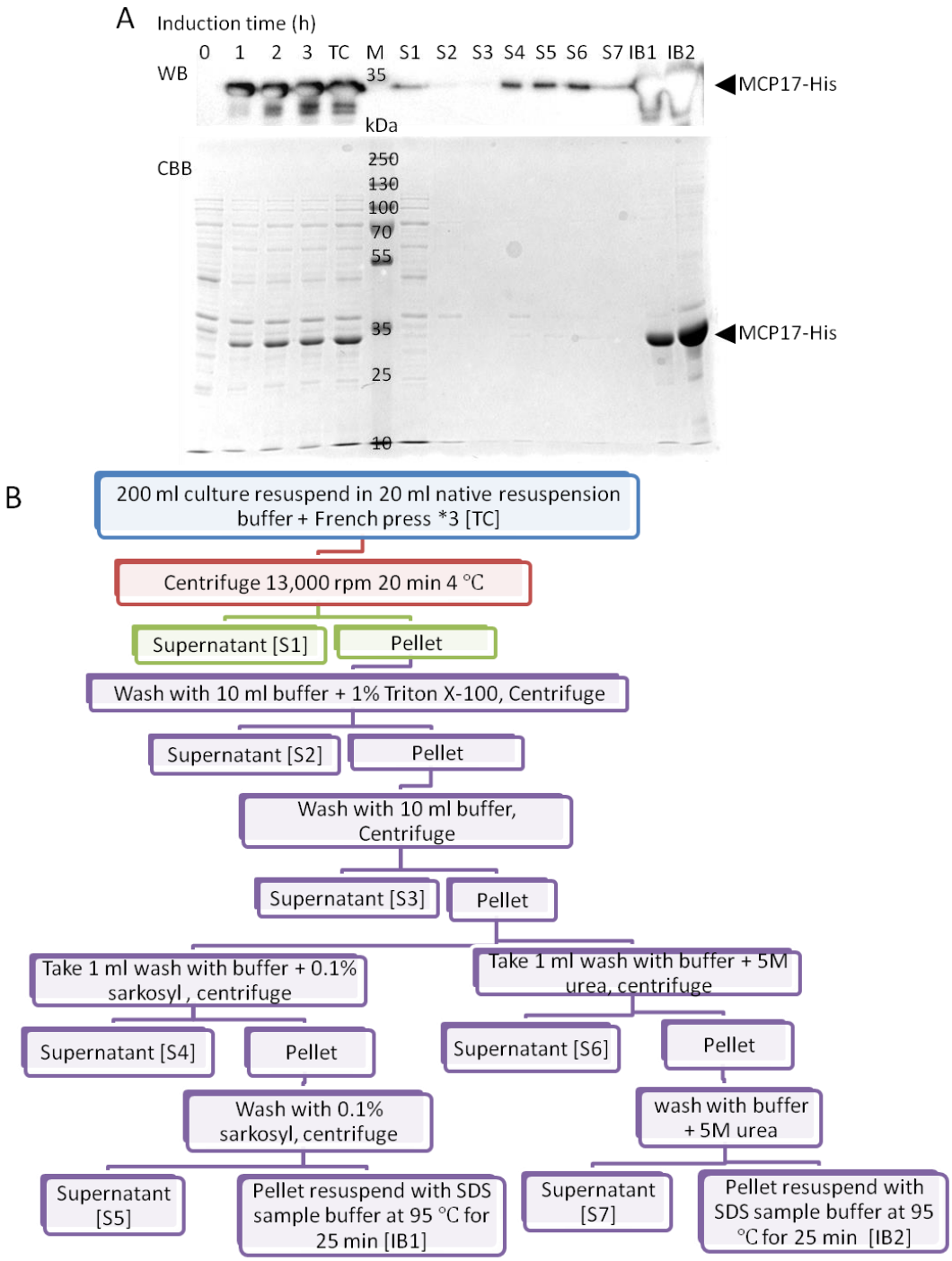

Figure 4-22 TbMCP17 protein solubility determination and wash of inclusion bodies

The left panel in A presents the induction of protein expression, and right panel of the marker shows different washes of inclusion bodies and final pellets. Figure B presents the samples collected for SDS-PAGE and WB. Basically, 200 ml of induced culture was resuspended in 20 ml native resuspension buffer and passed through French Press three times, and a sample of TC (total cell) was collected. Afterwards, high-speed centrifugation of 13,000 rpm for 20 minutes at 4 °C was performed to separate soluble protein (supernatant, S2) and inclusion bodies (pellet). The resulting pellet was washed once more with the same buffer, and then supernatant (S3) was collected. The washed pellet was resuspended in 10 ml of wash buffer. 1 ml aliquot of the resuspension was used

to wash twice with buffer containing 0.1% of sarkosyl (S4, S5) or 5M urea (S6, S7). The final inclusion bodies of the two are named IB1 and IB2. Each lane contains 200 µl induced culture.

Therefore, the procedure was optimised as follows: after lysis by French Press and the following centrifugation to remove soluble proteins, inclusion bodies were washed by native resuspension buffer containing 0.1% Triton X-100 to remove insoluble contaminants. Inclusion bodies were then solubilised and followed by purification steps. In Figure 4-23, a range of urea (1 M, 2 M and 4 M) and sarkosyl (0.2%, 0.5% and 1%) were added to wash buffer and supernatants (A1, A2, B1, B2, C1, C2, D1, D2, E1, E2, F1, F2) after washes were loaded onto the gel. As presented in lane A to C, only 4 M of urea was able to solubilise a minor amount of TbMCP17 (only visible in WB but not CBB&SS), but sarkosyl was clearly found to be more efficient than urea in solubilisation with a lower concentration. In the CBB and SS, a non-specific band at approximately 37 kDa was completely removed by sarkosyl but not urea because the 37 kDa band appeared only in the first wash of sarkosyl (D1, E1 and F1). Furthermore, less protein was detected in F lane than in the other pellet lanes, indicating that part of inclusion bodies was dissolved into wash solution instead of staying in the pellet. Thus, 1% of sarkosyl was selected to solubilise inclusion bodies.

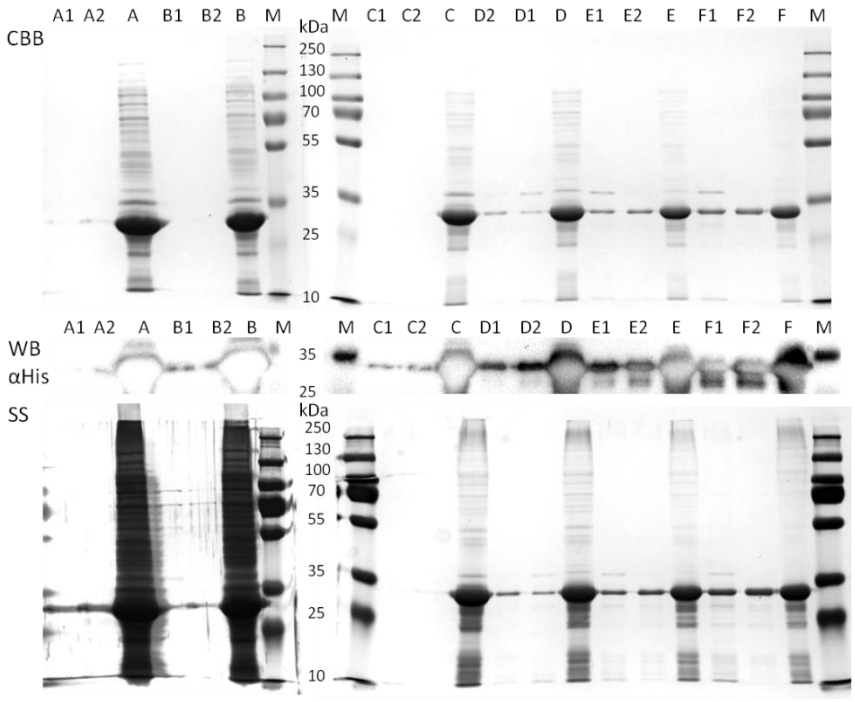

Figure 4-23 Purification and solubilisation of TbMCP17-His containing inclusion bodies

Chemicals with different concentrations tested one by one from group A to F are presented above. A: 1M urea; B: 2M urea; C: 4M urea; D: 0.2% sarkosyl; E: 0.5 % sarkosyl; F: 1% sarkosyl. The number (1 or 2) after letters is the supernatant of each wash. A letter without a number is the corresponding pellet from each group. TbMCP17 proteins detected with WB using His antibody are shown. A corresponding gel dyed with Coomassie Brilliant Blue (CBB) and silver stain (SS) is attached to visualise non-specific bands.

4.8.3 Ni-NTA protein purification and quantification

Washed inclusion bodies were loaded onto a Ni-NTA ageneose column for purification of the His-tagged recombinant TbMCP17. Ni-NTA agarose bound to His tags, while the unbound proteins flowed through the column. Unspecific bindings to Ni-NTA were removed by the following two washes, and TbMCP17-His were finally eluted. High molecular weight backgrounds were successfully removed from the sample. However, His tagged-Ni-NTA counteraction was found to be weak, and most of them found in the flow through (Figure 4-24). The failure of His-tagged binding might be due to: (i) a too high concentration of sarkosyl which interfered with binding; (ii) too short incubation time; (iii) the His tags of some proteins being not exposed to Ni-NTA due to an incomplete denaturation procedure; (iv) the too low binding capacity of Ni-NTA agarose. Experiments addressing all the problems mentioned above were performed, but the

binding efficiency was not increased. However, sufficient protein of the purification was obtained by reloading the flow through back to the column and repetition of the Ni-NTA binding procedure (Figure 4-25). The optimisation stopped accordingly.

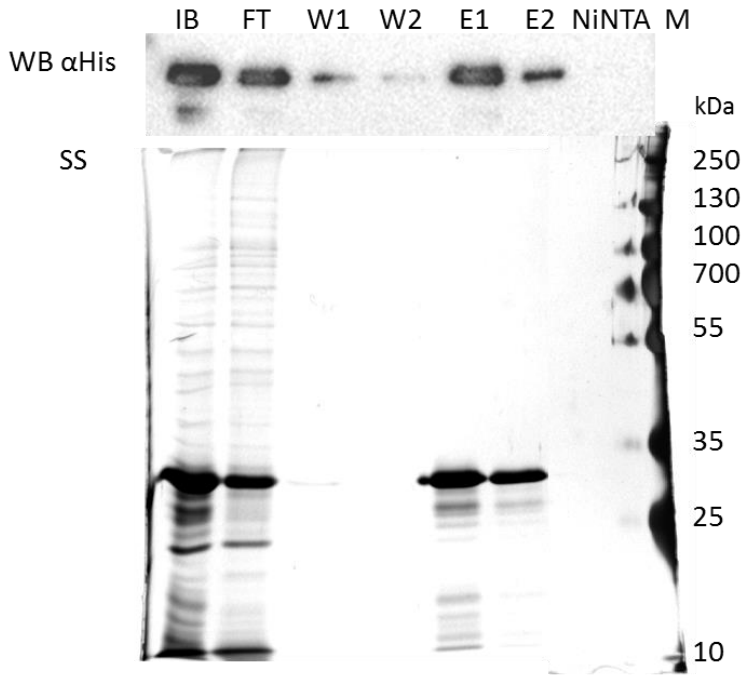

Figure 4-24 Inclusion bodies purified with Ni-NTA agarose
Inclusion bodies before loading onto Ni-NTA agarose (IB), the flow through (FT), washes (W1, W2), elutions (E1, E2) and the Ni-NTA agarose after elution (NiNTA) are presented on both WB probed with His antibody and on the silver stain (SS).

As mentioned earlier, TbMCP17 was only soluble in buffer containing a large amount of detergent (sarkosyl) which interfered with standard protein quantification methods like BCA protein assays. Thus, to quantify the protein concentration, BSA of various concentrations was run as standard alongside the protein sample and the density of which was compared with the target protein band on the CBB gel. Figure 4-25 showed that concentration of E 1:5 was larger than 1000 µg/ml, and concentration of E 1:10 roughly equalled to 600 µg/ml. Concentration of TbMCP17 elution under conservative estimation was 6000 µg/ml. 3 mg of protein (0.5 ml) was loaded onto a prep-gel, and the gel slice containing protein was cut out for antibody generation.

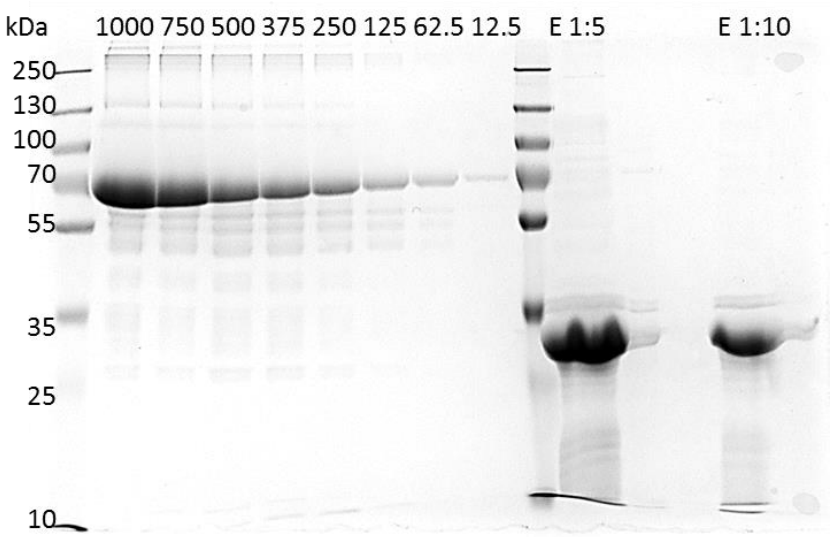

Figure 4-25 Quantification of TbMCP17 protein concentration in elution
BSA standard of different concentrations (from 12.5 µg/ml to 1000 µg/ml) is run on an SDS-PAGE gel and dyed with CBB. Elutions of TbMCP17-His were diluted five times or ten times before loaded onto the gel (labelled E 1:5 and E 1:10).

4.8.4 Antisera efficiency examination

The efficiency of two TbMCP17 antibodies (or antisera) generated from two rabbits were examined on both purified TbMCP17-His protein (Figure 4-26) and related *Trypanosoma brucei* cell lines (Figure 4-27). Both antisera were found to successfully recognise recombinant TbMCP17 (approximately 32 kDa) with antisera from rabbit 2 (called as antisera 2 below) showing higher titer. As for detecting TbMCP17 expressed in *Trypanosoma brucei*, only myc-tagged version of TbMCP17 was detected with TbMCP17 antisera 2 (see Figure 4-27). Thus, TbMCP17 antisera rabbit 2 was used in future experiments.

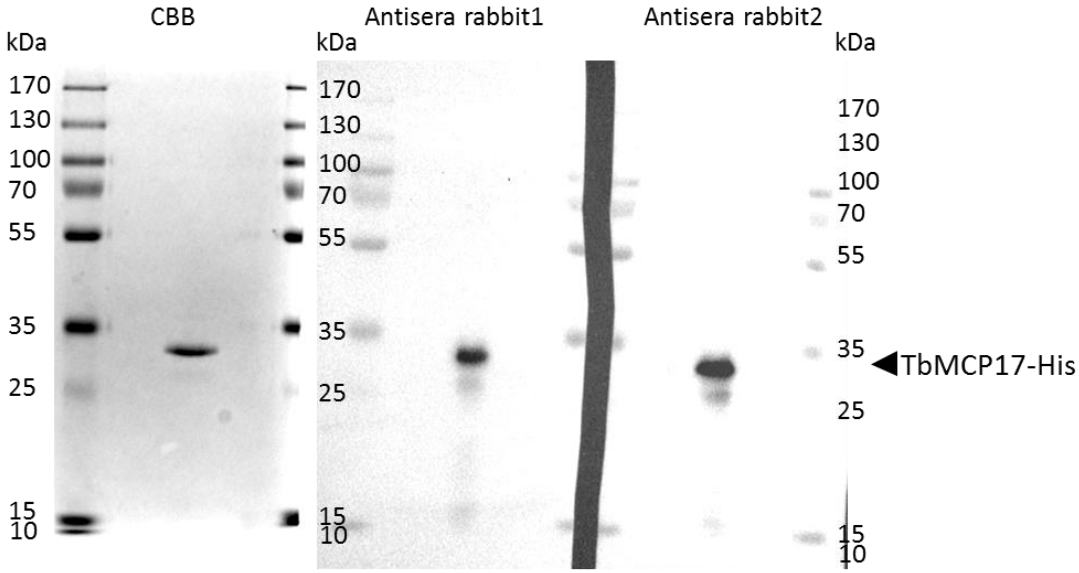

Figure 4-26 The detection of purified TbMCP17-His proteins using TbMCP17 antisera

WB results of TbMCP17-His proteins loaded in equal amount for the comparable results of the two antisera are displayed, and CBB lane contained 4 times more protein than WB to visualise the protein. Blank lanes added are to prevent overflow during loading. Both antisera 1 and 2 are diluted 1: 250 to serve as the primary antibody.

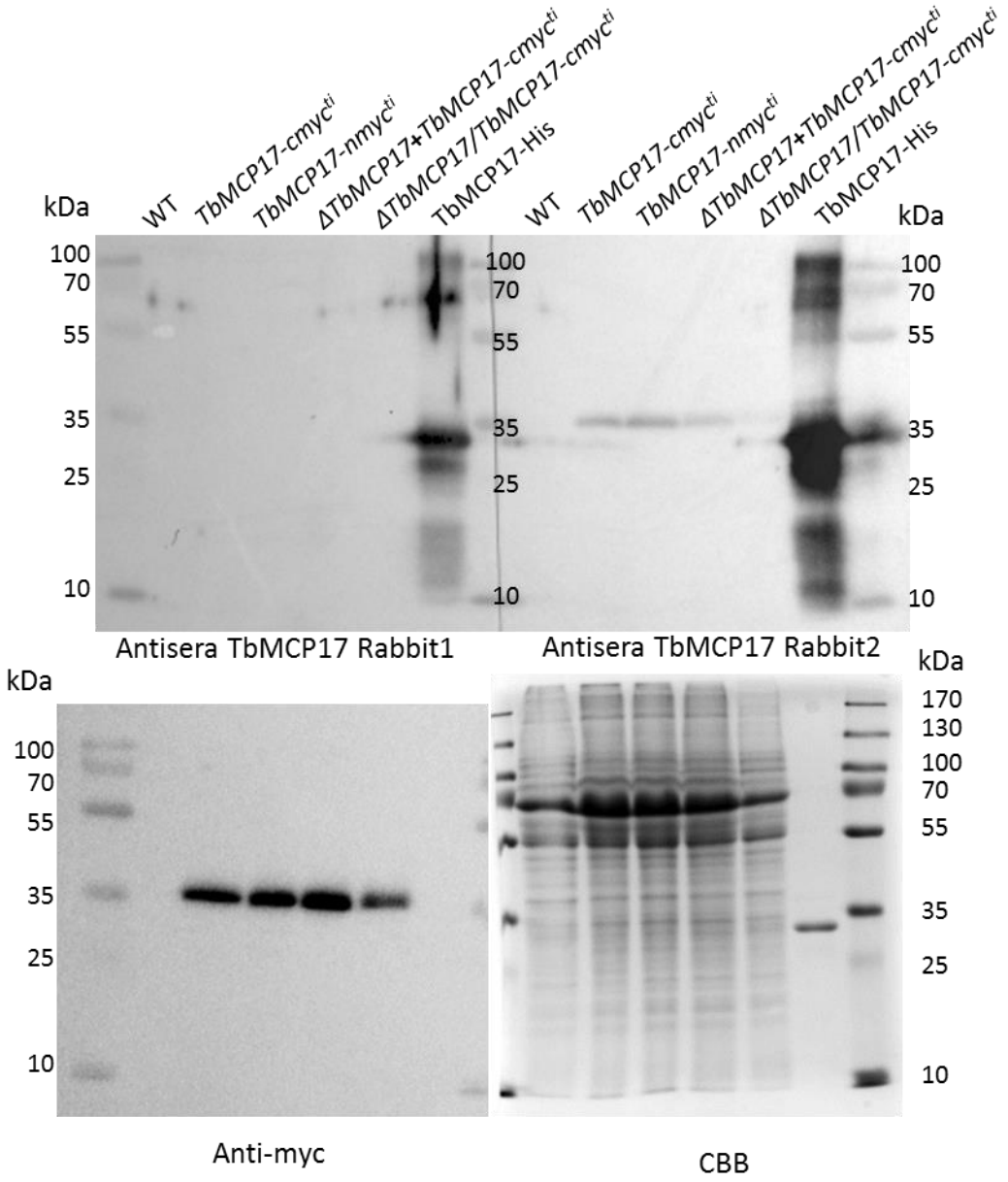

Figure 4-27 Detection of TbMCP17 from various *Trypanosoma brucei* cell lines using both antisera

Wildtype (WT), TbMCP17cmyc over-expression (*TbMCP17cmyc*^{ti}), TbMCP17nmyc over-expression (*TbMCP17nmyc*^{ti}), TbMCP17 conditional knockout containing inducible TbMCP17cmyc induced with tetracycline (*ΔTbMCP17+TbMCP17-cmyc*^{ti}), TbMCP17 conditional knockout without tetracycline (*ΔTbMCP17/TbMCP17-cmyc*^{ti}), and purified TbMCP17-His protein (TbMCP17-His) are examined. Primary antibodies used are TbMCP17 antisera 1, TbMCP17 antisera 2, and myc antibody. CBB gel is conducted to serve as a loading control.

4.9 TbMCP17 expression study

Since detecting TbMCP17 from WT cell line PCF449 remained problematic (discussed in Sections 4.8.4 and 4.9.1), two approaches were applied: (i) attempt to increase endogenous TbMCP17 level by growing cells in challenging conditions (iron depriving, minus heme, without glucose); (ii) optimisations of SDS-PAGE and WB conditions technically, such as improvements in sample preparation, blocking conditions, different types of membrane selection and purifications of crude antisera.

4.9.1 Endogenous TbMCP17 level was too low to be detected

TbMCP17 related cell lines (WT, *ΔTbMCP17/TbMCP17cmyc*^{ti}, TbMCP17 RNAi, *TbMCP17cmyc*^{ti} and *TbMCP17nmyc*^{ti}) were loaded on WB and tested with the antisera (Figure 4-28 left). TbMCP17 antisera detected myc tagged TbMCP17 (see the upper band of the lane 2, 5, and 6). However, the lower band was not endogenous TbMCP17 but background band, because it was present in both conditional double knockout and RNAi lane (labelled in Figure 4-28 unspecific band). The efficiency of TbMCP17 antisera was also tested on purified TbMCP17-His protein (Figure 4-28 right) and the same band of his antibody was detected by TbMCP17 antisera.

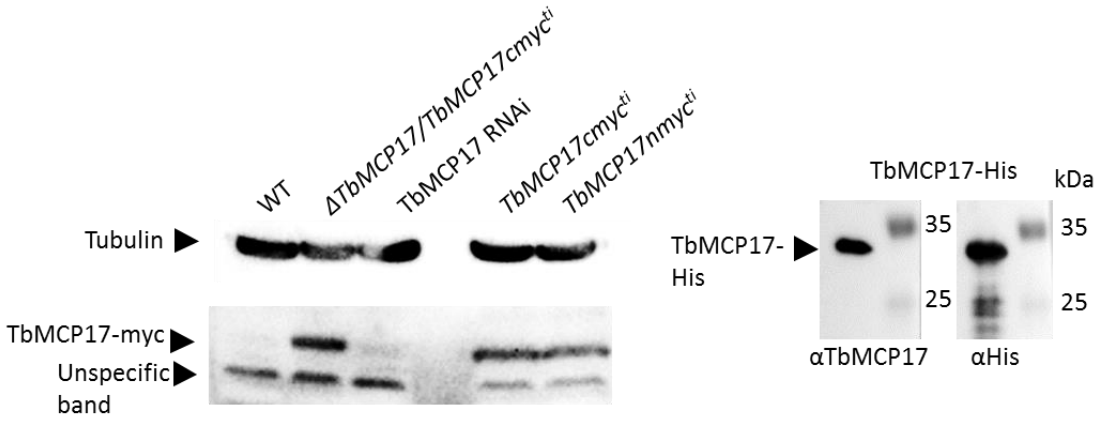

Figure 4-28 Endogenous TbMCP17 level was too low to be detected with TbMCP17 antisera

Multiple cell lines (WT, *ΔTbMCP17/TbMCP17cmyc*^{ti}, TbMCP17 RNAi, *TbMCP17cmyc*^{ti} and *TbMCP17nmyc*^{ti}) loaded onto an SDS-PAGE gel and incubated with tubulin and TbMCP17 antibodies are demonstrated. One blank lane was placed between TbMCP17RNAi and TbMCP17-cmyc to avoid the leak through of protein samples. On

the right panel, TbMCP17-His purified protein was loaded and probed with anti-TbMCP17 (αTbMCP17) and anti-His (αHis) antibodies. Each lane contains 1.25×10^7 cells.

4.9.2 TbMCP17 level under challenging conditions

Since TbMCP17 over-expression restored cell growth especially under iron-limiting conditions (see Section 4.3), it was possible for TbMCP17 to be regulated by iron concentrations. Thus, different concentrations of iron chelator deferoxamine were added to WT media, intending to see an up-regulation (detectable for WB analysis). However, no band other than the background band came up (Figure 4-29 A). Furthermore, the effects of heme and glucose depletion were examined by replacement of FCS to dialysed serum, and single compound depletion condition was achieved by adding back the same amount of heme or glucose as the standard medium setting. As presented in Figure 4-29 B, still no endogenous TbMCP17 was detected due to the extremely low abundance. To support that TbMCP17 antiserum was capable of detecting TbMCP17 proteins, a band around 35 kDa (the same size as TbMCP17-myc) was detected from *ΔTbMCP17+TbMCP17-cmyc*^{ti}. The correctness of this band as TbMCP17-myc was verified with myc antibody by detecting a band of the same size.

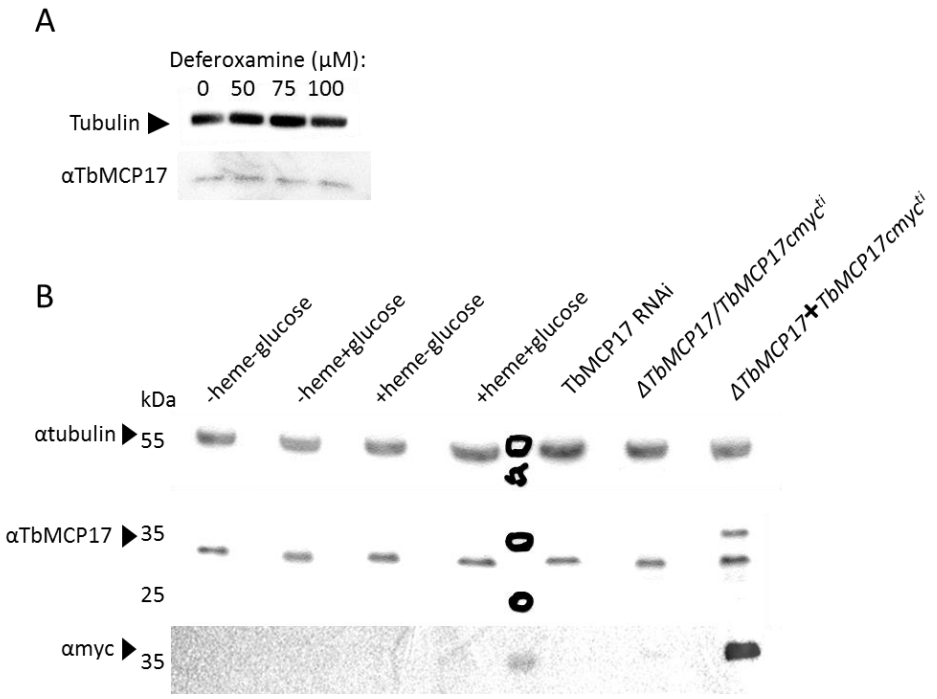

Figure 4-29 WB detection of TbMCP17 level under challenging conditions
A shows the WB result of 1.25×10^7 cells of WT treated with different concentrations of iron chelator deferoxamine probing with TbMCP17 antisera (αTbMCP17) and tubulin antibody (αtubulin) with the latter served as a loading control. The bands present in the αTbMCP17 were the background/contaminating bands, but not the TbMCP17. B displays WT cell line treated with either plus or minus heme/glucose probing with TbMCP17 antisera and tubulin antibody. TbMCP17 RNAi, *ΔTbMCP17/TbMCP17cmyc*^{ti} and *ΔTbMCP17+TbMCP17cmyc*^{ti} (with the induction of rescue copy by tetracycline) cell lines were loaded next to the experimental samples to eliminate the possibility that the non-specific background band might be taken as TbMCP17. The membrane was then incubated with myc antibody (αmyc).

Moreover, TbMCP17 mRNA level was also measured after 48 hours of culture in the specified medium by real time qPCR to determine whether the TbMCP17 level was regulated by the depletion of heme and/or glucose (Figure 4-30). As the qPCR results shown, TbMCP17 mRNA level was upregulated in the presence of heme regardless of glucose concentration (20% upregulation in glucose-depleted medium and 10% in glucose presence medium). The addition of glucose, on the other hand, resulted in a slight decrease in TbMCP17 mRNA levels (5% in heme-depleted and 10% in heme present conditions).

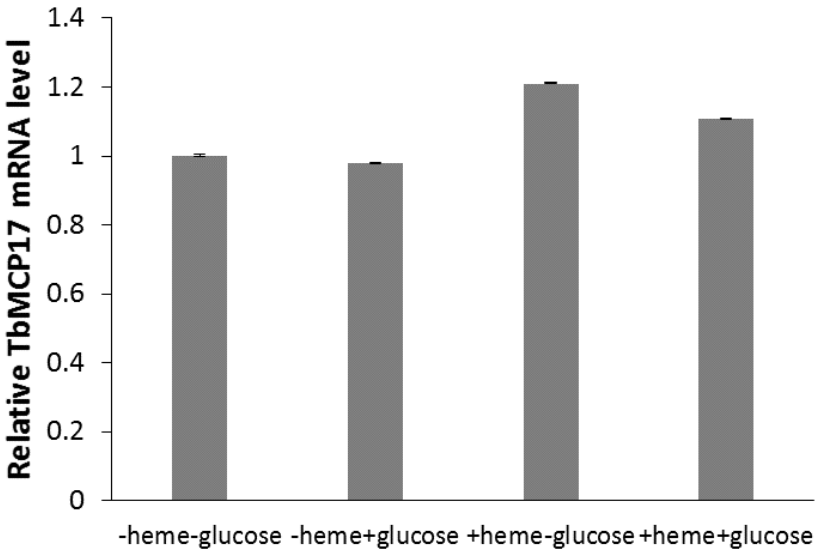

Figure 4-30 TbMCP17 mRNA level under variable heme and glucose conditions

Cells used in the experiment were cultured under specified conditions for 48 hours before harvesting. Dialysed serum was used in '-heme-glucose' group, 11.5 μM of heme and/or 5 mM of glucose were added accordingly. Data were derived from two separate real time qPCR experiments with triplicates in each experiment. TbMCP17 mRNA level was standardised against tubulin using respective primers. TbMCP17 mRNA level on double-depleted medium (-heme-glucose) was set to 100%.

In addition, because of the role iron played in electron transport chain, TbMCP17 level under oxidative stress was measured. WT cells were exposed to various concentrations of hydrogen peroxide for 48 hours, followed by the measurements of TbMCP17 mRNA and protein levels using quantitive PCR and WB, respectively. mRNA level of TbMCP17 was observed to be down-regulated by increasing concentrations of hydrogen peroxide: 90% of WT mRNA level under 50 nM hydrogen peroxide treatment and 75% under 100 nM hydrogen peroxide conditions (Figure 4-31). WB failed to recognise any specific band for TbMCP17 (data not shown), hence the regulation of TbMCP17 at protein level was in doubt. Combined qPCR with WB results demonstrated that TbMCP17 could be down-regulated by oxidative stress caused by hydrogen peroxide, but more convincing conclusion could not be drawn due to the detection limit of WB analysis.

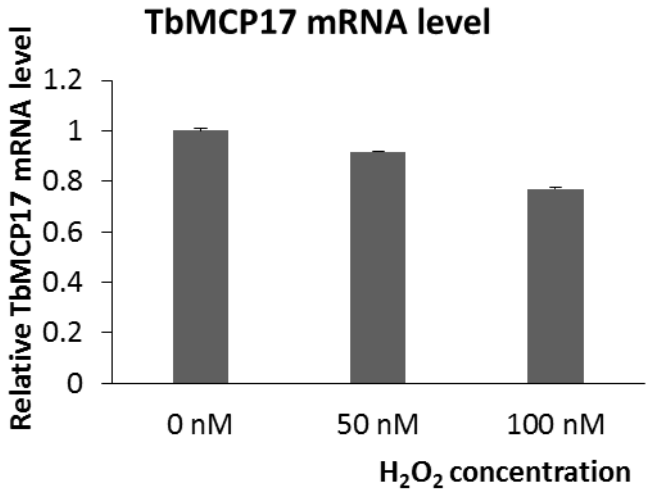

Figure 4-31 TbMCP17 mRNA level under variable hydrogen peroxide concentrations

Cells were cultured in media with the addition of 0 nM, 50 nM and 100 nM of H_2O_2 for 48 hours before the measurements. Data were derived from two separate real time qPCR experiments with triplicates in each experiment. TbMCP17 mRNA level was standardised against tubulin using respective primers. TbMCP17 mRNA level in standard culture medium (0 nM of hydrogen peroxide) was set to 100%.

4.9.3 Optimisations of SDS-PAGE and WB process

Since endogenous TbMCP17 could not be upregulated by the switch of carbon sources, iron limiting and heme depriving conditions, optimisations of SDS-PAGE and WB process were carried out trying to increase the sensitivity of the procedure so as to visualise TbMCP17 protein. In order to decrease background, different blocking reagents were tried. From the results (Figure 4-32 A), we could conclude that fish gelatin gave a clearer film than blocking with milk or BSA, so fish gelatin was chosen as the blocking reagent. Because TbMCP17 was a membrane protein, which tended to aggregate and form complexes like dimers, different sample preparation conditions were tested. As presented (Figure 4-32 second membrane), there was no remarkable difference among three preparations (95 °C for 5 min, 70 °C for 10 min, 37 °C for 30 min). Thus, the standard 95 °C for 5min preparation was applied to later experiments. Meanwhile, the nitrocellulose membrane was tested and showed a better signal with less background than PVDF membrane (Figure 4-32 B). Also, commercial blocking reagent superblock was tested to compare with 5% fish gelatin. The combination of nitrocellulose membrane

blocking with SuperBlock worked best (Figure 4-32 B). Consequently, this combination was applied for further experiments.

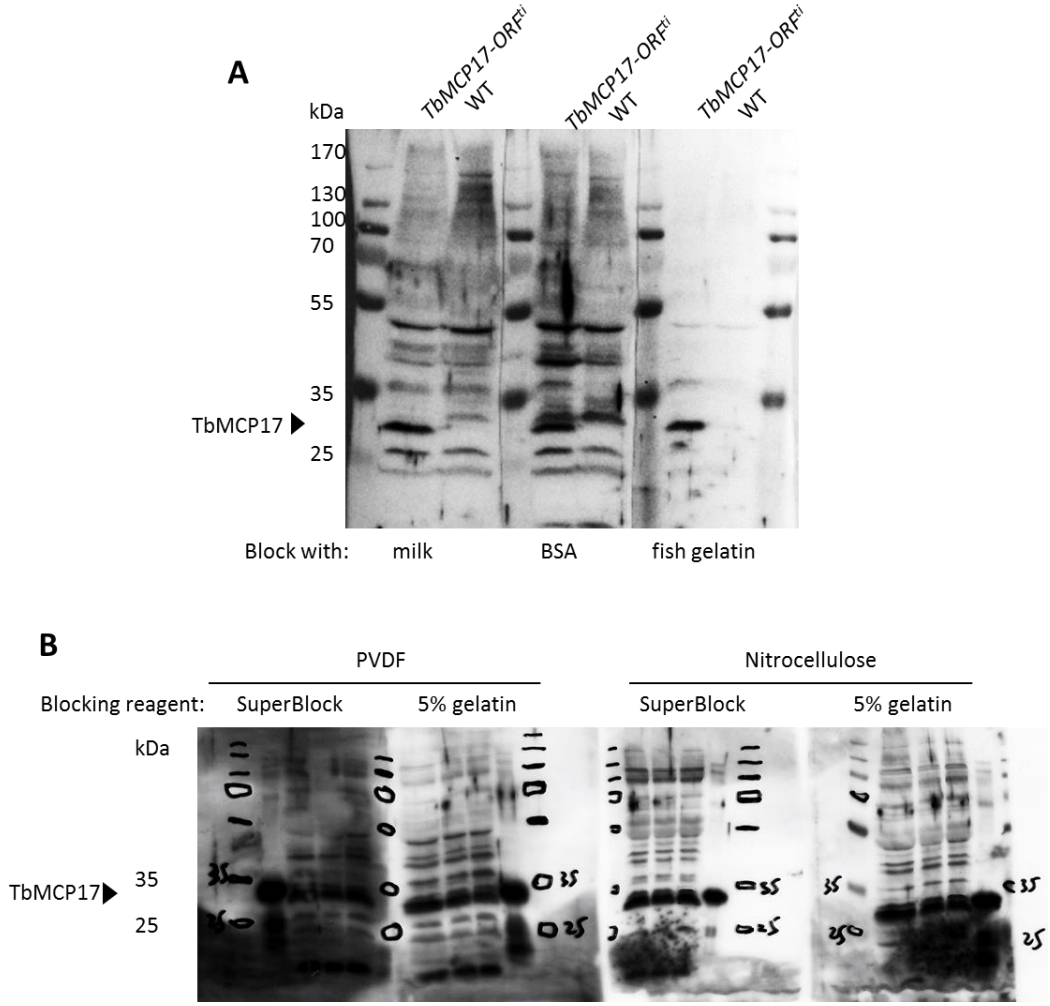

Figure 4-32 Optimisations of blocking reagents, membrane types and sample treatment

A demonstrates the same amount of WT and strain overexpressing TbMCP17 open reading frame without myc tag (*TbMCP17-ORF^{ti}*) blocked with 5% of milk, BSA or fish gelatin individually. B displays differently prepared *TbMCP17-ORF^{ti}* samples (lane 1, 95°C for 5 min; lane 2, 70°C for 10 min; lane 3, 37°C for 30 min) and lane 4 containing TbMCP17-His purified protein tested on both PVDF and nitrocellulose membrane, as well as on blocking reagent superblock and gelatin. Each lane contained 1.25×10^7 cells. The rest of the conditions stayed the same as standard WB procedure listed in Section 2.9.

Meanwhile, magnetic beads A/G (recognise both IgG binding domains: protein A and protein G) purification of TbMCP17 antisera was tested. As presented (Figure 4-33), the purified antibody produced less background than the crude antibody. In addition, cell numbers per lane were lowered to 5×10^6 cells (the same as standard WB settings for

Trypanosoma brucei). When comparing the upper panel with the lower panel in Figure 4-33, reduction of cell number led to clearer backgrounds and sharper bands.

Unfortunately, when looking at the result of 10 µl A/G purified antibody (Figure 4-33 right up panel), TbMCP17 was of the same size as background band (TbMCP17 ORF protein was the same height as the unspecific band from *ΔTbMCP17/TbMCP17cmyc*^{ti} and WT band), revealing that TbMCP17 could not be distinguished from the background band. Apart from that, no difference between WT and *ΔTbMCP17/TbMCP17cmyc*^{ti} patterns indicated that endogenous TbMCP17 amount was too low to be detected using TbMCP17 antisera by WB.

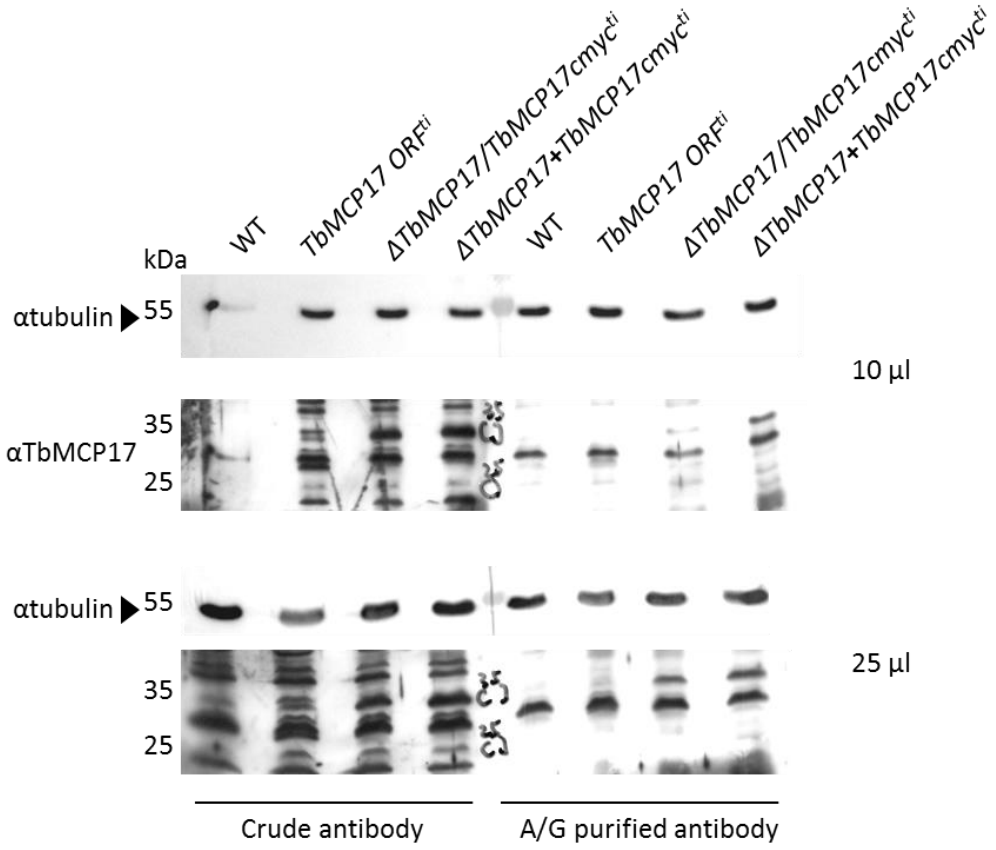

Figure 4-33 Optimisations of cell number per lane and purification of crude antisera

In the upper panel, 10 µl of samples containing 5×10^6 cells was loaded each lane, while 25 µl containing 1.25×10^7 cells in the lower panel. Four trypanosome strains were loaded, in which *TbMCP17-ORF*^{ti} served as a positive control and *ΔTbMCP17/TbMCP17cmyc*^{ti} as a negative control. The left part of the membrane shows result incubated with crude TbMCP17 antisera, and the right-hand side presents the outcome of A/G purified antibody. Tubulin is served as a loading control.

4.10 Conclusion

In this Chapter, the sequence of *TbMCP17* was analysed and shown to be the only homologue to mitochondrial iron transporters from humans and yeast by phylogenetic reconstruction, followed by sequence alignment with known mitochondrial iron transporters from different species, indicating that TbMCP17 could be a mitochondrial iron transporter in *Trypanosoma brucei.* TbMCP17 was found to be localised in mitochondria by immunofluorescent microscopy.

In addition, TbMCP17 overexpression helped restore cell growth under iron-limiting conditions (Figure 4-5). On the other hand, TbMCP17 down-regulation had a significant growth defect, while the re-introduction of TbMCP17-cmyc in conditional double knockout cells rescued cell growth which even reached WT level under iron limiting conditions. These results indicated that TbMCP17 was essential for cell growth. The iron content of those cell lines was then measured under both standard and heme-depleted conditions. Despite that WT and *TbMCP17-cmyc*^{ti} had similar values (no statistic difference), *TbMCP17 RNAi* demonstrated a down-regulation of iron content in mitochondria under both media conditions, and an up-regulation of total cell iron content in standard media with a decrease of total iron content in heme-depleted conditions, suggesting that TbMCP17 was likely to be an iron importer. The increase of total iron content in *TbMCP17 RNAi* cells cultured in the standard medium could be explained by feedback regulation of the cell which increased cytosolic iron content, attempting to promote iron import into the mitochondria. Noticeably, iron distribution (mitochondrial iron: total iron) stayed the same between standard and heme-depleted medium within the same cell line, suggesting that iron distribution in *T. brucei* was under tight control. The function of TbMCP17 was further confirmed by successful functional complementation in yeast. Yeast mitochondrial iron transporter knockout cell line (ΔMRS3/4) presented a significant growth defect under fermentable carbon source. By introduction of TbMCP17 into this cell line (ΔMRS3/4), the growth defect was rescued. This rescue suggested that TbMCP17 restored the function of MRS3/4 as a mitochondrial iron importer (Froschauer et al. 2009). The control experiment by re-introduction of MRS3 into MRS3/4-depleted cells, however, didn't result in a complete rescue of cell growth. The explanation for the growth defect could be that the expression level of MRS3 promoted by plasmid promoter

was different from the endogenous one, and might be too much for yeast cells in this case. In addition, the cells were cultured in the presence of iron chelator BPS. ΔMRS3/4 showed a more significant growth defect than WT as described in literature (Froschauer et al. 2009). This growth defect was also rescued by the introduction of TbMCP17.

At the same time, TbMCP17 antisera were generated by heterologous expression in *E. coli*, followed by protein isolation and purification. TbMCP17 antisera could detect TbMCP17 His tagged and myc tagged proteins. SDS-PAGE and WB procedure were optimised in sample preparation, blocking reagent and time, membrane transfer and developing method. But endogenous TbMCP17 was still under detection limit, suggesting that the failure of endogenous TbMCP17 detection was due to the limited amount of TbMCP17 protein. No signal of TbMCP17 protein level under iron-depriving or various heme and glucose conditions was observed, the possibilities were: (i) the increase of protein level was not significant enough for WB detection; (ii) TbMCP17 was down-regulated under these conditions; (iii) TbMCP17 protein level was not regulated under the examined conditions. mRNA level of TbMCP17 was clearly down-regulated by hydrogen peroxide, and it demonstrated a slight decrease in the presence of glucose. When heme was added back to the cell culture, TbMCP17 mRNA level was upregulated 10-20%. The mRNA results revealed that heme was an iron source that promoted TbMCP17 level, and that glucose addition caused a switch from proline consumption to glycolysis, resulting in a decrease of mitochondrial protein level. Too much iron in the mitochondria caused oxidative stress by producing highly toxic radicals. In order to defence oxidative stress, TbMCP17 was down-regulated.

Still, experiments on functional assays are suggested such as iron import assays using fluorescent probe PGSK or radioactive label of ^{55}Fe. Also, mitochondrial ATP production and aconitase activity measurements were attempted in this thesis, but no representative results were obtained (data not shown). More optimisations of experimental design or sample preparations could be carried out. In addition, it would be interesting to look at the oxygen consumption as TbMCP17 was found to be down-regulated at transcription level by oxidative stress. The oxidative stress caused by mitochondrial respiratory chain inhibitors could be rescued by Fe-superoxide dismutases (Fe-SODs) (Wang et al. 2015).

It is interesting to measure the mRNA and protein levels of TbMCP17 in cells culturing in various mitochondrial respiratory chain inhibitors or cells depleted in SODs.

A brief summary of investigations on TbMCP17:

- TbMCP17 was the only homologue to mitochondrial iron transporters.
- TbMCP17 over-expression rescued cell growth under iron-limiting conditions.
- TbMCP17 was essential to cell growth.
- TbMCP17 down-regulation caused a decrease of mitochondrial iron content.
- The introduction of TbMCP17 into yeast mitochondrial iron transporter depleted (ΔMRS3/4) cells rescued the growth defect.
- TbMCP17 protein level was below detection limit.
- TbMCP17 mRNA level was upregulated in the presence of heme and the absence of glucose. The addition of hydrogen peroxide suppressed the mRNA level of TbMCP17.
- More direct evidence of TbMCP17 as an iron transporter is needed.
- Further experiments on the physiological role TbMCP17 plays are suggested.

Chapter 5 Functional characterisation of TbSFNX

5.1 Introduction

The sideroflexin family was first identified in the mitochondrial membranes of rat and bovine, and they displayed the ability to transport citrate, isocitrate, malate, succinate, and phosphoenolpyruvate (Azzi et al. 1993). The depletion of sideroflexin in mice caused siderocytic anaemia (pathologic intramitochondrial iron deposited with siderotic granules present in erythrocytes rather than nucleated erythroid precursors (sideroblastic anaemia)) with a *flexed-tail* (*f*) phenotype, hence the gene was named as SFNX (Fleming et al. 2001). This depletion also resulted in mitochondrial iron accumulation, suggesting a potential role of SFNX in mitochondrial iron transport or metabolism (Fleming et al. 2001). But it was further suggested that the *flexed-tail* mutation (*f/f*) was caused by the mutation of Smad5 gene (Hegde et al. 2007). On the other hand, the fungal sfnx Fsf1p (Miotto et al. 2007), human sfnx2 (Ye et al. 2003), sfnx family in pancreatic islet (Yoshikumi et al. 2005), and developmental expression of sideroflexin family genes in *Xenopus* embryos (Li et al. 2010) were identified/studied, but the function information of sideroflexin family was limited. This evidence suggests the importance of functional characterisation of TbSFNX in *T. brucei*, as supportive information for the role(s) sideroflexin family protein plays in other organisms, especially in iron metabolism and carboxylate transport.

In this chapter, preliminary work has been done to identify a homologue SFNX in *Trypanosoma brucei*. TbSFNX was identified as a sideroflexin family protein, which contained a conserved mitochondrial tricarboxylate carrier motif (MTC, PF03820.8). Phylogenetic reconstruction revealed that TbSFNX in *Trypanosoma brucei* did not belong to any of the five sideroflexin classes in mammals identified before. *TbSFNX* gene over-expression with myc tag, surprisingly, led to cell death. However, TbSFNX conditional double knockout (*ΔTbSFNX/TbSFNX-cmyc*^{ti}) by the replacement of two *TbSFNX* copies with resistance cassettes using *TbSFNXcmyc*^{ti} cells presented no growth defect in the absence of tetracycline (when the rescue copy was not present). In order to eliminate the possibility that the growth of *ΔTbSFNX/TbSFNX-cmyc*^{ti} could be maintained by residual TbSFNXcmyc presented at the background level, TbSFNX RNAi was applied in this study. A long-term growth defect was observed from TbSFNX RNAi cells. Together with the overexpression result, the growth phenotype results indicated the tight control of TbSFNX level, and the disturbance caused growth defect. Metabolic

substrates (glucose and proline) and end products (succinate and acetate) content was measured on WT, *ΔTbSFNX/TbSFNX-cmyc*^{ti} and *TbSFNX-cmyc*^{ti} cells in both the presence and absence of glucose. The results revealed that both *ΔTbSFNX/TbSFNX-cmyc*^{ti} and *TbSFNX-cmyc*^{ti} caused an increase in proline consumption and acetate production, as well as an increase in succinate degradation/procession. In order to determine the endogenous TbSFNX protein level and the potential regulation under various conditions, TbSFNX was heterologously expressed in *E. coli* and purified to generate an antibody. The resulting antibody successfully detected the over-expressed TbSFNX-myc protein as well as the purified TbSFNX-His protein, while the endogenous protein was below the detection limit. Various attempts in optimisation to increase the detection limit or the removal of background, however, did not make endogenous TbSFNX detectable. In addition, TbSFNX mRNA and protein level were tested under various conditions, but no protein signal was detected in the conditions applied. mRNA level of TbSFNX was slightly down-regulated in the presence of hydrogen peroxide.

5.2 TbSFNX belongs to sideroflexin family

The only *TbSFNX* sequence (Tb09.160.2910) was identified by BLAST search (http://blast.ncbi.nlm.nih.gov/Blast.cgi?PAGE=Proteins) using known tricarboxylate carriers from *R. norvegicus* (Azzi et al. 1993) which belongs to the sideroflexin family. A reciprocal BLAST search using *TbSFNX* sequence showed hits predominately of sequences of sideroflexin from different species. A search against the Pfam (Protein Families) database (http://pfam.sanger.ac.uk) indicated that Tb09.160.2910 contained a conserved mitochondrial tricarboxylate carrier motif (MTC, PF03820.8).

The phylogenetic analysis was conducted using *TbSFNX*, sideroflexins, accompanied by citrate carriers, dicarboxylate carriers, di/tricarboxylate carriers and oxoglutarate carriers (Figure 5-1 A). The results show that *TbSFNX* indeed belongs to the sideroflexin family, supported by high bootstrap values of the formation of the same clade. In animals, the sideroflexin family contains five different classes which are highly related and functionally overlapping (Azzi et al. 1993; Fleming et al. 2001; Lockhart et al. 2002; Miyake et al. 2002; Ye et al. 2003; Murase et al. 2008). However, only one copy was identified in fungi (Miotto et al. 2007). To determine the class(es) of which TbSFNX belongs to, a phylogenetic tree was constructed using TbSFNX with sideroflexins of five different classes (sideroflexin 1 to 5) from different species (Figure 5-1 B), resulting in TbSFNX forming a separate clade with species from Kinetoplastea, and a distinct clade formed by fungi.

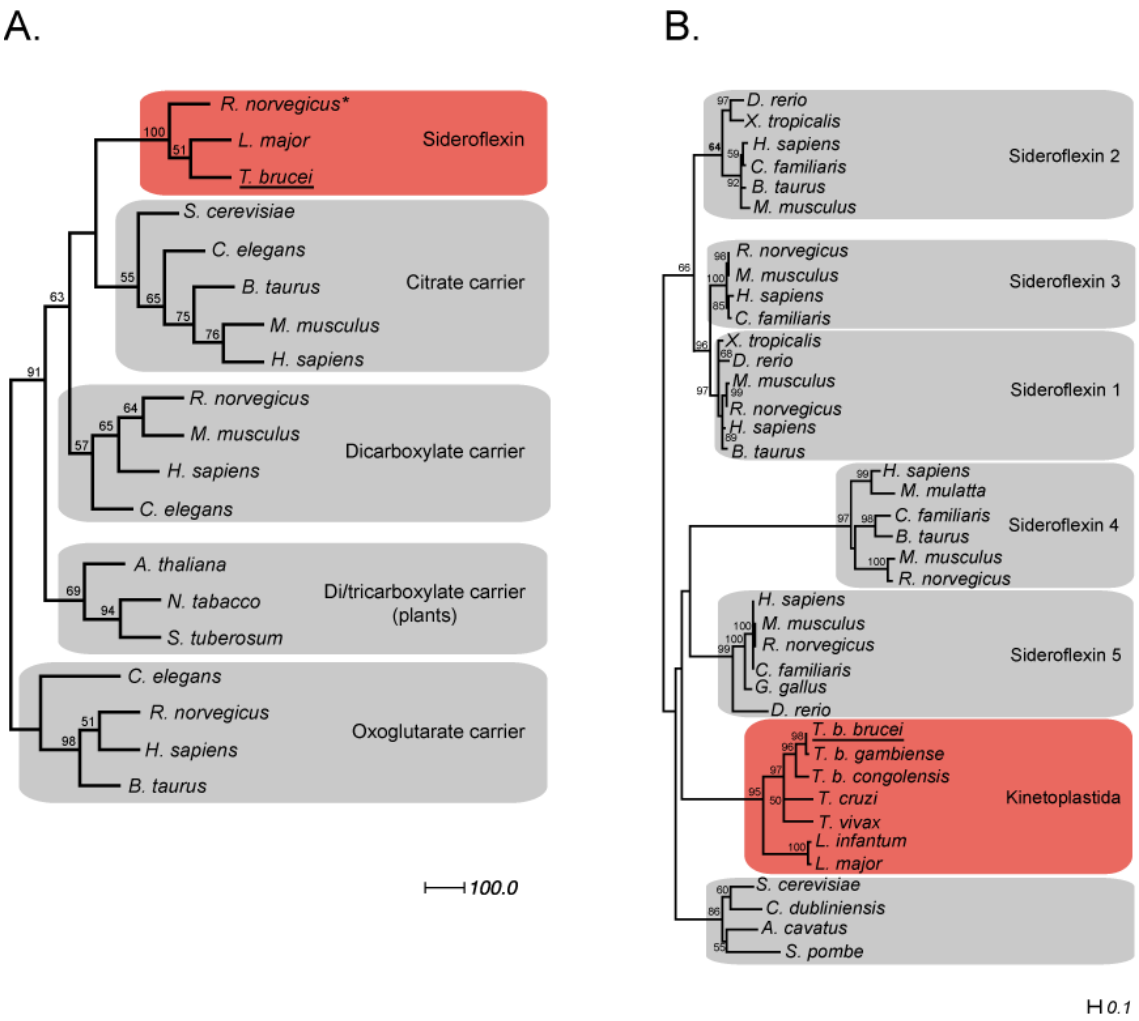

Figure 5-1 Phylogenetic analysis of TbSFNX towards various carboxylate carriers and sideroflexin family

The grey balloons indicate the five carrier groups found from phylogenetic reconstruction (A) or different classes of sideroflexins from various species (B). The *T.brucei* group is highlighted in an orange balloon with *T.brucei* protein underlined. An asterisk (*) is labelled next to sideroflexin from *R.norvegicus*, which has been functionally characterised. Bootstrap values smaller than 50% are not shown.

Sequence alignment using TbSFNX against sideroflexins from *H. sapiens* and *R. norvegicus* showed that the proteins of the sideroflexin family were highly conserved (Figure 5-2). TbSFNX sequence has an identity of 31% and similarity of about 51% with the human sideroflexins. Transmembrane prediction programs indicated the presence of 5 transmembrane domains.

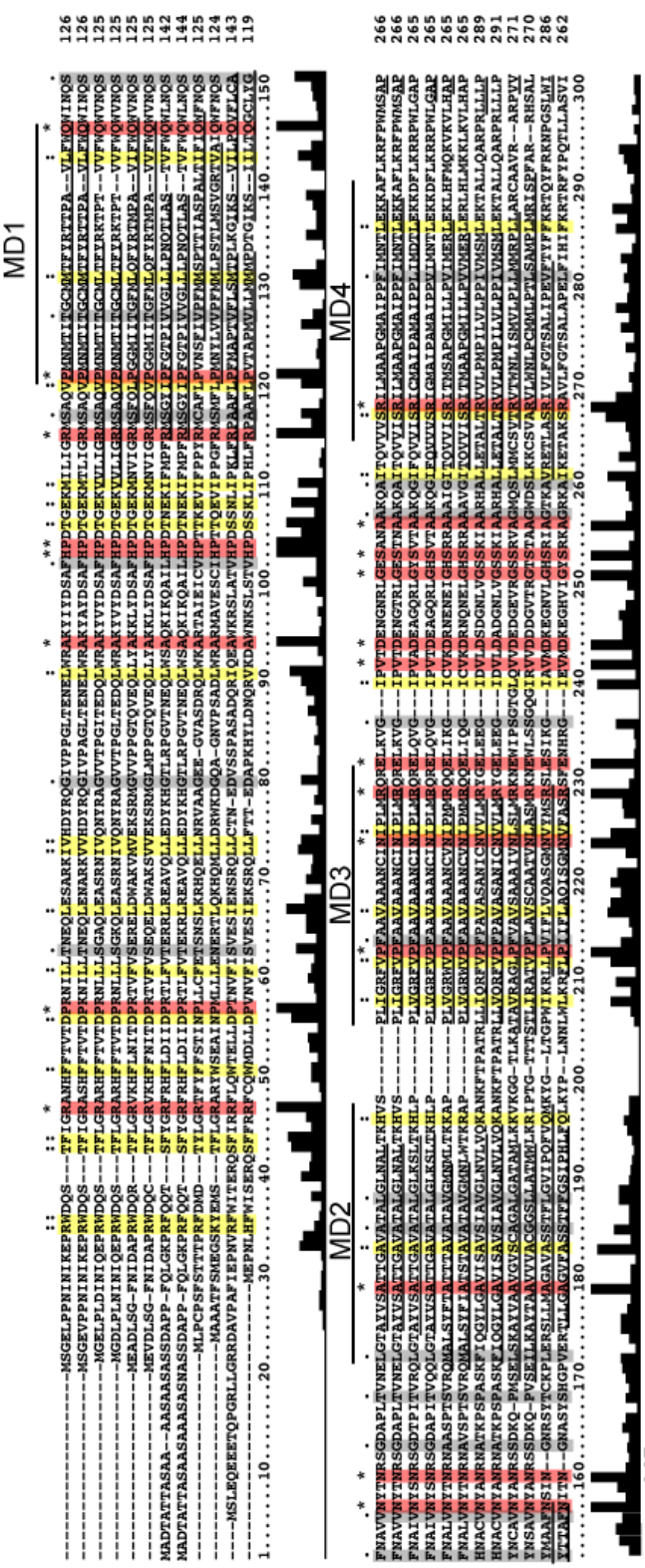

Figure 5-2 Alignment of the TbSFNX sequence with the sideroflexins of *H.sapiens* and *R.norvegicus*

The *T. brucei* sideroflexin (TbSFNX) is underlined. Membrane domains (MD1-5) are underlined and indicated. Bars designate the residue conservation within the sequences. (*) and red shadow indicate identical residues; (:) and yellow shadow represents conserved substitutions; (.) and grey shadow indicates semi-conserved substitutions.

5.3 TbSFNX is localised in the mitochondria

The tetracycline inducible TbSFNX overexpression cell line (*TbSFNXcmyc*^{ti}) was generated, and the expression of TbSFNX-cmyc was checked (Figure 5-3 A). Subcellular localisation of TbSFNX was determined by fractionation (Figure 5-3 B) and immunofluorescence microscopy (Figure 5-3 C) using the generated *TbSFNXcmyc*^{ti}. Results clearly show that *TbSFNX* is localised in the mitochondria, which is accordant with the subcellular location of characterised sideroflexins from *R.norvegicus*.

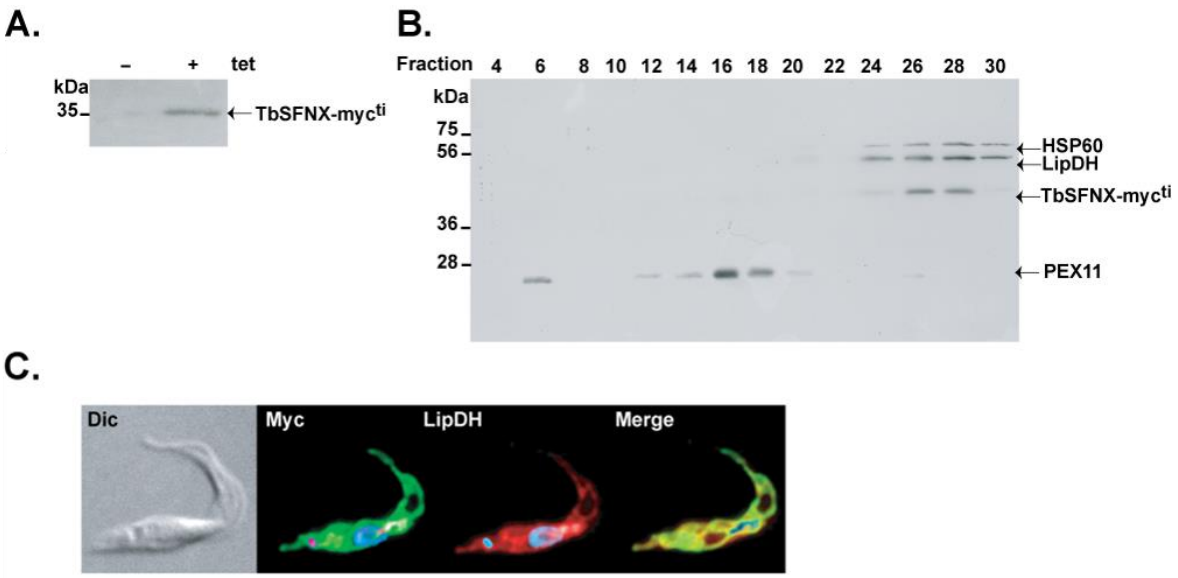

Figure 5-3 TbSFNX is localised in the mitochondria and predominantly expressed in the procyclic form

A. The successful expression of TbSFNX-cmyc protein is demonstrated by WB using *TbSFNX-cmyc*^{ti} cells upon the addition of tetracycline. B. fractionation result of induced *TbSFNXcmyc*^{ti} cell line is presented in WB. Antibodies against marker proteins of different cellular compartments were used: glycosome (PEX11) and mitochondria (LipDH and HSP60). TbSFXN-myc was detected using the myc antibody. C. Immunofluorescence microscopy is shown using the myc antibody for TbSFNX overexpression (green), LipDH (Lipoamide dehydrogenase) for mitochondria (red) and DAPI for nuclei and kinetoplasts (blue). The intact cell is indicated by digital interference contrast (DIC). Merge of myc and LipDH is displayed, too.

5.4 Both TbSFNX overexpression and knockout cause growth defect

A conventional *TbSFNX* gene depletion cell line could not be generated after many attempts, hence a TbSFNX depletion cell line carrying an inducible rescue copy of TbSFNX-cmyc (Δ*TbSFNX*::NEO/Δ*TbSFNX*::*BSD*/*TbSFNX-cmyc*^{ti}) was generated, which was referred to as Δ*TbSFNX/TbSFNX-cmyc*^{ti} below (the generated cell lines were checked by PCR and restriction enzyme digestions) (see Section 2.5.2 for details). This failure of knockout of duplicate copies suggests that TbSFNX is essential in procyclic form. Growth curves were performed in Δ*TbSFNX/TbSFNX-cmyc*^{ti} and *TbSFNX-cmyc*^{ti} cells when compared with WT PCF449 cells (labelled in the figure as *TbSFNX/TbSFNX*). The presence and depletion of TbSFNXcmyc protein (controlled by the presence and absence of tetracycline) were determined by WB (Figure 5-4 A&B). As shown in Figure 5-4 C, no significant difference in growth was observed in the TbSFNX conditional double knockout cells (Δ*TbSFNX/TbSFNX-cmyc*^{ti}), with or without the tetracycline-induced TbSFNX-cmyc protein. However, the over-expression cells *TbSFNX-cmyc*^{ti} stopped growing after 72 hours at a cell density of approximately 1.2×10^7 cells/ml.

The combination of results gathered from overexpression and knockout cells indicate that the TbSFNX level is tightly controlled in *T. brucei*, and that a slight increase of TbSFNX-myc (not detectable using the myc antibody in WB) is sufficient to cause a significant growth defect (Figure 5-4 D). This growth defect can be compromised by knocking out of the two endogenous copies, as no growth difference was found in Δ*TbSFNX/TbSFNX-cmyc*^{ti} cells (Figure 5-4 C).

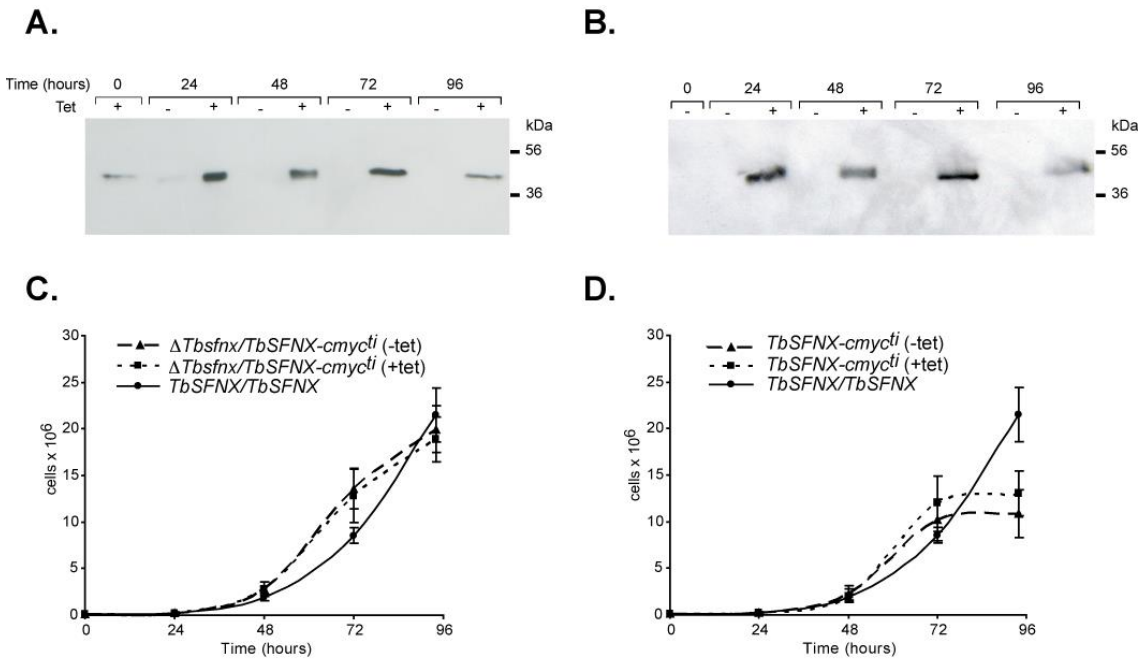

Figure 5-4 Growth phenotype analysis of *TbSFNX-cmyc*^{ti} and Δ*TbSFNX/TbSFNX-cmyc*^{ti} cell lines

A and B show WB control of *TbSFNX-cmyc*^{ti} and Δ*TbSFNX/TbSFNX-cmyc*^{ti} with (+) or without (-) tetracycline, respectively. *TbSFNX-cmyc* protein was detected with myc antibody. Growth curves compared with WT cell line are shown in C (Δ*TbSFNX/TbSFNX-cmyc*^{ti}) and D (*TbSFNX-cmyc*^{ti}) individually. Growth was followed every 24 hours for 96 hours, and WB samples were collected every 24 hours.

However, whether depletion of *TbSFNX* causes any growth defect has not been confirmed yet due to failing to remove TbSFNXcmyc rescue copy completely. Therefore, *TbSFNX* down-regulation was further achieved by RNAi.

RNAi was performed by expression of stem-loop 'sense/antisense' RNA molecules of the targeted sequences introduced in the pHD676 plasmid (Bringaud et al. 2000). Apa I is present in the MCS of pHD676 expression vectors with BamH I and Hind III at the two sides. Primers of *TbSFNX* antisense and sense were designed with BamH I & Apa I on the two ends of antisense, and Apa I & Hind III on the two ends of sense (Figure 5-5 A). Hence, after PCR amplification (Figure 5-5 B), the sense and antisense were digested with above enzymes and added directly into the pHD676. The resulting potential clones of pHD676 + *TbSFNX* were examined using PCR (Figure 5-5 C) and restriction enzyme mappings (data not shown). Plasmid from clone 1 was further sequenced and no functional mutation was found (See Appendix A4-5). Thus it was used in later experiments labelled as pHD676 + *TbSFNX* RNAi.

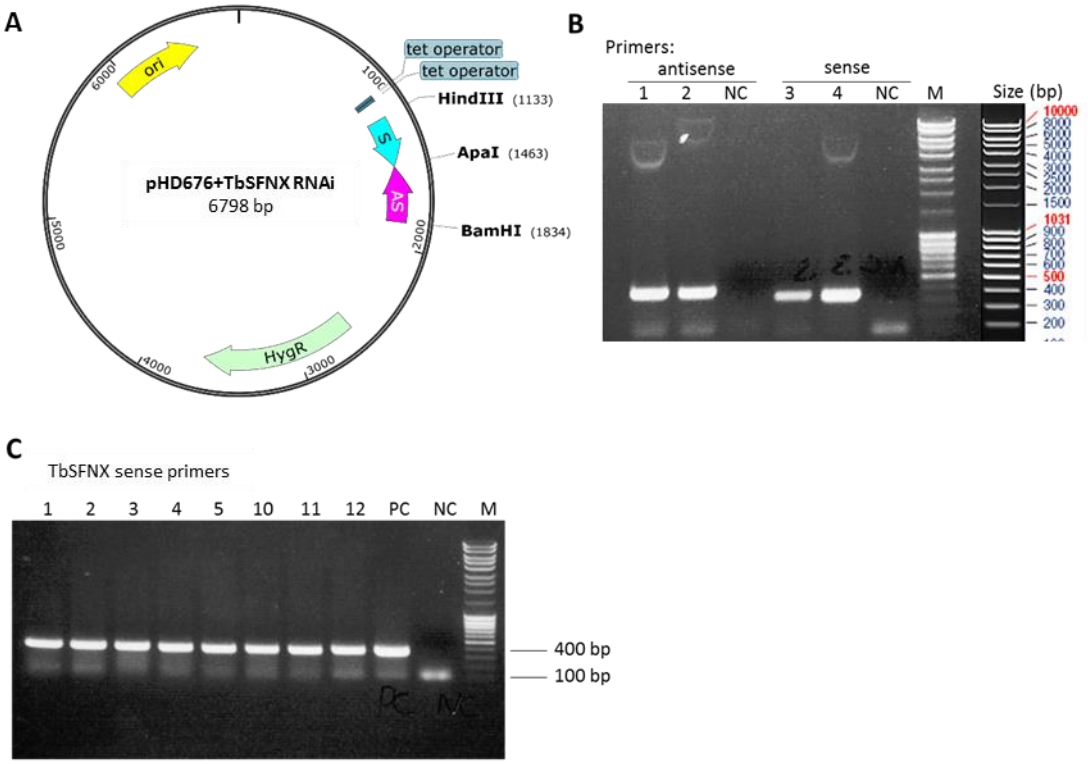

Figure 5-5 Construction of pHD676+TbSFNX RNAi plasmid

A. Plasmid map of pHD676+TbSFNX RNAi is displayed containing cloning restriction sites BamH I, Apa I and Hind III to insert sense (S) and antisense (AS) fragments of TbSFNX into pHD676 multiple cloning sites (MCS) in reversed direction. B. PCR amplification of TbSFNX antisense and sense fragments is demonstrated. Order: from left to right, the first three were the PCR results using *TbSFNX* antisense primers; the templates used in each lane were: 1: pLEW100+AS, 2: pLEW100v5+AS, NC: negative control without template. The next three lanes are amplification products using *TbSFNX* sense primers, the templates used in 3 and 4 are pDrive + *TbSFNX* S clone1 and 2, negative control. The last lane M is DNA MassRuler. C. Identification of pHD676+TbSFNX AS+S constructs is shown. The isolated 8 plasmids (1, 2, 3, 4, 5, 10, 11, and 12) were checked with PCR using *TbSFNX* sense primers. The positive control (PC) used pHD676+TbSFNX S construct as the template, while the negative control (NC) was performed without a template.

pH676+*TbSFNX* RNAi construct was transfected into PCF449, and positive *T. brucei TbSFNX* RNAi clones were isolated. Afterwards, growth experiments were performed with tetracycline-induced, non-induced *TbSFNX* RNAi cell line and tetracycline-induced WT cells. As presented in Figure 5-6 A, no difference was shown between induced and non-induced *TbSFNX* RNAi cell line, but a significant growth defect appeared after 3 days (72 hours) when compared the both *TbSFNX* RNAi cells (with or without tetracycline) with WT cells. This gave us a hint that the construct was leaky to some extent (similar leakage of plasmid found with TbMCP12, TbMCP17 knockout constructs). Meanwhile, mRNA from different time points of growth curve was isolated, and semi-

quantitive PCR was performed. As presented in Figure 5-6 B&C, the *TbSFNX* mRNA level was decreased during the induction. Furthermore, mRNA from non-induced TbSFNX RNAi cells was less than WT (70%), confirming partial knockdown of gene ongoing before the addition of tetracycline. When growth curves were taken into consideration with the RNAi efficiency result, a non-detrimental defect of growth was observed from TbSFNX RNAi cells, indicating that cellular TbSFNX level is under tight control.

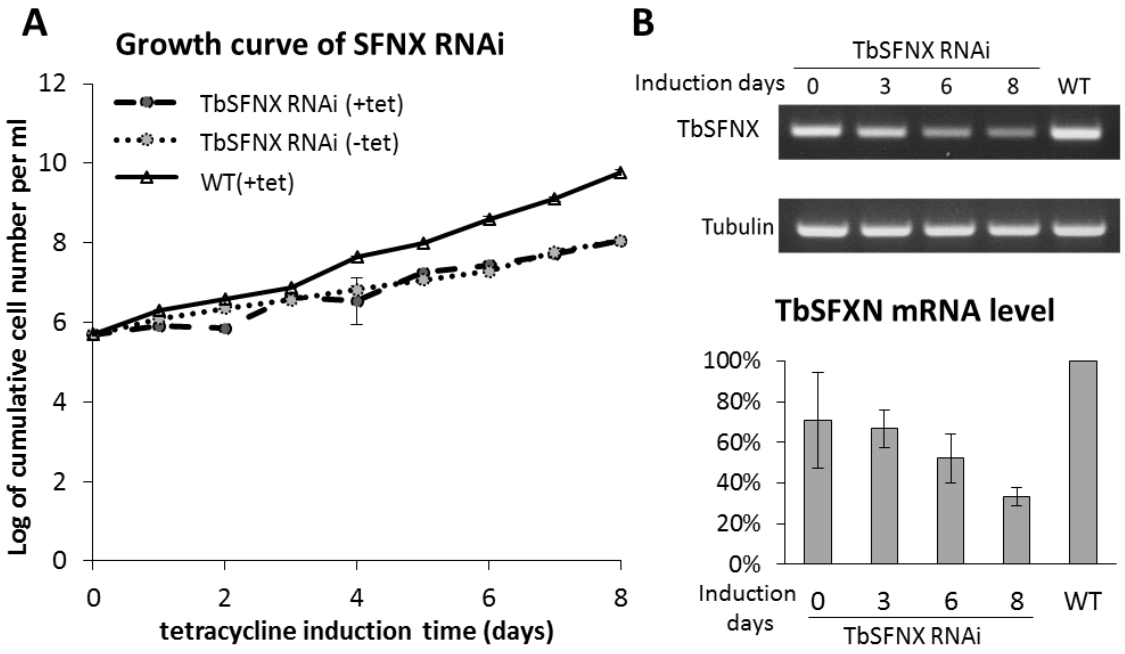

Figure 5-6 Growth effects of *TbSFNX* RNAi cells
A shows growth phenotype measured under induced and non-induced conditions of *TbSFNX* RNAi cells with WT (PCF449) cells plus tetracycline as a control. B displays semi-quantitive PCR result of *TbSFNX* mRNA level of the induced cell line, with tubulin as a loading control. C presents quantitive analysis of band density from TbSFNX mRNA level. Relative mRNA level of *SFXN* was first normalised with tubulin, then converted to percentages using mRNA level of WT *TbSFNX* as 100%. Error bars indicate the standard deviations of triplicates.

The TbSFNX RNAi results (Figure 5-6) in combination with the Δ*TbSFNX/TbSFNX-cmyc*^{ti} results (Figure 5-4) indicate that TbSFNX partial depletion causes a long-term significant growth defect (after 72 hours), while over-expressing TbSFNX is also detrimental for cell growth. This suggests that TbSFNX level is under tight control in low abundance.

5.5 Both TbSFNX OE and KO produce more acetate and consume more proline and succinate

In order to investigate the role(s) that TbSFNX played in energy metabolism, TbSFNX overexpression (OE; *TbSFNX-cmyc*^{ti}) and knockout (KO; Δ*TbSFNX/TbSFNX-cmyc*^{ti}) cells cultured in standard medium condition (0.23 mM glucose and 5 mM proline) were used to measure substrate (glucose and proline) consumption and end product (acetate and succinate) production (Figure 5-7). The same metabolic features were found from all three cells: (i) acetate was produced exclusively in the first 72 hours (Figure 5-7 A); (ii) succinate was accumulated in the first 72 hours then metabolised/progressed further in the next 24 hours (Figure 5-7 B); (iii) all glucose was consumed in the first 72 hours (Figure 5-7 C); (iv) proline consumption increased significantly from 72 hours to 96 hours (Figure 5-7 D). When comparing Δ*TbSFNX/TbSFNX-cmyc*^{ti} and *TbSFNX-cmyc*^{ti} with WT cells, both depletion and overexpression of TbSFNX caused increased acetate production (1.4× of WT) and proline consumption (2× of WT), which led to an increase in succinate consumption (or a decrease of succinate production). Δ*TbSFNX/TbSFNX-cmyc*^{ti} consumed more glucose in the first 48 hours, which was reflected in the slightly faster growth observed in Figure 5-4 C. Also, more consumption of succinate was found in Δ*TbSFNX/TbSFNX-cmyc*^{ti} cells when compared with *TbSFNX-cmyc*^{ti} cells.

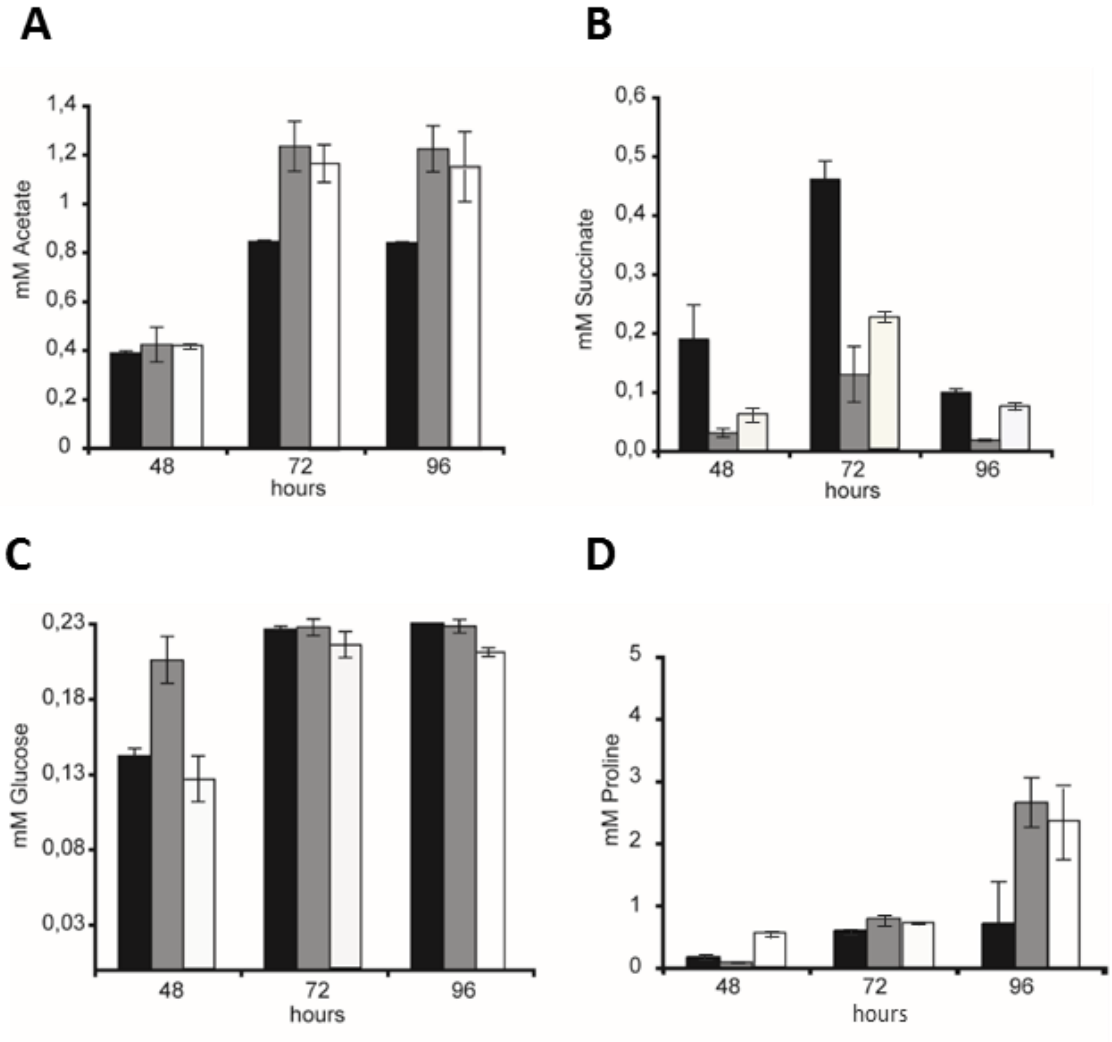

Figure 5-7 Determination of substrates and metabolites in *TbSFNX-cmyc^{ti}* and Δ*TbSFNX/TbSFNX-cmyc^{ti}* cultures

Consumption of glucose and proline are shown in C and D, respectively. The production of acetate and succinate are displayed in A and B, separately. Cell lines are distinguished by colours: WT (black), un-induced Δ*TbSFNX/TbSFNX-cmyc^{ti}* (grey) and induced *TbSFNXcmyc^{ti}* (white). Samples collected at 48 h, 72 h and 96 h are presented. Error bars indicate standard deviations of repeats.

5.6 Heterologous expression in *E. coli* and antibody generation

A similar approach to antibody generation of TbMCP17 (described in Section 4.8) was applied in TbSFNX. Processes including transformation in *E. coli*, induction and expression of protein, protein purification and quantification were performed. After four months of immunisation (completed by Thermo Fisher Scientific using purified protein), the efficiency of resulting antisera was tested against purified protein and *T.brucei* cell lines.

5.6.1 Plasmid generation and protein expression in *E.coli*

The gene of *TbSFNX* was cloned into the expression vector pET28 by inserting *TbSFNX* open reading frame (ORF) into the vector using BamH I and Hind III restriction enzymes. The obtained plasmid was checked by PCR and restriction enzyme digestion (Figure 5-8 A). TbSFNX ORF primers were used against the obtained plasmid (labelled as 1), and a single band around 1000 bp was amplified at the same size as *TbSFNX* (*TbSFNX* ORF: 981 bp), indicating the presence of the gene. The plasmid was digested with BamH I and Hind III into two fragments: a band of approximately 1000 bp is the *TbSFNX*, and the pET28 vector is 5369 bp corresponding to the band in gel picture between 5000 to 6000 bp. A schematic plasmid map of pET28+TbSFNX was presented (Figure 5-8 A). The inserted sequences were also checked for correctness, and the sequencing results showed no functional mutations (Appendix A4-6).

Protein expression was induced by IPTG for four hours. A protein band around 40 kDa was clearly visible in CBB with the size consistent with the predicted TbSFNX-His size of 39.17 kDa. This band was also detected by the His antibody, indicating the success of SFXN heterologous expression (Figure 5-8 B Non and Ind samples). The solubility of protein was further tested. As shown in the last two lands of Figure 5-8 B, TbSFNX-His was in the inclusion bodies, like other heterologously expressed proteins.

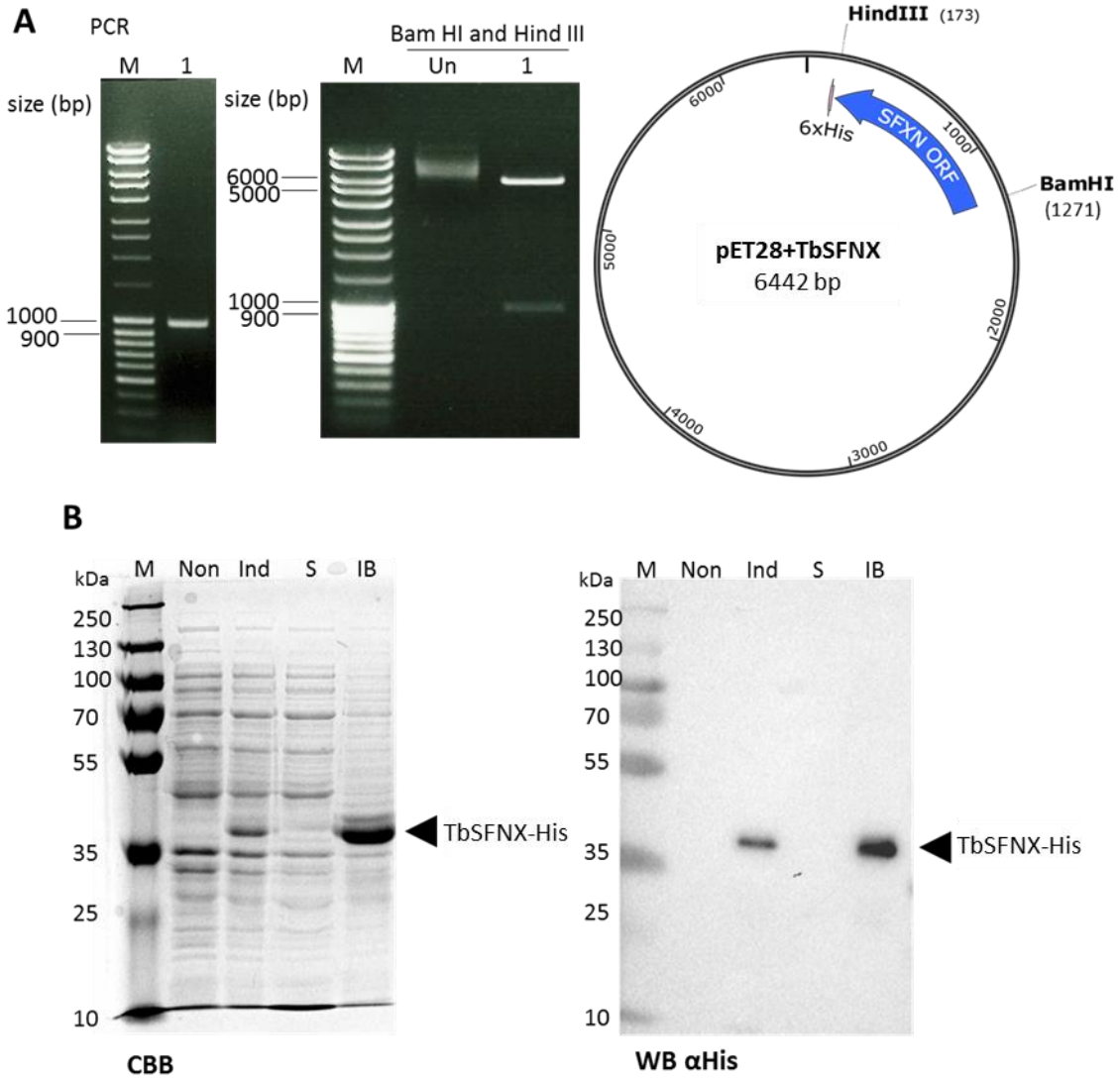

Figure 5-8 pET28+TbSFNX plasmid construction and induction of TbSFNX-His expression in Lemo21

A displays the generated plasmid examined by PCR using TbSFNX ORF forward and reverse primer (the detailed primer sequences can be found in Chapter 2) and by digestions with restriction enzymes (Bam H I and Hind III). M: marker; Un: undigest pET28+TbSFNX plasmid; 1: generated plasmid. Plasmid map of resulting construct is shown in A. The expression and solubility of TbSFNX-His is demonstrated in B. Lemo21 strain was transfected with pET28+*TbSFNX*, and TbSFNX-His protein expression was induced by IPTG for four hours. Cell pellet collected after induction was further treated with native resuspension buffer and French press to destroy bacterial membrane, and separated by centrifugation. Samples of non-induced cells (Non), induced cells (Ind), supernatant (S) and inclusion bodies (IB) were collected and loaded onto an SDS-PAGE gel followed by Coomassie Brilliant Blue (CBB) staining or WB using His antibody. The triangles indicate the TbSFNX-His protein bands.

5.6.2 Protein purification using Ni-NTA beads

Since sarkosyl is very efficient in solubilising of TbMCP17-His inclusion bodies, the same procedure was performed for TbSFNX-His IB. As observed from Figure 5-9 A, more than half of the protein failed to bind to Ni-NTA column and was found in the flow-through (FT). A minor amount of the protein was eluted successfully, while the majority was retained on the Ni-NTA resin (Figure 5-9 A). This failure of binding is most likely due to the insufficient exposure of His-tags on TbSFNX-His proteins. Thus, increased volume of 2% sarkosyl (5 folds more than the previous experiments) was applied to denature protein better, followed by the same Ni-NTA purification process. The results (Figure 5-9 B IB and FT lanes) revealed that increasing volume of solubilisation buffer denatured the protein sufficiently with His-tag exposed to Ni-NTA for binding. This increase of binding was confirmed by the observation that only non-specific proteins were washed out (lane W1, W2), and the target proteins successfully eluted from the column (lane E1, E2 and Ni-NTA).

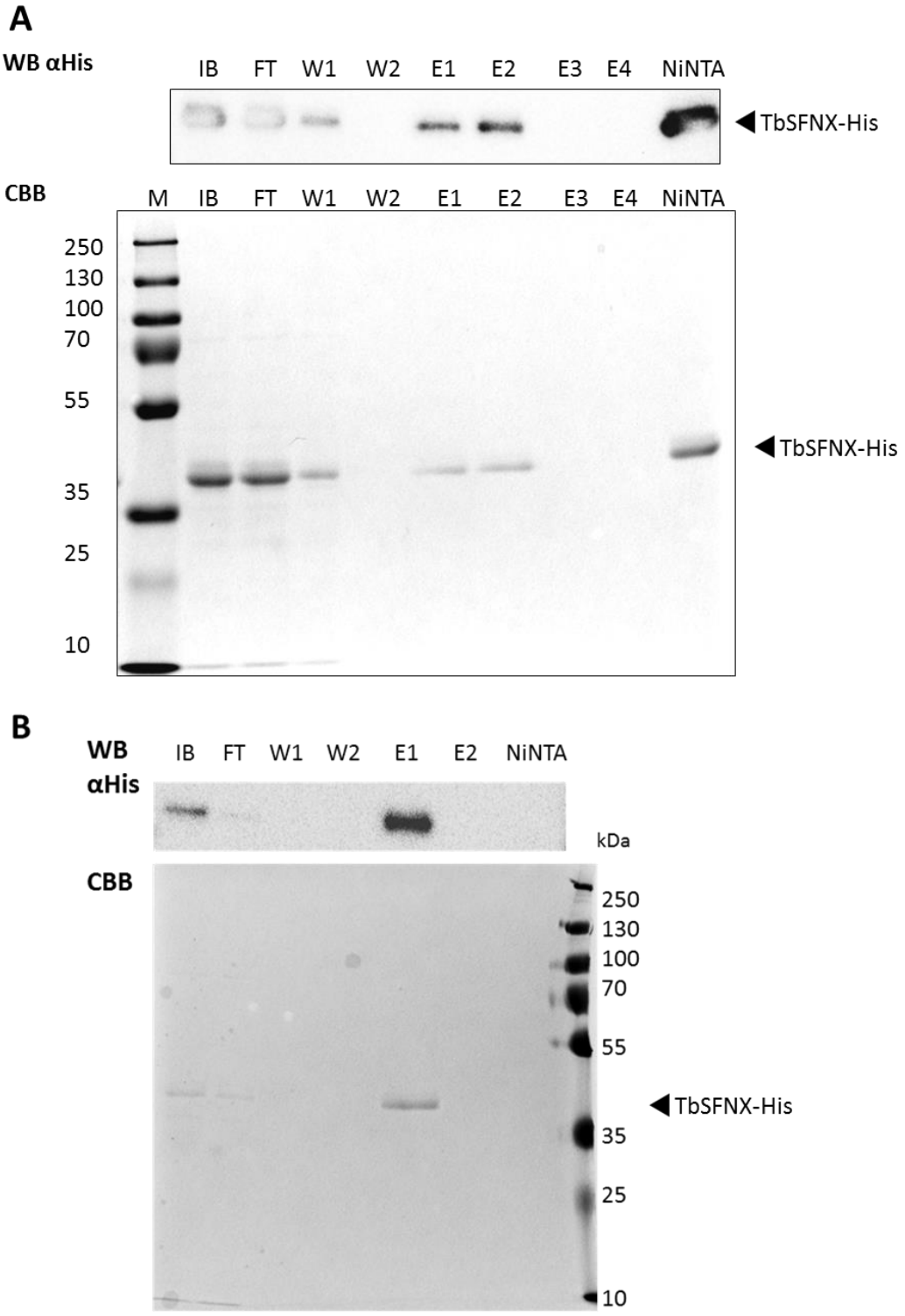

Figure 5-9 TbSFNX purification using Ni-NTA column

IB stands for inclusion bodies that were solubilised before loading onto Ni-NTA column. Samples at different steps were collected and tested with WB and CBB stain. His antibody was used for WB detection. FT: flow through; W1 and W2: two continuous washes; E1, E2, E3 and E4: elutions 1 to 4. NiNTA: NiNTA slurry. Protein marker (M) sizes are labelled next to the marker bands. A displays the IB solubilization process of 100 ml culture in 2 ml of 2% sarkosyl, while B presents the process using 10 ml of 2% sarkosyl of the same amount of culture.

5.6.3 Protein quantification

Elution containing pure TbSFNX-His proteins were concentrated and determined by using the BSA standard method discussed in Section 4.8.3. The protein concentration was determined to approximately 5 mg/ml (Figure 5-10). 3 mg of protein were loaded onto a prep gel and the gel slice containing protein was cut out for antibody generation.

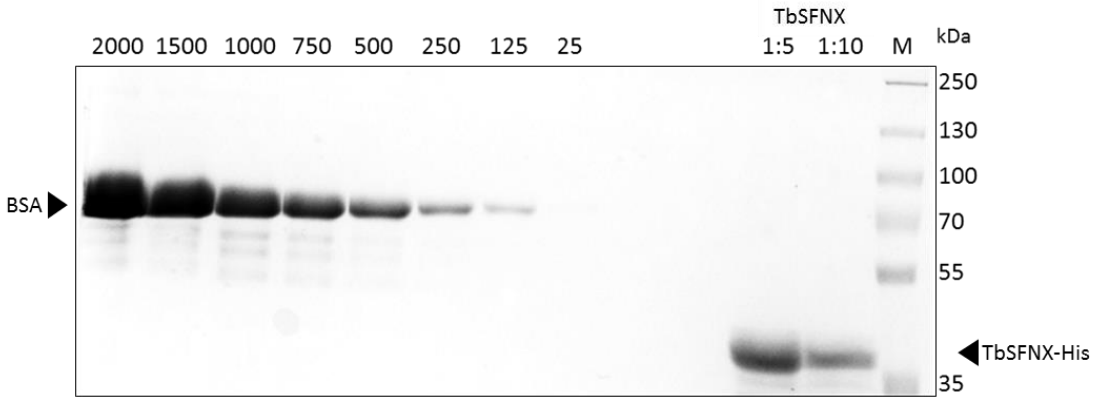

Figure 5-10 TbSFNX protein quantification
A series of BSA of different concentrations (from 25 µg/ml to 2000 µg/ml) are presented next to the 5-fold and 10-fold dilution samples of TbSFNX-His elutions (labelled as E 1:5 and E 1:10) on an SDS-PAGE gel and dyed with CBB.

5.6.4 Efficiency of antisera testing

Immunisation of purified TbSFNX-His protein was completed by TheromoFisher. The obtained 2 antisera were first tested against *T. brucei* WT PCF449 cells and the TbSFNX-His purified protein. As shown in Figure 5-11 A, TbSFNX antiserum 2 had a higher titre compared with antiserum 1. Also, antiserum 2 was more specific, while a non-specific band right below 35kDa was appearing in blot tested with antiserum 1. Thus, antiserum 2 was further used. Afterwards, TbSFNX antiserum 2 was applied on two *TbSFNX* down-regulation strains: TbSFNX RNAi and Δ*TbSFNX/TbSFNX-cmyc*^{ti} with the presence of tetracycline. The rescue copy (TbSFNXcmyc) in Δ*TbSFNX/TbSFNX-cmyc*^{ti} strain was successfully detected (Figure 5-11 B). However, the endogenous protein was not detected, and the band that was previously thought to be SFXN turned out to be a background band since it was present in all three tested cells. In order to detect endogenous TbSFNX, a

TbSFNX open reading frame (ORF) overexpression cell line was included in the cells used before. As observed from TbSFNX-ORF cells, unfortunately, the endogenous band is of the same size of background band on WB gels (Figure 5-11 C). Also, the loss of expression control on Δ*TbSFNX/TbSFNX-cmyc*^{ti} cell line was discovered by observing a band at around 37 kDa without the addition of tetracycline. Besides, various optimisations were performed, i.e., different blotting membrane, change of antibody diluent and purification of the antibody with A/G magnetic beads (data not shown). Unfortunately, those optimisations did not increase endogenous TbSFNX signal, suggesting the limit amount of endogenous TbSFNX in the *T.brucei* cells.

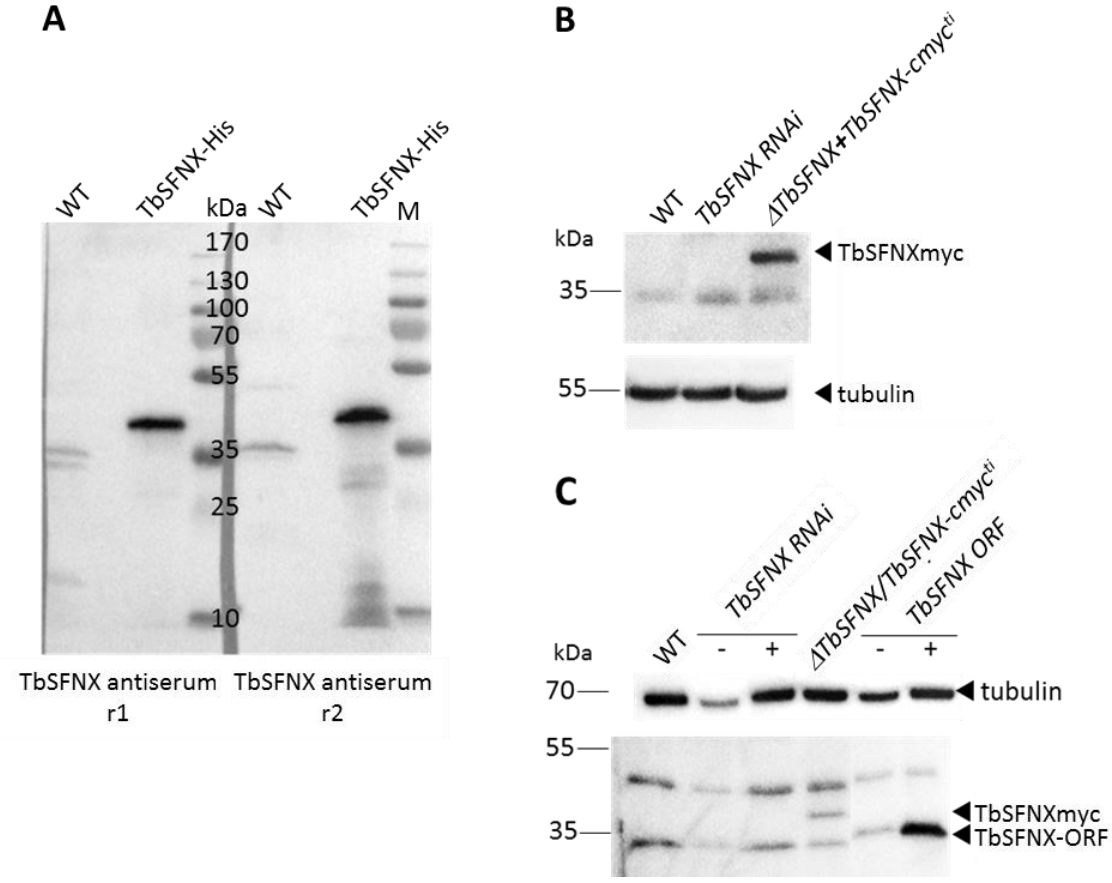

Figure 5-11 TbSFNX antisera testing

A displays TbSFNX antiserum from rabbit 1 (r1) and rabbit 2 (r2) testing results on *T.burcei* WT cells and TbSFNX-His purified protein (TbSFNX-His). M stands for mass ruler. B presents antisera 2 detection result on WT and TbSFNX down-regulation cell lines: RNAi strain (TbSFNX-RNAi) and tetracycline-induced knockout strain *ΔTbSFNX+TbSFNX-cmyc*^{ti}. Tubulin is served as a loading control. C shows further detection of TbSFNX on multiple strains including TbSFNX-ORF expression cell line. Protein bands are indicated with triangles with protein name next to them.

5.7 Endogenous TbSFXN not detectable under conditions tested

Changes of TbMCP12 and TbMCP17 mRNA and protein levels were observed under varying culture conditions, i.e. heme, glucose and oxidative stress caused by the addition of hydrogen peroxide (Sections 3.4, 3.5 and 4.9.2). As a potential carboxylate carrier as well as an iron homoeostasis regulator, TbSFNX level was examined under similar conditions to see whether it changed accordingly. TbSFNX protein level was tested under the presence and absence of heme, with Δ*TbSFNX/TbSFNXcmyc*^{ti} and TbSFNX RNAi cells served as negative controls. In addition, TbMCP17 over-expression cells (*TbMCP17cmyc*^{ti} and *TbMCP17nmyc*^{ti}) and TbMCP17 knockout cells (Δ*TbMCP17/TbMCP17-cmyc*^{ti} or TbMCP17 RNAi) cultured with the presence and absence of heme were tested at TbSFNX protein levels. The WB results (Figure 5-12 A) showed that the endogenous TbSFNX protein level remained under detection limit. Only TbSFNX-myc was detected in Δ*TbSFNX/TbSFNXcmyc*^{ti} cells without the addition of tetracycline, suggesting the leakage of rescue copy. Preliminary work was also performed on WT cells treated with hydrogen peroxide (H_2O_2), and mRNA levels observed decreased 10-20% compared with non-treated cells (Figure 5-12 B). More research needs to be conducted to unveil the conditions to regulate TbSFNX protein level in the future.

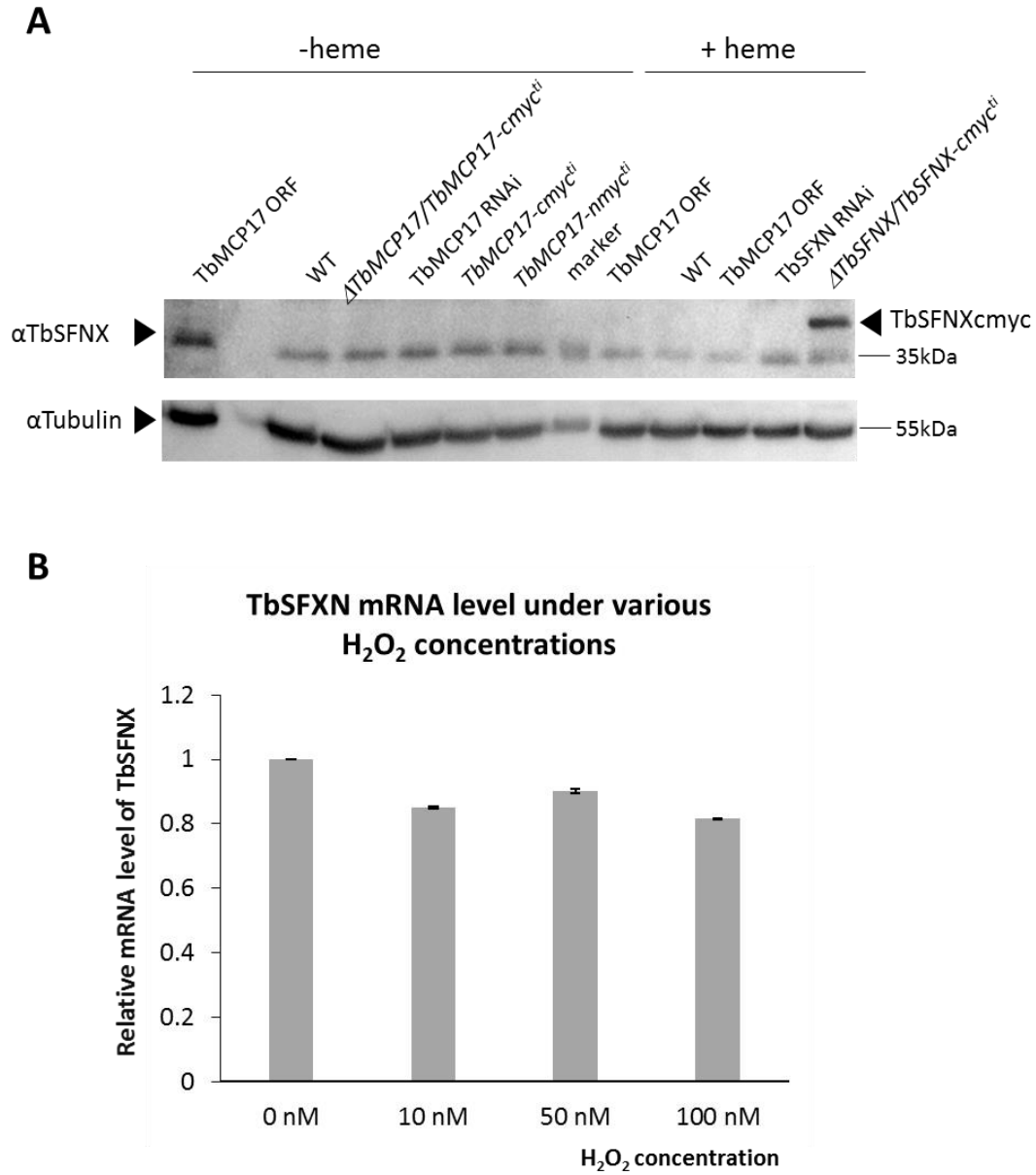

Figure 5-12 TbSFNX level detections under various medium conditions
A shows protein levels of WT, TbMCP17-ORF, *TbMCP17-myc*^{ti}, Δ*TbMCP17/TbMCP17-cmyc*^{ti} and TbMCP17 RNAi cells, as well as Δ*TbSFNX/TbSFNXcmyc*^{ti} and TbSFNX RNAi cells tested against the TbSFNX antibody (αTbSFNX). Tubulin was served as a loading control (αTubulin). Cells were cultured under either heme-depleted (-heme) or heme-available (+heme) conditions. B displays mRNA levels of WT cells cultured under various hydrogen peroxide concentrations. mRNA levels were tested by RT-quantitive PCR using primers generated from TbSFNX and TERT gene sequences (TbSNFNXqPCRFor, TbSNFNXqPCRRev, TERTqPCRFor, and TERTqPCRRev, sequence details can be found in Table 2-1). Relative TbSFNX mRNA level is calculated by setting the level of WT cells without the addition of hydrogen peroxide to 1.

5.8 Discussions and Conclusion

TbSFNX was found to belong to the sideroflexin family and formed a separate clade with high similarity to citrate transporters. This was consistent with the characterised sideroflexin family protein which was shown to transport citrate (Azzi et al. 1993). On the other hand, sideroflexin depletion was reported to cause iron accumulation in mitochondria and lead to siderocytic anaemia in mice and human (Fleming et al. 2001; Ye et al. 2003), indicating a potential role *TbSFNX* plays in iron metabolism. TbSFNX was found to be localised in mitochondria of *Trypanosoma brucei* in this study. The fact that conventional double knockout cell line (Δ*TbSFNX/TbSFNXcmyc*^{ti}) and the completely RNAi cell line cannot be generated, indicating the essentialness of TbSFNX. Both the over-expression (*TbSFNXcmyc*^{ti}) and the depletion (TbSFNX RNAi) caused a cell growth defect, suggesting that TbSFNX level is tightly controlled, which makes it possible to be a regulator by controlling its protein level. The possible explanations that RNA silencing induced by the addition of tetracycline did not show a further effect on cell growth between non-induced and induced cells were: (i) RNAi construct was leaky, thus TbSFNX depletion was also happening in non-induced cells; (ii) TbSFNX mRNA level of non-induced cells remained at 70%, which was efficient enough to present growth defect; (iii) post-translational modification was involved in the process and interfered with TbSFNX protein level. To justify the explanations, the mRNA level of TbSFNX RNAi (-tet) should be followed during the experiment, and the protein level of TbSFNX should be tested.

The potential role TbSFNX might play in energy metabolism was then assessed by measuring glucose & proline consumption and succinate & acetate production. The results observed were line with theories and findings in the field: (i) glucose, when present, is the preferred carbon source for PCF compared with proline (Lamour et al. 2005); (ii) succinate is not the end product for PCF, and it can be converted to acetate or fed into gluconeogenesis when glucose is completely depleted through pathway from fumarate to malate, pyruvate, phosphoenolpyruvate and further glyceraldehyde-3-phosphate, stepwise (van Weelden et al. 2005; van Hellemond et al. 2005); (iii) the 1.5-fold more acetate produced in both Δ*TbSFNX/TbSFNXcmyc*^{ti} and *TbSFNXcmyc*^{ti} cells (when compared with WT cells), regardless of the same amount of glucose consumed for all

three cells, is most likely derived from the pathway from succinate to malate, then pyruvate, and further to acetate from acetyl-CoA (Bringaud et al. 2015). These results indicate that the perturbation of TbSFNX level results in metabolic changes including more proline consumption, acetate formation from succinate and gluconeogenesis (Figure 5-7). This change of metabolism, in turn, leads to a growth defect in both Δ*TbSFNX/TbSFNXcmyc*^{ti} and *TbSFNXcmyc*^{ti} cells.

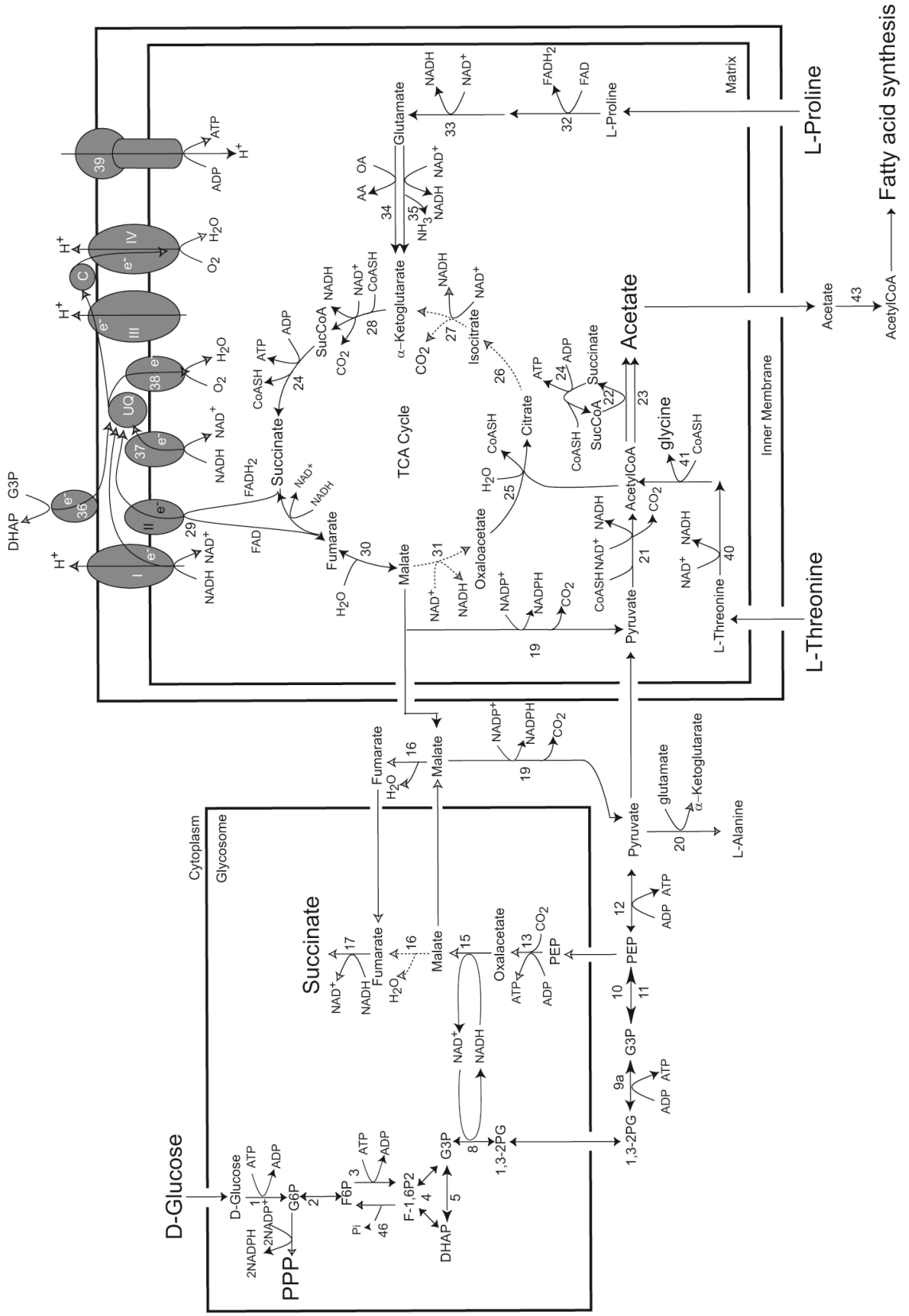

Figure 5-13 Schematic representation of the carbon flux in procyclic T. brucei energy metabolism

The figure is adapted from Besteiro (2005), Van Hellemond (2005) and Bringaud (2015). Legend: Black arrows, major flux route under the used culture conditions; dashed arrows, pathways with unclear function. Components of the respiratory chain are depicted as dark

grey ovals in the mitochondrial membrane. Excreted product acetate, succinate and substrates glucose, proline and threonine are shown in a larger font. The glycosomal and mitochondrial compartments and the TCA cycle are indicated. Enzymes are: 1, hexokinase: 2, glucose-6-phosphate isomerase; 3, phosphofructokinase; 4, aldolase; 5, triose-phosphate isomerase; 6, glycerol-3-phosphate dehydrogenase; 7, glycerol kinase; 8, glyceraldehyde-3-phosphate dehydrogenase; 9, phosphoglycerate kinase; 10, phosphoglycerate mutase; 11, enolase; 12, pyruvate kinase; 13, phosphoenolpyruvate carboxykinase; 14, pyruvate phosphate dikinase; 15, glycosomal malate dehydrogenase; 16, glycosomal fumarase; 17, NADH-dependent fumarate reductase; 18, glycosomal adenylate kinase; 19, malic enzyme; 20, alanine aminotransferase; 21, pyruvate dehydrogenase complex; 22, acetate:succinate CoA-transferase; 23, acetyl-CoA thioesterase; 24, succinyl-CoA synthetase; 25, citrate synthase; 26, aconitase; 27, isocitrate dehydrogenase; 28, a-ketoglutarate dehydrogenase complex; 29, succinate dehydrogenase (complex II of the respiratory chain); 30, mitochondrial fumarase; 31, mitochondrial malate dehydrogenase; 32, proline dehydrogenase; 33, pyrroline-5 carboxylate dehydrogenase; 34, glutamate aminotransferase; 35, glutamate dehydrogenase; 36, glycerol-3-phosphate oxidase; 37, rotenone-insensitive NADH dehydrogenase; 38, alternative oxidase; 39, F0/F1-ATP synthase; 40, threonine dehydrogenase; 41, acetylCoA:glycine C-acetyltransferase; 42, fructose 1,6 bisphosphatase; 43, AMP-dependent acetyl-CoA synthesis. Abbreviations: G6P: glucose 6-phosphate; F6P: fructose 6-phosphate; F-1,6P2: fructose 1,6-bisphosphate; DHAP: dihydroxyacetone phosphate; G3P:glyceraldehyde 3-phosphate; 1,3-2PG: 1,3-bisphosphoglycerate; PEP: phosphoenolpyruvate; PPP, pentose phosphate pathway; AA, amino acid; C, cytochrome c; CoASH, coenzyme A; OA, 2-oxoacid; Oxac, oxaloacetate; PEP, phosphoenolpyruvate; Pi, inorganic phosphate; PPi, inorganic pyrophosphate; SucCoA, succinyl-CoA; UQ, ubiquinone pool; e-, electrons; I, II, III and IV, complexes of the respiratory chain.

Apart from these results, the fairly low TbSFNX protein level was confirmed by the TbSFNX antibody, which was generated using heterologously expressed and purified TbSFNX-His protein. The generated TbSFNX antibody successfully detects TbSFNX-His and TbSFNX-myc proteins, but the endogenous TbSFNX is below detection limit regardless of all the efforts made in increasing detection sensitivity, removal of background and purification of the antibody. This indicates the low abundance of TbSFNX, which correlates with the growth defect observed in both Δ*TbSFNX/TbSFNXcmyc*^{ti} and *TbSFNXcmyc*^{ti} cell lines.

Preliminary results using various medium conditions did not result in a detectable increase of TbSFNX protein level under heme-depleted condition. The presence of hydrogen peroxide treatment led to an approximately 20% decrease of TbSFNX mRNA level. The change of TbMCP17 level (both up- and down-regulation) showed no link to WB-detectable TbSFNX protein level.

In future experiments, potential regulation of TbSFNX level is suggested to be tested in cells with different carbon sources (i.e., switch from low glucose to high glucose medium). Furthermore, as TbSFNX probably contains similar function as TbMCP12, the TbMCP12 depletion is likely to up-regulate TbSFNX so as to maintain cellular function. Thus, TbSFNX amount is advised to be examined in TbMCP12 knockout or over-expression cells.

Regardless of the results gathered, the transport function of TbSFNX remains elusive. Sideroflexins were reported to transport citrate and dicarboxylates (Azzi et al. 1993). To test potential substrate that TbSFNX transports, the mitochondrial ATP production assay or liposome reconstitution experiment using different metabolic intermediates is recommended. Besides, to support our hypothesis, nuclear magnetic resonance (NMR) analysis of the carbon flux through the mentioned metabolic routes is advised. It is also interesting to perform the measurement of fatty acid metabolisms in WT, Δ*TbSFNX/TbSFNXcmyc*^{ti} and *TbSFNXcmyc*^{ti} cell lines, since the upregulated acetate production from both knockout and overexpression directly feeds into fatty acid synthesis through acetyl-CoA (Rivière et al. 2009).

In addition to the transport function, sideroflexin depletion has been presented to lead to sideroblastic anaemia with iron accumulation in mitochondria (Fleming et al. 2001). This publication indicated a role of TbSFNX in mitochondrial iron homoeostasis. Thus, it is suggested to conduct iron content measurement of mitochondria and total cell in Δ*TbSFNX/TbSFNXcmyc*^{ti} and *TbSFNXcmyc*^{ti} cell lines. It is likely that as a sideroflexin family protein, Δ*TbSFNX/TbSFNXcmyc*^{ti} will lead to iron accumulation in the mitochondria, and *TbSFNXcmyc*^{ti} is prone to deprive iron in the mitochondria.

A brief summary of investigations on TbSFNX:

- TbSFNX belongs to the sideroflexin family.
- The endogenous protein level of TbSFNX is low and under tight control.
- Too much or too little of TbSFNX is detrimental for cell growth.
- The mRNA level of TbSFNX is decreased in the presence of hydrogen peroxide.

- Further experiments to unveil the functions of TbSFNX in tricarboxylate transport and/or mitochondrial iron homoeostasis are suggested.
- The physiological role(s) of TbSFNX should be further tested.

Chapter 6 Functional characterisation of TbMCP23

6.1 Introduction

The yeast mitochondrial pyrimidine carrier Rim2 has recently been shown to be essential in iron utilisation by enhancing heme and Fe-S cluster synthesis (Yoon et al. 2011). Rim2 has further been identified to mediate iron and other divalent metal ions to cross the mitochondrial inner membrane, which is dependent on pyrimidine nucleotide, especially when Mrs3 and Mrs4 are depleted, the removal of Rim2 causes more severe Fe-S protein maturation defect (Froschauer et al. 2013).

In this chapter, the Rim2 homologue in *T. brucei* was identified as TbMCP23 (Tb927.5.1550). TbMCP23 shared the conserved feature of mitochondrial carrier family proteins. Thus, the potential role TbMCP23 might play in iron usage or supply remains an interesting topic to study. In this chapter, due to time limit, only preliminary results were gathered including sequence analysis, TbMCP23 RNAi cell line generation and growth phenotype detection, followed by heterologous protein expression in *E. coli* for antibody generation.

6.2 Sequence analysis suggested TbMCP23 as a potential mitochondrial pyrimidine transporter

As discussed in other chapters, using conserved sequence and structural features, 24 mitochondrial carrier family proteins (TbMCP1-24) were identified from *T. brucei* (Colasante et al. 2009). TbMCP23 was identified as a homologue of known mitochondrial pyrimidine carriers (SLC35A33 homologues). To investigate more about TbMCP23 sequence, BLASTProtein (http://blast.ncbi.nlm.nih.gov/) was run using TbMCP23 protein sequence (Tb927.5.1550) against the genome database. The highest hits were sequences of different species from Kinetoplastea such as *T. b. gambiense* (I99/S100, identity % / similarity %), *Phytomonas sp.* (I60/S90), *L. seymouri* (I59/S95), *A. deanei* (I59/S92), followed by mammals SLC25A33 homologues, i.e *B. mutus* (I28/S87), *R. norveqicus* (I27/S92), *E. caballus* (I28/S87). Interestingly, parts of sequences of fungi coming out of BLASTP were potential folate transporters and deoxynucleotide carriers such as *C. immitis* (I33/S83) and *T. rubrum* (I31/S88). Afterwards, Rim2 protein sequence was also BLASTP against *S. cerevisiae* (taxid: 4932) and *Homo sapiens* (taxid: 9606) databases, separately. In the yeast database, the highest hits were Rim2 from different strains undoubtedly (I27/S86), followed by the L-ornithine transmembrane transporter Ort1p (I25/S86), the carnitine/acylcarnitine translocase Crc1p (I21/S90), the oxodicarboxylate carrier Odc2p (I22/S84), the citrate transporter Ctp1p (I24/S89) and the NAD^+ transporter Yia6p (I26/S51). Besides the best hit PNC1 (human mitochondrial pyrimidine transporter SLC25A33, I26/S91), protein sequences of various transport substrates were also found in *Homo sapiens* database: the calcium-binding mitochondrial carrier protein SCaMC-1 (I23/S89) and SCaMC-3 (I27/S84), the folate transporter (I26/S83), the thiamine pyrophosphate carrier (I22/S87) and the graves disease carrier (I26/S90). The rest of the homologues are linked to nucleotide synthesis: folate (folic acid) was needed for methylation reactions and nucleic acid synthesis, phosphate could be used in nucleotide synthesis too. Furthermore, the TbMCP23 sequence was aligned with (potential) mitochondrial iron transporters TbMCP17, Mrs3/4 and Mitoferrin 1/2.

Gathered sequences described above were aligned and a phylogenetic tree was generated using Mega7 (Figure 6-1). Sequences of trypanosomatids were highly conserved forming a separate clade which was close to yeast Rim2 and mammalian SLC25A33 proteins of

identified mitochondrial pyrimidine transporters (Hildyard & Halestrap 2003; Van Dyck et al. 1995; Marobbio et al. 2006; Favre et al. 2010; Da-Rè et al. 2014), indicating the possibility of TbMCP23 to be a pyrimidine transporter of mitochondria. The clade consisting of SLC25A33 and TbMCP23 homologues was somehow linked to certain nucleotide-related transporters (bootstrap value 57) such as folate carrier, FAD carrier and deoxynucleotide transporters. Noticeably, TbMCP17 and homologues in yeast or human formed a separate group (bootstrap value 99), but strongly connected with nucleotide or nucleotide-related proteins (bootstrap value 82), implying the potential relationship between iron exchange and pyrimidine transport. Besides, the ATP-Mg/Pi carriers, the SCaMC proteins and the thiamine pyrophosphate deoxynucleotide carrier formed an individual clade branching early from the tree. This further supported the highly homologous between TbMCP23 and pyrimidine transporters from the other aspect.

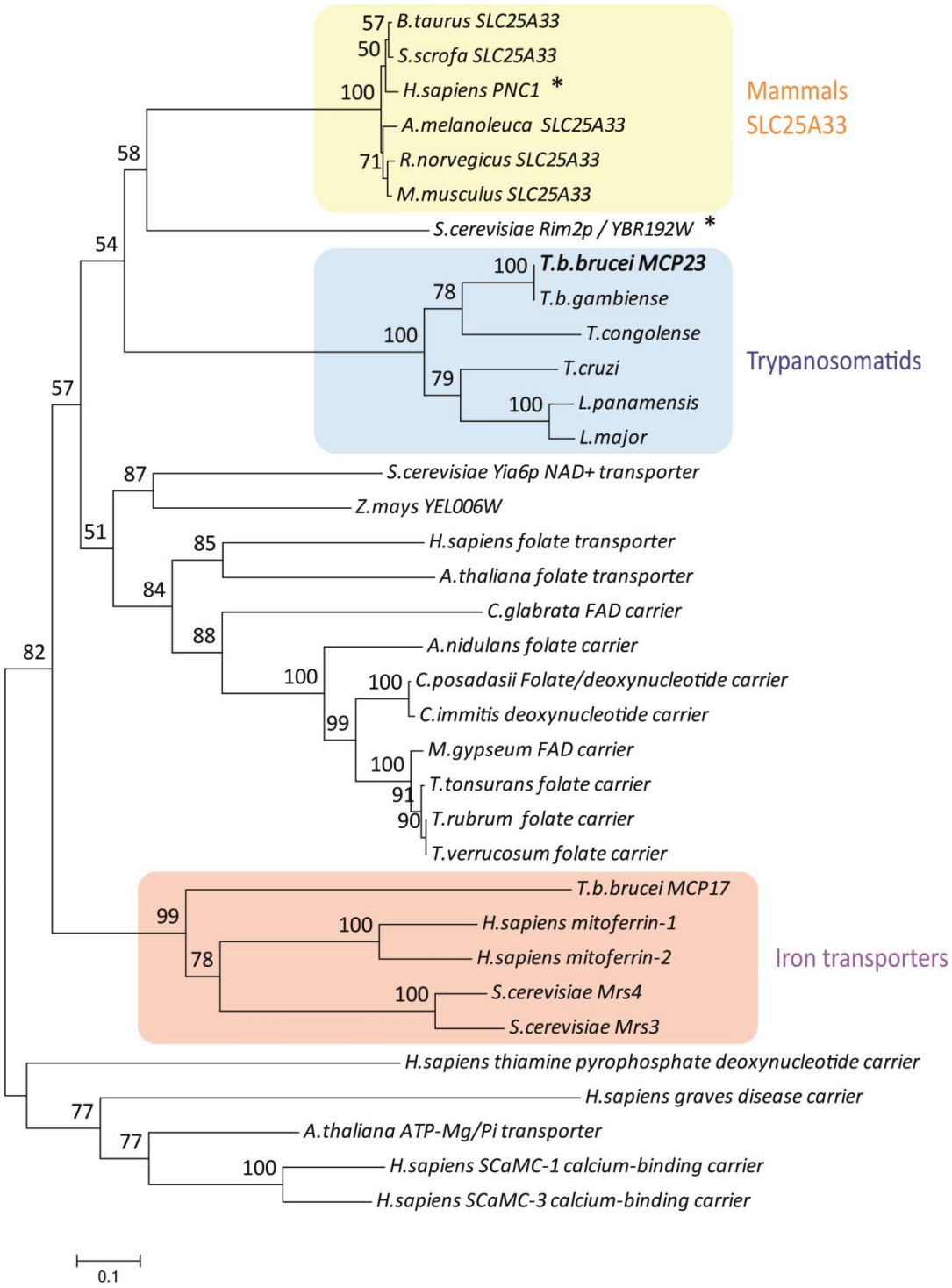

Figure 6-1 Evolutionary relationships of taxa of TbMCP23

The evolutionary history is inferred using the Neighbor-Joining method (Saitou & Nei 1987). The percentage of replicate trees in which the associated taxa clustered together in the bootstrap test (1000 replicates) are shown above the branches (Efron et al. 1996). The tree is drawn to scale, with branch lengths in the same units as those of the evolutionary distances used to infer the phylogenetic tree. The evolutionary distances are computed using the Poisson correction method (Zuckerkandl & Pauling 1965) and are in the units of the number of amino acid substitutions per site. The analysis involves 35 amino acid sequences. All positions containing gaps and missing data are eliminated. There is a total of 173 positions in the final dataset. Evolutionary analyses are conducted in MEGA7

(Kumar et al. 2016). Target protein sequence TbMCP23 is emphasised with larger font and bold, characterised pyrimidine transporters in human (PNC1) and yeast (Rim2) are labelled with an asterisk. Sequences/ species from Trypanosomatids are highlighted in a blue balloon, homologue to SLC25A33 from mammals are painted yellow with labels at the side, and (potential) iron transporters are circled and filled with orange.

As a potential pyrimidine transporter, the sequence of TbMCP23 was aligned with PNC1 and Rim2, as well as homologues from *Leishmania*, and the structural features were analysed. Sequence alignment of TbMCP23 with *L. major, S. cerevisiae* Rim2 and *H. sapiens* PNC1 showed that TbMCP23 contained all conserved sequences and structural features of mitochondrial carrier family proteins (Figure 6-2). The deduced amino acid sequence of TbMCP23 consists of 310 amino acids, and the predicted protein size is 34.1 kDa. TbMCP23 presents three transmembrane domains and contains six transmembrane alpha-helixes labelled as H1 to H6 identical to other MCF proteins. Moreover, in each transmembrane domain, signature sequence motif of 'Px[D/E]x2[K/R]x[K/R]' with 'x' representing any amino acid residue (Aquila et al. 1987; Saraste & Walker 1982) can be found at the end of H1, H3, and H5, labelled as M1a, M2a, and M3a. There were four exceptions, one of which was that [D/E] on M2a was replaced by nonpolar phenylalanine (F, see TbMCP23 and *L. major* homologue) or tryptophan (W, see Rim2 and PNC1). This polar mutation resulted from different transport mechanism for pyrimidine (Monné et al. 2012). On M3a, additionally, [D/E] in trypanosomatids (here represented as *T. brucei* and *L. major*) were replaced by asparagine (N), the first [K/R] in trypanosomatids by methionine (M), and the second [K/R] by histidine (H) of the same amino acid group (positively charged). Similarly, the second signature motif '[D/E]Gx4-5[W/F/Y][K/R]G' (labelled as M1b, M2b and M3b) was also conserved except for the starting two amino acids in M1b.

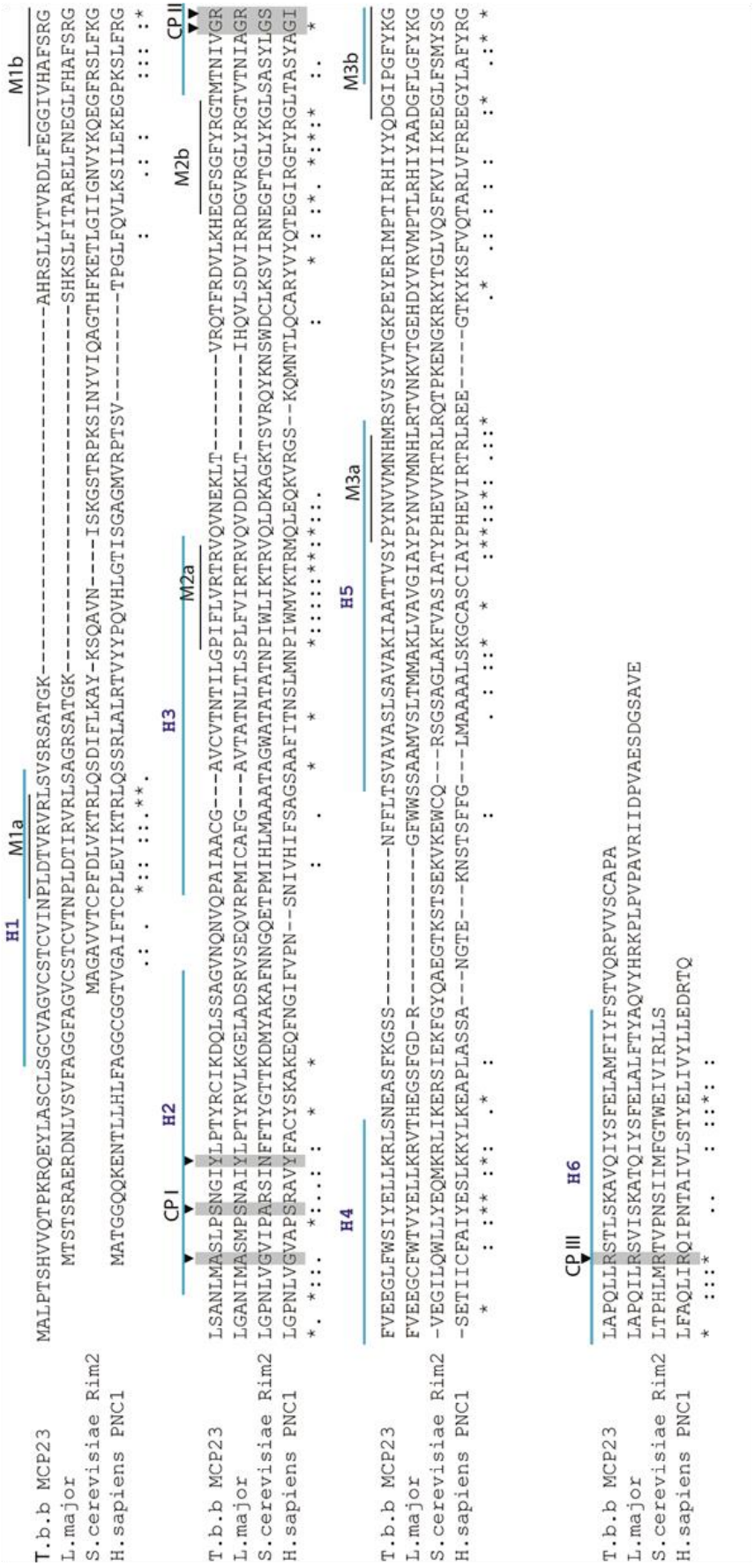

Figure 6-2 Sequence alignment of TbMCP23 with corresponding sequences from *L.major, S. cerevisiae* Rim2 and *H. sapiens* PNC1

Accession numbers can be found in Section 2.1. The six transmembrane helices are labelled from H1 to H6 with a blue line. The first part of the canonical signature sequence motifs locates at the end of H1, H3 and H5, labelled with M1a, M2a and M3a, and the second part motifs are labelled with M1b, M2b and M3b. Substrate contact points (CP I, CP II, and CP III) are located downstream of M1b, M2b, and M3b and boxed grey. An asterisk (*) indicates positions which have a single, fully conserved residue. Colon (:) signifies conservation between groups of strongly similar properties - scoring > 0.5 in the Gonnet PAM 250 matrix. Period (.) stands for conservation between groups of weakly similar properties - scoring =< 0.5 in the Gonnet PAM 250 matrix.

In MCF proteins, groups of conserved amino acids located downstream of each signature motif participate in substrate discrimination, recognition and binding. Three well-conserved substrate contact points called CP I, CP II and CP III are extrapolated from all MCF proteins transporting similar substrates (Kunji & Robinson 2006). As shown by the protein sequence alignments of mitochondrial pyrimidine carriers, the three amino acids for CP I are relatively conserved. The first amino acid on CP I was either a hydrophobic alanine (A) in trypanosomatids or a hydrophobic glycine (G) in yeast and human. The second amino acid was a hydrophilic serine (S) or hydrophobic alanine (A) (in yeast), and the third amino acid was either a tyrosine (Y) in trypanosomatids or asparagine (N) in yeast. For contact point II, the first glycine (G) was conserved in all four sequences as Kunji predicted. The second amino acid differed among positively charged arginine (R), hydrophilic serine (S) and hydrophobic isoleucine (I). The positively charged arginine (R) in contact point III was proved to be involved in phosphate binding (Kunji & Robinson 2006).

6.3 TbMCP23 RNAi presented a slight increase in growth

In order to determine whether TbMCP23 was essential for cell growth, gene knockdown (RNAi) was conducted, and related growth phenotype was observed.

6.3.1 RNAi plasmid construction

Using the same method as that of TbSFNX RNAi plasmid via Apa I, BamH I and Hind III restriction enzyme sites, pHD676+TbMCP23 RNAi plasmid was constructed (see Section 5.4). The resulting potential clones were first examined with PCR using TbMCP23 sense primers, and all of them showed a band of predicted size (Figure 6-3 A). 5 potential clones were then digested with BamH I and Hind III for antisense plus sense fragment (AS+S, Figure 6-3 B), and with BamH I, Hind III and Apa I enzyme sets for both antisense and sense fragments (AS&S, Figure 6-3 C). As shown in Figure 6-3 B, after the BamH I & Hind III digestion, a band of approximately 900 bp was observed, which was identical to the size of TbMCP23 antisense and sense (AS+S 832 bp, Appendix A1). The triple enzyme digestion resulted in two bands of similar size, which was in accordance with the size of antisense (AS 444 bp) and sense (S 388 bp). Among the five positive clones, clone 1 was further sequenced and confirmed, thus used for later experiments.

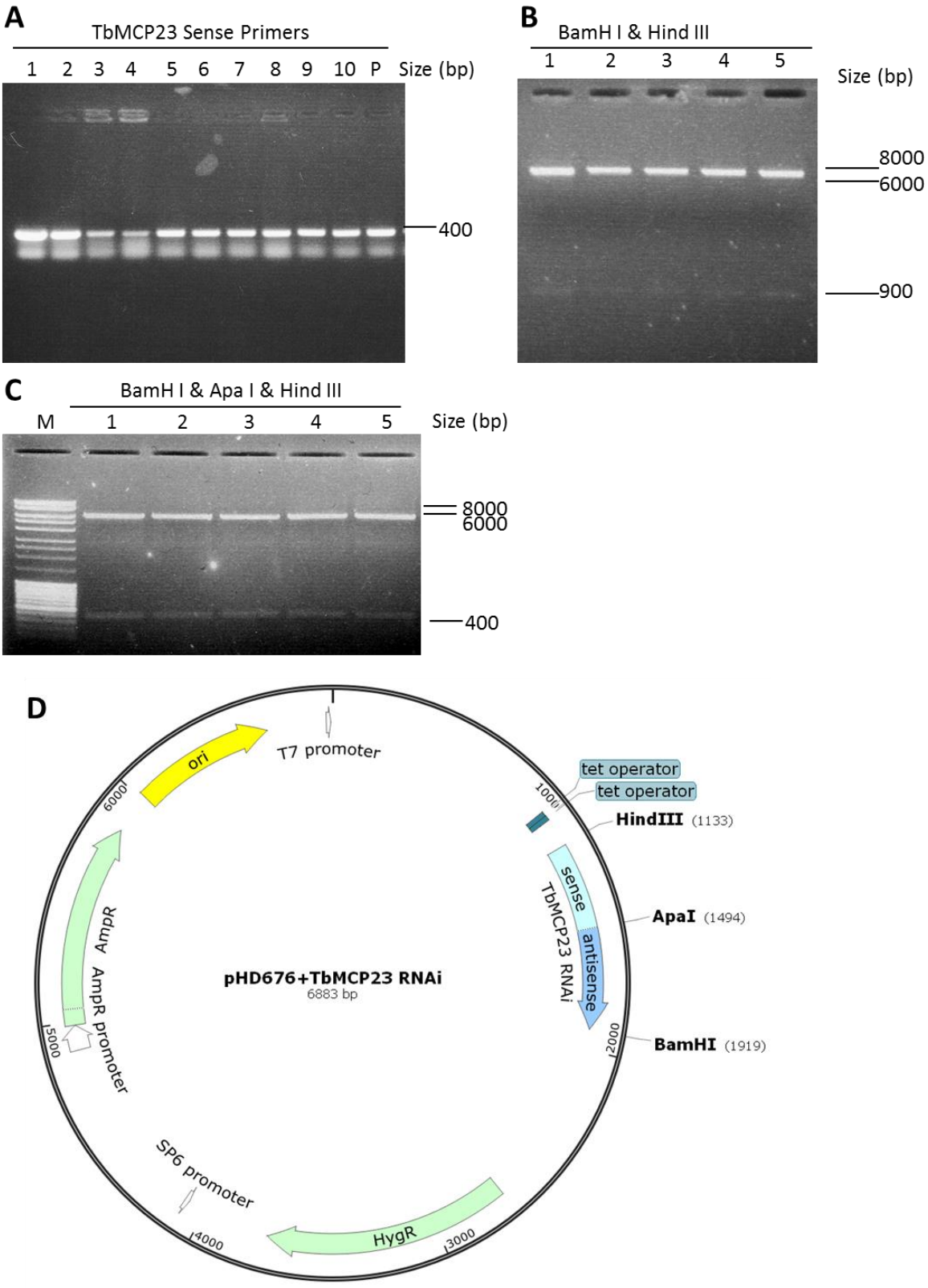

Figure 6-3 The examination of potential pHD676+TbMCP23 RNAi clones
A displays PCR examination using TbMCP23 sense forward and reverse primers to test 10 colonies. P stands for positive control using pHD676+TbMCP23 sense plasmid. B and C show restriction enzymes digestions on first 5 clones using BamH I, Apa I, and Hind III. M stands for the marker, U represents undigested plasmid isolated from clone 1.

Samples 1 to 5 are five plasmids isolated from five individual clones. The resulting plasmid map is attached to D.

6.3.2 Growth of TbMCP23 RNAi cells increased slightly

PCF449 was transfected with pHD676+TbMCP23 RNAi plasmid. The generated TbMCP23 RNAi cell line was induced by the addition of tetracycline. The growth of TbMCP23 RNAi cells was followed for 6 days and compared with that of WT. Surprisingly, TbMCP23 RNAi cells grew slightly faster than WT (shown in Figure 6-4). TbMCP23 knockdown efficiency was checked using quantitive real time PCR (Table 6-1). mRNA level of TbMCP23 was 100 folds less expressed than WT, confirming that mRNA level of TbMCP23 was significantly down-regulated (Table 6-1).

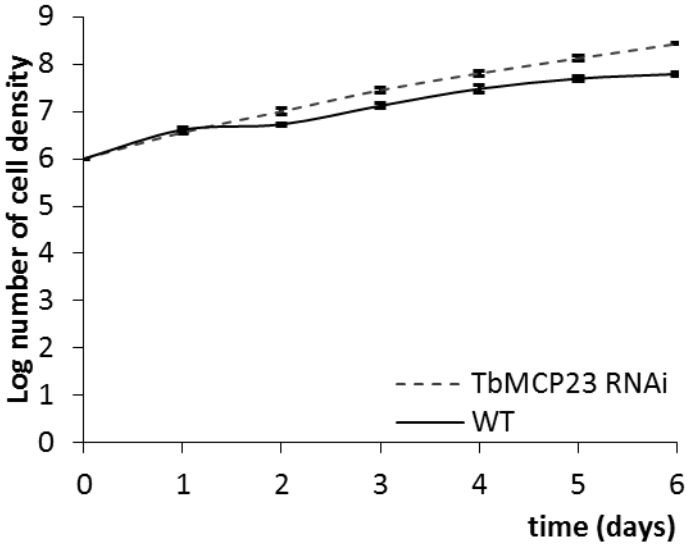

Figure 6-4 The growth effect on TbMCP23 down-regulation
The growth of TbMCP23RNAi cell line induced by tetracycline is presented in the graph with WT cells. The growth was followed for 6 days. Cell density is presented in log10. The solid line indicates WT growth and the dashed line for TbMCP23RNAi cell line. Error bars are added representing standard deviation but too small to be visualised.

Table 6-1 TbMCP23 mRNA level detection

Cell sample	**$C_{T\ (TbMCP23)}$**	**$C_{T\ (TERT)}$**	**ΔC_T ($C_{T\ (TbMCP23)}$ - $C_{T\ (TERT)}$)**	**$\Delta\Delta C_T$ (Avg. $\Delta C_{T\ (TbMCP23RNAi)}$- Avg. $\Delta C_{T(PCF449)}$)**	**Relative mRNA ($2^{-\Delta\Delta C_T}$)**
PCF449	**$C_{T\ (TbMCP23)}$**	**$C_{T\ (TERT)}$**	**ΔC_T ($C_{T\ (TbMCP23)}$ - $C_{T\ (TERT)}$)**	**$\Delta\Delta C_T$ (Avg. $\Delta C_{T\ (TbMCP23RNAi)}$- Avg. $\Delta C_{T(PCF449)}$)**	**Relative mRNA ($2^{-\Delta\Delta C_T}$)**
Average	23.06721 23.10966 23.06608	25.23888 25.29084 25.51281	-2.17 -2.18 -2.45		
PCF449			-2.27±0.13	0.00±0.13	1.0 (0.91-1.10)
Average	33.0185 32.80369 32.28911	24.74456 24.85074 24.78175	8.27 7.95 7.51		
TbMCP23 RNAi			7.91±0.31	10.18±0.31	0.000862 (0.0007-0.001)

RT-PCR performed in PCF449 and TbMCP23 cells using two sets of primers, i.e., TbMCP23 and TERT in triplicates is presented as C_T values (threshold cycles). ΔC_T is calculated by subtracting $C_{T\ (TERT)}$ from $C_{T\ (TbMCP23)}$ within each cell sample. $\Delta\Delta C_T$ is calculated by subtracting the averages of ΔC_T of PCF449 from ΔC_T of TbMCP23 RNAi cells. The normalised mRNA amount of TbMCP23 relative to PCF449 is calculated by $2^{-\Delta\Delta CT}$ with WT TbMCP23 mRNA level set to 1.

Noticeably, mRNA depletion does not reflect exactly the same situation at the protein level. Hence, this growth phenotype should be further confirmed by WB analysis at protein level.

6.4 Heterologous protein expression

In order to detect TbMCP23 at the protein level, TbMCP23 was induced to express in *E. coli* and further purified for antibody generation.

6.4.1 Plasmid construction

The expression vector pET28 was inserted with TbMCP23 open reading frame (ORF) using BamH I and Hind III restriction enzyme sites. After amplification with PCR, TbMCP23 ORF was first ligated into pGEM T-easy. Isolated plasmids were tested using restriction enzyme digestions (Figure 6-5 A). Then, the TbMCP23 fragment was double digested using BamH I and Hind III, and further inserted into the pET28 vector. The resulting pET28+TbMCP23 plasmids were examined by PCR using TbMCP23 primers (Figure 6-5 B). Plasmid No.1 was sequenced and aligned with TbMCP23 gene sequence (Tb927.5.1550) to confirm that plasmid No.1 can be used for further experiments (Appendix A4-7).

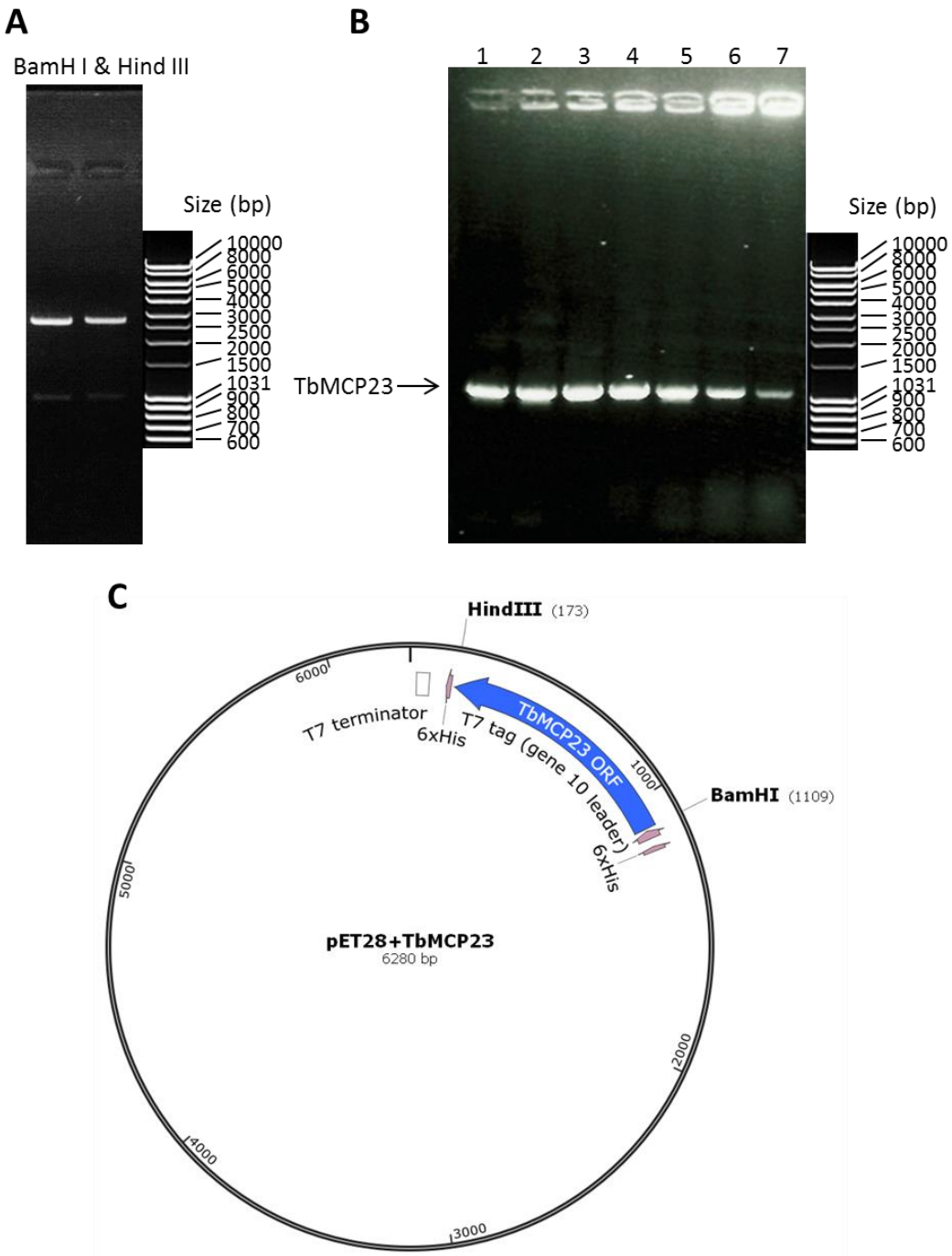

Figure 6-5 The construction and examination of pET28+TbMCP23
A displays digestion result of two potential pGEM T easy + TbMCP23 plasmids digested with BamH I and Hind III enzymes. B presents PCR result of potential pET28+TbMCP23 constructs using TbMCP23 primers. C demonstrated the plasmid map of pET28+TbMCP23.

6.4.2 Protein expression

The isolated pET28 +TbMCP23 construct was transformed into Lemo21 *E.coli* strain, and the protein expression was induced. As shown in Figure 6-6, a band of predicted size for TbMCP23-His (around 35 kDa) was observed and confirmed with His antibody, indicating that TbMCP23 was successfully expressed after IPTG induction.

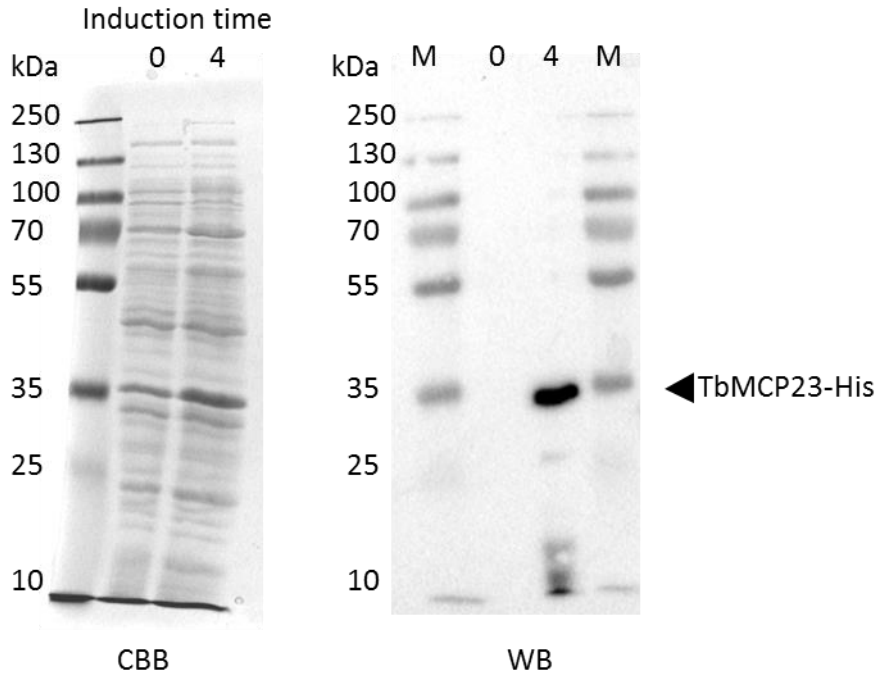

Figure 6-6 Heterologous protein expression of TbMCP23

CBB results of cell extracts before (0) and after (4) induction is shown in the left panel, and WB result probed with His antibody in the right panel. OD600=0.1 is used for WB per lane, and OD600=0.2 for CBB.

6.4.3 Protein purification

Followed by the expression of TbMCP23, the protein was isolated from *E. coli* cell lysate and purified using Ni-NTA beads. In principle, Ni-NTA binds His-tagged protein, here TbMCP23-His, and unbound proteins went through the column and collected as flow through (FT) sample. Afterwards, Ni-NTA were washed three times to remove any possible impurities, followed by two elutions using elution buffer that contained detergents to remove His-tagged protein from the column. As presented in Figure 6-7 A,

no protein was detected from WB in FT and three wash samples, indicating that protein binding step was efficient. This finding was also supported by CBB results that multiple bands were detected in FT suggesting successful removal of the majority of impurities (Figure 6-7 B). In two elutions, sufficient amount of protein was observed with some degraded products, whereas around 1/3 still remained in the Ni-NTA beads. The results can be accounted for (i) not enough volume of elution buffer was added; (ii) elution buffer was not efficient enough.

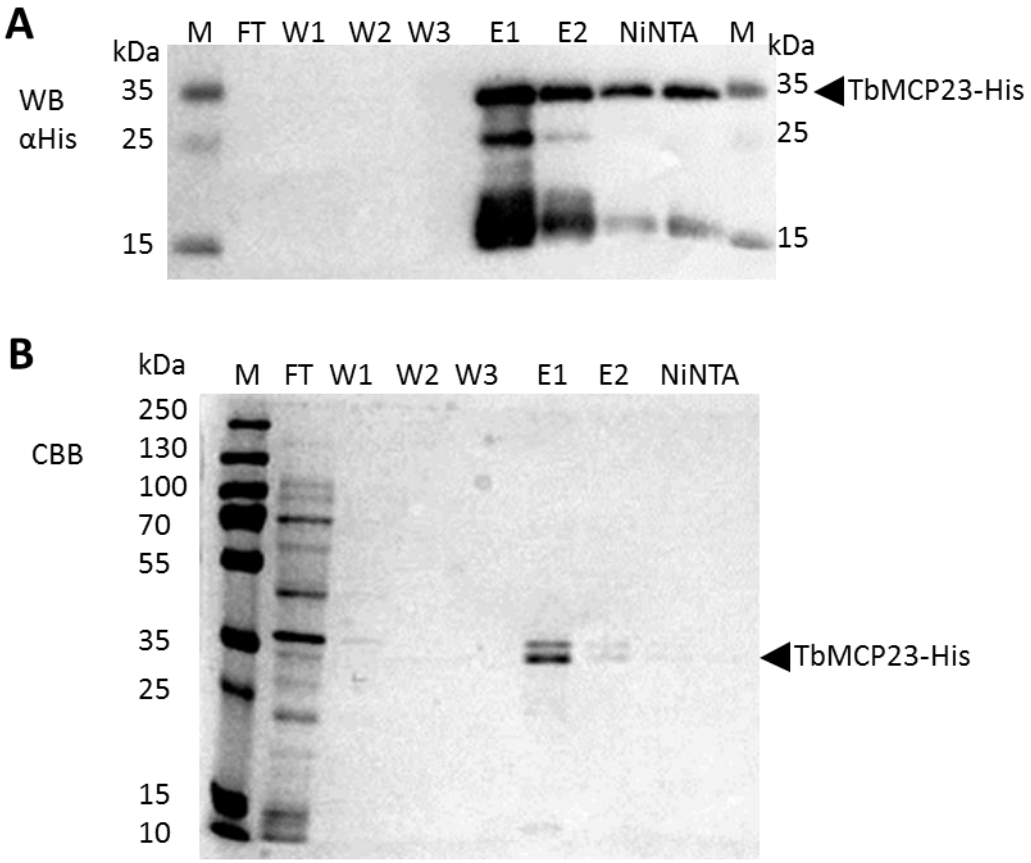

Figure 6-7 TbMCP23-His protein purification using Ni-NTA column
Protein purification using Ni-NTA column procedure was followed and samples in between different steps were collected and loaded onto WB (A) and CBB (B) gel. M stands for the marker; FT for flow through; W1, W2 and W3 are three continuous washes; E1 and E2 indicate two elutions; the last two lanes were Ni-NTA beads slurry. For WB, His antibody is used to detect target protein, and CBB demonstrates the purity of samples from different steps.

6.5 Conclusion

In this chapter, preliminary steps for identification and characterisation of TbMCP23 were taken. Sequence alignment of TbMCP23 with mitochondrial pyrimidine transporters from other species and the phylogenetic tree indicates that TbMCP23 is a potential nucleotide transporter, especially for pyrimidine. Interestingly, the pyrimidine carriers were more closely linked to mitochondrial iron carriers (TbMCP17, Mrs3/4) than other nucleotide-related carriers, as shown in the phylogenetic tree (Figure 6-1). No growth defect of TbMCP23 knockdown (RNAi) was observed in this study. In drosophila, however, TbMCP23 homologue drim2 double knockout presented some growth effect at the larvae stage, a significant defect at the pupae stage and no survival at the adult stage, but no growth effect presented when one of the gene copies was depleted (Da-Rè et al. 2014). Similar growth defect was found in yeast (Van Dyck et al. 1995). This contradicting result suggested that either a tiny percentage of TbMCP23 mRNA is sufficient for cell growth or TbMCP23 is not essential for cell growth, which implied alternative transporters in *T. brucei.* The depletion of mRNA is not necessarily related to down-regulation at the protein level since low copies of mRNA can be sufficient enough for protein expression. Thus, an antibody for detecting TbMCP23 protein level was performed. Heterologous expression of TbMCP23-His protein in *E. coli* was completed, and the protein was successfully bound to Ni-NTA column.

For future study, the following experiments are suggested to be included. First of all, concerning antibody generation, more elution steps or larger volume of elution buffer should be applied. If the same problem turns up again, more powerful detergent or higher concentrations should be tested. At the same time, conventional gene double knockout cell line could be generated to achieve 100% gene removal. Furthermore, the generation of TbMCP23 over-expression (with myc tag) cells is recommended. The generated cell line can be used for cellular localisation by immunofluorescence microscopy, and potential growth phenotype can be examined. Functional experiments such as measurement of the nucleotide production or pyrimidine transport assays can be conducted to disclose the function of TbMCP23. Moreover, experiments related to iron transport and heme synthesis are suggested. As proved by Wiesenberger and Dancis, Rim2, the pyrimidine nucleotide exchanger in yeast, can co-import pyrimidine and iron

(Froschauer et al. 2013; Yoon et al. 2011). It is interesting to investigate whether in *T. brucei,* TbMCP23 can rescue cell growth defect and/or restore iron transport function in the ΔTbMCP17 cell line.

A brief summary of investigations on TbMCP23:

- TbMCP23 is a potential pyrimidine transporter suggested by sequence analysis.
- Mitochondrial pyrimidine carriers are more closely linked to mitochondrial iron carriers compared with nucleotide related carriers.
- TbMCP23 RNAi did not result in growth defect.
- Heterologous TbMCP23-His protein expression and purification are applicable but need further optimisation.
- The subcellular localisation is suggested to be tested.
- Function experiments are suggested such as the nucleotide transport assays or the examination of nucleotide production rate.
- The link between TbMCP23 and TbMCP17 or the rest potential iron related transporters should be tested.

Chapter 7 Discussions and conclusion

To sum up, this thesis successfully identified and characterise potential mitochondrial iron-related proteins TbMCP12, TbMCP17, TbSFNX and TbMCP23 in *Trypanosoma brucei*. In this study, TbMCP12 is proved to be a dicarboxylate-tricarboxylate mitochondrial carrier (DTC). TbMCP17 is strongly suggested to be an iron transporter. The functions of TbMCP23 and TbSFNX need further investigations.

Mitochondrial carrier family (MCF) proteins are involved in many physiologically important processes, including the maintenance of the cellular ATP balance and the regulation of the intricate cytoplasmic-mitochondrial redox state. MCF proteins further provide the eukaryotic cell with vital biosynthetic building blocks, which are derived from the tricarboxylic acid cycle in the mitochondrial matrix. MCF proteins exert flux control on a wide range of metabolic pathways (see Palmieri 2014 and references therein). Iron is a fundamental element for various processes including electron transport, DNA synthesis and repair, oxidative stress defence and energy metabolism (see Bruno Manta 2011 and references therein). However, free iron is toxic to cell by the spread of reactive oxygen species and the generation of highly reactive radicals. The homoeostasis of iron has to be tightly regulated.

Sequence analysis of TbMCP12 suggested its phylogenetic relationship with carboxylate carriers such as dicarboxylate carriers (DICs), dicarboxylate-tricarboxylate carriers (DTCs) and oxoglutarate carriers (OGCs). TbMCP12 showed a closer relationship with DTCs and OGCs than with DICs from the phylogenetic tree (Colasante, unpublished data). It is worth mentioning that no specific hit was found using tricarboxylate carriers (also known as citrate carriers, CICs) against *Trypanosoma brucei* genome by BLASTP (GeneDB, Colasante, unpublished data). OGCs catalyse the exchange between oxoglutarate and malate, and play a role in the malate-asperate shuttle and the oxoglutarate-citrate shuttle (see Monné et al. 2012 and references therein). DTC is responsible for the exchange of a tricarboxylate with a dicarboxylate in plants and combines the characteristics of both the oxoglutarate-malate and tricarboxylate carriers (Picault et al. 2002). It catalyses electroneutral metabolites transport that plays a number of roles involved in organic acid flux to or from the mitochondria, including fatty acid elongation, redox equivalents for photorespiration, nitrogen assimilation (Gálvez et al. 1999), ATP synthesis and respiratory flux (Kanellis & Roubelakis - Angelakis 1993). The

DTC counterpart in animals is the CIC, which not only catalyses a tricarboxylate for a dicarboxylate (the same as DTC) but also transports a tricarboxylate in exchange of another tricarboxylate or phosphoenolpyruvate (PEP) across the mitochondrial inner membrane. Like DTCs, CIC proteins play a role in fatty acid biosynthesis, maintaining redox balance and other processes such as gluconeogenesis, insulin secretion, histone acetylation, inflammation and differentiation of fibroblasts into adipocytes (Joseph et al. 2006; Siculella et al. 2004; Morciano et al. 2009; Siculella et al. 2010; Cappello et al. 2012; Bonofiglio et al. 2013; Catalina-Rodriguez et al. 2012; Kolukula et al. 2014; Wakil 1989; Kuhajda 2006; Kuhajda 2000; Santolla et al. 2012; Serviddio et al. 2014). Accordingly, TbMCP12 is very likely to transport tricarboxylate, dicarboxylate and oxoglutarate, and thus function as a DTC in plants. The stronger relatedness of DTC to OGC than to other characterised carriers, which indicates that DTC and OGC originate from the same ancestor. This ancestor in plants evolves to DTC, whereas in animals it duplicates into two proteins: CIC and OGC. TbMCP12 also supports this hypothesis with only one homologue of OGC and DIC discovered from *Trypanosoma brucei* by BLASTP.

The expression level of TbMCP12 protein is 29 folds higher in PCF than BSF (Colasante, unpublished data). The various mRNA and protein expression levels of CIC are also found in human tissues: high in liver, pancreas and kidney but low or absent in brain, heart, skeletal muscle and lungs (Huizing et al. 1998). The rat OGC has found to be expressed in heart, liver and brain (Dolce et al. 1994), while the human OGC is more abundant in heart and skeletal muscle (Huizing et al. 1998). Human DIC protein is found in liver, kidney, heart brain, lung, pancreas and adipose tissue (Fiermonte et al. 1998; Huizing et al. 1998; Das et al. 1999). DTC transcript level is the highest in the flower bud of Arabidopsis, yet the lowest level in the root (Picault et al. 2002). On the other hand, many mitochondrial-related proteins (Chi et al. 1998; Colasante et al. 2006; Saas et al. 2000; Peña-Diaz et al. 2012) have presented a life-cycle regulatory expression pattern: highly expressed in PCF and low expression level or absent in BSF in *T. Brucei*, which is related to the repressed mitochondrial function in BSF (Bringaud et al. 2015).

The failure of generating a conventional double knockout cell line (*ΔTbMCP12*) indicates the indispensable role TbMCP12 plays in PCF. Yeast DIC is also found to be essential for cell growth, and the DIC-depleted cells failed to grow in ethanol or acetate acting as

the sole carbon source (Palmieri et al. 1999). The primary function of DIC is to import succinate into mitochondria, providing intermediates for Kerb's cycle. Moreover, the successful growth rescued by introducing TbMCP12 into DIC-depleted cells cultured in acetate medium suggests that TbMCP12 can functionally complement DIC, indicating that TbMCP12 can transport succinate into the mitochondria as yeast DIC.

The transport function of TbMCP12 was further tested using the mitochondrial ATP production assay. Until now, the most successful strategy to identify the substrate specificity of the transport function is characterised by the EPRA method of gene expression, purification of the recombinant proteins, their reconstitution into liposomes and transport assays (Fiermonte et al. 1993). Due to the failure of reconstitution of TbMCP12 into liposomes, another method: mitochondrial ATP production assay (Allemann & Schneider 2000) was performed. The assay was applied to digitonin-isolated mitochondria from TbMCP12 knockout cells, overexpression and WT cells of *T. brucei*. The complete depletion of ATP production from citrate and isocitrate in TbMCP12 knockout mitochondria strongly suggests that TbMCP12 transports tricarboxylates (citrate and isocitrate). The transport properties of CIC from different species are confirmed by the purification of carriers from mitochondria and liposomal reconstitution (LaNoue & Schoolwerth 1979; Palmieri et al. 1972; Robinson 1971) as well as recombinant expression and reconstitution (Xu et al. 1995; Kaplan et al. 1995; Zara et al. 2007; Capobianco et al. 2011; Madeo et al. 2009) from rat, eel, drosophila and yeast. The results prove that CIC transports citrate, *cis*-aconitate, threo-isocitrate, phosphoenolpyruvate, L-malate, malonate and succinate. In yeast, the second isoform of CIC, CIC2 (also known as YHM2 or citrate/OGC) has been identified, and this protein efficiently transports citrate, oxoglutarate, succinate and fumarate, while inefficiently transports isocitrate, *cis*-aconitate and malate (Castegna et al. 2010). In plants, DTCs are capable of transporting dicarboxylates, tricarboxylates and sulphate but not PEP (Picault et al. 2002; Regalado et al. 2013). In Protista *Plasmodium falciparum*, a DTC transporting dicarboxylates (oxoglutarate, oxaloacetate, malate, succinate and fumarate), citrate and sulphate is identified (Nozawa et al. 2011). Moreover, the ATP production of citrate can be completely ablated by the impermeable substrate analogue 1,2,3-benzenetricarboxylate (BTA), which has been previously proved to specifically inhibit

CIC (Palmieri et al. 1972; Robinson & Oei 1975; Stipani & Palmieri 1983). This result further confirms the citrate transport function of TbMCP12.

An increase of the expression level of TbMCP12 has been observed under different culture conditions such as the presence of glucose, heme addition as well as hydrogen peroxide addition. These results indicate a role TbMCP12 plays in oxidative stress defence. The role was further confirmed by the growth phenotype of TbMCP12 knockout and overexpression under increasing hydrogen peroxide concentrations that TbMCP12 overexpression cells grew better under oxidative stress than WT or knockout. $NADP^+$/NADPH ratio of TbMCP12 knockout, overexpression and WT cells were also measured, revealing a significant increase of the ratio of knockout cells cultured on low glucose medium and a remarkable decrease of the ratio of overexpression cells cultured on high glucose medium. This result is consistent with the finding that TbMCP12 level was higher in high glucose condition, so that a further overexpression of TbMCP12-myc resulted in a significant phenotype and vice versa. Human DIC plays a role in the transfer of reducing equivalents (NADPH), which is supported by the fact that DIC knockdown caused a less malignant phenotype (growth more sensitive to oxidative stress) (Zhou et al. 2015). Apart from this finding, the overexpression of DIC and OGC in a renal proximal tubule-derived cell line, NRK-52E cells, presented an increase of protection against oxidative stress and chemically induced apoptosis (Xu et al. 2006).

TbMCP17 is the only homologue of mitochondrial iron carrier found in *T. brucei* with high similarities to mitochondrial iron transporters characterised in *Leishmania amazonensis:* LMIT1 at I53%/S69% (Mittra et al. 2016), in *Saccharomyces cerevisiae:* MRS3 and MRS4 at I31%/S48% (Muhlenhoff et al. 2003; Froschauer et al. 2009) and in *Homo sapiens:* Mitoferrin 1 and Mitoferrin 2 at I32%/S48% (Shaw et al. 2006; Paradkar et al. 2009). Conserved contact points were found in the species above. Also, in mammals and yeast, there are two isoforms with the second ones (Mitoferrin2 and MRS4) as backups (Troadec et al. 2011; Paradkar et al. 2009), while in plants and insects, only one copy is found (Metzendorf et al. 2010).This difference indicates the same ancestor in evolution, which duplicated in certain circumstances such as Mitoferrin 1 for erythropoiesis (Troadec et al. 2011), while in other species such as drosophila, trypanosomes and plants, only one protein form is enough for the full function.

In this study, the generation of conventional double knockout in TbMCP17 encountered the same failure as in TbMCP12, suggesting the essentiality of TbMCP17 in PCF. The generated conditional knockout and RNAi cell lines indeed presented a significant growth defect under both standard and iron depleted conditions. Correspondingly, the rescue of growth under iron depriving conditions were observed in TbMCP17 overexpression cells, as well as in TbMCP17-myc expressed conditional knockout cells. Under iron depleted conditions, TbMCP17 overexpression cells grew better than WT, suggesting a positive role TbMCP17 plays against iron-deprival. The growth phenotypes clearly show that TbMCP17 is an iron transporter. The growth defect caused by TbMCP17 depletion was found by Mittra et al (Mittra et al. 2016). The similar growth defect was also found in mutants of mitochondrial iron transporter from other species: MRS3/4 mutants presented growth failure in acetate and ethanol (Froschauer et al. 2009); LMIT1 half-knockout presented a reduction in growth rate, and in promastigotes of *L. amazonensis* LMIT1 null mutant cannot be generated (Mittra et al. 2016); partial lethality was found when the only mitoferrin gene was deleted in *Drosophila* (Metzendorf et al. 2010). The consistency further confirms that mitochondrial iron carriers are vital to cell growth.

Additionally, the mitochondrial iron content of TbMCP17 RNAi cells was decreased under standard condition, and this decrease was more predominant under heme-depleted conditions. Similar results in *Leishmania* was found in half LMIT1 knockout (Mittra et al. 2016).This result confirms that TbMCP17 functions as an iron importer. Functional complementation was further performed on yeast mitochondrial iron importer MRS3/4 depleted strain. The rescue of growth defect of MRS3/4 depleted strain by the introduction of TbMCP17 further confirmed the iron transport function. The poor growth of MRS3/4 depleted strain in yeast has shown to be corrected by expression of vertebrate mitoferrin proteins (Li & Kaplan 2004; Wang et al. 2011; Shaw et al. 2006). Thus, TbMCP17 is very likely to be a mitochondrial iron importer in *T.brucei.*

The expression level of TbMCP17 mRNA is upregulated when heme is added or glucose is removed from the media. Also, the introduction of oxidative stress created by the addition of H_2O_2 resulted in a decrease of TbMCP17 mRNA level. Though no protein-level results are available, the removal of glucose promotes PCF to rely more on mitochondrial energy metabolism, thus increases the mitochondrial membrane proteins

activities, which was also found in TbMCP12. Heme cannot be synthesised inside the trypanosomes (Allen et al. 2008). After transporting host heme into the trypanosomal cytosol by TbHrg protein in PCF (Huynh et al. 2012) or by HpHb receptor in BSF (Vanhollebeke et al. 2008), heme needs to be imported into mitochondria for the formation of cytochrome *c* oxidase (Allen 2011), but the transporter of this remains enigmatic. It's possible that TbMCP17 plays a role in heme import because the addition of heme promotes TbMCP17 expression. As discussed before, H_2O_2 can produce extremely reactive hydroxyl radical (OH·) when it reacts with metal cations (Fe^{2+} or Cu^{+}) via the Fenton reaction. There's a hint that TbMCP17 level is regulated by oxidative stress.

TbSFNX belongs to sideroflexin family. Unlike metazoan that has a group of sideroflexins, only one protein form is found in Kinetoplastea, and it forms a separate clade. This finding is supported by *in silico* analyses of fungal Fsf1, in which Fsf1 proteins form a distinct clade (Miotto et al. 2007). The localisation result found in this study demonstrated that TbSFNX is localised in the mitochondria, same as other sideroflexin family proteins (Hildick-Smith et al. 2013; Miyake et al. 2002). Generation of conventional double knockout resulted in the same problem found in TbMCP12 and TbMCP17, thus an inducible rescue copy was added, resulting in a conditional double knockout cell line. Growth defect was found in both TbSFNX knockout and overexpression cells, implying that the protein level has to be controlled tightly. The growth defect is possibly linked to an increased metabolic flux found in both TbSFNX knockout and overexpression cells, suggesting that the change of TbSFNX level causes perturbation in energy metabolism.

Due to time limit, functional experiments were not performed on TbSFNX. The functions of sideroflexin family proteins have been suggested to be related to iron and tricarboxylates. The first protein found in this family is the SFXN1 from mice, the mutation of which was linked to flexed-tail mouse with sideroblastic anaemia (Fleming et al. 2001). However, it was subsequently reported that the defect in flexed-tail mice was in the transcription-factor-encoding gene *Smad5* rather than *Sfnx1* (Hegde et al. 2007). SFNX1 expression was also found to be reduced in Alzheimer's disease patients (Minjarez et al. 2016). The macrocytic anaemia was caused by *SFXN4* mutation (Hildick-Smith et al. 2013). In lambs, *SFNX1* was presented to link to hair follicle development

(Lv et al. 2016; Sun et al. 2013). In rat brain, SFXN5 (BBG-TCC) was found to exchange citrate *in vitro* (Miyake et al. 2002). A study on Xenopus embryos via whole-mount *in situ* hybridization analysis revealed that the 5 sideroflexin proteins are differently expressed in different tissues, indicating roles SFNXs play developmentally (Li et al. SFXN3 has been suggested to be a novel auto-antigen in the patients with oral squamous cell carcinoma (Murase et al. 2008). Another study on SFXN3 in pancreatic islet suggested its role in the differentiation of pancreatic beta-cells, and its relation to the regeneration of the cells (Yoshikumi et al. 2005). However, no direct evidence has been presented to support the transport function of SFNX as a tricarboxylate carrier or iron-related transporter. Thus, function experiments on TbSFNX are important not only for understanding this gene in Kinetoplastea, but also for providing sideroflexin family proteins in other species with supportive information on functions.

Sequence analysis indicated that TbMCP23 is a potential pyrimidine carrier in the mitochondria of *T.brucei*. Yeast pyrimidine transporter RIM2 has been found to co-transport nucleotides with iron (Yoon et al. 2011; Froschauer et al. 2013). Also, the phylogenetic tree revealed a significant relation between TbMCP17-homologues and nucleotide or nucleotide related transporters, suggesting the link between pyrimidine and iron transporters. No growth defect was observed from the generated TbMCP23 RNAi cells, with a little increase of growth rate instead.

Apart from gene identification and function characterisation, heterologous protein expression and antibody generation were performed on TbMCP17, TbMCP23 and TbSFNX. All three proteins were successfully expressed in *E.coli.* The purification steps were initially optimised in TbMCP17 and further used for TbSFNX and TbMCP23 with minor amends. The antisera of TbMCP17 and TbSFNX were generated and examined with efficiency. Both of the antisera were able to detect overexpressed protein (with and without myc tag) as well as His tag recombinant proteins, but not endogenous proteins. This failure of detecting endogenous proteins suggested that TbMCP17 and TbSFNX are of low abundance.

In this study, the failure of generating double gene knockout of TbMCP12, TbMCP17 and TbSFXN, and the severe growth defects caused by gene depletion suggested critical

roles the proteins play. The proteins are essential for parasite viability, implying that the proteins are potential drug targets. Human cells also depend on the mitochondrial iron and di/tricarboxylate carriers for the transport of metabolites and iron, which in turn affects mitochondrial energy metabolism and iron-related functions such as electron transport chain and iron-sulfur cluster assembly. Thus, the lack of selectivity between human and *T.brucei* TbMCP12, TbMCP17 and TbSFNX will be a potential toxicity issue in downstream drug development. Therefore, further modifications of the drugs should be applied for specific targeting.

To the best of our knowledge, TbMCP12 is the first mitochondrial di/tri-carboxylate carrier characterised in Kinetoplastea and plays a role in oxidative stress defence. From the aspect of iron transport, TbMCP17 is most likely a mitochondrial iron importer. Although not much functional experiments were performed on TbSFNX, sequence analysis confirmed that it is the only sideroflexin family protein in *T. brucei.* Depletion of sideroflexin was previously observed to cause mitochondrial iron accumulation (Hildick-Smith et al. 2013), suggesting that TbSFNX might be an iron exporter. Together with mitochondrial iron importer TbMCP17, TbSFNX helps maintain iron balance in the mitochondria. Besides the link with iron transport, sideroflexin proteins are proved to be a tricarboxylate carrier (Azzi et al. 1993; Miyake et al. 2002) linked to TbMCP12. TbMCP23, the only homologue to yeast pyrimidine carrier RIM2, is likely to co-import iron with nucleotides (Froschauer et al. 2013) especially in the absence of the main iron transporter TbMCP17.

Future functional characterisation experiments on TbMCP17, TbSFNX and TbMCP23 functions are therefore highly recommended. The measurements of iron-related enzyme activities such as FeSODs, aconitase and alternative oxidases, as well as that of iron-sulfur cluster assembly, are suggested to further confirm the physiological role TbMCP17 plays. Also, the link among TbMCP12, TbMCP17, TbMCP23 and TbSFNX is interesting to be investigated. Knockout TbSFNX in TbMCP12 is highly recommended, and the mitochondrial ATP production assay on the resulting strain should be completely abolished with all mitochondrial substrates tested. Similar knockout or knockdown can be performed on TbMCP23 in TbMCP17 mutant strain, and growth phenotype and potential iron transport activity of TbMCP23 can be obtained. The thesis pose a new

direction on the collaborative working system of mitochondrial iron transport in *Trypanosoma brucei*. The findings lay solid foundation for future research and novel drug invention.

References

Abreu, I.A. & Cabelli, D.E., 2010. Superoxide dismutases-a review of the metal-associated mechanistic variations. *Biochimica et biophysica acta*, 1804(2), pp.263–74.

Adl, S.M., Simpson, A.G.B., Farmer, M.A., Andersen, R.A., Anderson, O.R., Barta, J.R., Bowser, S.S., Brugerolle, G., Fensome, R.A., Fredericq, S., James, T.Y., Karpov, S., Kugrens, P., Krug, J., Lane, C.E., Lewis, L.A., Lodge, J., Lynn, D.H., Mann, D.G., McCourt, R.M., Mendoza, L., Moestrup, O., Mozley-Standridge, S.E., Nerad, T.A., Shearer, C.A., Smirnov, A. V, Spiegel, F.W. & Taylor, M.F.J.R., 2005. The new higher level classification of eukaryotes with emphasis on the taxonomy of protists. *The Journal of eukaryotic microbiology*, 52(5), pp.399–451.

Aisen, P., Enns, C. & Wessling-Resnick, M., 2001. Chemistry and biology of eukaryotic iron metabolism. *Int J Biochem Cell Biol*, 33(10), pp.940–959.

Aisen, P. & Listowsky, I., 1980. Iron transport and storage proteins. *Annual review of biochemistry*, 49, pp.357–93.

Allemann, N. & Schneider, 2000. ATP production in isolated mitochondria of procyclic Trypanosoma brucei. *Molecular and biochemical parasitology*, 111(1), pp.87–94.

Allen, J.W.A., 2011. Cytochrome c biogenesis in mitochondria - Systems III and V. *FEBS Journal*, 278(22), pp.4198–4216.

Allen, J.W.A., Ferguson, S.J. & Ginger, M.L., 2008. Distinctive biochemistry in the trypanosome mitochondrial intermembrane space suggests a model for stepwise evolution of the MIA pathway for import of cysteine-rich proteins. *FEBS Letters*, 582(19), pp.2817–2825.

Allmann, S., Morand, P., Ebikeme, C., Gales, L., Biran, M., Hubert, J., Brennand, A., Mazet, M., Franconi, J.-M., Michels, P.A.M., Portais, J.-C., Boshart, M. & Bringaud, F., 2013. Cytosolic NADPH homeostasis in glucose-starved procyclic Trypanosoma brucei relies on malic enzyme and the pentose phosphate pathway fed by gluconeogenic flux. *The Journal of biological chemistry*, 288(25), pp.18494–505.

Aquila, H., Link, T.A. & Klingenberg, M., 1987. Solute carriers involved in energy transfer of mitochondria form a homologous protein family. *FEBS Lett*, 212(1), pp.1–9.

Azzi, A., Glerum, M., Koller, R., Mertens, W. & Spycher, S., 1993. The mitochondrial tricarboxylate carrier. *J Bioenerg Biomembr*, 25(5), pp.515–524.

Babcock, M., De, S. D., Oaks, R., Davis-Kaplan, S., Jiralerspong, S., Montermini, L., Pandolfo, M. & Kaplan, J., 1997. Regulation of mitochondrial iron accumulation by yfh1p, a putative homolog of frataxin. *Science*,276(5319), 1709.

Barrett, M.P., Burchmore, R.J., Stich, A., Lazzari, J.O., Frasch, A.C., Cazzulo, J.J. & Krishna, S., 2003. The trypanosomiases. *Lancet*, 362(9394), pp.1469–1480.

Basu, S., Horáková, E., & Lukeš, J., 2016. Iron-associated biology of trypanosoma brucei. *Biochimica Et Biophysica Acta*, 1860(2), pp.363–370.

Basu, S., Netz, D.J., Haindrich, A.C., Herlerth, N., Lagny, T.J., Pierik, A.J., Lill, R. & Lukeš, J., 2014. Cytosolic iron-sulphur protein assembly is functionally conserved and essential in procyclic and bloodstream *T rypanosoma brucei*. *Molecular Microbiology*, 93(5), pp.897–910.

Becker, T., Böttinger, L. & Pfanner, N., 2012. Mitochondrial protein import: from transport pathways to an integrated network. *Trends in biochemical sciences*, 37(3), pp.85–91.

Bedhomme, M., Hoffmann, M., McCarthy, E.A., Gambonnet, B., Moran, R.G., Rébeillé, F. & Ravanel, S., 2005. Folate metabolism in plants: an Arabidopsis homolog of the mammalian mitochondrial folate transporter mediates folate import into chloroplasts. *The Journal of biological chemistry*, 280(41), pp.34823–31.

Beinert, H., Holm, R.H. & Munck, E., 1997. Iron-sulfur clusters: nature's modular, multipurpose structures. *Science*, 277(5326), pp.653–659.

Bekri, S., Kispal, G., Lange, H., Fitzsimons, E., Tolmie, J., Lill, R. & Bishop, D.F., 2000. Human ABC7 transporter: gene structure and mutation causing X-linked sideroblastic anemia with ataxia with disruption of cytosolic iron-sulfur protein

maturation. *Blood*, 96(9), pp.3256–64.

Bergmeyer, H.U. & Gawehn, K., 1974. *Methods of enzymatic analysis Volume 2*, Verlag Chemie.

Bertani, G., 2004. Lysogeny at mid-twentieth century: P1, P2, and other experimental systems. *Journal of bacteriology*, 186(3), pp.595–600.

Besteiro, S., Barrett, M.P., Rivière, L. & Bringaud, F., 2005. Energy generation in insect stages of Trypanosoma brucei: Metabolism in flux. *Trends in Parasitology*, 21(4), pp.185–191.

Besteiro, S., Biran, M., Biteau, N., Coustou, V., Baltz, T., Canioni, P. & Bringaud, F., 2002. Succinate secreted by Trypanosoma brucei is produced by a novel and unique glycosomal enzyme, NADH-dependent fumarate reductase. *J Biol Chem*, 277(41), pp.38001–38012.

Blattner, J., Helfert, S., Michels, P. & Clayton, C., 1998. Compartmentation of phosphoglycerate kinase in Trypanosoma brucei plays a critical role in parasite energy metabolism. *Proceedings of the National Academy of Sciences of the United States of America*, 95(20), pp.11596–600.

Bochud-Allemann, N. & Schneider, A., 2002. Mitochondrial substrate level phosphorylation is essential for growth of procyclic Trypanosoma brucei. *The Journal of biological chemistry*, 277(36), pp.32849–54.

Bojunga, N., Kötter, P. & Entian, K.D., 1998. The succinate/fumarate transporter Acr1p of Saccharomyces cerevisiae is part of the gluconeogenic pathway and its expression is regulated by Cat8p. *Molecular & general genetics: MGG*, 260(5), pp.453–61.

Bonofiglio, D., Santoro, A., Martello, E., Vizza, D., Rovito, D., Cappello, A.R., Barone, I., Giordano, C., Panza, S., Catalano, S., Iacobazzi, V., Dolce, V. & Andò, S., 2013. Mechanisms of divergent effects of activated peroxisome proliferator-activated receptor-γ on mitochondrial citrate carrier expression in 3T3-L1 fibroblasts and mature adipocytes. *Biochimica et Biophysica Acta (BBA) - Molecular and Cell Biology of Lipids*, 1831(6), pp.1027–1036.

Boothroyd, J.C., Paynter, C.A., Coleman, S.L. & Cross, G.A., 1982. Complete nucleotide sequence of complementary DNA coding for a variant surface glycoprotein from Trypanosoma brucei. *J Mol Biol*, 157(3), pp.547–56.

Bouvier, F., Linka, N., Isner, J.-C., Mutterer, J., Weber, A.P.M. & Camara, B., 2006. Arabidopsis SAMT1 defines a plastid transporter regulating plastid biogenesis and plant development. *The Plant cell*, 18(11), pp.3088–105.

Brachmann, C.B., Davies, A., Cost, G.J., Caputo, E., Li, J., Hieter, P., Boeke, J.D., 1998. Designer deletion strains derived from Saccharomyces cerevisiae S288C: a useful set of strains and plasmids for PCR-mediated gene disruption and other applications. *Yeast*. Jan;14(2) 115-132.

Breidbach, T., Scory, S., Krauth-Siegel, R.L.L. & Steverding, D., 2002. Growth inhibition of bloodstream forms of Trypanosoma brucei by the iron chelator deferoxamine. *International Journal for Parasitology*, 32(4), pp.473–479.

Bresgen, N. & Eckl, P.M., 2015. Oxidative stress and the homeodynamics of iron metabolism. *Biomolecules*, 5(2), pp.808–47.

Bringaud, F., Biran, M., Millerioux, Y., Wargnies, M., Allmann, S. & Mazet, M., 2015. Combining reverse genetics and nuclear magnetic resonance-based metabolomics unravels trypanosome-specific metabolic pathways. *Molecular microbiology*, 96(5), pp.917–26.

Bringaud, F., Robinson, D.R., Barradeau, S., Biteau, N., Baltz, D. & Baltz, T., 2000. Characterization and disruption of a new Trypanosoma brucei repetitive flagellum protein, using double-stranded RNA inhibition. *Molecular and biochemical parasitology*, 111(2), pp.283–97.

Brun, R., Blum, J., Chappuis, F. & Burri, C., 2010. Human African trypanosomiasis. *Lancet*, 375(9709), pp.148–159.

Bryla, J. & Frackowiak, B., 1968. Integration of mitochondrial respiration and cytoplasmic glycolysis. *Postepy biochemii*, 14(2), pp.167–84.

Cappello, A.R., Guido, C., Santoro, A., Santoro, M., Capobianco, L., Montanaro, D.,

Madeo, M., Andò, S., Dolce, V. & Aquila, S., 2012. The Mitochondrial Citrate Carrier (CIC) Is Present and Regulates Insulin Secretion by Human Male Gamete. *Endocrinology*, 153(4), pp.1743–1754.

Capobianco, L., Iacopetta, D., Carrisi, C., Madeo, M., Cappello, A.R. & Dolce, V., 2011. An effective strategy for cloning the mitochondrial citrate carrier: identification, characterization and tissue distribution in silver eel. *Advances in Bioscience and Biotechnology*, 2, pp.157–162.

Cappello, A.R., Miniero, D. V., Curcio, R., Ludovico, A., Daddabbo, L., Stipani, I., Robinson, A.J., Kunji, E.R.S.S. & Palmieri, F., 2007. Functional and structural role of amino acid residues in the odd-numbered transmembrane alpha-helices of the bovine mitochondrial oxoglutarate carrier. *Journal of molecular biology*, 369(2), pp.400–12.

Castegna, A., Scarcia, P., Agrimi, G., Palmieri, L., Rottensteiner, H., Spera, I., Germinario, L. & Palmieri, F., 2010. Identification and functional characterization of a novel mitochondrial carrier for citrate and oxoglutarate in Saccharomyces cerevisiae. *The Journal of biological chemistry*, 285(23), pp.17359–70.

Catalina-Rodriguez, O., Kolukula, V.K., Tomita, Y., Preet, A., Palmieri, F., Wellstein, A., Byers, S., Giaccia, A.J., Glasgow, E., Albanese, C. & Avantaggiati, M.L., 2012. The mitochondrial citrate transporter, CIC, is essential for mitochondrial homeostasis. *Oncotarget*, 3(10), pp.1220–1235.

Chi, T.B., Brown B, S. V & Williams, N., 1998. Subunit 9 of the mitochondrial ATP synthase of Trypanosoma brucei is nuclearly encoded and developmentally regulated. *Molecular and biochemical parasitology*, 92(1), pp.29–38.

Chisi, J.E., Misiri, H., Zverev, Y., Nkhoma, A. & Sternberg, J.M., 2004. Anaemia in human African trypanosomiasis caused by Trypanosoma brucei rhodesiense. *East African medical journal*, 81(10), pp.505–8.

Clarkson, A.B., Bienen, E.J., Pollakis, G. & Grady, R.W., 1989. Respiration of bloodstream forms of the parasite Trypanosoma brucei brucei is dependent on a plant-like alternative oxidase. *The Journal of biological chemistry*, 264(30),

pp.17770–6.

Clayton, C.E., 2002. Life without transcriptional control? From fly to man and back again. *The EMBO Journal*, 21(8), pp.1881–1888.

Clayton, C.E. & Michels, P., 1996. Metabolic compartmentation in African trypanosomes. *Parasitology today (Personal ed.)*, 12(12), pp.465–71.

Colasante, C., Alibu, V.P., Kirchberger, S., Tjaden, J., Clayton, C. & Voncken, F., 2006. Characterization and developmentally regulated localization of the mitochondrial carrier protein homologue MCP6 from Trypanosoma brucei. *Eukaryotic Cell*, 5(8), pp.1194–1205.

Colasante, C., Peña Diaz, P., Clayton, C. & Voncken, F., 2009. Mitochondrial carrier family inventory of Trypanosoma brucei brucei: Identification, expression and subcellular localisation. *Molecular and Biochemical Parasitology*, 167(2), pp.104–117.

Colasante, C., Zheng, F., & Voncken, F. Identification and functional characterisation of potential mitchondrial di-/tri-carboxylate carriers from the human pathegon *Trypanosoma brucei.* Unpublished data.

Cotruvo, J.A. & Stubbe, J., 2011. Class I ribonucleotide reductases: metallocofactor assembly and repair in vitro and in vivo. *Annual review of biochemistry*, 80, pp.733–67.

Coustou, V., Besteiro, S., Biran, M., Diolez, P., Bouchaud, V., Voisin, P., Michels, P.A., Canioni, P., Baltz, T. & Bringaud, F., 2003. ATP generation in the Trypanosoma brucei procyclic form: cytosolic substrate level is essential, but not oxidative phosphorylation. *J Biol Chem*, 278(49), pp.49625–49635.

Coustou, V., Besteiro, S., Riviere, L., Biran, M., Biteau, N., Franconi, J.M., Boshart, M., Baltz, T. & Bringaud, F., 2005. A mitochondrial NADH-dependent fumarate reductase involved in the production of succinate excreted by procyclic Trypanosoma brucei. *J Biol Chem*, 280(17), pp.16559–16570.

Csere, P., Lill, R., & Kispal, G. (1998). Identification of a human mitochondrial abc

transporter, the functional orthologue of yeast atm1p. *Febs Letters*,441(2), 266–270.

Czichos, J., Nonnengaesser, C. & Overath, P., 1986. Trypanosoma brucei: cis-aconitate and temperature reduction as triggers of synchronous transformation of bloodstream to procyclic trypomastigotes in vitro. *Exp Parasitol*, 62(2), pp.283–291.

Da-Rè, C., Franzolin, E., Biscontin, A., Piazzesi, A., Pacchioni, B., Gagliani, M.C., Mazzotta, G., Tacchetti, C., Zordan, M. a., Zeviani, M., Bernardi, P., Bianchi, V., De Pittà, C. & Costa, R., 2014. Functional characterization of drim2, the Drosophila melanogaster homolog of the yeast mitochondrial deoxynucleotide transporter. *Journal of Biological Chemistry*, 289(11), pp.7448–7459.

Daniel Gietz, R. & Woods, R., 2002. Guide to Yeast Genetics and Molecular and Cell Biology - Part B. *Methods in Enzymology*, 350(2001), pp.87–96.

Das, A., Li, H., Liu, T. & Bellofatto, V., 2006. Biochemical characterization of *Trypanosoma brucei* RNA polymerase II. *Molecular and biochemical parasitology*, 150(2), pp.201–10.

Das, K., Lewis, R.Y., Combatsiaris, T.P., Lin, Y., Shapiro, L., Charron, M.J. & Scherer, P.E., 1999. Predominant expression of the mitochondrial dicarboxylate carrier in white adipose tissue. *The Biochemical journal*, 344 Pt 2, pp.313–20.

Dolce, V., Messina, A., Cambria, A. & Palmieri, F., 1994. Cloning and sequencing of the rat cDNA encoding the mitochondrial 2-oxoglutarate carrier protein. *DNA sequence: the journal of DNA sequencing and mapping*, 5(2), pp.103–9.

Dolce, V., Rita Cappello, A. & Capobianco, L., 2014. Mitochondrial tricarboxylate and dicarboxylate-tricarboxylate carriers: from animals to plants. *IUBMB life*, 66(7), pp.462–71.

Dormeyer, M., Schöneck, R., Dittmar, G.A. & Krauth-Siegel, R.L., 1997. Cloning, sequencing and expression of ribonucleotide reductase R2 from Trypanosoma brucei. *FEBS letters*, 414(2), pp.449–53.

Dreesen, O., Li, B. & Cross, G.A.M., 2005. Telomere structure and shortening in telomerase-deficient Trypanosoma brucei. *Nucleic acids research*, 33(14), pp.4536–

43.

Dufernez, F., Yernaux, C., Gerbod, D., Noël, C., Chauvenet, M., Wintjens, R., Edgcomb, V.P., Capron, M., Opperdoes, F.R. & Viscogliosi, E., 2006. The presence of four iron-containing superoxide dismutase isozymes in trypanosomatidae: characterization, subcellular localization, and phylogenetic origin in Trypanosoma brucei. *Free radical biology & medicine*, 40(2), pp.210–25.

Dupuy, J., Volbeda, A., Carpentier, P., Darnault, C., Moulis, J.-M. & Fontecilla-Camps, J.C., 2006. Crystal structure of human iron regulatory protein 1 as cytosolic aconitase. *Structure (London, England: 1993)*, 14(1), pp.129–39.

Van Dyck, E., Jank, B., Ragnini, A., Schweyen, R.J., Duyckaerts, C., Sluse, F. & Foury, F., 1995. Overexpression of a novel member of the mitochondrial carrier family rescues defects in both DNA and RNA metabolism in yeast mitochondria. *MGG Molecular & General Genetics*, 246(4), pp.426–436.

Efron, B., Halloran, E. & Holmes, S., 1996. Bootstrap confidence levels for phylogenetic trees. *Proceedings of the National Academy of Sciences of the United States of America*, 93(14), pp.7085–90.

Evans, D.A. & Brown, R.C., 1972. The utilization of glucose and proline by culture forms of Trypanosoma brucei. *J Protozool*, 19(4), pp.686–690.

Fairlamb, A.H. & Bowman, I.B., 1977. Trypanosoma brucei: suramin and other trypanocidal compounds' effects on sn-glycerol-3-phosphate oxidase. *Experimental parasitology*, 43(2), pp.353–61.

Fast, B., Kremp, K., Boshart, M. & Steverding, D., 1999. Iron-dependent regulation of transferrin receptor expression in Trypanosoma brucei. *The Biochemical journal*, 342 Pt 3, pp.691–696.

Favre, C., Zhdanov, A., Leahy, M., Papkovsky, D. & O'Connor, R., 2010. Mitochondrial pyrimidine nucleotide carrier (PNC1) regulates mitochondrial biogenesis and the invasive phenotype of cancer cells. *Oncogene*, 29(27), pp.3964–76.

Felice, M.R., De Domenico, I., Li, L., Ward, D.M., Bartok, B., Musci, G. & Kaplan, J.,

2005. Post-transcriptional regulation of the yeast high affinity iron transport system. *J Biol Chem*, 280(23), pp.22181–22190.

Felsenstein, J., 1985. Confidence Limits on Phylogenies: An Approach Using the Bootstrap on JSTOR. *Evolution*, 39(4), pp.783–791.

Fenton, H. J. H., 1894. Lxxiii.—oxidation of tartaric acid in presence of iron. *J.chem.soc.trans*, 65, 899-910.

Fernández-Moya, S.M. & Estévez, A.M. 2010. Posttranscriptional control and the role of RNA-binding proteins in gene regulation in trypanosomatid protozoan parasites. *Wiley interdisciplinary reviews. RNA*, 1(1), pp.34–46.

Fernandez, E., Fernandez, M. & Rodicio, R., 1993. Two structural genes are encoding malate synthase isoenzymes in Saccharomyces cerevisiae. *FEBS letters*, 320(3), pp.271–5.

Ferro, M., Salvi, D., Riviere-Rolland, H., Vermat, T., Seigneurin-Berny, D., Grunwald, D., Garin, J., Joyard, J. & Rolland, N., 2002. Integral membrane proteins of the chloroplast envelope: identification and subcellular localization of new transporters. *Proceedings of the National Academy of Sciences of the United States of America*, 99(17), pp.11487–92.

Fiermonte, G., Palmieri, L., Dolce, V., Lasorsa, F.M., Palmieri, F., Runswick, M.J. & Walker, J.E., 1998. The sequence, bacterial expression, and functional reconstitution of the rat mitochondrial dicarboxylate transporter cloned via distant homologs in yeast and Caenorhabditis elegans. *The Journal of biological chemistry*, 273(38), pp.24754–9.

Fiermonte, G., Walker, J.E. & Palmieri, F., 1993. Abundant bacterial expression and reconstitution of an intrinsic membrane-transport protein from bovine mitochondria. *The Biochemical journal*, pp.293–9.

Fleming, M.D., Campagna, D.R., Haslett, J.N., Trenor, C.C., Andrews, N.C., Trenor 3rd, C.C. & Andrews, N.C., 2001. A mutation in a mitochondrial transmembrane protein is responsible for the pleiotropic hematological and skeletal phenotype of flexed-tail (f/f) mice. *Genes and Development*, 15(6), pp.652–657.

Foury, F., & Cazzalini, O., 1997. Deletion of the yeast homologue of the human gene associated with friedreich's ataxia elicits iron accumulation in mitochondria. *Febs Letters*, 411(2-3), 373.

Foury, F. & Roganti, T., 2002. Deletion of the mitochondrial carrier genes MRS3 and MRS4 suppresses mitochondrial iron accumulation in a yeast frataxin-deficient strain. *J Biol Chem*, 277(27), pp.24475–24483.

Froschauer, E.M., Rietzschel, N., Hassler, M.R., Binder, M., Schweyen, R.J., Lill, R., Mühlenhoff, U. & Wiesenberger, G., 2013. The mitochondrial carrier Rim2 co-imports pyrimidine nucleotides and iron. *The Biochemical journal*, 455(1), pp.57–65.

Froschauer, E.M., Schweyen, R.J. & Wiesenberger, G., 2009. The yeast mitochondrial carrier proteins Mrs3p/Mrs4p mediate iron transport across the inner mitochondrial membrane. *Biochimica et biophysica acta*, 1788(5), pp.1044–50.

Gálvez, Lancien & Hodges, 1999. Are isocitrate dehydrogenases and 2-oxoglutarate involved in the regulation of glutamate synthesis? *Trends in plant science*, 4(12), pp.484–490.

de Gaudenzi, J.G., Noé, G., Campo, V.A., Frasch, A.C. & Cassola, A., 2011. Gene expression regulation in trypanosomatids. *Essays in biochemistry*, 51, pp.31–46.

Gehrig, S. & Efferth, T., 2008. Development of drug resistance in Trypanosoma brucei rhodesiense and Trypanosoma brucei gambiense. Treatment of human African trypanosomiasis with natural products (Review). *Int J Mol Med*, 22(4), pp.411–419.

GeneDB. Available at: http://www.genedb.org/Homepage [Accessed November 3, 2015].

Girard, M., Giraud, S., Courtioux, B., Jauberteau-Marchan, M.-O. & Bouteille, B., 2005. Endothelial cell activation in the presence of African trypanosomes. *Molecular and biochemical parasitology*, 139(1), pp.41–9.

Grab, D.J., Shaw, M.K., Wells, C.W., Verjee, Y., Russo, D.C., Webster, P., Naessens, J. & Fish, W.R., 1993. The transferrin receptor in African trypanosomes: identification, partial characterization and subcellular localization. *European journal of cell*

biology, 62(1), pp.114–26.

Grab, D.J., Wells, C.W., Shaw, M.K., Webster, P. & Russo, D.C., 1992. Endocytosed transferrin in African trypanosomes is delivered to lysosomes and may not be recycled. *European journal of cell biology*, 59(2), pp.398–404.

Gull, K., 2003. Host-parasite interactions and trypanosome morphogenesis: a flagellar pocketful of goodies. *Curr Opin Microbiol*, 6(4), pp.365–370.

Haile, S. & Papadopoulou, B., 2007. Developmental regulation of gene expression in trypanosomatid parasitic protozoa. *Current opinion in microbiology*, 10(6), pp.569–77.

Hall, J.P., Wang, H. & Barry, J.D., 2013. Mosaic VSGs and the scale of Trypanosoma brucei antigenic variation. *PLoS Pathog*, 9(7), p.e1003502.

Hannaert, V., 2010. Sleeping sickness pathogen (Trypanosoma brucei) and natural products: therapeutic targets and screening systems. *Planta Med*, 77(6), pp.586–597.

Hannaert, V. & Michels, P.A., 1994. Structure, function, and biogenesis of glycosomes in kinetoplastida. *J Bioenerg Biomembr*, 26(2), pp.205–212.

Hannaert, V., Saavedra, E., Duffieux, F., Szikora, J.-P., Rigden, D.J., Michels, P.A.M. & Opperdoes, F.R., 2003. Plant-like traits associated with metabolism of Trypanosoma parasites. *Proceedings of the National Academy of Sciences of the United States of America*, 100(3), pp.1067–71.

Hegde, S., Lenox, L. E., Lariviere, A., Porayette, P., Perry, J. M., & Yon, M., et al., 2007. An intronic sequence mutated in flexed-tail, mice regulates splicing of smad5. Mammalian Genome, 18(12), 852-860.

Helfert, S., Estévez, A.M., Bakker, B., Michels, P. & Clayton, C., 2001. Roles of triosephosphate isomerase and aerobic metabolism in Trypanosoma brucei. *The Biochemical journal*, 357(Pt 1), pp.117–25.

Hell, K., 2008. The erv1-mia40 disulfide relay system in the intermembrane space of mitochondria. *Biochimica Et Biophysica Acta Molecular Cell Research*, 1783(4), 601-609.

van Hellemond, J.J., Opperdoes, F.R. & Tielens, A.G., 1998. Trypanosomatidae produce acetate via a mitochondrial acetate:succinate CoA transferase. *Proc Natl Acad Sci U S A*, 95(6), pp.3036–3041.

van Hellemond, J.J., Opperdoes, F.R. & Tielens, a G.M., 2005. The extraordinary mitochondrion and unusual citric acid cycle in Trypanosoma brucei. *Biochemical Society transactions*, 33(Pt 5), pp.967–971.

Henderson, P. J., & Lardy, H. A., 1970. Bongkrekic acid. an inhibitor of the adenine nucleotide translocase of mitochondria. Journal of Biological Chemistry, 245(6), 1319-1326.

Henson, C.P. & Cleland, W.W., 1967. Purification and kinetic studies of beef liver cytoplasmic aconitase. *The Journal of biological chemistry*, 242(17), pp.3833–8.

Hildick-Smith, G.J., Cooney, J.D., Garone, C., Kremer, L.S., Haack, T.B., Thon, J.N., Miyata, N., Lieber, D.S., Calvo, S.E., Akman, H.O., Yien, Y.Y., Huston, N.C., Branco, D.S., Shah, D.I., Freedman, M.L., Koehler, C.M., Italiano, J.E., Merkenschlager, A., Beblo, S., Strom, T.M., Meitinger, T., Freisinger, P., Donati, M.A., Prokisch, H., Mootha, V.K., DiMauro, S., Paw, B.H. & Paw, B.H., 2013. Macrocytic anemia and mitochondriopathy resulting from a defect in sideroflexin 4. *American journal of human genetics*, 93(5), pp.906–14.

Hildyard, J.C.W. & Halestrap, A.P., 2003. Identification of the mitochondrial pyruvate carrier in Saccharomyces cerevisiae. *The Biochemical journal*, 374(Pt 3), pp.607–11.

Hofer, A., Schmidt, P.P., Gräslund, A. & Thelander, L., 1997. Cloning and characterization of the R1 and R2 subunits of ribonucleotide reductase from Trypanosoma brucei. *Proceedings of the National Academy of Sciences of the United States of America*, 94(13), pp.6959–64.

Horvath, A., Horakova, E., Dunajcikova, P., Verner, Z., Pravdova, E., Slapetova, I., Cuninkova, L. & Lukes, J., 2005. Downregulation of the nuclear-encoded subunits of the complexes III and IV disrupts their respective complexes but not complex I in procyclic Trypanosoma brucei. *Mol Microbiol*, 58(1), pp.116–130.

Huizing, M., Ruitenbeek, W., van den Heuvel, L.P., Dolce, V., Iacobazzi, V., Smeitink, J.A., Palmieri, F. & Trijbels, J.M., 1998. Human mitochondrial transmembrane metabolite carriers: tissue distribution and its implication for mitochondrial disorders. *Journal of bioenergetics and biomembranes*, 30(3), pp.277–84.

Huynh, C., Yuan, X., Miguel, D.C., Renberg, R.L., Protchenko, O., Philpott, C.C., Hamza, I. & Andrews, N.W., 2012. Heme uptake by Leishmania amazonensis is mediated by the transmembrane protein LHR1. *PLoS pathogens*, 8(7), p.e1002795.

Infantino, V., Convertini, P., Cucci, L., Panaro, M.A., Di Noia, M.A., Calvello, R., Palmieri, F. & Iacobazzi, V., 2011. The mitochondrial citrate carrier: a new player in inflammation. *Biochemical Journal*, 438(3), pp.433–436.

Joseph, J.W., Jensen, M. V., Ilkayeva, O., Palmieri, F., Alarcon, C., Rhodes, C.J. & Newgard, C.B., 2006. The Mitochondrial Citrate/Isocitrate Carrier Plays a Regulatory Role in Glucose-stimulated Insulin Secretion. *Journal of Biological Chemistry*, 281(47), pp.35624–35632.

Kabiri, M. & Steverding, D., 2001. Identification of a developmentally regulated iron superoxide dismutase of Trypanosoma brucei. *The Biochemical journal*, 360(Pt 1), pp.173–7.

Kajimoto, K., Terada, H., Baba, Y. & Shinohara, Y., 2005. Essential role of citrate export from mitochondria at early differentiation stage of 3T3-L1 cells for their effective differentiation into fat cells, as revealed by studies using specific inhibitors of mitochondrial di- and tricarboxylate carriers. *Molecular genetics and metabolism*, 85(1), pp.46–53.

Kanellis, A.K. & Roubelakis - Angelakis, K.A., 1993. Grape. In *Biochemistry of Fruit Ripening*. Dordrecht: Springer Netherlands, pp. 189–234.

Kaplan, R.S., Mayor, J.A., Gremse, D.A. & Wood, D.O., 1995. High level expression and characterization of the mitochondrial citrate transport protein from the yeast Saccharomyces cerevisiae. *The Journal of biological chemistry*, 270(8), pp.4108–14.

Kennedy, P.G., 2006. Human African trypanosomiasis: in and out of Africa. *Neurology*, 66(7), pp.962–963.

Kispal, G., Csere, P., Guiard, B., & Lill, R., 1997. The abc transporter atm1p is required for mitochondrial iron homeostasis. *Febs Letters*, 418(3), 346–350.

Knight, S.A., Sepuri, N.B., Pain, D. & Dancis, A., 1998. Mt-Hsp70 homolog, Ssc2p, required for maturation of yeast frataxin and mitochondrial iron homeostasis. *The Journal of biological chemistry*, 273(29), pp.18389–93.

Kolukula, V.K., Sahu, G., Wellstein, A., Rodriguez, O.C., Preet, A., Iacobazzi, V., D'Orazi, G., Albanese, C., Palmieri, F. & Avantaggiati, M.L., 2014. SLC25A1, or CIC, is a novel transcriptional target of mutant p53 and a negative tumor prognostic marker. *Oncotarget*, 5(5), pp.1212–1225.

Kramer, S., Marnef, A., Standart, N. & Carrington, M., 2012. Inhibition of mRNA maturation in trypanosomes causes the formation of novel foci at the nuclear periphery containing cytoplasmic regulators of mRNA fate. *Journal of cell science*, 125(Pt 12), pp.2896–909.

Krieger, S., Schwarz, W., Ariyanayagam, M.R., Fairlamb, A.H., Krauth-Siegel, R.L. & Clayton, C., 2000. Trypanosomes lacking trypanothione reductase are avirulent and show increased sensitivity to oxidative stress. *Molecular microbiology*, 35(3), pp.542–52.

Kuhajda, F.P., 2000. Fatty-acid synthase and human cancer: new perspectives on its role in tumor biology. *Nutrition (Burbank, Los Angeles County, Calif.)*, 16(3), pp.202–8.

Kuhajda, F.P., 2006. Fatty acid synthase and cancer: new application of an old pathway. *Cancer research*, 66(12), pp.5977–80.

Kuhn, J., Tengler, U. & Binder, S., 2001. Transcript lifetime is balanced between stabilizing stem-loop structures and degradation-promoting polyadenylation in plant mitochondria. *Molecular and cellular biology*, 21(3), pp.731–42.

Kumar, S., Stecher, G. & Tamura, K., 2016. MEGA7: Molecular Evolutionary Genetics Analysis Version 7.0 for Bigger Datasets. *Molecular biology and evolution*, 33(7), pp.1870–4.

Kunji, E.R.S. & Robinson, A.J., 2006. The conserved substrate binding site of

mitochondrial carriers. *Biochimica et Biophysica Acta - Bioenergetics*, 1757(9–10), pp.1237–1248.

Laemmli, 1970. Cleavage of Structural Proteins during the Assembly of the Head of Bacteriophage T4. *Nature*, 227(5259), pp.680–685.

Lamour, N., Riviere, L., Coustou, V., Coombs, G.H., Barrett, M.P. & Bringaud, F., 2005. Proline metabolism in procyclic Trypanosoma brucei is down-regulated in the presence of glucose. *J Biol Chem*, 280(12), pp.11902–11910.

Lange, H., Kispal, G. & Lill, R., 1999. Mechanism of iron transport to the site of heme synthesis inside yeast mitochondria. *Journal of Biological Chemistry*, 274(27), pp.18989–18996.

LaNoue, K.F. & Schoolwerth, A.C., 1979. Metabolite transport in mitochondria. *Annual review of biochemistry*, 48, pp.871–922.

Leroux, A. E., Maugeri, D. A., Cazzulo, J. J., & Nowicki, C. (2011). Functional characterization of nadp-dependent isocitrate dehydrogenase isozymes from trypanosoma cruzi. *Molecular & Biochemical Parasitology*, 177(1), 61-64.

Le Trant, N., Meshnick, S.R., Kitchener, K., Eaton, J.W. & Cerami, A., 1983. Iron-containing superoxide dismutase from Crithidia fasciculata. Purification, characterization, and similarity to Leishmanial and trypanosomal enzymes. *The Journal of biological chemistry*, 258(1), pp.125–30.

Li, F.Y., Leibiger, B., Leibiger, I. & Larsson, C., 2002. Characterization of a putative murine mitochondrial transporter homology of hMRS3/4. *Mamm Genome*, 13(1), pp.20–23.

Li, L. & Kaplan, J., 2004. A Mitochondrial-Vacuolar Signaling Pathway in Yeast That Affects Iron and Copper Metabolism. *Journal of Biological Chemistry*, 279(32), pp.33653–33661.

Li, W., Cowley, A., Uludag, M., Gur, T., McWilliam, H., Squizzato, S., Park, Y.M., Buso, N. & Lopez, R., 2015. The EMBL-EBI bioinformatics web and programmatic tools framework. *Nucleic acids research*, 43(W1), pp.W580-4.

Li, X., Han, D., Kam, R.K.T., Guo, X., Chen, M., Yang, Y., Zhao, H. & Chen, Y., 2010. Developmental expression of sideroflexin family genes in Xenopus embryos. *Developmental Dynamics*, 239(10), pp.2742–2747.

Liang, X., Haritan, A., Uliel, S. & Michaeli, S., 2003. trans and cis splicing in trypanosomatids: mechanism, factors, and regulation. *Eukaryotic cell*, 2(5), pp.830–40.

Lin, H., Li, L., Jia, X., Ward, D.M. & Kaplan, J., 2011. Genetic and biochemical analysis of high iron toxicity in yeast: Iron toxicity is due to the accumulation of cytosolic iron and occurs under both aerobic and anaerobic conditions. *Journal of Biological Chemistry*, 286(5), pp.3851–3862.

Linden, M., Gellerfors, P. & Nelson, B.D., 1982. Pore protein and the hexokinase-binding protein from the outer membrane of rat liver mitochondria are identical. *FEBS Lett*, 141(2), pp.189–192.

Liniger, M., Urwyler, S., Studer, E., Oberle, M., Renggli, C.K. & Roditi, I., 2004. Role of the N-terminal domains of EP and GPEET procyclins in membrane targeting and the establishment of midgut infections by Trypanosoma brucei. *Molecular and biochemical parasitology*, 137(2), pp.247–51.

Lockhart, P.J., Holtom, B., Lincoln, S., Hussey, J., Zimprich, A., Gasser, T., Wszolek, Z.K., Hardy, J. & Farrer, M.J., 2002. The human sideroflexin 5 (SFXN5) gene: sequence, expression analysis and exclusion as a candidate for PARK3. *Gene*, 285(1–2), pp.229–237.

Long, S., Changmai, P., Tsaousis, A.D., Skalický, T., Verner, Z., Wen, Y.-Z.Z., Roger, A.J. & Lukeš, J., 2011. Stage-specific requirement for Isa1 and Isa2 proteins in the mitochondrion of Trypanosoma brucei and heterologous rescue by human and Blastocystis orthologues. *Molecular microbiology*, 81(6), pp.1403–18.

Long, S., Jirků, M., Mach, J., Ginger, M.L., Sutak, R., Richardson, D.R., Tachezy, J. & Lukeš, J., 2008. Ancestral roles of eukaryotic frataxin: Mitochondrial frataxin function and heterologous expression of hydrogenosomal Trichomonas homologues in trypanosomes. *Molecular Microbiology*, 69(1), pp.94–109.

Lu, W., Wei, G., Pan, W. & Tabel, H., 2011. Trypanosoma congolense Infections: Induced Nitric Oxide Inhibits Parasite Growth In Vivo. *Journal of parasitology research*, 2011, p.316067.

Lundkvist, G.B., Kristensson, K. & Bentivoglio, M., 2004. Why trypanosomes cause sleeping sickness. *Physiology (Bethesda, Md.)*, 19, pp.198–206.

Lv, X.Y., Ni, R., Sun, W., Su, R., Musa, H.H., Yin, J.F., Wang, Q.Z., Gao, W. & Chen, L., 2016. Candidate genes for the development of hair follicles in Hu sheep. *Genetics and Molecular Research*, 15(3).

de Macêdo, J. P. D., Burkard, G. S., Niemann, M., Barrett, M. P., Vial, H., & Mäser, P., et al., 2015. An atypical mitochondrial carrier that mediates drug action in trypanosoma brucei. *Plos Pathogens*, 11(5), e1004875.

Madeo, M., Carrisi, C., Iacopetta, D., Capobianco, L., Cappello, A.R., Bucci, C., Palmieri, F., Mazzeo, G., Montalto, A. & Dolce, V., 2009. Abundant expression and purification of biologically active mitochondrial citrate carrier in baculovirus-infected insect cells. *Journal of Bioenergetics and Biomembranes*, 41(3), pp.289–297.

Makiuchi, T., Annoura, T., Hashimoto, M., Hashimoto, T., Aoki, T. & Nara, T., 2011. Compartmentalization of a Glycolytic Enzyme in Diplonema, a Non-kinetoplastid Euglenozoan. *Protist*, 162(3), pp.482–489.

Man, W.C., Miyazaki, M., Chu, K. & Ntambi, J.M., 2006. Membrane topology of mouse stearoyl-CoA desaturase 1. *The Journal of biological chemistry*, 281(2), pp.1251–60.

Manta,B., Fleitas, L., & Comini, M., 2012. Iron Metabolism in Pathogenic Trypanosomes. *Iron Metabolism,*2012. InTechOpen

Marobbio, C.M.T., Di Noia, M.A. & Palmieri, F., 2006. Identification of a mitochondrial transporter for pyrimidine nucleotides in Saccharomyces cerevisiae: bacterial expression, reconstitution and functional characterization. *The Biochemical journal*, 393(Pt 2), pp.441–446.

Martin, K.L. & Smith, T.K., 2006. The glycosylphosphatidylinositol (GPI) biosynthetic pathway of bloodstream-form Trypanosoma brucei is dependent on the de novo synthesis of inositol. *Mol Microbiol*, 61(1), pp.89–105.

Martínez-Calvillo, S., Yan, S., Nguyen, D., Fox, M., Stuart, K. & Myler, P.J., 2003. Transcription of Leishmania major Friedlin chromosome 1 initiates in both directions within a single region. *Molecular cell*, 11(5), pp.1291–9.

Maser, P., Luscher, A. & Kaminsky, R., 2003. Drug transport and drug resistance in African trypanosomes. *Drug Resist Updat*, 6(5), pp.281–290.

Matovu, E., Stewart, M.L., Geiser, F., Brun, R., Maser, P., Wallace, L.J., Burchmore, R.J., Enyaru, J.C., Barrett, M.P., Kaminsky, R., Seebeck, T. & de Koning, H.P., 2003. Mechanisms of arsenical and diamidine uptake and resistance in Trypanosoma brucei. *Eukaryot Cell*, 2(5), pp.1003–1008.

Matthews, K.R., Ellis, J.R. & Paterou, A., 2004. Molecular regulation of the life cycle of African trypanosomes. *Trends Parasitol*, 20(1), pp.40–47.

Merschjohann, K. & Steverding, D., 2006. In vitro growth inhibition of bloodstream forms of Trypanosoma brucei and Trypanosoma congolense by iron chelators. *Kinetoplastid biology and disease*, 5, p.3.

Metzendorf, C., Lind, M.I., Andrews, N., Dunn, L., Rahmanto, Y., Tricoire, H., et al., 2010. Drosophila mitoferrin is essential for male fertility: evidence for a role of mitochondrial iron metabolism during spermatogenesis. *BMC Developmental Biology*, 10(1), p.68.

Michels, P.A., Hannaert, V. & Bringaud, F., 2000. Metabolic aspects of glycosomes in trypanosomatidae - new data and views. *Parasitol Today*, 16(11), pp.482–489.

Millar, A.H. & Heazlewood, J.L., 2003. Genomic and proteomic analysis of mitochondrial carrier proteins in Arabidopsis. *Plant physiology*, 131(2), pp.443–53.

Minjarez, B., Calderón-González, K.G., Rustarazo, M.L.V., Herrera-Aguirre, M.E., Labra-Barrios, M.L., Rincon-Limas, D.E., del Pino, M.M.S., Mena, R. & Luna-Arias, J.P., 2016. Identification of proteins that are differentially expressed in brains

with Alzheimer's disease using iTRAQ labeling and tandem mass spectrometry. *Journal of Proteomics*, 139, pp.103–121.

Miotto, G., Tessaro, S., Rotta, G.A. & Bonatto, D., 2007. In silico analyses of Fsf1 sequences, a new group of fungal proteins orthologous to the metazoan sideroblastic anemia-related sideroflexin family. *Fungal Genetics and Biology*, 44(8), pp.740–753.

Mittra, B., Cortez, M., Haydock, A., Ramasamy, G., Myler, P. J., Andrews, N. W., 2013. Iron uptake controls the generation of Leishmania infective forms through regulation of ROS levels. The Journal of Experimental Medicine, 210(2), 401–416.

Mittra, B., Laranjeira-Silva, M.F., Perrone Bezerra de Menezes, J., Jensen, J., Michailowsky, V., Belkaid, Y., 2016. A Trypanosomatid Iron Transporter that Regulates Mitochondrial Function Is Required for Leishmania amazonensis Virulence. D. Horn, ed. *PLoS pathogens*, 12(1), p.e1005340.

Miyake, S., Yamashita, T., Taniguchi, M., Tamatani, M., Sato, K. & Tohyama, M., 2002. Identification and characterization of a novel mitochondrial tricarboxylate carrier. *Biochemical and biophysical research communications*, 295(2), pp.463–8.

Monné, M., Miniero, D.V., Daddabbo, L., Robinson, A.J., Kunji, E.R.S. & Palmieri, F., 2012. Substrate specificity of the two mitochondrial ornithine carriers can be swapped by single mutation in substrate binding site. *The Journal of biological chemistry*, 287(11), pp.7925–34.

Morciano, P., Carrisi, C., Capobianco, L., Mannini, L., Burgio, G., Cestra, G., De Benedetto, G.E., Corona, D.F. V., Musio, A. & Cenci, G., 2009. A conserved role for the mitochondrial citrate transporter Sea/SLC25A1 in the maintenance of chromosome integrity. *Human Molecular Genetics*, 18(21), pp.4180–4188.

Moreira, D., López-García, P., & Vickerman, K., 2004. An updated view of kinetoplastid phylogeny using environmental sequences and a closer outgroup: proposal for a new classification of the class kinetoplastea. *Int J Syst Evol Microbiol*, 54(5), 1861-1875.

Muhlenhoff, U., Stadler, J. a., Richhardt, N., Seubert, A., Eickhorst, T., Schweyen, R.J., Lill, R., Wiesenberger, G., Mühlenhoff, U., Stadler, J. a., Richhardt, N., Seubert, A.,

Eickhorst, T., Schweyen, R.J., Lill, R. & Wiesenberger, G., 2003. A Specific Role of the Yeast Mitochondrial Carriers Mrs3/4p in Mitochondrial Iron Acquisition under Iron-limiting Conditions. *Journal of Biological Chemistry*, 278(42), pp.40612–40620.

Murase, R., Abe, Y., Takeuchi, T., Nabeta, M., Imai, Y., Kamei, Y., Kagawa-Miki, L., Ueda, N., Sumida, T., Hamakawa, H. & Kito, K., 2008. Serum autoantibody to sideroflexin 3 as a novel tumor marker for oral squamous cell carcinoma. *Proteomics-Clinical Applications*, 2(4), pp.517–527.

Nancolas, B., Guo, L., Zhou, R., Nath, K., Nelson, D. S., & Leeper, D. B., et al, 2016. The anti-tumour agent lonidamine is a potent inhibitor of the mitochondrial pyruvate carrier and plasma membrane monocarboxylate transporters. *Biochemical Journal*, 473(7), 929.

Ngô, H., Tschudi, C., Gull, K. & Ullu, E., 1998. Double-stranded RNA induces mRNA degradation in Trypanosoma brucei. *Proceedings of the National Academy of Sciences of the United States of America*, 95(25), pp.14687–92.

Nozawa, A., Fujimoto, R., Matsuoka, H., Tsuboi, T. & Tozawa, Y., 2011. Cell-free synthesis, reconstitution, and characterization of a mitochondrial dicarboxylate–tricarboxylate carrier of Plasmodium falciparum. *Biochemical and Biophysical Research Communications*, 414(3), pp.612–617.

Nury, H., Dahout-Gonzalez, C., Trézéguet, V., Lauquin, G.J.M., Brandolin, G. & Pebay-Peyroula, E., 2006. Relations between structure and function of the mitochondrial ADP/ATP carrier. *Annual review of biochemistry*, 75, pp.713–741.

O'Brien, T.C., Mackey, Z.B., Fetter, R.D., Choe, Y., O'Donoghue, A.J., Zhou, M., Craik, C.S., Caffrey, C.R. & McKerrow, J.H., 2008. A parasite cysteine protease is key to host protein degradation and iron acquisition. *The Journal of biological chemistry*, 283(43), pp.28934–43.

Opperdoes, F.R., Borst, P. & Spits, H., 1977. Particle-bound enzymes in the bloodstream form of Trypanosoma brucei. *Eur J Biochem*, 76(1), pp.21–28.

Ouellette, M. & Papadopoulou, B., 2009. Coordinated gene expression by post-

transcriptional regulons in African trypanosomes. *Journal of biology*, 8(11), p.100.

Overath, P., Czichos, J. & Haas, C., 1986. The effect of citrate/cis-aconitate on oxidative metabolism during transformation of Trypanosoma brucei. *European journal of biochemistry / FEBS*, 160(1), pp.175–82.

Overath, P. & Engstler, M., 2004. Endocytosis, membrane recycling and sorting of GPI-anchored proteins: Trypanosoma brucei as a model system. *Mol Microbiol*, 53(3), pp.735–744.

Palmieri, F., 2014. Mitochondrial transporters of the SLC25 family and associated diseases: A review. *Journal of Inherited Metabolic Disease*, 37(4), pp.565–575.

Palmieri, F., 2004. The mitochondrial transporter family (SLC25): physiological and pathological implications. *Pflugers Arch*, 447(5), pp.689–709.

Palmieri, F., Agrimi, G., Blanco, E., Castegna, A., Di Noia, M.A., Iacobazzi, V., Lasorsa, F.M., Marobbio, C.M.T., Palmieri, L., Scarcia, P., Todisco, S., Vozza, A. & Walker, J., 2006. Identification of mitochondrial carriers in Saccharomyces cerevisiae by transport assay of reconstituted recombinant proteins. *Biochimica et biophysica acta*, 1757(9–10), pp.1249–62.

Palmieri, F., Pierri, C.L., De Grassi, A., Nunes-Nesi, A. & Fernie, A.R., 2011. Evolution, structure and function of mitochondrial carriers: a review with new insights. *The Plant journal: for cell and molecular biology*, 66(1), pp.161–81.

Palmieri, F., Stipani, I., Quagliariello, E. & Klingenberg, M., 1972. Kinetic Study of the Tricarboxylate Carrier in Rat Liver Mitochondria. *European Journal of Biochemistry*, 26(4), pp.587–594.

Palmieri, L., Lasorsa, F.M., De Palma, A., Palmieri, F., Runswick, M.J. & Walker, J.E., 1997. Identification of the yeast ACR1 gene product as a succinate-fumarate transporter essential for growth on ethanol or acetate. *FEBS letters*, 417(1), pp.114–8.

Palmieri, L., Vozza, A., Hönlinger, A., Dietmeier, K., Palmisano, A., Zara, V. & Palmieri, F., 1999. The mitochondrial dicarboxylate carrier is essential for the growth of

Saccharomyces cerevisiae on ethanol or acetate as the sole carbon source. *Molecular microbiology*, 31(2), pp.569–77.

Paradkar, P.N., Zumbrennen, K.B., Paw, B.H., Ward, D.M. & Kaplan, J., 2009. Regulation of mitochondrial iron import through differential turnover of mitoferrin 1 and mitoferrin 2. *Molecular and cellular biology*, 29(4), pp.1007–1016.

Parsons, M., 2004. Glycosomes: parasites and the divergence of peroxisomal purpose. *Mol Microbiol*, 53(3), pp.717–724.

Parsons, M., Furuya, T., Pal, S. & Kessler, P., 2001. Biogenesis and function of peroxisomes and glycosomes. *Mol Biochem Parasitol*, 115(1), pp.19–28.

Peña-Diaz, P., Pelosi, L., Ebikeme, C., Colasante, C., Gao, F., Bringaud, F. & Voncken, F., 2012. Functional characterization of TbMCP5, a conserved and essential ADP/ATP carrier present in the mitochondrion of the human pathogen Trypanosoma brucei. *Journal of Biological Chemistry*, 287(50), pp.41861–41874.

Picault, N., Hodges, M., Palmieri, L. & Palmieri, F., 2004. The growing family of mitochondrial carriers in Arabidopsis. *Trends in plant science*, 9(3), pp.138–46.

Picault, N., Palmieri, L., Pisano, I., Hodges, M. & Palmieri, F., 2002. Identification of a novel transporter for dicarboxylates and tricarboxylates in plant mitochondria. Bacterial expression, reconstitution, functional characterization, and tissue distribution. *The Journal of biological chemistry*, 277(27), pp.24204–11.

Ponka, P., 1999. Cellular iron metabolism. *Kidney Int Suppl*, 69, pp.S2-11.

Prathalingham, S.R., Wilkinson, S.R., Horn, D. & Kelly, J.M., 2007. Deletion of the Trypanosoma brucei Superoxide Dismutase Gene sodb1 Increases Sensitivity to Nifurtimox and Benznidazole. *Antimicrobial Agents and Chemotherapy*, 51(2), pp.755–758.

Rees, D.C., 2002. Great metalloclusters in enzymology. *Annu Rev Biochem*, 71, pp.221–246.

Regalado, A., Pierri, C.L., Bitetto, M., Laera, V.L., Pimentel, C., Francisco, R., Passarinho, J., Chaves, M.M. & Agrimi, G., 2013. Characterization of mitochondrial

dicarboxylate/tricarboxylate transporters from grape berries. *Planta*, 237(3), pp.693–703.

Rivière, L., Moreau, P., Allmann, S., Hahn, M., Biran, M., Plazolles, N., Franconi, J.-M., Boshart, M. & Bringaud, F., 2009. Acetate produced in the mitochondrion is the essential precursor for lipid biosynthesis in procyclic trypanosomes. *Proceedings of the National Academy of Sciences of the United States of America*, 106(31), pp.12694–9.

Riviere, L., van Weelden, S.W., Glass, P., Vegh, P., Coustou, V., Biran, M., van Hellemond, J.J., Bringaud, F., Tielens, A.G. & Boshart, M., 2004. Acetyl:succinate CoA-transferase in procyclic Trypanosoma brucei. Gene identification and role in carbohydrate metabolism. *J Biol Chem*, 279(44), pp.45337–45346.

Robinson, B.H., 1971. Transport of phosphoenolpyruvate by the tricarboxylate transporting system in mammalian mitochondria. *FEBS letters*, 14(5), pp.309–312.

Robinson, B.H. & Oei, J., 1975. Citrate transport in guinea pig heart mitochondria. *Canadian journal of biochemistry*, 53(5), pp.643–7.

Rocha, G., Martins, A., Gama, G., Brandão, F. & Atouguia, J., 2004. Possible cases of sexual and congenital transmission of sleeping sickness. *Lancet (London, England)*, 363(9404), p.247.

Rodgers, J., 2009. Human African trypanosomiasis, chemotherapy and CNS disease. *J Neuroimmunol*, 211(1–2), pp.16–22.

Roditi, I., Furger, A., Ruepp, S., Schürch, N. & Bütikofer, P., 1998. Unravelling the procyclin coat of Trypanosoma brucei. *Molecular and biochemical parasitology*, 91(1), pp.117–30.

van Roermund, C.W., Drissen, R., van Den Berg, M., Ijlst, L., Hettema, E.H., Tabak, H.F., Waterham, H.R. & Wanders, R.J., 2001. Identification of a peroxisomal ATP carrier required for medium-chain fatty acid beta-oxidation and normal peroxisome proliferation in Saccharomyces cerevisiae. *Mol Cell Biol*, 21(13), pp.4321–4329.

Rosano, G.L. & Ceccarelli, E.A., 2014. Recombinant protein expression in Escherichia

coli: advances and challenges. *Frontiers in microbiology*, 5, p.172.

Rostovtseva, T.K. & Bezrukov, S.M., 1998. ATP transport through a single mitochondrial channel, VDAC, studied by current fluctuation analysis. *Biophys J*, 74(5), pp.2365–2373.

Rouault, T.A. & Tong, W.H., 2005. Iron-sulphur cluster biogenesis and mitochondrial iron homeostasis. *Nat Rev Mol Cell Biol*, 6(4), pp.345–351.

Runswick, M.J., Walker, J.E., Bisaccia, F., Iacobazzi, V. & Palmieri, F., 1990. Sequence of the bovine 2-oxoglutarate/malate carrier protein: structural relationship to other mitochondrial transport proteins. *Biochemistry*, 29(50), pp.11033–40.

Ryter, S.W. & Tyrrell, R.M., 2000. The heme synthesis and degradation pathways: role in oxidant sensitivity. Heme oxygenase has both pro- and antioxidant properties. *Free radical biology & medicine*, 28(2), pp.289–309.

Saas, J., Ziegelbauer, K., von Haeseler, A., Fast, B. & Boshart, M., 2000. A developmentally regulated aconitase related to iron-regulatory protein-1 is localized in the cytoplasm and in the mitochondrion of Trypanosoma brucei. *Journal of Biological Chemistry*, 275(4), pp.2745–2755.

Saitou, N. & Nei, M., 1987. The neighbor-joining method: a new method for reconstructing phylogenetic trees. *Molecular biology and evolution*, 4(4), pp.406–25.

Santolla, M.F., Lappano, R., De Marco, P., Pupo, M., Vivacqua, A., Sisci, D., Abonante, S., Iacopetta, D., Cappello, A.R., Dolce, V. & Maggiolini, M., 2012. G protein-coupled estrogen receptor mediates the up-regulation of fatty acid synthase induced by 17β-estradiol in cancer cells and cancer-associated fibroblasts. *The Journal of biological chemistry*, 287(52), pp.43234–45.

Saraste, M. & Walker, J.E., 1982. Internal sequence repeats and the path of polypeptide in mitochondrial ADP/ATP translocase. *FEBS Letters*, 144(2), pp.250–254.

Sather, S. & Agabian, N., 1985. A 5’ spliced leader is added in trans to both alpha- and beta-tubulin transcripts in Trypanosoma brucei. *Proc Natl Acad Sci U S A*, 82(17),

pp.5695–5699.

Schneider, A., Bouzaidi-Tiali, N., Chanez, A.-L. & Bulliard, L., 2007. ATP production in isolated mitochondria of procyclic Trypanosoma brucei. *Methods in molecular biology (Clifton, N.J.)*, 372, pp.379–387.

Serviddio, G., Bellanti, F., Stanca, E., Lunetti, P., Blonda, M., Tamborra, R., Siculella, L., Vendemiale, G., Capobianco, L. & Giudetti, A.M., 2014. Silybin exerts antioxidant effects and induces mitochondrial biogenesis in liver of rat with secondary biliary cirrhosis. *Free Radical Biology and Medicine*, 73, pp.117–126.

Shabnam, N., Tripathi, I., Sharmila, P. & Pardha-Saradhi, P., 2015. A rapid, ideal, and eco-friendlier protocol for quantifying proline. *Protoplasma*.

Shaw, G.C., Cope, J.J., Li, L., Corson, K., Hersey, C., Ackermann, G.E., Gwynn, B., Lambert, A.J., Wingert, R.A., Traver, D., Trede, N.S., Barut, B.A., Zhou, Y., Minet, E., Donovan, A., Brownlie, A., Balzan, R., Weiss, M.J., Peters, L.L., Kaplan, J., Zon, L.I. & Paw, B.H., 2006. Mitoferrin is essential for erythroid iron assimilation. *Nature*, 440(7080), pp.96–100.

Sheftel, A.D., Zhang, A.S., Brown, C., Shirihai, O.S. & Ponka, P., 2007. Direct interorganellar transfer of iron from endosome to mitochondrion. *Blood*, 110(1), pp.125–132.

Shongwe, M.S., Smith, C.A., Ainscough, E.W., Baker, H.M., Brodie, A.M. & Baker, E.N., 1992. Anion binding by human lactoferrin: results from crystallographic and physicochemical studies. *Biochemistry*, 31(18), pp.4451–8.

Shvartsman, M., Kikkeri, R., Shanzer, A. & Cabantchik, Z.I., 2007. Non-transferrin-bound iron reaches mitochondria by a chelator-inaccessible mechanism: biological and clinical implications. *Am J Physiol Cell Physiol*, 293(4), pp.C1383-94.

Siculella, L., Damiano, F., Sabetta, S. & Gnoni, G. V, 2004. n-6 PUFAs downregulate expression of the tricarboxylate carrier in rat liver by transcriptional and posttranscriptional mechanisms. *Journal of lipid research*, 45(7), pp.1333–40.

Siculella, L., Damiano, F., Di Summa, R., Tredici, S.M., Alduina, R., Gnoni, G. V. &

Alifano, P., 2010. Guanosine 5′-diphosphate 3′-diphosphate (ppGpp) as a negative modulator of polynucleotide phosphorylase activity in a “rare” actinomycete. *Molecular Microbiology*, 77(3), pp.716–729.

Sievers, F., Wilm, A., Dineen, D., Gibson, T.J., Karplus, K., Li, W., Lopez, R., McWilliam, H., Remmert, M., Söding, J., Thompson, J.D. & Higgins, D.G., 2011. Fast, scalable generation of high-quality protein multiple sequence alignments using Clustal Omega. *Molecular systems biology*, 7, p.539.

Simpson, A.G.B., 2003. Cytoskeletal organization, phylogenetic affinities and systematics in the contentious taxon Excavata (Eukaryota). *International Journal of Systematic and Evolutionary Microbiology*, 53(6), pp.1759–1777.

Simpson, A.G.B. & Roger, A.J., 2004. The real “kingdoms” of eukaryotes. *Current Biology*, 14(17), pp.R693–R696.

Smíd, O., Horákova, E., Vilímova, V., Hrdy, I., Cammack, R., Horváth, A., Lukes, J., Tachezy, J., Horáková, E., Vilímová, V., Hrdy, I., Cammack, R., Horváth, A., Lukes, J. & Tachezy, J., 2006. Knock-downs of iron-sulfur cluster assembly proteins IscS and IscU down-regulate the active mitochondrion of procyclic Trypanosoma brucei. *Journal of Biological Chemistry*, 281(39), pp.28679–28686.

Sogin, M. L., Elwood, H. J., & Gunderson, J. H., 1986. Evolutionary diversity of eukaryotic small-subunit rrna genes. *Proceedings of the National Academy of Sciences of the United States of America*, 83(5), 1383-1387.

Steverding, D., 2008. The history of African trypanosomiasis. *Parasit Vectors*, 1(1), p.3.

Steverding, D., Stierhof, Y.D., Fuchs, H., Tauber, R. & Overath, P., 1995. Transferrin-binding protein complex is the receptor for transferrin uptake in Trypanosoma brucei. *The Journal of cell biology*, 131(5), pp.1173–82.

Stich, A., Abel, P.M. & Krishna, S., 2002. Human African trypanosomiasis. *Bmj*, 325(7357), pp.203–206.

Stijlemans, B., Vankrunkelsven, A., Brys, L., Magez, S. & De Baetselier, P., 2008. Role of iron homeostasis in trypanosomiasis-associated anemia. *Immunobiology*, 213(9–

10), pp.823–35.

Stipani, I. & Palmieri, F., 1983. Purification of the active mitochondrial tricarboxylate carrier by hydroxylapatite chromatography. *FEBS letters*, 161(2), pp.269–74.

Stuart, K., Brun, R., Croft, S., Fairlamb, A., Gurtler, R.E., McKerrow, J., Reed, S. & Tarleton, R., 2008. Kinetoplastids: related protozoan pathogens, different diseases. *J Clin Invest*, 118(4), pp.1301–1310.

Sun, W., Ni, R., Yin, J.F., Musa, H.H., Ding, T. jia, Yang, S., et al., 2013. Genome Array of Hair Follicle Genes in Lambskin with Different Patterns G. E. Woloschak, ed. *PLoS ONE*, 8(7), p.e68840.

Taketani, S., Kakimoto, K., Ueta, H., Masaki, R. & Furukawa, T., 2003. Involvement of ABC7 in the biosynthesis of heme in erythroid cells: interaction of ABC7 with ferrochelatase. *Blood*, 101(8), pp.3274–80.

Taniguchi, M. & Sugiyama, T., 1997. The Expression of 2-Oxoglutarate/Malate Translocator in the Bundle-Sheath Mitochondria of Panicum miliaceum, a NAD-Malic Enzyme-Type C4 Plant, Is Regulated by Light and Development. *Plant physiology*, 114(1), pp.285–293.

Taylor, M.C. & Kelly, J.M., 2010. Iron metabolism in trypanosomatids, and its crucial role in infection. *Parasitology*, 137(6), pp.899–917.

Tielens, A.G. & van Hellemond, J.J., 1998. Differences in energy metabolism between trypanosomatidae. *Parasitol Today*, 14(7), pp.265–272.

Tielens, A. G. M., & van Hellemond, J. J. V., 2009. Surprising variety in energy metabolism within trypanosomatidae. *Trends in Parasitology*, 25(10), 482-490.

Le Trant, N., Meshnick, S.R., Kitchener, K., Eaton, J.W. & Cerami, A., 1983. Iron-containing superoxide dismutase from Crithidia fasciculata. Purification, characterization, and similarity to Leishmanial and trypanosomal enzymes. *The Journal of biological chemistry*, 258(1), pp.125–30.

Tripodi, K.E.J., Menendez Bravo, S.M. & Cricco, J.A., 2011. Role of heme and heme-proteins in trypanosomatid essential metabolic pathways. *Enzyme research*, 2011,

p.873230.

Troadec, M.-B., Warner, D., Wallace, J., Thomas, K., Spangrude, G.J., Phillips, J., Khalimonchuk, O., Paw, B.H., Ward, D.M. & Kaplan, J., 2011. Targeted deletion of the mouse Mitoferrin1 gene: from anemia to protoporphyria. *Blood*, 117(20).

Tsuda, A., Witola, W.H., Konnai, S., Ohashi, K. & Onuma, M., 2006. The effect of TAO expression on PCD-like phenomenon development and drug resistance in Trypanosoma brucei. *Parasitology international*, 55(2), pp.135–42.

Tsuda, A., Witola, W.H., Ohashi, K. & Onuma, M., 2005. Expression of alternative oxidase inhibits programmed cell death-like phenomenon in bloodstream form of Trypanosoma brucei rhodesiense. *Parasitology international*, 54(4), pp.243–51.

Týč, J., Klingbeil, M.M. & Lukeš, J., 2015. Mitochondrial heat shock protein machinery hsp70/hsp40 is indispensable for proper mitochondrial DNA maintenance and replication. *mBio*, 6(1), pp.e02425-14.

Vanhollebeke, B., De Muylder, G., Nielsen, M.J., Pays, A., Tebabi, P., Dieu, M., Raes, M., Moestrup, S.K. & Pays, E., 2008. A haptoglobin-hemoglobin receptor conveys innate immunity to Trypanosoma brucei in humans. *Science (New York, N.Y.)*, 320(5876), pp.677–681.

Verner, Z., Basu, S., Benz, C., Dixit, S., Dobáková, E., Faktorová, D., Hashimi, H., Horáková, E., Huang, Z., Paris, Z., Peña-Diaz, P., Ridlon, L., Týč, J., Wildridge, D., Zíková, A. & Lukeš, J., 2015. Chapter Three – Malleable Mitochondrion of Trypanosoma brucei. *International Review of Cell and Molecular Biology*, 315, pp.73–151.

Vickerman, K., 1985. Developmental cycles and biology of pathogenic trypanosomes. *Br Med Bull*, 41(2), pp.105–114.

Vignais, P. V., Vignais, P. M., Lauquin, G., & Morel, F., 1973. Binding of adenosine diphosphate and of antagonist ligands to the mitochondrial ADP carrier. *Biochimie*, 55(6–7), 763-778.

Vidilaseris, K., Shimanovskaya, E., Esson, H.J., Morriswood, B. & Dong, G., 2014.

Assembly mechanism of Trypanosoma brucei BILBO1, a multidomain cytoskeletal protein. *The Journal of biological chemistry*, 289(34), pp.23870–81.

Voncken, F., Boxma, B., Tjaden, J., Akhmanova, A., Huynen, M., Verbeek, F., Tielens, A.G., Haferkamp, I., Neuhaus, H.E., Vogels, G., Veenhuis, M. & Hackstein, J.H., 2002. Multiple origins of hydrogenosomes: functional and phylogenetic evidence from the ADP/ATP carrier of the anaerobic chytrid Neocallimastix sp. *Mol Microbiol*, 44(6), pp.1441–1454.

Voncken, F., Van Hellemond, J.J., Pfisterer, I., Maier, A., Hillmer, S. & Clayton, C., 2003. Depletion of GIM5 causes cellular fragility, a decreased glycosome number, and reduced levels of ether-linked phospholipids in trypanosomes. *Journal of Biological Chemistry*, 278(37), pp.35299–35310.

Wakil, S.J., 1989. Fatty acid synthase, a proficient multifunctional enzyme. *Biochemistry*, 28(11), pp.4523–30.

Walden, W.E., Selezneva, A.I., Dupuy, J., Volbeda, A., Fontecilla-Camps, J.C., Theil, E.C. & Volz, K., 2006. Structure of dual function iron regulatory protein 1 complexed with ferritin IRE-RNA. *Science (New York, N.Y.)*, 314(5807), pp.1903–8.

Wang, L., Duan, Q., Wang, T., Ahmed, M., Zhang, N., & Li, Y., et al., 2015. Mitochondrial respiratory chain inhibitors involved in ros production induced by acute high concentrations of iodide and the effects of sod as a protective factor. *Oxidative Medicine & Cellular Longevity*, 2015(3), 217670.

Wang, Y., Langer, N.B., Shaw, G.C., Yang, G., Li, L., Kaplan, J., Paw, B.H. & Bloomer, J.R., 2011. Abnormal mitoferrin-1 expression in patients with erythropoietic protoporphyria. *Experimental hematology*, 39(7), pp.784–94.

van Weelden, S.W., van Hellemond, J.J., Opperdoes, F.R. & Tielens, A.G., 2005. New functions for parts of the Krebs cycle in procyclic Trypanosoma brucei, a cycle not operating as a cycle. *J Biol Chem*, 280(13), pp.12451–12460.

van Weelden, S.W.H., Fast, B., Vogt, A., van der Meer, P., Saas, J., van Hellemond, J.J., Tielens, A.G.M. & Boshart, M., 2003. Procyclic Trypanosoma brucei do not use

Krebs cycle activity for energy generation. *The Journal of biological chemistry*, 278(15), pp.12854–12863.

WHO, 2017. WHO | World Health Organization.

Wiesenberger, G., Waldherr, M. & Schweyen, R.J., 1992. The nuclear gene MRS2 is essential for the excision of group II introns from yeast mitochondrial transcripts in vivo. *The Journal of biological chemistry*, 267(10), pp.6963–9.

Wilkinson, S. R., Prathalingam, S. R., Taylor, M. C., Ahmed, A., Horn, D., & Kelly, J. M., 2006. Functional characterisation of the iron superoxide dismutase gene repertoire in *Trypanosoma brucei*. *Free Radical Biology & Medicine*, 40(2), 198-209.

Wingfield, P.T., Palmer, I. & Liang, S.M., 2001. Folding and purification of insoluble (inclusion body) proteins from Escherichia coli. *Current protocols in protein science / editorial board, John E. Coligan ... [et al.]*, Chapter 6, p.Unit 6.5.

Xu, F., Putt, D.A., Matherly, L.H. & Lash, L.H., 2006. Modulation of expression of rat mitochondrial 2-oxoglutarate carrier in NRK-52E cells alters mitochondrial transport and accumulation of glutathione and susceptibility to chemically induced apoptosis. *The Journal of pharmacology and experimental therapeutics*, 316(3), pp.1175–86.

Xu, Y., Mayor, J.A., Gremse, D., Wood, D.O. & Kaplan, R.S., 1995. High-Yield Bacterial Expression, Purification, and Functional Reconstitution of the Tricarboxylate Transport Protein from Rat Liver Mitochondria. *Biochemical and Biophysical Research Communications*, 207(2), pp.783–789.

Ye, X., Xu, J., Cheng, C., Yin, G., Zeng, L., Ji, C., Gu, S., Xie, Y. & Mao, Y., 2003. Isolation and characterization of a novel human putative anemia-related gene homologous to mouse sideroflexin. *Biochem Genet*, 41(3–4), pp.119–125.

Yoon, H., Zhang, Y., Pain, J., Lyver, E.R., Lesuisse, E., Pain, D. & Dancis, A., 2011. Rim2, a pyrimidine nucleotide exchanger, is needed for iron utilization in mitochondria. *Biochemical Journal*, 440(1), pp.137–146.

Yoshikumi, Y., Mashima, H., Ueda, N., Ohno, H., Suzuki, J., Tanaka, S., Hayashi, M., Sekine, N., Ohnishi, H., Yasuda, H., Iiri, T., Omata, M., Fujita, T. & Kojima, I., 2005. Roles of CTPL/Sfxn3 and Sfxn family members in pancreatic islet. *Journal of Cellular Biochemistry*, 95(6), pp.1157–1168.

Zara, V., Dolce, V., Capobianco, L., Ferramosca, A., Papatheodorou, P., Rassow, J. & Palmieri, F., 2007. Biogenesis of eel liver citrate carrier (CIC): negative charges can substitute for positive charges in the presequence. *Journal of molecular biology*, 365(4), pp.958–67.

Zhang, Y., Lyver, E.R., Knight, S.A., Lesuisse, E. & Dancis, A., 2005. Frataxin and mitochondrial carrier proteins, Mrs3p and Mrs4p, cooperate in providing iron for heme synthesis. *J Biol Chem*, 280(20), pp.19794–19807.

Zhang, Y., Lyver, E. R., Knight, S. A. B., Pain, D., Lesuisse, E., & Dancis, A., 2006. Mrs3p, mrs4p, and frataxin provide iron for fe-s cluster synthesis in mitochondria. *Journal of Biological Chemistry*, 281(32), 22493-502.

Zhou, X., Paredes, J.A., Krishnan, S., Curbo, S. & Karlsson, A., 2015. The mitochondrial carrier SLC25A10 regulates cancer cell growth. *Oncotarget*, 6(11), pp.9271–9283.

Zuckerkandl, E. & Pauling, L., 1965. Molecules as documents of evolutionary history. *Journal of theoretical biology*, 8(2), pp.357–66.

Appendix

A1 Sequences of genes related in this study

TbMCP12 sequence (Tb10.389.0690) (915 bp):

ATGTCGAAAGAGACAAAGGCGCCCGCGAATGCGCCCCTTCCTAAGGTCTACA
CGATCGGGATTGCTGGTTTTTCCGGCATGTTTGCATGGTTGTTCACGCACCCT
TATGAAATGTGGAAGAATACGGTGATGACTGCACCCAAAGGTACCTCACAGA
AGGAATGTTTGGTTAAGGTGTGGGAACGTGGACCATTCAGGGGTTTGTCTAC
GGGAATCCTCCGCCAGGCCGTGTACGCTCCTGCAAGACTTGGGTGTTATCCC
ATATTTCGTGATGCCATCATGTCTCTGAAGGGTGACGCCGACGGCATGCCAAC
AGTTGCCGAGCGTGCACTTGCTGGCGCCCTGGCTGGTGTCTTTTCCAGTATCC
TCACTTCCCCAGTGGAGGTTTGTCTCGTTCTGCAAATGACCGGTGCATCGAA
GCAGTCGTTGACGCGTGCGGCGATTACCGTATACTCAACTAACGGAATCACG
GGATATTGGCGTGGTGTCAGTGCCCTTGCTTCTCGTGCAGCACTGGTGGGCG
TTGCCCAAGTCGCTGTGCATGATCAAGTCCTTTCCGCGTTGCGGCGTCGTAAT
GTTTCCTACTCTCAATTGCACGGAACCCAACCATACGGAGACAACATTGTCG
TCAATGCAGCGAGCATCCTTACAGCATTGTTTTATTCCGTTATCACGATGCCAG
TTGAATTCGCACGTGTACGTATGTCCGCTGATACCACCAAAGCAAAGTATAAG
AGTGTGACTCAGACGATAGGACGAGTCGTTCGTGAGGAGGGGGCATTGGCG
GTGTACGACTCCTTCGCGCCGTACTTTTTCCGCTGTGCGACACACACAGTGG
TGTGCTTCTTCACAATTGAATACATCACAAGAAAGGTGAAGGGGTGGCGTGC
CGCCAAGCTTCAGGCAAAGCAGTAG

TbMCP17 sequence (Tb927.3.2980) (870 bp):

ATGGTTTCCGAGGGCACTTCCGCTGCAGGTCGCCTGGAGGGCGAGTCGCCG
CTTGCGCTGCGCGTCGATACTGGCGAAATTGTCGCGGGATGCCTCGCCGGTT
TTGTGGAACATTTCTTTATGTTCCCGTTTGACACTTTGAAGACACGGGTTCAG
AGTGGGGACTCGACGAATGTCATATTAGCGGCAAAGCGTATTTCGCGGAATG
AGCGACTTGCACATCTTTACCGCGGATTCGCGCCCATCATCGTTTCTGCCGTT
CCAGCGCATGGTGCATATTACAGCACATATGAGGCTGCGAAGCGTGTCTTTGG
TGAGGATTCCACAGTGTCTATAACGGTCTCTGCCAGTTGTGCGGTCGCTGCTC
ATGACACCATTTCCACCCCATTTGATGTTATCAAGCAGCGGATGCAGATGGAC

GGGAGCCGGAAGTTTGCTTCATCGCTTCAGTGTGGTCAATGTGCAGTTGCGG
AAGGGGGCGTGCGGTGCCTTCTCCTCTCTTTGCCCACCACTATTTTAATGAAC
ATTCCACATTTCTCAGCCTACTGGTTAGTTTATGAGGGGTTTCTTGCATACTTG
GGTGGTGAGCGGCGCAATAGGGAAACGGAAGTTGCGGGAGATTACATAACC
GGGGGCCTCCTGGCAGGCACTGTGGCTTCTATTGTCTCGTCACCGTTAGACG
TTGTAAAGACTCAGCTGCAACTCGGTCTTAGAAAGAATATCCCCGATGCGGT
GCGCTATGTCTTAGTCAATCGTGGCACCAAAGGTTTCTTTGCCGGGGTTACGG
CGAGAGTTATGTGTACCGCTCCTGCTGGTGCCCTGTCAATGATCACATATGAA
ACGGCCAAGAAGTTCATGGAGGAACGGTAA

MCP17 RNAi sequence with BamH I, Xho I and Hind III (836 bp):

CGGATCCCCATTTGATGTTATCAAGCAGCGGATGCAGATGGACGGGAGCCGG
AAGTTTGCTTCATCGCTTCAGTGTGGTCAATGTGCAGTTGCGGAAGGGGGCG
TGCGGTGCCTTCTCCTCTCTTTGCCCACCACTATTTTAATGAACATTCCACATT
TCTCAGCCTACTGGTTAGTTTATGAGGGGTTTCTTGCATACTTGGGTGGTGAG
CGGCGCAATAGGGAAACGGAAGTTGCGGGAGATTACATAACCGGGGGCCTC
CTGGCAGGCACTGTGGCTTCTATTGTCTCGTCACCGTTAGACGTTGTAAAGAC
TCAGCTGCAACTCGGTCTTAGAAAGAATATCCCCGATGCGGTGCGCTATGTCT
TAGTCAATCGTGGCACCAAAGGTTTCTTTGCCGGGGTTACGGCGAGAGTTAT
GTGTACCGCTCCTGCTGGTGCCCTGTCAATGCTCGAGTGACTAAGACATAGC
GCACCGCATCGGGGATATTCTTTCTAAGACCGAGTTGCAGCTGAGTCTTTACA
ACGTCTAACGGTGACGAGACAATAGAAGCCACAGTGCCTGCCAGGAGGCCC
CCGGTTATGTAATCTCCCGCAACTTCCGTTTCCCTATTGCGCCGCTCACCACC
CAAGTATGCAAGAAACCCCTCATAAACTAACCAGTAGGCTGAGAAATGTGGA
ATGTTCATTAAAATAGTGGTGGGCAAAGAGAGGAGAAGGCACCGCACGCCC
CCTTCCGCAACTGCACATTGACCACACTGAAGCGATGAAGCAAACTTCCGGC
TCCCGTCCATCTGCATCCGCTGCTTGATAACATCAAATGGGGTGGAAGCTTG

MCP17 5'UTR sequence (500 bp):

TGGGTGTTCCGTGTCGTGAGGTGGAGAGGTGATGGAAAATAATAAGAGTTGC
GGAAGGGAGTATGTGAGGTGCACCACTTTTGGACGGTGAGATAAGCAGGGA

GGAGTTTGAGGGTACTTGTGGTACAGTACTCCCCCTCTTTTATATTCTTTTGAT
TTAAGGCAGTCACTTGTCTGCTAGCAACCCCTCTCTTTCTGTGTATATCTGTTT
TTTTGTTTTATTATTGTTGGTGCAGTTACCCCCTTCCTTTTCTTGTCGTGGTACT
GTCGCTGATGCGTCATTACCCCTCTATTTTGTTTCCATATGCGTCTTCACGAAA
GCGTCGTCGCAGACGTTTGCATATTTTTGTCTTCCATGCACCACTCCACGTTC
ATTTCTTGCCTCTGTTCATCTTTTCTTTTTTTTCTTTTCTCTCGCTCGTTCCCCG
TGTTGCCGTTGTTTTGCTTGGCTGCGGTGATGTGTGTATTATCTGCTGATGTTT
GCTTCTGTTTTATTGTAG

MCP17 3'UTR sequence (492 bp):

GCATGGATCCCCGTGTTCTTGTTTCAGGTGTGAACCCCGGGGTTATCAATATG
AGAAGGGTGCATGTGATGCAGTGGGTGGAAAGCTTTTCACTATTTCCAGTAA
TAACCGCTGTCGATTTCACTTTTCATTTTGTTGAGGAAGGGGTTTACAATTCA
CCATATGGACGGTGTCGGAAGTGATGATGAAACCAGCTGATACACTTCCCTTT
ATTACAAAAAAAAAAGAGGTTTTATTTTTGTACGGTTAGCGCAGAACACACA
GGTATAACCATCGGTATCGTCTTTGGTAGTCTGCGAATATACTTTTTTCCTTTTT
TAAACACAGGATTCATAAACGGGTAAGAGCCAGACAGTGGCTGACAAGGGT
GTTAGGGGCCTTACATTGTAAACTTATCTGTATTTTTTTTTTCCCCCGTAGACC
TCTTATGTCTCATTCTTGTCAGTAGCCGCTTCCCTTCCCGCTCCAGTAATGTGT
TTGACGGGCCCATAG

TbSFXN sequence (Tb927.9.4310) (981 bp)

ATGCTTCCATGTCCGTCGTTCTCTACCACAACTCCAAGGTTTGACATGGACAC
CTATCTGGGTCGTACTTTTTACTTTTTTTCCACCATCAACCCACTGTTGTGCTT
TGAGACGTCAAACTCATTGAAGCGCCATCAGGAGCTGCTCAATCGTGTGGCA
GCGGGAGAGGAAGGGGTTGCAAGCGACAGACAACTGTGGAAAGCACGCAC
TGCAATAGAAATATGCGTGCATCCCACCACTAAGGAAGTTATATTTCCACCTT
ACAGGATGTGTGCTTTCCTTCCTGTGAATAGTTTTATCGTACCCTTCATGATGT
CACCGACGACCATTGCAAGCCCTGCGCTCACAATATTCATTCAGTGGTTTAAC
CAGAGCTATAACTGCGCGGTGAATTATGCAAATCGCTCCTCCGATAAGCAACC
GATGTCGGAACTATCTAAGGCGTACGTCGCCGCTGTTGGTGTTTCCTGCGCCG

GAGCACTAGGTGCTACAGCAATGCTGAAGAAAGTAAAAGGTGGCACATTGA
AAGCCACAGCTGTTCGTGCGGGGTTACCTTTCGTGGCGGTATCTGCGGCGGC
AATTGTGAATCTTTCTCTAATGCGTAAGAATGAGTGGATTCCATCAGGCACTG
GCCTACAAGTTGTTGACGAGGATGGTGAGGTGCGGGGCAGCAGTCGTGTTG
CCGGCATGCAAAGTCTCATGATGTGTTCCGTCACGCGTGTTACATGGAACCTT
ATTTCCATGGTGTTGCCGCTTTTGATGATGCGACCACTCCTTGCCCGCTGTGC
AGCTGTTCGGGCTCGACCTGTTGTGTATGAAACAGCACTGCAGATTGCCAGC
CTCGGCGTCGGTGTTCCGCTTGCATTGGGTGCATTTAGCACAACAGTGAGTG
TACCTGCGAATCGGTTGGAGCCGGAACTTCGTGGGTTGAAGCGAAAGGACG
GCTCGCCTGTTGAAATATTCACGTATTACAAGGGTTTG

SFXN antisense sequence with BamH I, Xho I and Hind III (395 bp):

CGATGTCGGATCCATCTAAGGCGTACGTCGGCGCTGTTGGTGTTTCCTGCGCC
GGAGCACTAGGTGCTACAGCAATGCTGAAGAAAGTAAAAGGTGGCACATTG
AAAGCCACAGCTGTTCGTGCGGGGTTACCTTTCGTGGCGGTATCTGCGGCGG
CAATTGTGAATCTTTCTCTAATGCGTAAGAATGAGTGGATTCCATCAGGCACT
GGCCTACAAGTTGTTGACGAGGATGGTGAGGTGCGGGGCAGCAGTCGTGTT
GCCGGCATGCAAAGTCTCATGATGTGTTCCGTCACGCGTGTTACATGGAACCT
TATTTCCATGGTGTTGCCGCTTTTGATGATGCGACCACTCCTTGCCCGCTGTG
CAGCTGTTCGGGCTCGAGCTGAAGCTTAT

SFXN sense sequence with Xho I and Hind III (345 bp):

CGATGTCGGAAGCTTCTAAGGCGTACGTCGCCGCTGGTTGGTGTTTCCTGCG
CCGGAGCACTAGGTGCTACAGCAATGCTGAAGAAAGTAAAAGGTGGCACAT
TGAAAGCCACAGCTGTTCGTGCGGGGTTACCTTTCGTGGCGGTATCTGCGGC
GGCAATTGTGAATCTTTCTCTAATGCGTAAGAATGAGTGGATTCCATCAGGCA
CTGGCCTACAAGTTGTTGACGAGGATGGTGAGGTGCGGGGCAGCAGTCGTG
TTGCCGGCATGCAAAGTCTCATGATGTGTTCCGTCACGCGTGTTACATGGAAC
CTTATTTCCATGGTGTTGCCGCTCTCGAGGATG

SFXN antisense sequence with BamH I and Apa I (390 bp):

CGATGTCGGATCCATCTAAGGCGTACGTCGGCGCTGTTGGTGTTTCCTGCGCC
GGAGCACTAGGTGCTACAGCAATGCTGAAGAAAGTAAAAGGTGGCACATTG
AAAGCCACAGCTGTTCGTGCGGGGTTACCTTTCGTGGCGGTATCTGCGGCGG
CAATTGTGAATCTTTCTCTAATGCGTAAGAATGAGTGGATTCCATCAGGCACT
GGCCTACAAGTTGTTGACGAGGATGGTGAGGTGCGGGGCAGCAGTCGTGTT
GCCGGCATGCAAAGTCTCATGATGTGTTCCGTCACGCGTGTTACATGGAACCT
TATTTCCATGGTGTTGCCGCTTTTGATGATGCGACCACTCCTTGCCCGCTGTG
CAGCTGTTCGGGCTCGGGGCCCTG

SFXN sense sequence with Apa I and Hind III (343 bp):

CGATGTCGGAAGCTTCTAAGGCGTACGTCGCCGCTGGTTGGTGTTTCCTGCG
CCGGAGCACTAGGTGCTACAGCAATGCTGAAGAAAGTAAAAGGTGGCACAT
TGAAAGCCACAGCTGTTCGTGCGGGGTTACCTTTCGTGGCGGTATCTGCGGC
GGCAATTGTGAATCTTTCTCTAATGCGTAAGAATGAGTGGATTCCATCAGGCA
CTGGCCTACAAGTTGTTGACGAGGATGGTGAGGTGCGGGGCAGCAGTCGTG
TTGCCGGCATGCAAAGTCTCATGATGTGTTCCGTCACGCGTGTTACATGGAAC
CTTATTTCCATGGTGTTGCCGCTGGGCCCAG

TbMCP23 antisense sequence with BamH I and Apa I (444 bp):

ACCAGAAGGATCCACCTGCCATTGCGGCTTGTGGTGCCGTGTGTGTGACAAA
CACGATCCGTGCCGTGTGTGTGACAAACACGATCCTAGGGCCGATATTTCTG
GTGCGGACTCGCGTGCAAGTTAACGAAAAACTAACTGTGCGGCAAACGTTT
AGAGATGTGCTGAAGCACGAAGGCTTCAGTGGTTTCTACCGCGGGACCATGA
CCAATATTGTGGGTCGGTTCGTCGAAGAGGGCCTCTTCTGGAGCATCTATGAA
CTTCTTAAGCGGTTGTCAAACGAAGCAAGTTTCAAGGGTTCCAGCAACTTTT
TTCTGACATCTGTCGCGGTAGCATCGCTTTCGGCCGTGGCGAAGATTGCCGCC
ACCACCGTCTCTTATCCTTACAACGTCGTTATGAATCACATGCGCAGCGTCAG
CTATCGTGACAGGGAAACGGGCCCCT

TbMCP23 sense sequence with Apa I and Hind III (338 bp):

GTGCCGTGTGTGTGACAAACACGATCCTAGGGCCGATATTTCTGGTGCGGAC
TCGCGTGCAAGTTAACGAAAAACTAACTGTGCGGCAAACGTTTAGAGATGTG
CTGAAGCACGAAGGCTTCAGTGGTTTCTACCGCGGGACCATGACCAATATTG
TGGGTCGGTTCGTCGAAGAGGGCCTCTTCTGGAGCATCTATGAACTTCTTAA
GCGGTTGTCAAACGAAGCAAGTTTCAAGGGTTCCAGCAACTTTTTTCTGACA
TCTGTCGCGGTAGCATCGCTTTCGGCCGTGGCGAAGATTGCCGCCACCACCG
TCTCTTATCCTTACAACGGGCCCATG

TbMCP23 gene sequence (Tb927.5.1550):

ATGGCACTCCCGACATCGCATGTGGTTCAAACCCCCAAAAGACAAGAATACC
TTGCATCCTGTTTGTCTGGTTGTGTTGCCGGTGTCTGCTCCACCTGCGTCATA
AACCCATTGGATACCGTCCGTGTGCGCCTCTCTGTAAGCCGAAGTGCCACTG
GAAAGGCACACAGGAGCCTCTTGTACACTGTTAGGGACCTCTTCGAGGGAG
GCATTGTCCACGCCTTTTCGCGTGGTCTCTCGGCAAATCTAATGGCCTCGCTT
CCCTCCAATGGTATTTATCTTCCTACATACCGCTGCATTAAGGACCAACTTTCC
TCTGCCGGAGTCAACCAGAATGTTCAACCTGCCATTGCGGCTTGTGGTGCCG
TGTGTGTGACAAACACGATCCTAGGGCCGATATTTCTGGTGCGGACTCGCGT
GCAAGTTAACGAAAAACTAACTGTGCGGCAAACGTTTAGAGATGTGCTGAA
GCACGAAGGCTTCAGTGGTTTCTACCGCGGGACCATGACCAATATTGTGGGT
CGGTTCGTCGAAGAGGGCCTCTTCTGGAGCATCTATGAACTTCTTAAGCGGT
TGTCAAACGAAGCAAGTTTCAAGGGTTCCAGCAACTTTTTTCTGACATCTGT
CGCGGTAGCATCGCTTTCGGCCGTGGCGAAGATTGCCGCCACCACCGTCTCT
TATCCTTACAACGTCGTTATGAATCACATGCGCAGCGTCAGCTACGTGACAGG
GAAACCCGAGTATGAGCGCATTATGCCAACAATACGACACATTTATTACCAAG
ACGGCATACCCGGTTTTTACAAGGGGCTTGCGCCGCAGCTGTTACGGAGCAC
GCTAAGTAAGGCTGTACAGATATATTCTTTTGAACTGGCCATGTTCATTTACTT
CAGCACTGTCCAACGTCCCGTTGTTTCTTGCGCTCCCGCATAA

NEO sequence (438 bp):

ATGCGGCGGCTGCATACGCTTGATCCGGCTACCTGCCCATTCGACCACCAAG
CGAAACATCGCATCGAGCGAGCACGTACTCGGATGGAAGCCGGTCTTGTCGA

TCAGGATGATCTGGACGAAGAGCATCAGGGGCTCGCGCCAGCCGAACTGTT
CGCCAGGCTCAAGGCGCGCATGCCCGACGGCGAGGATCTCGTCGTGACCCAT
GGCGATGCCTGCTTGCCGAATATCATGGTGGAAAATGGCCGCTTTTCTGGATT
CATCGACTGTGGCCGGCTGGGTGTGGCGGACCGCTATCAGGACATAGCGTTG
GCTACCCGTGATATTGCTGAAGAGCTTGGCGGCGAATGGGCTGACCGCTTCC
TCGTGCTTTACGGTATCGCCGCTCCCGATTCGCAGCGCATCGCCTTCTATCGC
CTTCTTGACGAGTTCTTCTGA

BSD sequence (399 bp):

ATGGCCAAGCCTTTGTCTCAAGAAGAATCCACCCTCATTGAAAGAGCAACGG
CTACAATCAACAGCATCCCCATCTCTGAAGACTACAGCGTCGCCAGCGCAGC
TCTCTCTAGCGACGGCCGCATCTTCACTGGTGTCAATGTATATCATTTTACTGG
GGGACCTTGTGCAGAACTCGTGGTGCTGGGCACTGCTGCTGCTGCGGCAGC
TGGCAACCTGACTTGTATCGTCGCGATCGGAAATGAGAACAGGGGCATCTTG
AGCCCCTGCGGACGGTGCCGACAGGTGCTTCTCGATCTGCATCCTGGGATCA
AAGCCATAGTGAAGGACAGTGATGGACAGCCGACGGCAGTTGGGATTCGTG
AATTGCTGCCCTCTGGTTATGTGTGGGAGGGCTAA

A2 Plasmid maps and cloning strategies

A2-1 Plasmid map of pHD676

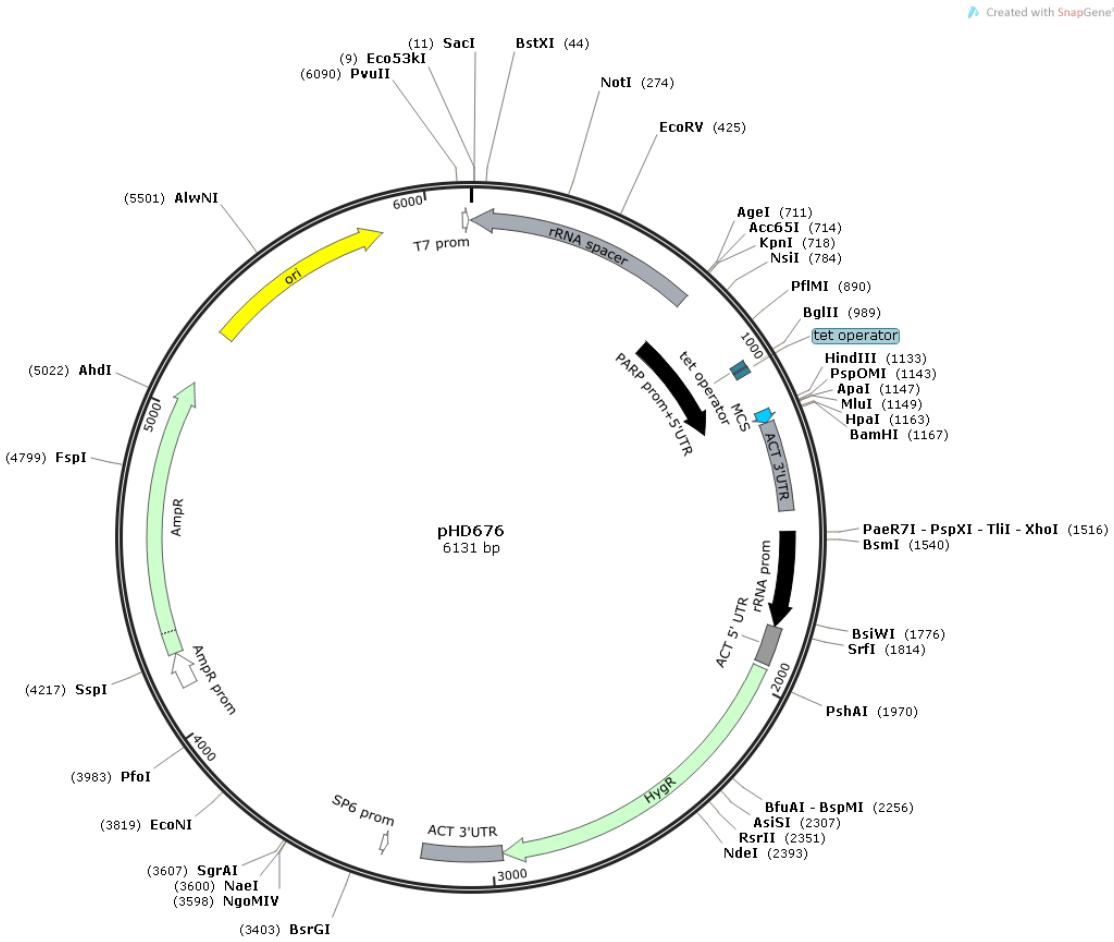

A2-2 Plasmid map of pHD677

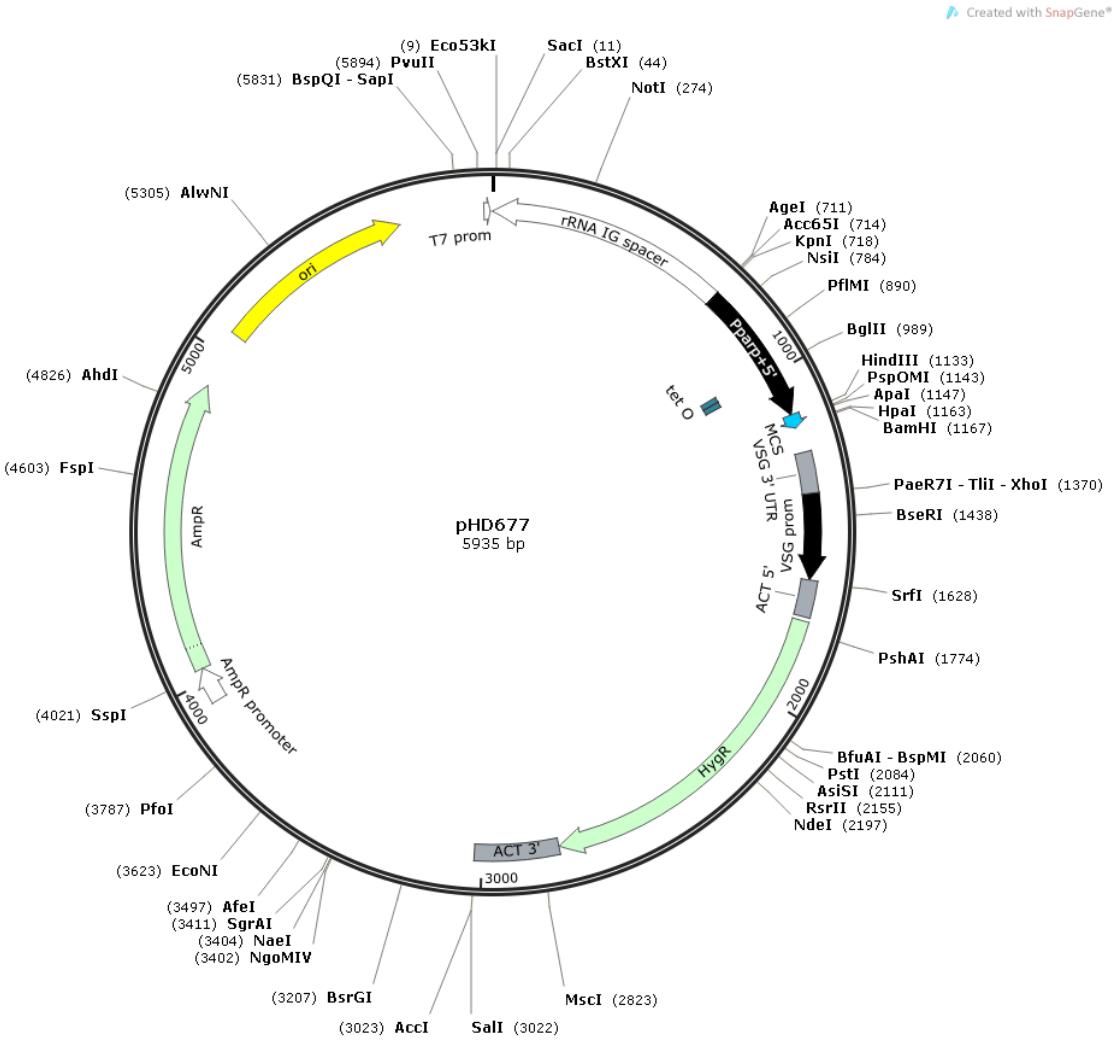

A2-3 Plasmid map of pHD678

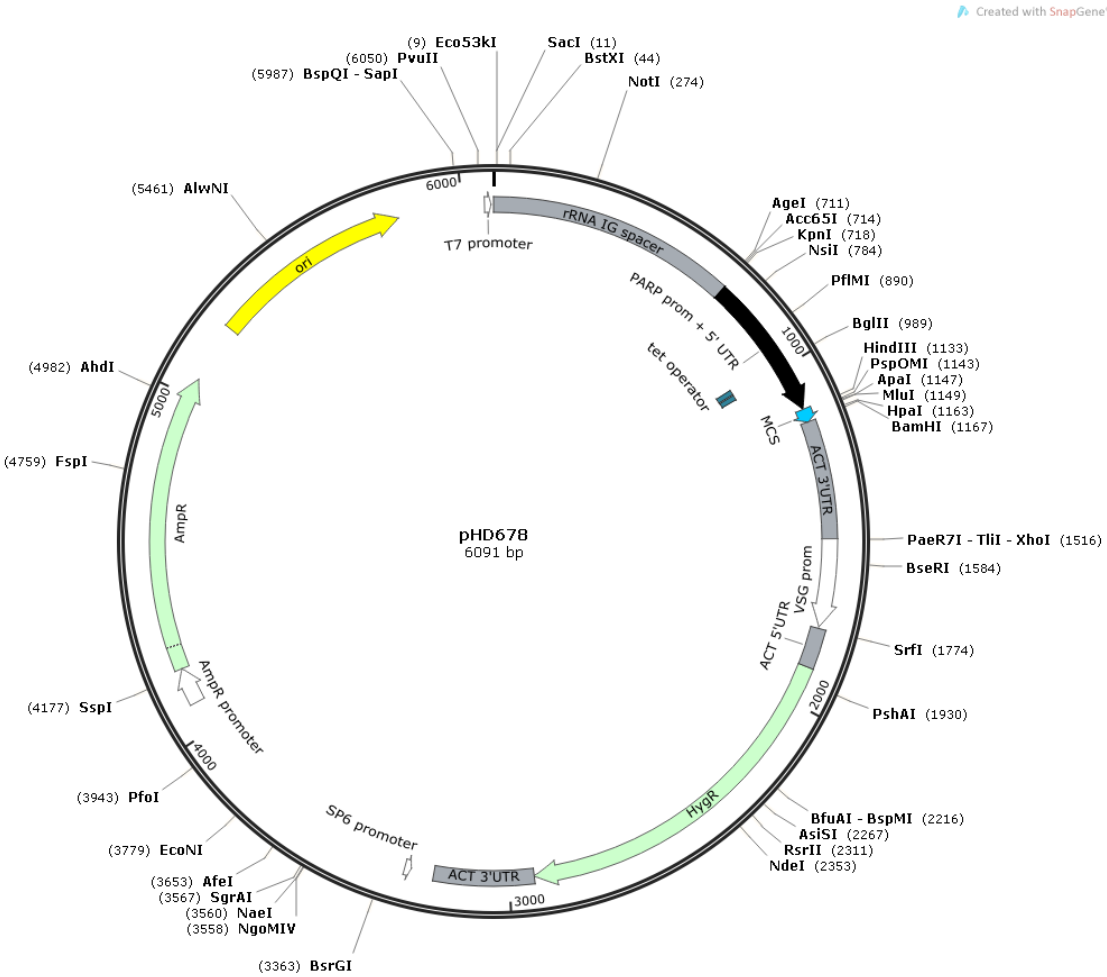

A2-4 Plasmid map of pLEW100

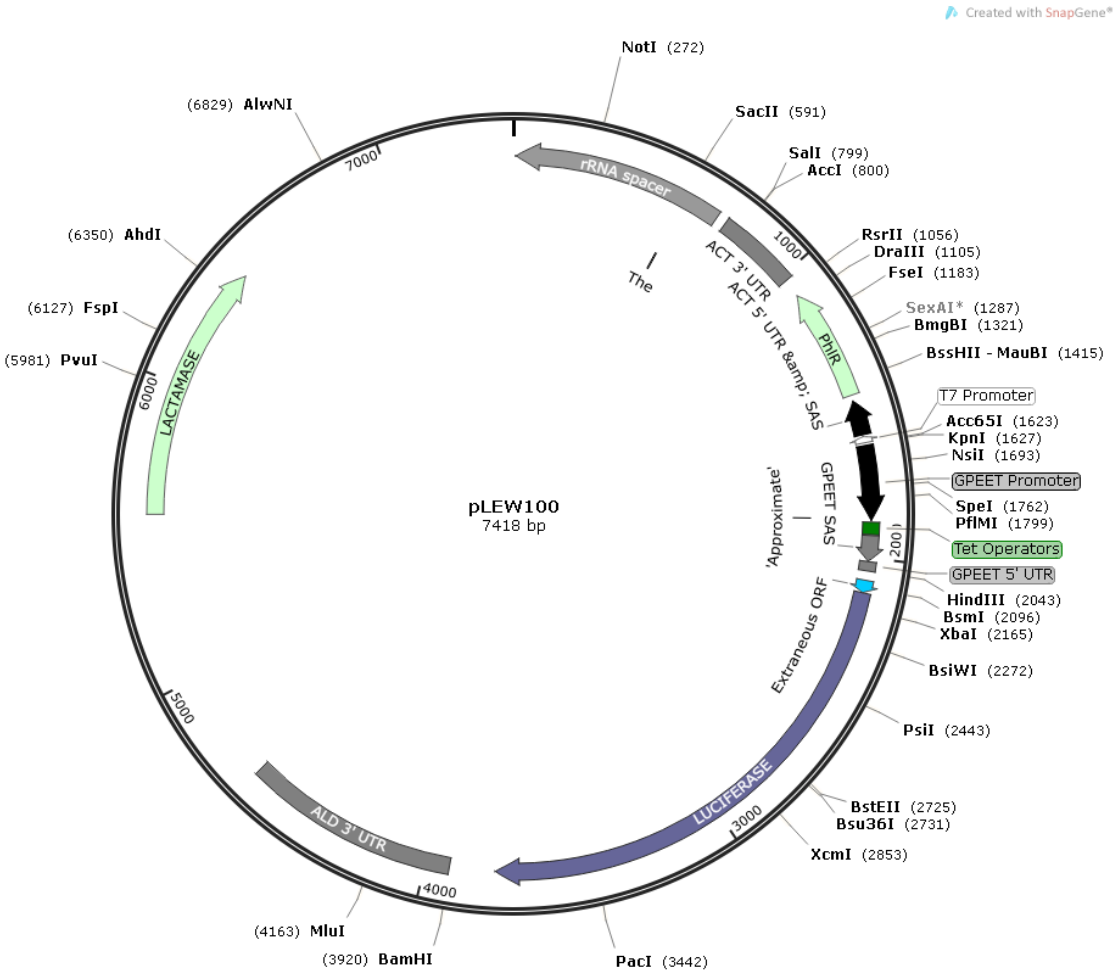

A2-5 Plasmid map of pHD1034

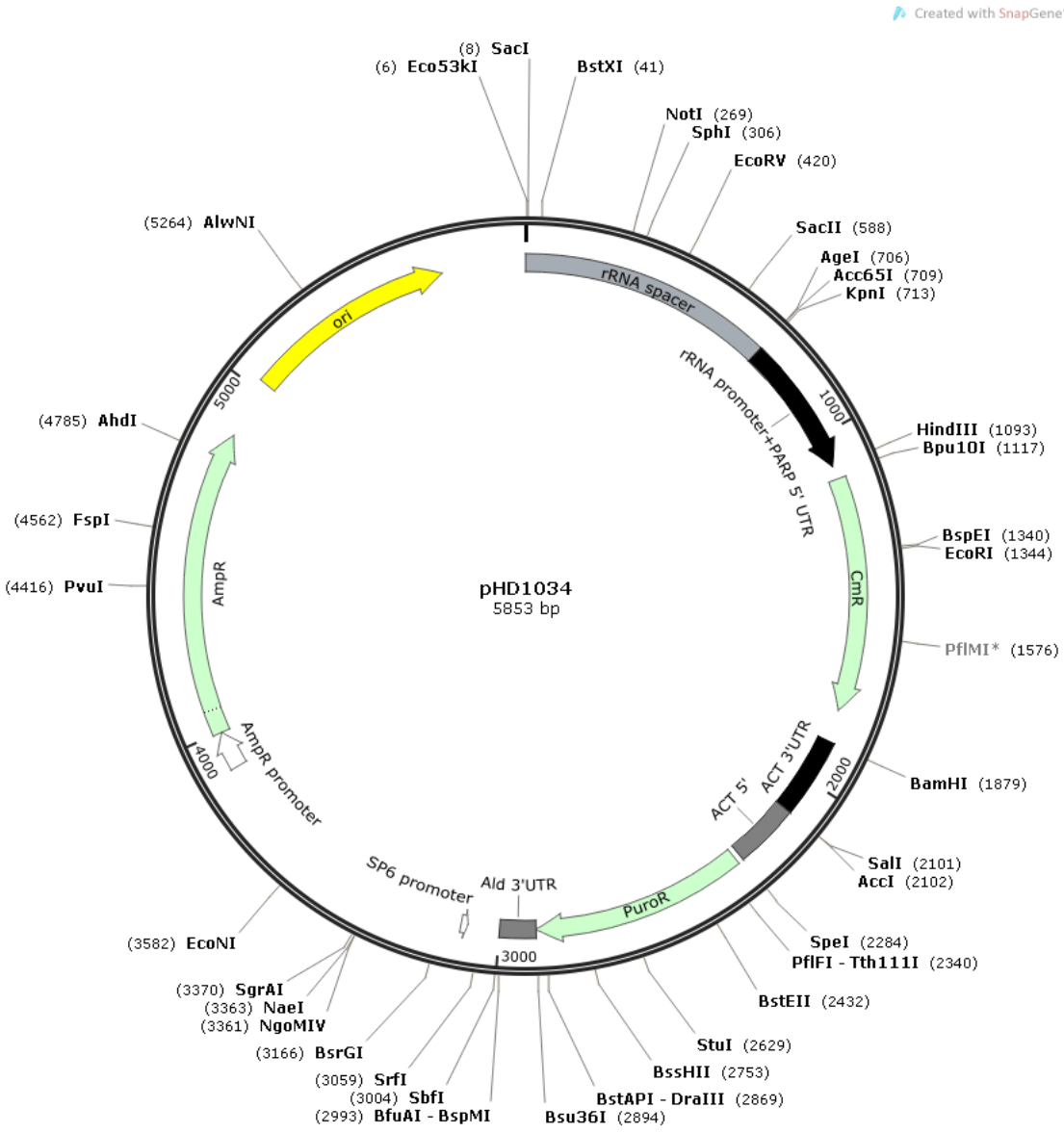

A2-6 Plasmid map of pLEW100v5BSD

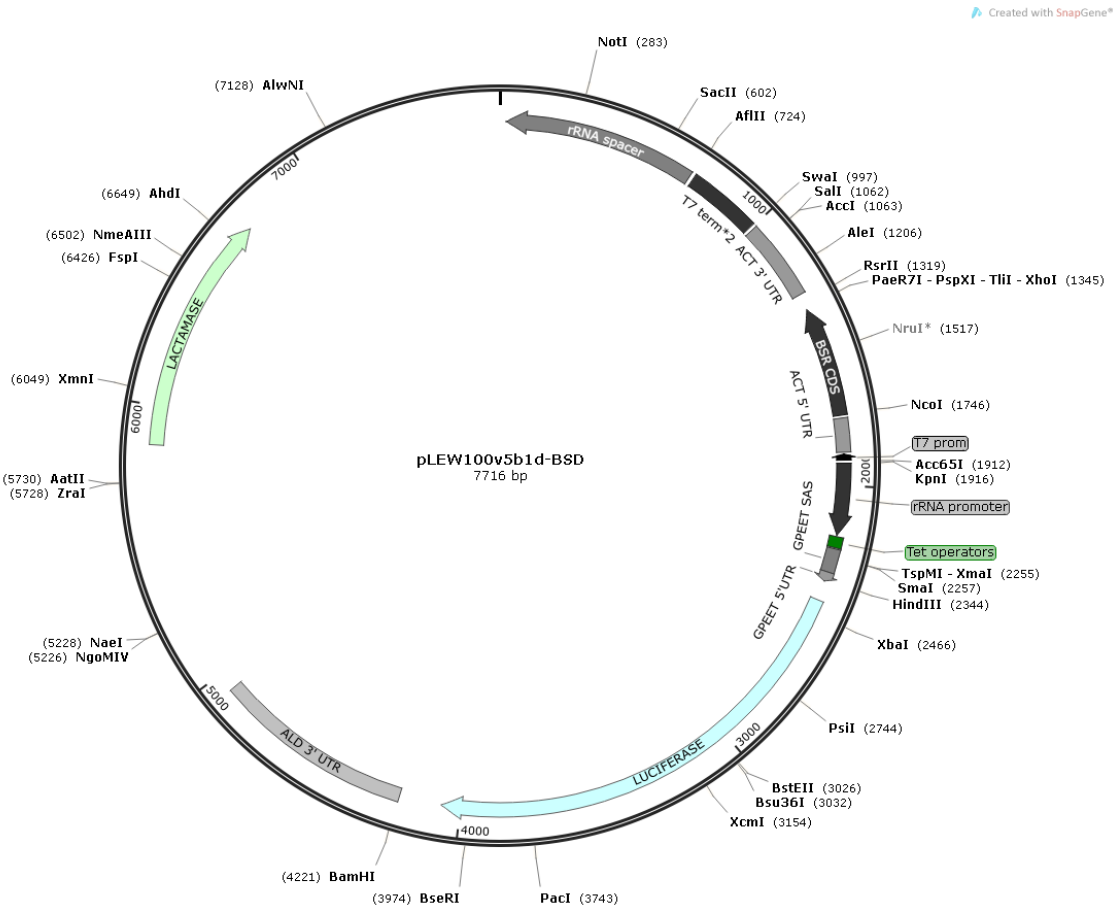

A2-7 pDrive cloning vector map (QIAGEN)

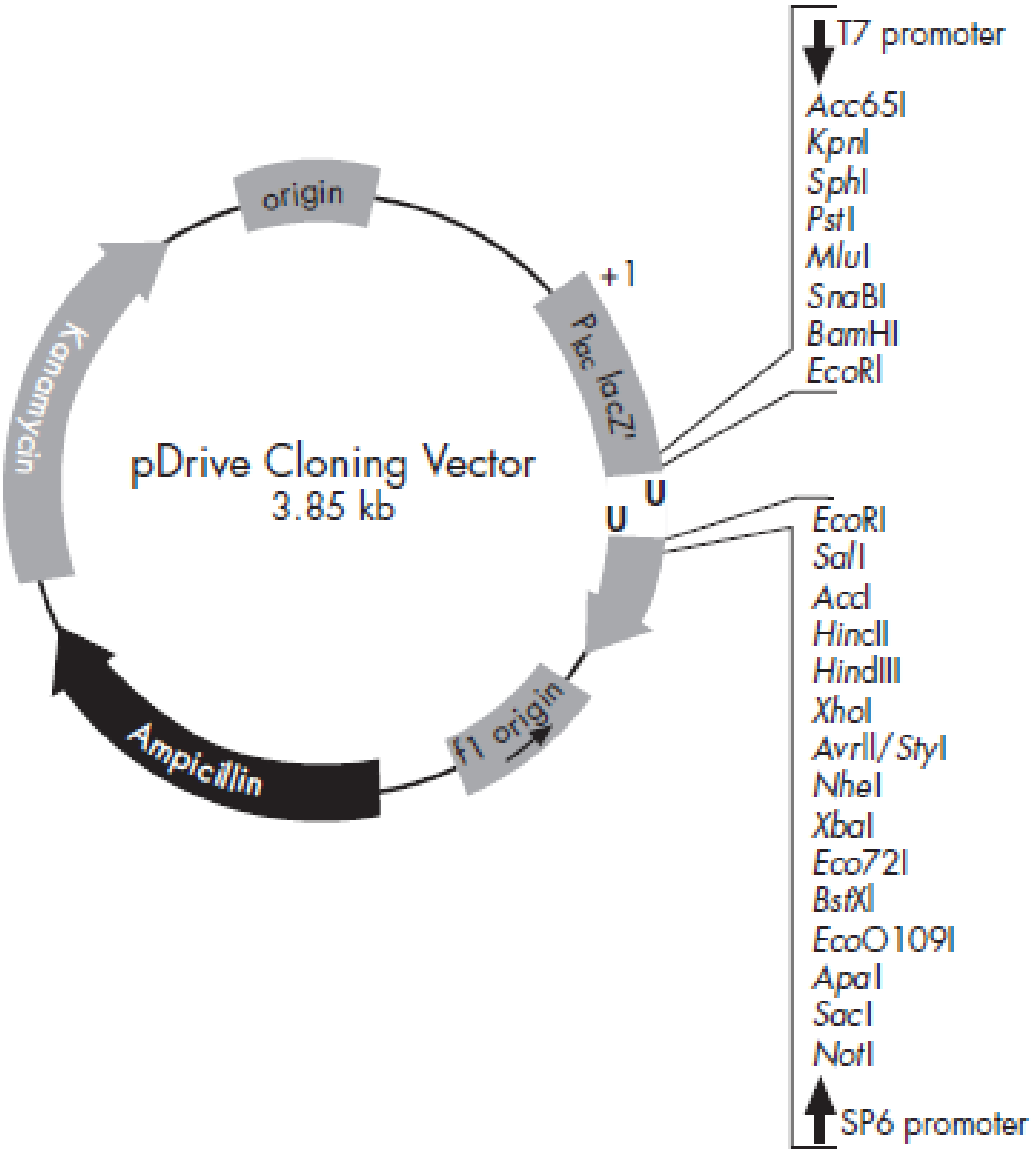

A2-8 Plasmid map of pBlueScript KS

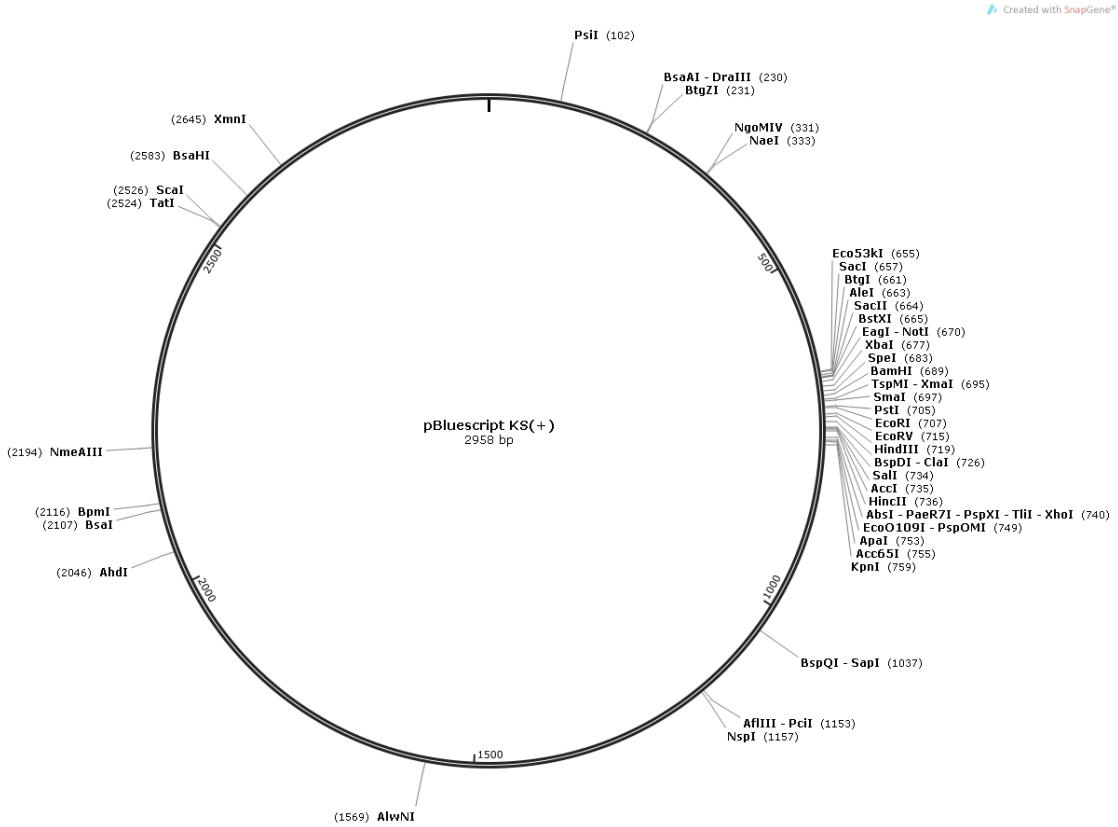

A2-9 Plasmid map of pET28a

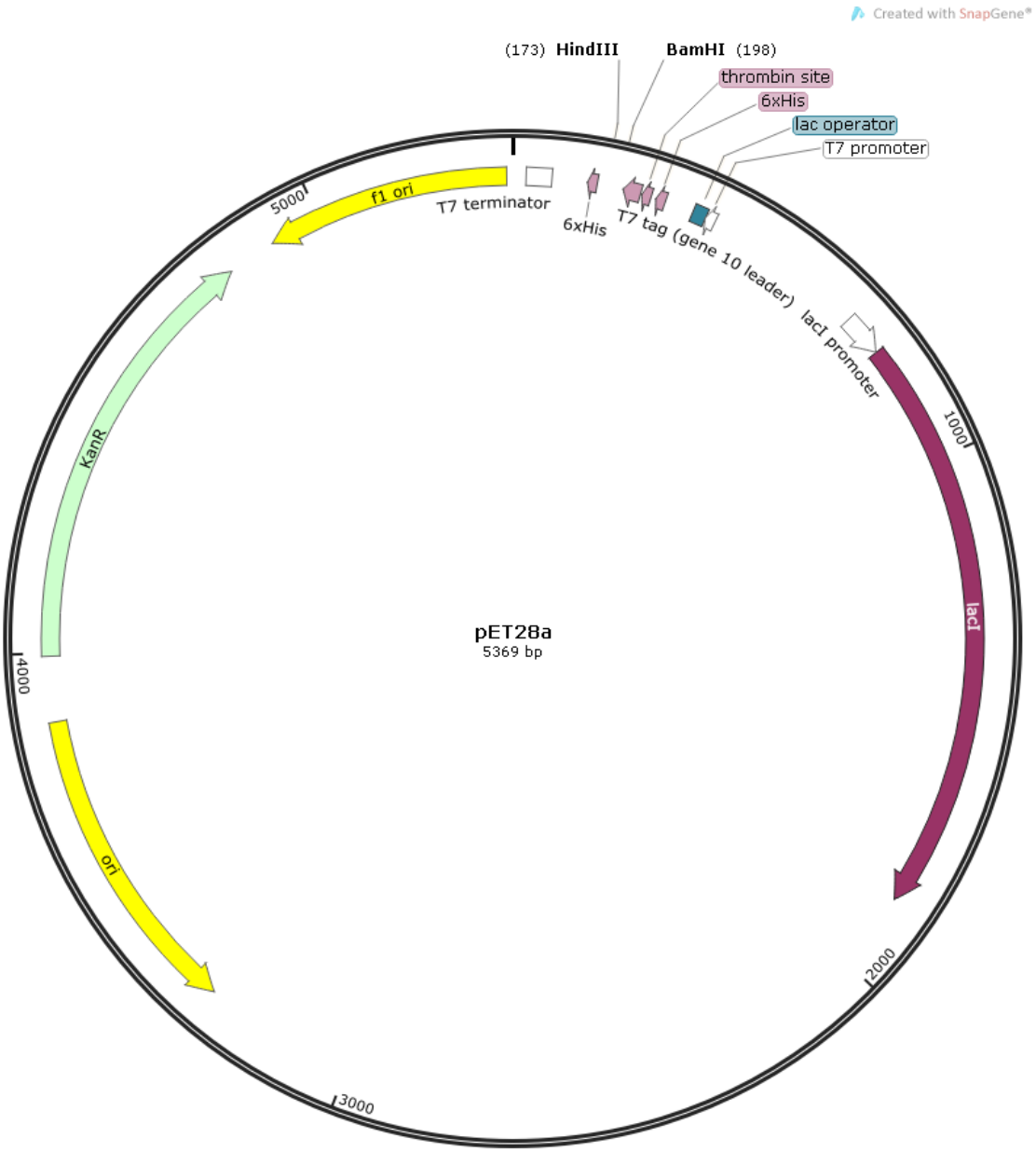

A2-10 Plasmid map of pET28a+TbMCP17

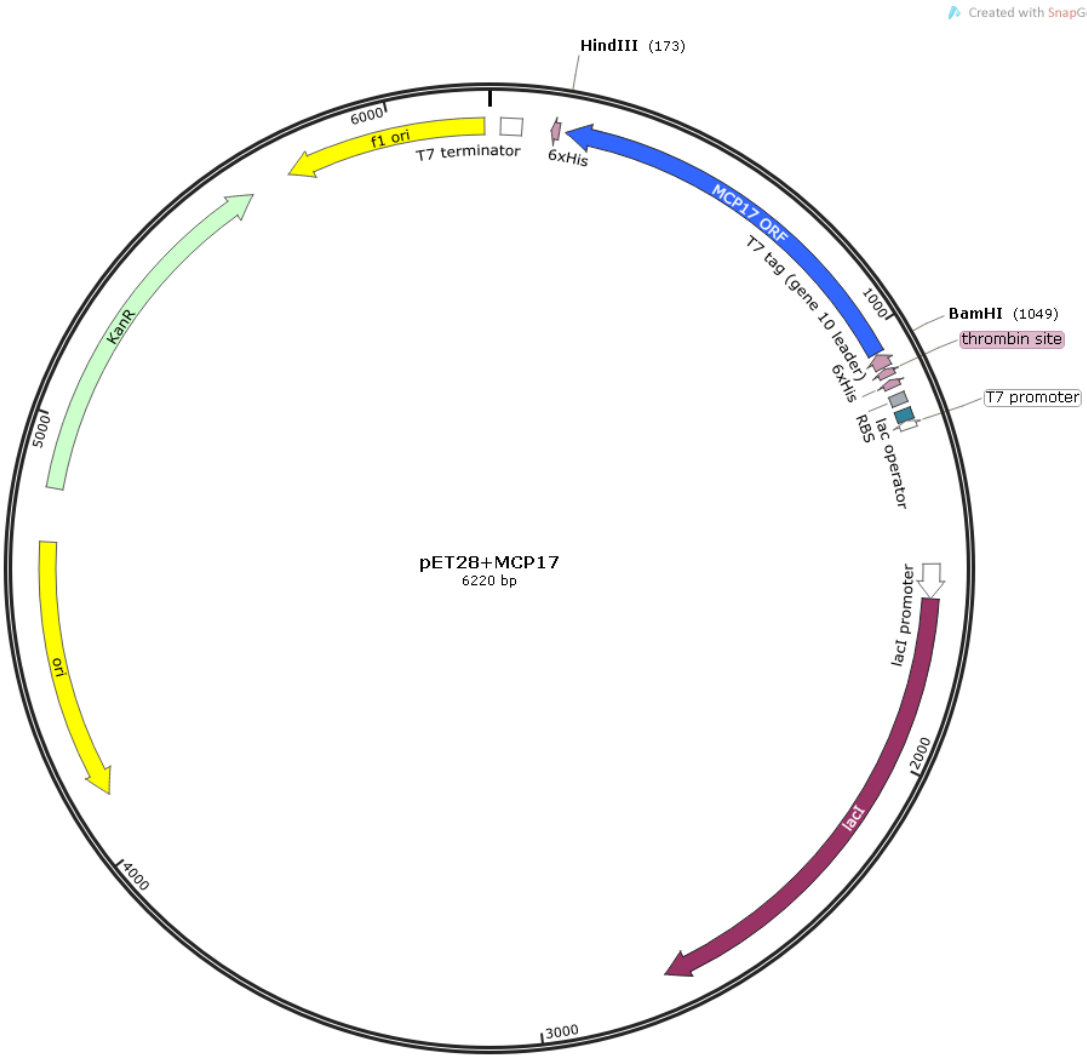

A2-11 Plasmid map of pET28a+SFXN

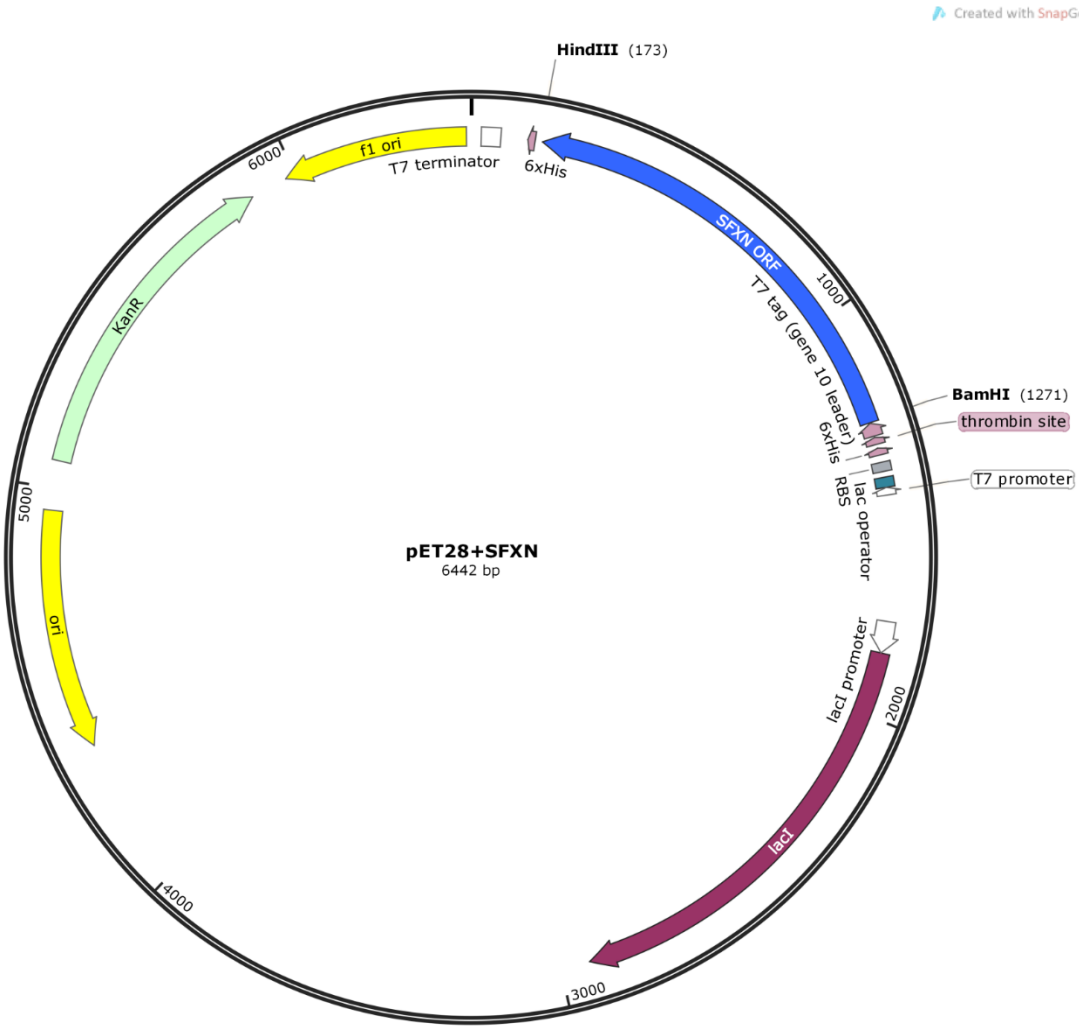

A3 Protocols

A3-1 SDM-79 media

	mM	MW	gram	vol. (ml)	product code
Dulbecco's modified Eagle medium (DMEM) powder	**Custom-made : pyridoxal, not pyridoxine**		3.50		**Gibco 23800** NOT 31600-083
Medium 199, Hank salt			1.00		Gibco 10012-037
Glucose·H_2O	5.5	198	0.55		Riedel de Haën 16301
HEPES	33.6	238.3	4.00		Gibco 11344-033
MOPS	23.9	209.3	2.50		Duchefa M1502
$NaHCO_3$	23.8	84.0	1.00		Sigma S-5761
Adenosine	0.037	267.2	0.005		Sigma A9251
Guanosine	0.035	283.2	0.005		Sigma G6752
D(+)-glucosamine HCl	0.23	215.6	0.025		Sigma G4875
Folic acid	0.009	441.4	0.002		Sigma F7876
p-Aminobenzoic acid	0.011	175.2	0.001		Sigma A0254
D(+)-biotin	0.82 µM	244.3	0.1 mg		Merck 124514
Amino-acids					
L-alanine	2.24	89.1	0.10		Merck 101007
L-arginine HCl	0.47	210.7	0.050		Sigma A5131
L-methionine	0.47	149.2	0.035		Sigma M9625
L-phenylalanine	0.48	165.2	0.040		Aldrich P1 700-8
L-proline	5.21	115.1	0.30		Sigma P0380
L-serine	0.57	105.1	0.030		Aldrich S260-0
Taurine	1.28	125.1	0.080		Sigma T0625
L-threonine	2.94	119.1	0.175		Sigma T8625

L-tyrosine	0.55	181.2	0.05		Sigma T3754
Demi-water				500	

Dissolve in ca. ½ of final volume, then add following solutions:

	mM	MW	gram	volume (ml)	product code
MEM amino acid solution 50X				4.0	Gibco 11130-036
MEM non-essent. AA solution 100X				3.0	Gibco 11140-035

Adjust to pH 7.3 using NaOH, adjust to final volume and stir for 2-3 h.

Filter sterilise (use a 0.2 μm cellulose acetate membrane-filter) and dispense in sterile flasks in usable portions (generally 5×100 ml) and store these at 4 °C.

Prior to use, add to 100 ml medium the following compounds:

	mM	MW	gram	volume (ml)	product code
Foetal bovine serum (lot. nr. 40q2021k)				11.1 (→10%)	Gibco-BRL 10270-106
Hemin stock solution				0.22	
Penicillin/Streptomycin solution (500×)				0.22	Roche 1074440

Prepare the Hemin stock solution by dissolving 0.10 g Hemin in 40 ml NaOH, 50 mM.

Stirr at least 30 minutes, filter sterilise (use a 0.2 μm cellulose acetate membrane-filter), and make aliquots of 1.1 ml in sterile eppendorfs.

Store at -20 °C.

A3-2 MEM-PROS medium

For 10 L of medium

- $CaCl_2 \cdot H_2O$ 2.65 g
- KCl 4.00 g
- $MgSO_4 \cdot 7H_2O$ 2.00 g
- NaCl 68.00 g
- $NaH_2PO_4 \cdot H_2O$ 1.40 g
- HEPES 71.40 g
- L-Arg.HCl 1.26 g
- L-Cys 0.24 g
- L-Gln 2.92 g
- L-His.HCl.H_2O 0.42 g
- L-Ile 0.52 g
- L-Leu 0.52 g
- L-Lys 0.73 g
- L-Met 0.15 g
- L-Phe 1.00 g
- L-Thr 0.48 g
- L-Trp 0.10 g
- L-Tyr 1.00 g
- L-Val 0.46 g
- L-Pro 6.00 g
- Adenosine 0.12 g
- Ornithine.HCl 0.10 g
- Phenol red 0.1 g
- MEM non-essential amino acids (100x, Sigma M-7145) 100 ml
- MEM vitamins (100x, Sigma M-6895) 100 ml

Make salt solution including HEPES in a volume of about 4 litres and adjust pH to 7.4 with NaOH. Add all the others solids and wait until dissolved. Dilute up to about 9 litres. Add the MEM solutions, make up to final volume and sterile-filter. Leave out overnight to check for contamination. Store in 450 ml aliquots at 4 °C.

Add before use:

• Heat-inactivated foetal bovine serum (Gibco-BRL #10270-106) 50 ml
(heat 30 minutes at 56°C to inactivate it, make 50-ml aliquots at –20 °C)
• Penicillin/Streptomycin solution (Sigma P-0906) 5 ml
(each vial has 20 ml containing 5000 U of penicillin and 5 mg of streptomycin in 0.9% NaCl)
• 2.5 mg/ml haemin (in 100 mM NaOH, autoclaved and stored at 4°C) 1.5 ml

A3-3 HMI-9 medium

For 5 L of medium:

Dissolve medium powder in ~3 L ultra pure water
Add 15.12 g $NaHCO_3$
Adjust pH to 7.5 with 10 M NaOH
Make volume up to 5 L
Filter sterilize and dispense 450 ml into 500-ml bottles and freeze at -20°C.

Before use, add to one bottle (500ml):

20 mM β-mercapto-ethanol	5 ml (7 µl)
150 mM L-Cysteine.HCl.H2O	5 ml (0.1317 g)
serum	50 ml
Penicillin/ Streptomycin solution	5 ml

A3-4 ZPFM and Cytomix protocol

ZPFM (Zimmerman's Post Fusion Medium):

132 mM NaCl, 8 mM KCl, 8 mM Na_2HPO_4, 1.5 mM KH_2PO_4,1.5 mM $MgAc \cdot 4H_2O$, 90 µM $Ca(OAc)_2$; pH 7.0, filter-sterilized and stored at 4 °C.

Cytomix:

EGTA p.H. 7.6	2 mM
KCl	120 mM
$CaCl_2$	0.15 mM
[1]K_2HPO_4/KH_2PO_4 p.H 7.6	10 mM
HEPES p.H 7.6	25 mM
$MgCl_2 \cdot 6H_2O$	5 mM
Glucose (Dextrose)	0.5%
BSA	100 ug/ml
[2]Hypoxanthine	1 mM

Adjust to p.H. 7.6 (KOH), filter sterilise and store at 4 ºC.

[1] Prepare 10× K_2HPO_4/KH_2PO_4 p.H 7.6 by mixing 8.66 ml 1 M K_2HPO_4 with 1.34 ml 1 M KH_2PO_4 in 90 mls H_2O.

[2] Same 100× as for HMI-9 (13.6 mg/ml in 0.1 M NaOH).

A4 Sequencing results

A4-1 *TbMCP17* double knockout constructs sequencing result

```
 Fast alignment of DNA sequences BSD53UTRMCP17T3 and TbMCP17-5pr UTR,
BSD-ORF

Upper line: BSD53UTR TbMCP17 T3, from 1 to 946
Lower line: TbMCP17-5pr UTR.txt, from 13 to 471
            BSD-ORF, from 1 to 272
5'UTR 475 bp + 214 bp + BSD 399 bp = 1088 bp
1   ............GTCGTGAGGTGGAGAGGTGATGTAAAATAATAAGAGTTGCGGAAGGGA
                ||||||||||||||||||||| |||||||||||||||||||||||||
1   CTAGAGCTCCGTGTCGTGAGGTGGAGAGGTGATGGAAAATAATAAGAGTTGCGGAAGGGA
    TbMCP17 5'UTR Sac Forward
49  GTATGTGAGGTGCACCACTTTTGGACGGTGAGATAAGCAGGGAGGAGTTTGAGGGTACTT
    ||||||||||||||||||||||||||||||||||||||||||||||||||||||||||||
61  GTATGTGAGGTGCACCACTTTTGGACGGTGAGATAAGCAGGGAGGAGTTTGAGGGTACTT

109 GTGGTACAGTACTCCCCCTCTTTTATATTTTTTTGATTTAAGGCAGTCACTTGTCCGCTA
    |||||||||||||||||||||||||||| ||||||||||||||||||||||||| ||||
121 GTGGTACAGTACTCCCCCTCTTTTATATTCTTTTGATTTAAGGCAGTCACTTGTCTGCTA

169 GCAACCCCTCTCTTTCTGTGTATATCTGTTTTTTTGTTTTATTATTGTTGGTACAGTTAC
    |||||||||||||||||||||||||||||||||||||||||||||||||||| |||||||
181 GCAACCCCTCTCTTTCTGTGTATATCTGTTTTTTTGTTTTATTATTGTTGGTGCAGTTAC

229 CCCCTTCCTTTTCTTGTCGTGGTACTGTCGCTGATGCGTCATTACCCCTCTATTTTGTTT
    ||||||||||||||||||||||||||||||||||||||||||||||||||||||||||||
241 CCCCTTCCTTTTCTTGTCGTGGTACTGTCGCTGATGCGTCATTACCCCTCTATTTTGTTT

289 CCATATGCGTCTTCACGAAAGCGTCGTCGCAGACGTTTGCATATTTTTGTCTTCCATGCA
    ||||||||||||||||||||||||||||||||||||||||||||||||||||||||||||
301 CCATATGCGTCTTCACGAAAGCGTCGTCGCAGACGTTTGCATATTTTTGTCTTCCATGCA

349 CCACTCCACGTTCATTTCTTGCCTCTGTTCATCTTTTCTTTTTTTTTCTTTTCTCTCGCT
    |||||||||||||||||||||||||||||||||||| ||||||||||||||||||||||
361 CCACTCCACGTTCATTTCTTGCCTCTGTTCATCTTTTC.TTTTTTTTCTTTTCTCTCGCT

409 CGTTCCCCGTGTTGCCGTTGTTTTGCTTGGCTGCGGTGATGTGTGACTAGTGGTAATGAA
    ||||||||||||||||||||||||||||||||||||||||||||||||||||
420 CGTTCCCCGTGTTGCCGTTGTTTTGCTTGGCTGCGGTGATGTGTGACTAGT
                  TbMCP17 3'UTR Spe Reverse
469 GATGCTCGAGCCCGGGCACAGCAAGGTCTTCTGAAATTCATGTTTTTTTTTTTTTTACTC


529 TGCATTGCAGCCTCCGCTCTTATTTAGTTTTGCTTTACGTAAGGTCTCGTTGCTGCCATA


589 AAATAAGCTCTAGAACTGTGTTGACAATTAATCATCGGCATAGTATATCGGCATAGTATA


649 ATACGACAAGGTGAGGAACTAAACCATGGCCAAGCCTTTGTCCCAAGAAGAATCCACCCT
                            |||||||||||||||| ||||||||||||||||
```

```
1    ........................ATGGCCAAGCCTTTGTCTCAAGAAGAATCCACCCT
                              BSD Forward primer
709  CATTGAAAGAGCAACGGCTACAATCAACAGCATCCCCATCTCTGAAGACTACAGCGTCG
     ||||||||||||||||||||||||||||||||||||||||||||||||||||||||||||
36   CATTGAAAGAGCAACGGCTACAATCAACAGCATCCCCATCTCTGAAGACTACAGCGTCG

769  CCAGCGCAGCTCTCTCTAGCGACGGCCGCATCTTCACTGGTGTCAATGTATATCATTTTA
     ||||||||||||||||||||||||||||||||||||||||||||||||||||||||||||
96   CCAGCGCAGCTCTCTCTAGCGACGGCCGCATCTTCACTGGTGTCAATGTATATCATTTTA

829  CTGGGGGACCTTGTGCAGAACTCGTGGTGCTGGGCACTGCTGCTGCTGCGGCAGCTGGC.
     ||||||||||||||||||||||||||||||||||||||||||||||||||||||||||||
156  CTGGGGGACCTTGTGCAGAACTCGTGGTGCTGGGCACTGCTGCTGCTGCGGCAGCTGGCA

889  ACCTGACTTGTATCGTCGCGATCGGAAATGAG.ACAGGGGCATCTTGAG.CCCTGCGA
     |||||||||||||||||||||||||||||| ||||||||||||||| |||||||
216  ACCTGACTTGTATCGTCGCGATCGGAAATGAGAACAGGGGCATCTTGAGCCCCTGCGG
```

```
Fast alignment of DNA sequences RC-BSD53UTR TbMCP17 T7 and TbMCP17-3pr
UTR.txt

Ktuple=2 Gap_open=2 Gap_extend=1

Upper line: RC-BSD53UTR TbMCP17 T7, from 320 to 810
Lower line: TbMCP17-3pr UTR.txt, from 5 to 490

RC-BSD53UTR TbMCP17 T7: TbMCP17-3pr UTR.txt identity= 98.57%(483/490)
gap=1.80%(9/499)

316  GCTAGGATCCCCGTGTTCTTGTTTCAGGTGTGAACCCCGGAGTTATCAATATGAGAAGGG
     ||  |||||||||||||||||||||||||||||||||| |||||||||||||||||||
1    GCATGGATCCCCGTGTTCTTGTTTCAGGTGTGAACCCCGGGGTTATCAATATGAGAAGGG
     TbMCP17 3'UTR BamHI Forward primer

376  TGCATGTGATGCAGTGGGTGGAAAGCTTTTCACTATTTCCAGTAATAACCGCTGTCGAGT
     |||||||||||||||||||||||||||||||||||||||||||||||||||||||||| |
61   TGCATGTGATGCAGTGGGTGGAAAGCTTTTCACTATTTCCAGTAATAACCGCTGTCGATT

436  TCACTTTTTTTTTCATTTTGTTGAGGAAGGGGTTTACAATTCACCATATGGACGGTGTCG
     ||||     ||||||||||||||||||||||||||||||||||||||||||||||||||||
121  TCAC.....TTTTCATTTTGTTGAGGAAGGGGTTTACAATTCACCATATGGACGGTGTCG

496  GAAGTGATGATGAAACCAGCTGATACACTTCCCTTTATTACAAAAAAAAA..AGGTTTTA
     ||||||||||||||||||||||||||||||||||||||||||||||||  ||||||||
176  GAAGTGATGATGAAACCAGCTGATACACTTCCCTTTATTACAAAAAAAAAAGAGGTTTTA

554  TTTTTGTACGGTTAGCGCAGAACACACAGGTATAACCATCGGTATCGTCTTTGGTAGTCT
     ||||||||||||||||||||||||||||||||||||||||||||||||||||||||||||
236  TTTTTGTACGGTTAGCGCAGAACACACAGGTATAACCATCGGTATCGTCTTTGGTAGTCT

614  GCGAATATACTTTTTTCCTTTTTTAAACACAGGATTCATAAACGGGTAAGAGCCAGACAG
     ||||||||||||||||||||||||||||||||||||||||||||||||||||||||||||
296  GCGAATATACTTTTTTCCTTTTTTAAACACAGGATTCATAAACGGGTAAGAGCCAGACAG

674  TGGCTGACAAGGGTGTTAGGGGCCTTACATTGTAAACTTATCTGTATTTTTTTTTTTTTC
     ||||||||||||||||||||||||||||||||||||||||||||  |||||||||| |
356  TGGCTGACAAGGGTGTTAGGGGCCTTACATTGTAAACTTATCTGTA..TTTTTTTTTTCC

734  CCCGTAGACCTCTTATGTCTCATTCTTGTCAGTAGCCGCTTCCCTTCCCGCTCCAGTAAT
     ||||||||||||||||||||||||||||||||||||||||||||||||||||||||||||
414  CCCGTAGACCTCTTATGTCTCATTCTTGTCAGTAGCCGCTTCCCTTCCCGCTCCAGTAAT

794  GTGTTTGACGGGCCCAGAATCGAATTCCCGCGGCCGCCATGGCGGCCGGGAGCATGCGAC
     |||||||||||||||| |
474  GTGTTTGACGGGCCCATAG
     TbMCP17 3'UTR ApaI Reverse primer
```

```
Fast alignment of DNA sequences NEO53UTR TbMCP17 T3 and TbMCP17-5pr
UTR.xdna

Ktuple=2 Gap_open=2 Gap_extend=1

Upper line: NEO53UTR TbMCP17 T3, from 1 to 470
Lower line: TbMCP17-5pr UTR.xdna, from 18 to 464

NEO53UTRMCP17T3:   TbMCP17-5pr   UTR.xdna   identity=   93.58%(452/483)
gap=3.59%(18/501)
1   ..................GAGGTGGAGAGGTGATGTAAAATAATAAGAGTTGCGGAAGGGA
                       |||||||||||||||| |||||||||||||||||||||||||
1   CTAGAGCTCCGTGTCGTGAGGTGGAGAGGTGATGGAAAATAATAAGAGTTGCGGAAGGGA
    TbMCP17 5'UTR SacI Forward primer

44  GTATGTGAGGTGCACCACTTTTGGACGGTGAGATAAGCAGGGAGGAGTTTGAGGGTACTT
    ||||||||||||||||||||||||||||||||||||||||||||||||||||||||||||
61  GTATGTGAGGTGCACCACTTTTGGACGGTGAGATAAGCAGGGAGGAGTTTGAGGGTACTT

104 GTGGTACAGTACTCCCCCTCTTTTATATTTTTTTGATTTAAGGCAGTCACTTGTCCGCTA
    |||||||||||||||||||||||||||| ||||||||||||||||||||||||| ||||
121 GTGGTACAGTACTCCCCCTCTTTTATATTCTTTTGATTTAAGGCAGTCACTTGTCTGCTA

164 GCAACCCCTCTCTTTCTGTGTATATCTGTTTTTTTGTTTTATTATTGTTGGTACAGTTAC
    |||||||||||||||||||||||||||||||||||||||||||||||||||||| |||||||
181 GCAACCCCTCTCTTTCTGTGTATATCTGTTTTTTTGTTTTATTATTGTTGGTGCAGTTAC

224 CCCCTTCCTTTTCTTGTCGTGGTACTGTCGCTGATGCGTCATTACCCCTCTATTTTGTTT
    ||||||||||||||||||||||||||||||||||||||||||||||||||||||||||||
241 CCCCTTCCTTTTCTTGTCGTGGTACTGTCGCTGATGCGTCATTACCCCTCTATTTTGTTT

284 CCATATGCGTCTTCACGAAAGCGTCGTCGCAGACGTTTGCATATTTTTGTCTTCCATGCA
    ||||||||||||||||||||||||||||||||||||||||||||||||||||||||||||
301 CCATATGCGTCTTCACGAAAGCGTCGTCGCAGACGTTTGCATATTTTTGTCTTCCATGCA

344 CCACTCCACGTTCATTTCTTGCCTCTGTTCATCTTTTCTTTTTTTTTCTTTTCTCTCGCT
    |||||||||||||||||||||||||||||||||||| ||||||||||||||||||||||
361 CCACTCCACGTTCATTTCTTGCCTCTGTTCATCTTTTC.TTTTTTTTCTTTTCTCTCGCT

404 CGTTCCCCGTGTTGCCGTTGTTTTGCTTGGCTGCGGTGATGTGTGACTAGTGGTAATGAA
    ||||||||||||||||||||||||||||||||||||||||||||||||||||||||||||
420 CGTTCCCCGTGTTGCCGTTGTTTTGCTTGGCTGCGGTGATGTGTGACTAGTTAGC

464 GATGCTCGAGCCCGGGCACAGCAAGGTCTTCTGAAATTCATGTTTTTTTTTTTTTTACTC

524 TGCATTGCAGCCTCCGCTCTTATTTAGTTTTGCTTTACGTAAGGTCTCGTTGCTGCCATA

584 AAATAAGCTCTAGAACTAGATACCAACAAGCCCGAAAACAGATACTCAACTGCAACGAAG

644 CTTACAGGAGAAAGAATAGTAACCCTTTCATCAAGAAAATAGTTCAAACGAATTATGCGC

704 GAAATCGTCTGCGTTCAGCTGGCCAATGCGGTAACCAGATCGGCTCAAAGTTCTGGGAGG

764 TGATCCGGCCAAGCTTGGATGGATTGCACGCAGGTTCTCCGGCCGCTTG
                       |||||||||||||||||||||||||||||||
                     GATGGATTGCACGCAGGTTCTCCGGCCGCTTG
                     Neo full length Forward primer

326 bp in between 5'UTR and NEO full length gene.
```

```
Fast alignment of DNA sequences RC-NEO53UTR TbMCP17 T7 and NEO-ORF,
TbMCP17-3pr UTR.txt
13 bp in between NEO and 3'UTR
Upper line: RC-NEO53UTR TbMCP17 T7, from 1 to 377
Lower line: NEO-ORF, from 61 to 438
Lower line: MCP17-3pr UTR.txt, from 5 to 476

RC-NEO53UTR TbMCP17 T7: NEO-ORF identity= 100.00%(377/377)
gap=0.26%(1/378)
RC-NEO53UTR TbMCP17 T7: TbMCP17-3pr UTR.txt identity= 98.73%(468/474)
gap=1.86%(9/483)

1    CGCATCGAGCGAGCACGTACTCGGATGGAAGCCGGTC.TGTCGATCAGGATGATCTGGAC
     |||||||||||||||||||||||||||||||||||||| ||||||||||||||||||||||
61   CGCATCGAGCGAGCACGTACTCGGATGGAAGCCGGTCTTGTCGATCAGGATGATCTGGAC

60   GAAGAGCATCAGGGGCTCGCGCCAGCCGAACTGTTCGCCAGGCTCAAGGCGCGCATGCCC
     ||||||||||||||||||||||||||||||||||||||||||||||||||||||||||||||
121  GAAGAGCATCAGGGGCTCGCGCCAGCCGAACTGTTCGCCAGGCTCAAGGCGCGCATGCCC

120  GACGGCGAGGATCTCGTCGTGACCCATGGCGATGCCTGCTTGCCGAATATCATGGTGGAA
     ||||||||||||||||||||||||||||||||||||||||||||||||||||||||||||||
181  GACGGCGAGGATCTCGTCGTGACCCATGGCGATGCCTGCTTGCCGAATATCATGGTGGAA

180  AATGGCCGCTTTTCTGGATTCATCGACTGTGGCCGGCTGGGTGTGGCGGACCGCTATCAG
     ||||||||||||||||||||||||||||||||||||||||||||||||||||||||||||||
241  AATGGCCGCTTTTCTGGATTCATCGACTGTGGCCGGCTGGGTGTGGCGGACCGCTATCAG

240  GACATAGCGTTGGCTACCCGTGATATTGCTGAAGAGCTTGGCGGCGAATGGGCTGACCGC
     ||||||||||||||||||||||||||||||||||||||||||||||||||||||||||||||
301  GACATAGCGTTGGCTACCCGTGATATTGCTGAAGAGCTTGGCGGCGAATGGGCTGACCGC

300  TTCCTCGTGCTTTACGGTATCGCCGCTCCCGATTCGCAGCGCATCGCCTTCTATCGCCTT
     ||||||||||||||||||||||||||||||||||||||||||||||||||||||||||||||
361  TTCCTCGTGCTTTACGGTATCGCCGCTCCCGATTCGCAGCGCATCGCCTTCTATCGCCTT
                                                 Neo Reverse primer

360  CTTGACGAGTTCTTCTGAGCGGGACTCTGGGGTTCGGATCCCCGTGTTCTTGTTTCAGGT
     ||||||||||||||||||              |   ||||||||||||||||||||||||||
421  CTTGACGAGTTCTTCTGA         1   GCATGGATCCCCGTGTTCTTGTTTCAGGT
                                  TbMCP17 3'UTR BamHI Forward primer

420  GTGAACCCCGGAGTTATCAATATGAGAAGGGTGCATGTGATGCAGTGGGTGGAAAGCTTT
     |||||||||| |||||||||||||||||||||||||||||||||||||||||||||||||||
30   GTGAACCCCGGGGTTATCAATATGAGAAGGGTGCATGTGATGCAGTGGGTGGAAAGCTTT

480  TCACTATTTCCAGTAATAACCGCTGTCGAGTTCACTTTTTTTTTCATTTTGTTGAGGAAG
     |||||||||||||||||||||||||||||| |||||     ||||||||||||||||||||
90   TCACTATTTCCAGTAATAACCGCTGTCGATTTCAC.....TTTTCATTTTGTTGAGGAAG

540  GGGTTTACAATTCACCATATGGACGGTGTCGGAAGTGATGATGAAACCAGCTGATACACT
     ||||||||||||||||||||||||||||||||||||||||||||||||||||||||||||||
150  GGGTTTACAATTCACCATATGGACGGTGTCGGAAGTGATGATGAAACCAGCTGATACACT

600  TCCCTTTATTACAAAAAAAAA..AGGTTTTATTTTTGTACGGTTAGCGCAGAACACACAG
     ||||||||||||||||||||  |||||||||||||||||||||||||||||||||||||||
210  TCCCTTTATTACAAAAAAAAAAGAGGTTTTATTTTTGTACGGTTAGCGCAGAACACACAG

660  GTATAACCATCGGTATCGTCTTTGGTAGTCTGCGAATATACTTTTTTCCTTTTTTAAACA
     ||||||||||||||||||||||||||||||||||||||||||||||||||||||||||||||
270  GTATAACCATCGGTATCGTCTTTGGTAGTCTGCGAATATACTTTTTTCCTTTTTTAAACA
```

```
720  CAGGATTCATAAACGGGTAAGAGCCAGACAGTGGCTGACAAGGGTGTTAGGGGCCTTACA
     ||||||||||||||||||||||||||||||||||||||||||||||||||||||||||||
330  CAGGATTCATAAACGGGTAAGAGCCAGACAGTGGCTGACAAGGGTGTTAGGGGCCTTACA

780  TTGTAAACTTATCTGTATTTTTTTTTTTTTCCCCGTAGACCTCTTATGTCTCATTCTTGT
     ||||||||||||||||  ||||||||||  ||||||||||||||||||||||||||||||
390  TTGTAAACTTATCTGTA..TTTTTTTTTTCCCCCGTAGACCTCTTATGTCTCATTCTTGT

840  CAGTAGCCGCTTCCCTTCCCGCTCCAGTAATGTG
     ||||||||||||||||||||||||||||||||||
450  CAGTAGCCGCTTCCCTTCCCGCTCCAGTAATGTGTTTGACGGGCCCATAG
                      TbMCP17 3'UTR ApaI Reverse primer
```

A4-2 pGEM T easy+*MCP17* ORF constructs: sequencing result

```
Fast alignment of DNA sequences MCP17ORF-BH.txt and pGemMCP17ORFBH1T7-insert only

Ktuple=2 Gap_open=2 Gap_extend=1

Upper line: MCP17ORF-BH.txt, from 1 to 886
Lower line: pGemMCP17ORFBH1T7-insert only, from 1 to 887

MCP17ORF-BH.txt:pGemMCP17ORFBH1T7-insert only identity= 99.44%(881/886) gap=0.11%(1/887)
1   GAGGATCCATGGTTTCCGAGGGCACTTCCGCTGCAGGTCGCCTGGAGGGCGAGTCGCCGC
    ||||||||||||||||||||||||||||||||||||||||||||||||||||||||||||
1   GAGGATCCATGGTTTCCGAGGGCACTTCCGCTGCAGGTCGCCTGGAGGGCGAGTCGCCGC

61  TTGCGCTGCGCGTCGATACTGGCGAAATTGTCGCGGGATGCCTCGCCGGTTTTGTGGAAC
    ||||||||||||||||||||||||||||||||||||||||||||||||||||||||||||
61  TTGCGCTGCGCGTCGATACTGGCGAAATTGTCGCGGGATGCCTCGCCGGTTTTGTGGAAC

121 ATTTCTTTATGTTCCCGTTTGACACTTTGAAGACACGGGTTCAGAGTGGGGACTCGACGA
    ||||||||||||||||||||||||||||||||||||||||||||||||||||||||||||
121 ATTTCTTTATGTTCCCGTTTGACACTTTGAAGACACGGGTTCAGAGTGGGGACTCGACGA

181 ATGTCATATTAGCGGCAAAGCGTATTTCGCGGAATGAGCGACTTGCACATCTTTACCGCG
    ||||||||||||||||||||||||||||||||||||||||||||||||||||||||||||
181 ATGTCATATTAGCGGCAAAGCGTATTTCGCGGAATGAGCGACTTGCACATCTTTACCGCG

241 GATTCGCGCCCATCATCGTTTCTGCCGTTCCAGCGCATGGTGCATATTACAGCACATATG
    |||||||||||||||| ||||||||||||||||||||||||||||||||||||||||||
241 GATTCGCGCCCATCATTGTTTCTGCCGTTCCAGCGCATGGTGCATATTACAGCACATATG

301 AGGCTGCGAAGCGTGTCTTTGGTGAGGATTCCACAGTGTCTATAACGGTCTCTGCCAGTT
    ||||||||||||||||||||||||||||||||||||||||||||||||||||||||||||
301 AGGCTGCGAAGCGTGTCTTTGGTGAGGATTCCACAGTGTCTATAACGGTCTCTGCCAGTT

361 GTGCGGTCGCTGCTCATGACACCATTTCCACCCCATTTGATGTTATCAAGCAGCGGATGC
    ||||||||||||||||||||||||||||||||||||||||||||||||||||||||||||
361 GTGCGGTCGCTGCTCATGACACCATTTCCACCCCATTTGATGTTATCAAGCAGCGGATGC

421 AGATGGACGGGAGCCGGAAGTTTGCTTCATCGCTTCAGTGTGGTCAATGTGCAGTTGCGG
    |||||||||||||||||||||||| ||||||||||||||||||||||||||||||||||
421 AGATGGACGGGAGCCGGAAGTTTGCCTCATCGCTTCAGTGTGGTCAATGTGCAGTTGCGG

481 AAGGGGGCGTGCGGTGCCTTCTCCTCTCTTTGCCCACCACTATTTTAATGAACATTCCAC
    ||||||||||||||||||||||||||||||||||||||||||||||||||||||||||||
481 AAGGGGGCGTGCGGTGCCTTCTCCTCTCTTTGCCCACCACTATTTTAATGAACATTCCAC

541 ATTTCTCAGCCTACTGGTTAGTTTATGAGGGGTTTCTTGCATACTTGGGTGGTGAGCGGC
    ||||||||||||||||||||||||||||||||||||||||||||||||||||||||||||
541 ATTTCTCAGCCTACTGGTTAGTTTATGAGGGGTTTCTTGCATACTTGGGTGGTGAGCGGC

601 GCAATAGGGAAACGGAAGTTGCGGGAGATTACATAACCGGGGGCCTCCTGGCAGGCACTG
    |||||||||||||||||||||||||||||||||||||||||||||||||||||||||| ||
601 GCAATAGGGAAACGGAAGTTGCGGGAGATTACATAACCGGGGGCCTCCTGGCAGGCAGTG

661 TGGCTTCTATTGTCTCGTCACCGTTAGACGTTGTAAAGACTCAGCTGCAACTCGGTCTTA
    ||||||||||||||||||||||||||||||||||||||||||||||||||||||||||||
661 TGGCTTCTATTGTCTCGTCACCGTTAGACGTTGTAAAGACTCAGCTGCAACTCGGTCTTA

721 GAAAGAATATCCCCGATGCGGTGCGCTATGTCTTAGTCAATCGTGGCACCAAAGGTTTCT
    |||||||||||||| ||||||||||||||||||||||||||||||||||||||||||||
721 GAAAGAATATCCCTGATGCGGTGCGCTATGTCTTAGTCAATCGTGGCACCAAAGGTTTCT

781 TTGCCGGGGTTACGGCGAGAGTTATGTGTACCGCTCCTGCTGGTGCCCTGTCAATGATCA
    ||||||| ||||||||||||||||||||||||||||||||||||||||||||||||||||
781 TTGCCGGAGTTACGGCGAGAGTTATGTGTACCGCTCCTGCTGGTGCCCTGTCAATGATCA

841 CATATGAAAC.GGCCAAGAAGTTCATGGAGGAACGGTAAAAGCTTCG
    |||||||||| ||||||||||||||||||||||||||||||||||
841 CATATGAAACGGGCCAAGAAGTTCATGGAGGAACGGTAAAAGCTTCG
```

A4-3 pCM190+MCP17 and MCP17-Myc sequencing result

```
Upper line: TbMCP17; Lower line: TbMCP17-full transcript. Identity=
99.43%
      BamH I
1   GAGGATCCATGGTTTCCGAGGGCACTTCCGCTGCAGGTCGCCTGGAGGGCGAGTCGCCGC
           ||||||||||||||||||||||||||||||||||||||||||||||||||||||||
1   ........ATGGTTTCCGAGGGCACTTCCGCTGCAGGTCGCCTGGAGGGCGAGTCGCCGC

61  TTGCGCTGCGCGTCGATACTGGCGAAATTGTCGCGGGATGCCTCGCCGGTTTTGTGGAAC
    ||||||||||||||||||||||||||||||||||||||||||||||||||||||||||||
53  TTGCGCTGCGCGTCGATACTGGCGAAATTGTCGCGGGATGCCTCGCCGGTTTTGTGGAAC

121 ATTTCTTTATGTTCCCGTTTGACACTTTGAAGACACGGGTTCAGAGTGGGGACTCGACGA
    ||||||||||||||||||||||||||||||||||||||||||||||||||||||||||||
113 ATTTCTTTATGTTCCCGTTTGACACTTTGAAGACACGGGTTCAGAGTGGGGACTCGACGA

181 ATGTCATATTAGCGGCAAAGCGTATTTCGCGGAATGAGCGACTTGCACATCTTTACCGCG
    ||||||||||||||||||||||||||||||||||||||||||||||||||||||||||||
173 ATGTCATATTAGCGGCAAAGCGTATTTCGCGGAATGAGCGACTTGCACATCTTTACCGCG

241 GATTCGCGCCCATCATTGTTTCTGCCGTTCCAGCGCATGGTGCATATTACAGCACATATG
    |||||||||||||||| ||||||||||||||||||||||||||||||||||||||||||
233 GATTCGCGCCCATCATCGTTTCTGCCGTTCCAGCGCATGGTGCATATTACAGCACATATG

301 AGGCTGCGAAGCGTGTCTTTGGTGAGGATTCCACAGTGTCTATAACGGTCTCTGCCAGTT
    ||||||||||||||||||||||||||||||||||||||||||||||||||||||||||||
293 AGGCTGCGAAGCGTGTCTTTGGTGAGGATTCCACAGTGTCTATAACGGTCTCTGCCAGTT

361 GTGCGGTCGCTGCTCATGACACCATTTCCACCCCATTTGATGTTATCAAGCAGCGGATGC
    ||||||||||||||||||||||||||||||||||||||||||||||||||||||||||||
353 GTGCGGTCGCTGCTCATGACACCATTTCCACCCCATTTGATGTTATCAAGCAGCGGATGC

421 AGATGGACGGGAGCCGGAAGTTTGCCTCATCGCTTCAGTGTGGTCAATGTGCAGTTGCGG
    |||||||||||||||||||||||| ||||||||||||||||||||||||||||||||||
413 AGATGGACGGGAGCCGGAAGTTTGCTTCATCGCTTCAGTGTGGTCAATGTGCAGTTGCGG

481 AAGGGGGCGTGCGGTGCCTTCTCCTCTCTTTGCCCACCACTATTTTAATGAACATTCCAC
    ||||||||||||||||||||||||||||||||||||||||||||||||||||||||||||
473 AAGGGGGCGTGCGGTGCCTTCTCCTCTCTTTGCCCACCACTATTTTAATGAACATTCCAC

541 ATTTCTCAGCCTACTGGTTAGTTTATGAGGGGTTTCTTGCATACTTGGGTGGTGAGCGGC
    ||||||||||||||||||||||||||||||||||||||||||||||||||||||||||||
533 ATTTCTCAGCCTACTGGTTAGTTTATGAGGGGTTTCTTGCATACTTGGGTGGTGAGCGGC

601 GCAATAGGGAAACGGAAGTTGCGGGAGATTACATAACCGGGGGCCTCCTGGCAGGCAGTG
    |||||||||||||||||||||||||||||||||||||||||||||||||||||||||| ||
593 GCAATAGGGAAACGGAAGTTGCGGGAGATTACATAACCGGGGGCCTCCTGGCAGGCACTG

661 TGGCTTCTATTGTCTCGTCACCGTTAGACGTTGTAAAGACTCAGCTGCAACTCGGTCTTA
    ||||||||||||||||||||||||||||||||||||||||||||||||||||||||||||
653 TGGCTTCTATTGTCTCGTCACCGTTAGACGTTGTAAAGACTCAGCTGCAACTCGGTCTTA

721 GAAAGAATATCCCCGATGCGGTGCGCTATGTCTTAGTCAATCGTGGCACCAAAGGTTTCT
    ||||||||||||||||||||||||||||||||||||||||||||||||||||||||||||
713 GAAAGAATATCCCCGATGCGGTGCGCTATGTCTTAGTCAATCGTGGCACCAAAGGTTTCT
```

```
781 TTGCCGGAGTTACGGCGAGAGTTATGTGTACCGCTCCTGCTGGTGCCCTGTCAATGACCA
    ||||||| |||||||||||||||||||||||||||||||||||||||||||||||||| ||
773 TTGCCGGGGTTACGGCGAGAGTTATGTGTACCGCTCCTGCTGGTGCCCTGTCAATGATCA
                                                    Not I
841 CATATGAAACGGCCAAGAAGTTCATGGAGGAACGGTAAGCGGCCGC
    |||||||||||||||||||||||||||||||||||||
833 CATATGAAACGGCCAAGAAGTTCATGGAGGAACGGTAA
```

Upper line: TbMCP17Myc; Lower line: MCP17-full transcript. identity= 99.43%

```
      BamH I
1   GAGGATCCATGGTTTCCGAGGGCACTTCCGCTGCAGGTCGCCTGGAGGGCGAGTCGCCGC
           ||||||||||||||||||||||||||||||||||||||||||||||||||||||||
1   ........ATGGTTTCCGAGGGCACTTCCGCTGCAGGTCGCCTGGAGGGCGAGTCGCCGC

61  TTGCGCTGCGCGTCGATACTGGCGAAATTGTCGCGGGATGCCTCGCCGGTTTTGTGGAAC
    ||||||||||||||||||||||||||||||||||||||||||||||||||||||||||||
53  TTGCGCTGCGCGTCGATACTGGCGAAATTGTCGCGGGATGCCTCGCCGGTTTTGTGGAAC

121 ATTTCTTTATGTTCCCGTTTGACACTTTGAAGACACGGGTTCAGAGTGGGGACTCGACGA
    ||||||||||||||||||||||||||||||||||||||||||||||||||||||||||||
113 ATTTCTTTATGTTCCCGTTTGACACTTTGAAGACACGGGTTCAGAGTGGGGACTCGACGA

181 ATGTCATATTAGCGGCAAAGCGTATTTCGCGGAATGAGCGACTTGCACATCTTTACCGCG
    ||||||||||||||||||||||||||||||||||||||||||||||||||||||||||||
173 ATGTCATATTAGCGGCAAAGCGTATTTCGCGGAATGAGCGACTTGCACATCTTTACCGCG

241 GATTCGCGCCCATCATTGTTTCTGCCGTTCCAGCGCATGGTGCATATTACAGCACATATG
    ||||||||||||||| ||||||||||||||||||||||||||||||||||||||||||||
233 GATTCGCGCCCATCATCGTTTCTGCCGTTCCAGCGCATGGTGCATATTACAGCACATATG

301 AGGCTGCGAAGCGTGTCTTTGGTGAGGATTCCACAGTGTCTATAACGGTCTCTGCCAGTT
    ||||||||||||||||||||||||||||||||||||||||||||||||||||||||||||
293 AGGCTGCGAAGCGTGTCTTTGGTGAGGATTCCACAGTGTCTATAACGGTCTCTGCCAGTT

361 GTGCGGTCGCTGCTCATGACACCATTTCCACCCCATTTGATGTTATCAAGCAGCGGATGC
    ||||||||||||||||||||||||||||||||||||||||||||||||||||||||||||
353 GTGCGGTCGCTGCTCATGACACCATTTCCACCCCATTTGATGTTATCAAGCAGCGGATGC

421 AGATGGACGGGAGCCGGAAGTTTGCCTCATCGCTTCAGTGTGGTCAATGTGCAGTTGCGG
    ||||||||||||||||||||||||| ||||||||||||||||||||||||||||||||||
413 AGATGGACGGGAGCCGGAAGTTTGCTTCATCGCTTCAGTGTGGTCAATGTGCAGTTGCGG

481 AAGGGGGCGTGCGGTGCCTTCTCCTCTCTTTGCCCACCACTATTTTAATGAACATTCCAC
    ||||||||||||||||||||||||||||||||||||||||||||||||||||||||||||
473 AAGGGGGCGTGCGGTGCCTTCTCCTCTCTTTGCCCACCACTATTTTAATGAACATTCCAC

541 ATTTCTCAGCCTACTGGTTAGTTTATGAGGGGTTTCTTGCATACTTGGGTGGTGAGCGGC
    ||||||||||||||||||||||||||||||||||||||||||||||||||||||||||||
533 ATTTCTCAGCCTACTGGTTAGTTTATGAGGGGTTTCTTGCATACTTGGGTGGTGAGCGGC

601 GCAATAGGGAAACGGAAGTTGCGGGAGATTACATAACCGGGGGCCTCCTGGCAGGCAGTG
    |||||||||||||||||||||||||||||||||||||||||||||||||||||||||| ||
593 GCAATAGGGAAACGGAAGTTGCGGGAGATTACATAACCGGGGGCCTCCTGGCAGGCACTG

661 TGGCTTCTATTGTCTCGTCACCGTTAGACGTTGTAAAGACTCAGCTGCAACTCGGTCTTA
    ||||||||||||||||||||||||||||||||||||||||||||||||||||||||||||
653 TGGCTTCTATTGTCTCGTCACCGTTAGACGTTGTAAAGACTCAGCTGCAACTCGGTCTTA

721 GAAAGAATATCCCCGATGCGGTGCGCTATGTCTTAGTCAATCGTGGCACCAAAGGTTTCT
```

```
    ||||||||||||||||||||||||||||||||||||||||||||||||||||||||||||||||||||||||
713 GAAAGAATATCCCCGATGCGGTGCGCTATGTCTTAGTCAATCGTGGCACCAAAGGTTTCT

781 TTGCCGGAGTTACGGCGAGAGTTATGTGTACCGCTCCTGCTGGTGCCCTGTCAATGATCA
    ||||||| ||||||||||||||||||||||||||||||||||||||||||||||||||||
773 TTGCCGGGGTTACGGCGAGAGTTATGTGTACCGCTCCTGCTGGTGCCCTGTCAATGATCA
```

Myc sequence

```
841 CATATGAAACGGCCAAGAAGTTCATGGAGGAACGGGAACAAAACTCATCTCAGAAGA
    ||||||||||||||||||||||||||||||||||| ||
833 CATATGAAACGGCCAAGAAGTTCATGGAGGAACGGTAA
```

Tb927.3.2.2980

GGATCTGTAAGCGGCCGC

Not I

A4-4 pCM190+MRS3 sequencing result

Sequence alignment of MRS3 in pCM190+MRS3 construct with MRS3 sequence GB: S288C.

```
Upper line: pCM190-MRS3; Lower line: MRS3_genomic. Identity= 100.00%

1   GAGGATCCATGGTAGAAAACTCGTCGAGTAATAATTCAACAAGGCCAATTCCAGCAATAC
            ||||||||||||||||||||||||||||||||||||||||||||||||||||||
1   ........ATGGTAGAAAACTCGTCGAGTAATAATTCAACAAGGCCAATTCCAGCAATAC

61  CTATGGATCTACCCGATTATGAGGCGCTCCCCACCCACGCGCCATTGTACCATCAACTTA
    ||||||||||||||||||||||||||||||||||||||||||||||||||||||||||||
53  CTATGGATCTACCCGATTATGAGGCGCTCCCCACCCACGCGCCATTGTACCATCAACTTA

121 TAGCGGGTGCATTTGCTGGTATAATGGAACATTCAGTGATGTTCCCGATAGATGCCCTTA
    ||||||||||||||||||||||||||||||||||||||||||||||||||||||||||||
113 TAGCGGGTGCATTTGCTGGTATAATGGAACATTCAGTGATGTTCCCGATAGATGCCCTTA

181 AGACGCGAATACAATCAGCCAACGCGAAATCGCTGTCTGCCAAGAATATGCTTTCGCAAA
    ||||||||||||||||||||||||||||||||||||||||||||||||||||||||||||
173 AGACGCGAATACAATCAGCCAACGCGAAATCGCTGTCTGCCAAGAATATGCTTTCGCAAA

241 TATCTCACATCTCTACTTCCGAAGGAACTCTAGCCCTATGGAAGGGTGTTCAGTCTGTCA
    ||||||||||||||||||||||||||||||||||||||||||||||||||||||||||||
233 TATCTCACATCTCTACTTCCGAAGGAACTCTAGCCCTATGGAAGGGTGTTCAGTCTGTCA

301 TACTAGGTGCGGGACCTGCGCATGCAGTGTATTTTGGTACGTATGAGTTCTGCAAAAAAA
    ||||||||||||||||||||||||||||||||||||||||||||||||||||||||||||
293 TACTAGGTGCGGGACCTGCGCATGCAGTGTATTTTGGTACGTATGAGTTCTGCAAAAAAA

361 ATCTTATCGATTCGAGTGATACGCAAACGCACCATCCTTTTAAGACAGCTATCAGTGGTG
    ||||||||||||||||||||||||||||||||||||||||||||||||||||||||||||
353 ATCTTATCGATTCGAGTGATACGCAAACGCACCATCCTTTTAAGACAGCTATCAGTGGTG

421 CCTGTGCCACCACGGCATCTGACGCATTAATGAACCCATTCGACACAATAAAACAGAGAA
    ||||||||||||||||||||||||||||||||||||||||||||||||||||||||||||
413 CCTGTGCCACCACGGCATCTGACGCATTAATGAACCCATTCGACACAATAAAACAGAGAA

481 TCCAACTCAATACCTCGGCATCAGTATGGCAAACCACAAAGCAGATTTACCAATCTGAAG
    ||||||||||||||||||||||||||||||||||||||||||||||||||||||||||||
473 TCCAACTCAATACCTCGGCATCAGTATGGCAAACCACAAAGCAGATTTACCAATCTGAAG

541 GTTTGGCAGCATTTTATTATTCTTACCCAACCACCCTAGTAATGAACATCCCATTTGCAG
    ||||||||||||||||||||||||||||||||||||||||||||||||||||||||||||
533 GTTTGGCAGCATTTTATTATTCTTACCCAACCACCCTAGTAATGAACATCCCATTTGCAG

601 CATTTAATTTCGTCATATATGAATCATCCACAAAATTTTTAAACCCATCAAATGAGTACA
    ||||||||||||||||||||||||||||||||||||||||||||||||||||||||||||
593 CATTTAATTTCGTCATATATGAATCATCCACAAAATTTTTAAACCCATCAAATGAGTACA

661 ACCCCCTCATACATTGTCTGTGTGGCAGTATCAGCGGATCGACATGTGCGGCGATCACAA
    ||||||||||||||||||||||||||||||||||||||||||||||||||||||||||||
653 ACCCCCTCATACATTGTCTGTGTGGCAGTATCAGCGGATCGACATGTGCGGCGATCACAA

721 CACCTTTAGACTGCATAAAGACAGTACTGCAGATAAGGGGCAGTCAAACAGTTTCGTTGG
```

```
    ||||||||||||||||||||||||||||||||||||||||||||||||||||||||||||||||
713 CACCTTTAGACTGCATAAAGACAGTACTGCAGATAAGGGGCAGTCAAACAGTTTCGTTGG

781 AAATTATGAGAAAGGCGGATACTTTTAGTAAAGCAGCCAGTGCCATATATCAAGTTTATG
    ||||||||||||||||||||||||||||||||||||||||||||||||||||||||||||||||
773 AAATTATGAGAAAGGCGGATACTTTTAGTAAAGCAGCCAGTGCCATATATCAAGTTTATG

841 GCTGGAAAGGGTTTTGGAGAGGTTGGAAACCAAGGATAGTGGCAAACATGCCGGCTACTG
    ||||||||||||||||||||||||||||||||||||||||||||||||||||||||||||||||
833 GCTGGAAAGGGTTTTGGAGAGGTTGGAAACCAAGGATAGTGGCAAACATGCCGGCTACTG

901 CTATATCATGGACAGCTTATGAATGTGCAAAACATTTCCTAATGACGTATTAGAAGCTTC
    ||||||||||||||||||||||||||||||||||||||||||||||||||||||||||
893 CTATATCATGGACAGCTTATGAATGTGCAAAACATTTCCTAATGACGTATTAG

816 GGGTTTTGGAGAGGTTGGAAACCAAGGATAGTGGCAAACATGCCGGCTACTGCTATATCA
    ||||||||||||||||||||||||||||||||||||||||||||||||||||||||||||||||
841 GGGTTTTGGAGAGGTTGGAAACCAAGGATAGTGGCAAACATGCCGGCTACTGCTATATCA

876 TGGACAGCTTATGAATGTGCAAAACATTTCCTAATGACGTATTAGCTGCAG
    ||||||||||||||||||||||||||||||||||||||||||||||||
901 TGGACAGCTTATGAATGTGCAAAACATTTCCTAATGACGTATTAG
```

A4-5 pHD676+*SFXN* RNAi construct sequencing result

```
Upper line: pGEM-SFXNAS1-BA-T7, from 3 to 383
Lower line: SFXNAS+S-HAB.txt, from 327 to 707

pGEM-SFXNAS1-BA-T7:SFXNAS+S-HAB.txt identity= 98.69%(378/383)
        Apa I
1    CAGGGCCCCGAGCCCGAACAGCTGCACAGCGGGCAAGGAGTGGCCGCATCATCAAAAGCG
     | |||||||||||||||||||||||||||||||||||||||||| ||||||||||||||||
325  CTGGGCCCCGAGCCCGAACAGCTGCACAGCGGGCAAGGAGTGGTCGCATCATCAAAAGCG

61   GCAACACCATGGAAATAAGGTTCCATGTAACACGCGTGACGGAACACATCATGAGACTTT
     ||||||||||||||||||||||||||||||||||||||||||||||||||||||||||||
385  GCAACACCATGGAAATAAGGTTCCATGTAACACGCGTGACGGAACACATCATGAGACTTT

121  GCATGCCGGCAACACGACTGCTGCCCCTCACCTCACCATCCTCGTCAACAACTTGTAGGC
     |||||||||||||||||||||||||| ||||||||||||||||||||||||||||||||
445  GCATGCCGGCAACACGACTGCTGCCCCGCACCTCACCATCCTCGTCAACAACTTGTAGGC

181  CAGTGCCTGATGGAATCCACTCATTCTTACGCATTAGAGAAAGATTCACAATTGCCGCCG
     ||||||||||||||||||||||||||||||||||||||||||||||||||||||||||||
505  CAGTGCCTGATGGAATCCACTCATTCTTACGCATTAGAGAAAGATTCACAATTGCCGCCG

241  CAGATACCGTCACGAAAGGTAACCCCGCACGAACAGCTGTGGCTTTCAATGTGCCACCTT
     |||||||| ||||||||||||||||||||||||||||||||||||||||||||||||||||
565  CAGATACCGCCACGAAAGGTAACCCCGCACGAACAGCTGTGGCTTTCAATGTGCCACCTT

301  TTACTTTCTTCAGCATTGCTGTAGCACCTAGTGCTCCGGCGCAGGAAACACCAACAGCGG
     ||||||||||||||||||||||||||||||||||||||||||||||||||||||||||||
625  TTACTTTCTTCAGCATTGCTGTAGCACCTAGTGCTCCGGCGCAGGAAACACCAACAGCGC

361  CGACGTACGCCTTAGATGGATCCGACATCG
     |||||||||||||||||||||||
685  CGACGTACGCCTTAGATGGATCC
                     BamH I
```

A4-6 pET28+SFNX sequencing result

```
Upper line: pET28+SFNX sequence result.
Lower line: His-sfnx.
Identity= 99.34%

1   GGTACATTCCCCTCTAGAAATAATTTTGTTTAACTTTAAGAAGGAGATATACCATGGGCA
                                                        |||||||
1   ..................................................ATGGGCA

61  GCAGCCATCATCATCATCATCACAGCAGCGGCCTGGTGCCGCGCGGCAGCCATATGGCTA
    ||||||||||||||||||||||||||||||||||||||||||||||||||||||||||||
8   GCAGCCATCATCATCATCATCACAGCAGCGGCCTGGTGCCGCGCGGCAGCCATATGGCTA
                                  BamH I
121 GCATGACTGGTGGACAGCAAATGGGTCGCGGATCCATGCTTCCATGTCCGTCGTTCTCTA
    ||||||||||||||||||||||||||||||||||||||||||||||||||||||||||||
68  GCATGACTGGTGGACAGCAAATGGGTCGCGGATCCATGCTTCCATGTCCGTCGTTCTCTA

181 CCACAACTCCAAGGTTTGACATGGACACCTATCTGGGTCGTACCTTTTACTTTTTTTCCA
    |||||||||||||||||||||||||||||||||||||||| ||||||||||||||||
128 CCACAACTCCAAGGTTTGACATGGACACCTATCTGGGTCGTACTTTTTACTTTTTTTCCA

241 CCATCAACCCACTGTTGTGCTTTGAGACGTCAAACTCATTGAAGCGCCATCAGGAGCTGC
    ||||||||||||||||||||||||||||||||||||||||||||||||||||||||||||
188 CCATCAACCCACTGTTGTGCTTTGAGACGTCAAACTCATTGAAGCGCCATCAGGAGCTGC

301 TCAATCGTGTGGCAGCGGGAGAGGAAGGGGTTGCAAGCGACAGACAACTGTGGAAAGCAC
    ||||||||||||||||||||||||||||||||||||||||||||||||||||||||||||
248 TCAATCGTGTGGCAGCGGGAGAGGAAGGGGTTGCAAGCGACAGACAACTGTGGAAAGCAC

361 GCACTGCAATAGAAATATGCGTGCATCCCACCACTAAGGAAGTTATATTTCCACCTTACA
    ||||||||||||||||||||||||||||||||||||||||||||||||||||||||||||
308 GCACTGCAATAGAAATATGCGTGCATCCCACCACTAAGGAAGTTATATTTCCACCTTACA

421 GGATGTGTGCTTTCCTTCCTGTGAATAGTTTTATCGTACCCTTCATGATGTCACCGACGA
    ||||||||||||||||||||||||||||||||||||||||||||||||||||||||||||
368 GGATGTGTGCTTTCCTTCCTGTGAATAGTTTTATCGTACCCTTCATGATGTCACCGACGA

481 CCATTGCAAGCCCTGCGCTCACAATATTCATTCAGTGGTTTAACCAGAGCTATAACTGCG
    ||||||||||||||||||||||||||||||||||||||||||||||||||||||||||||
428 CCATTGCAAGCCCTGCGCTCACAATATTCATTCAGTGGTTTAACCAGAGCTATAACTGCG

541 CGGTGAATTATGCAAATCGCTCCTCCGATAAGCAACCGATGTCGGAACTATCTAAGGCGT
    ||||||||||||||||||||||||||||||||||||||||||||||||||||||||||||
488 CGGTGAATTATGCAAATCGCTCCTCCGATAAGCAACCGATGTCGGAACTATCTAAGGCGT

601 ACGTCGCCGCTGTTGGTGTTTCCTGCGCCGGAGCACTAGGTGCTACAGCAATGCTGAAGA
    ||||||||||||||||||||||||||||||||||||||||||||||||||||||||||||
548 ACGTCGCCGCTGTTGGTGTTTCCTGCGCCGGAGCACTAGGTGCTACAGCAATGCTGAAGA

661 AAGTAAAAGGTGGCACATTGAAAGCCACAGCTGTTCGTGCGGGGTTACCTTTCGTGACGG
    |||||||||||||||||||||||||||||||||||||||||||||||||||||| |||
608 AAGTAAAAGGTGGCACATTGAAAGCCACAGCTGTTCGTGCGGGGTTACCTTTCGTGGCGG

721 TATCTGCGGCGGCAATTGTGAATCTTTCTCTAATGCGTAAGAATGAGTGGATTCCATCAG
    ||||||||||||||||||||||||||||||||||||||||||||||||||||||||||||
668 TATCTGCGGCGGCAATTGTGAATCTTTCTCTAATGCGTAAGAATGAGTGGATTCCATCAG

781 GCACTGGCCTACAAGTTGTTGACGAGGATGGTGAGGTGAGGGGCAGCAGTCGTGTTGCCG
```

```
    |||||||||||||||||||||||||||||||||||||| ||||||||||||||||||||
728 GCACTGGCCTACAAGTTGTTGACGAGGATGGTGAGGTGCGGGGCAGCAGTCGTGTTGCCG

841 GCATGCAAAGTCTCATGATGTGTTCCGTCACGCGTGTTACATGGAACCTTATTTCCATGG
    ||||||||||||||||||||||||||||||||||||||||||||||||||||||||||||
788 GCATGCAAAGTCTCATGATGTGTTCCGTCACGCGTGTTACATGGAACCTTATTTCCATGG

901 TGTTGCCGCTTTTGATGATGCGGCCACTCCTTGCCCGCTGTGCAGCTGTTCCCGCTCGAC
    |||||||||||||||||||||| |||||||||||||||||||||||||||  |||||||
848 TGTTGCCGCTTTTGATGATGCGACCACTCCTTGCCCGCTGTGCAGCTGTTCGGGCTCGAC

961 CTGTTGTGTATGAAACGGCACTGCAGATTGCCAGCCTCGGCGTCGGTGTTCCGCTTGCAT
    ||||||||||||||| ||||||||||||||||||||||||||||||||||||||||||||
908 CTGTTGTGTATGAAACAGCACTGCAGATTGCCAGCCTCGGCGTCGGTGTTCCGCTTGCAT

1021 TGGGTGCATTTAGCACAACAGTGAGTGTACCTGCGAATCGGTTGGAGCCGGAACTTCGT
     ||||||||||||||||||||||||||||||||||||||||||||||||||||||||||||
968  TGGGTGCATTTAGCACAACAGTGAGTGTACCTGCGAATCGGTTGGAGCCGGAACTTCGT

841  GGGTTGAAGCGAAAGGACGGCTCGCCTGTTGAAATATTCACGTATTACAAGGGTTTGTG
     ||||||||||||||||||||||||||||||||||||||||||||||||||||||||||||
1002 GGGTTGAAGCGAAAGGACGGCTCGCCTGTTGAAATATTCACGTATTACAAGGGTTTGTG
     stop codon
901  AAAGCTT Hind III
     |
   1062     A
```

A4-7 pET28+TbMCP23 sequencing result

```
Upper line: TbMCP23. Lower line: TbMCP23(pET28). Identity= 99.64%

1   ATGGCACTCCCGACATCGCATGTGGTTCAAACCCCCAAAAGACAAGAATACCTTGCATCC
    ||||||||||||||||||||||||||||||||||||||||||||||||||||||||||||
73  ATGGCACTCCCGACATCGCATGTGGTTCAAACCCCCAAAAGACAAGAATACCTTGCATCC

61  TGTTTGTCTGGTTGTGTTGCCGGTGTCTGCTCCACCTGCGTCATAAACCCATTGGATACC
    ||||||||||||||||||||||||||||||||||||||||||||||||||||||||||||
133 TGTTTGTCTGGTTGTGTTGCCGGTGTCTGCTCCACCTGCGTCATAAACCCATTGGATACC

121 GTCCGTGTGCGCCTCTCTGTAAGCCGAAGTGCCACTGGAAAGGCACACAGGAGCCTCTTG
    ||||||||||||||||||||||||||||||||||||||||||||||||||||||||||||
193 GTCCGTGTGCGCCTCTCTGTAAGCCGAAGTGCCACTGGAAAGGCACACAGGAGCCTCTTG

181 TACACTGTTAGGGACCTCTTCGAGGGAGGCATTGTCCACGCCTTTTCGCGTGGTCTCTCG
    ||||||||||||||||||||||||||||||||||||||||||||||||||||||||||||
253 TACACTGTTAGGGACCTCTTCGAGGGAGGCATTGTCCACGCCTTTTCGCGTGGTCTCTCG

241 GCAAATCTAATGGCCTCGCTTCCCTCCAATGGTATTTATCTTCCTACATACCGCTGCATT
    ||||||||||||||||||||||||||||||||||||||||||||||||||||||||||||
313 GCAAATCTAATGGCCTCGCTTCCCTCCAATGGTATTTATCTTCCTACATACCGCTGCATT

301 AAGGACCAACTTTCCTCTGCCGGAGTCAACCAGAATGTTCAACCTGCCATTGCGGCTTGT
    ||||||||||||||||||||||||||||||||||||||||||||||||||||||||||||
373 AAGGACCAACTTTCCTCTGCCGGAGTCAACCAGAATGTTCAACCTGCCATTGCGGCTTGT

361 GGTGCCGTGTGTGTGACAAACACGATCCTAGGGCCGATATTTCTGGTGCGGACTCGCGTG
    |||||||||||||||||||||||||||||||||||||||||||||||||||||||| |||
433 GGTGCCGTGTGTGTGACAAACACGATCCTAGGGCCGATATTTCTGGTGCGGACTCGGGTG

421 CAAGTTAACGAAAAACTAACTGTGCGGCAAACGTTTAGAGATGTGCTGAAGCACGAAGGC
    ||||||||||||||||||||||||||||||||||||||||||||||||||||||||||||
493 CAAGTTAACGAAAAACTAACTGTGCGGCAAACGTTTAGAGATGTGCTGAAGCACGAAGGC

481 TTCAGTGGTTTCTACCGCGGGACCATGACCAATATTGTGGGTCGGTTCGTCGAAGAGGGC
    ||||||||||||||||||||||||||||||||||||||||||||||||||||||||||||
553 TTCAGTGGTTTCTACCGCGGGACCATGACCAATATTGTGGGTCGGTTCGTCGAAGAGGGC

541 CTCTTCTGGAGCATCTATGAACTTCTTAAGCGGTTGTCAAACGAAGCAAGTTTCAAGGGT
    |||||||||||||||||||||||||||||||||||||||| ||||||||||||||||||
613 CTCTTCTGGAGCATCTATGAACTTCTTAAGCGGTTGTCAAGCGAAGCAAGTTTCAAGGGT

601 TCCAGCAACTTTTTTCTGACATCTGTCGCGGTAGCATCGCTTTCGGCCGTGGCGAAGATT
    ||||||||||||||||||||||||||||||||||||||||||||||||||||||||||||
673 TCCAGCAACTTTTTTCTGACATCTGTCGCGGTAGCATCGCTTTCGGCCGTGGCGAAGATT

661 GCCGCCACCACCGTCTCTTATCCTTACAACGTCGTTATGAATCACATGCGCAGCGTCAGC
    ||||||||||||||||||||||||||||||||||||||||||||||||||||||||||||
733 GCCGCCACCACCGTCTCTTATCCTTACAACGTCGTTATGAATCACATGCGCAGCGTCAGC

721 TACGTGACAGGGAAACCCGAGTATGAGCGCATTATGCCAACAATACGACACATTTATTAC
    ||||||||||||||||||||||||||||||||||||||||||||||||||||||||||||
793 TACGTGACAGGGAAACCCGAGTATGAGCGCATTATGCCAACAATACGACACATTTATTAC

781 CAAGACGGCATACCCGGTTTTTACAAGGGGCTTGCGCCGCAGCTGTTACGGAGCACGCTA
    |||||||||||||||| ||||||||||||||||||||||||||||||||||||||||||
853 CAAGACGGCATACCCGGCTTTTACAAGGGGCTTGCGCCGCAGCTGTTACGGAGCACGCTA
```

```
841 AGTAAGGCTGTACAGATATATTCTTTTGAACTGGCCATGTTCATTTACTTCAGCACTGTC
    ||||||||||||||||||||||||||||||||||||||||||||||||||||||||||||
825 AGTAAGGCTGTACAGATATATTCTTTTGAACTGGCCATGTTCATTTACTTCAGCACTGTC

901 CAACGTCCCGTTGTTTCTTGCGCTCCCGCATAA
    |||||||||||||||||||||||||||||||||
885 CAACGTCCCGTTGTTTCTTGCGCTCCCGCATAAAAGCTT  Hind III
```

A5 Growth curves of TbMCP17 overexpression and depletion cell lines

A5-1 Overexpression of TbMCP17 helps cells defense iron limiting conditions

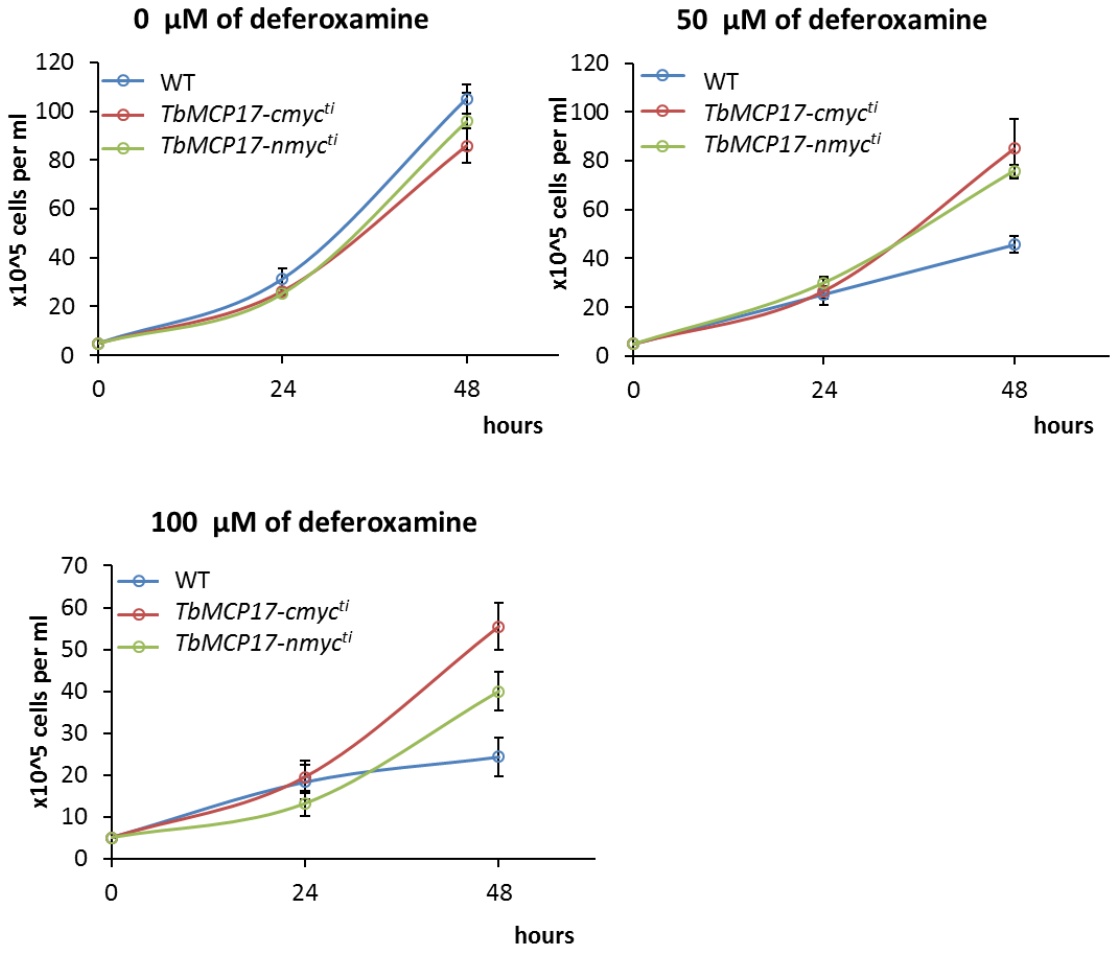

Figure A5-1 Cell densities of wild-type (WT) cells (blue), TbMCP17-cmyc expression cells (red) and TbMCP17-nmyc expression cells (green) treated with different concentrations of iron chelator deferoxamine measured every 24 hours of subculture are presented above. Error bars correspond to standard deviation of triplicates.

A5-2 Conditional double knockout of TbMCP17 causes growth defect and which is rescued by TbMCP17 overexpression

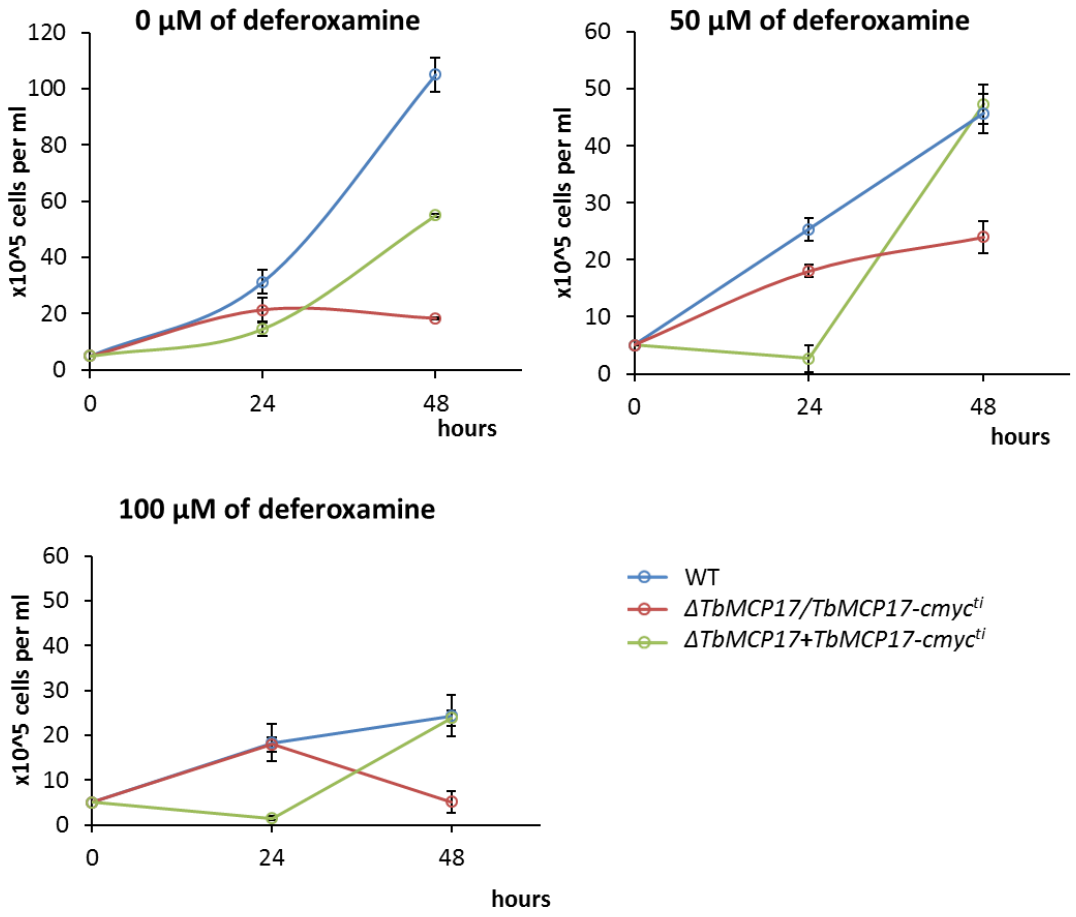

Figure A5-2 Cell densities of wild-type (WT) cells (blue), conditional double knockout *ΔTbMCP17/TbMCP17-cmyc*^{ti} (red) and *ΔTbMCP17+TbMCP17-cmyc*^{ti} (green) treated with different concentrations of iron chelator deferoxamine measured every 24 hours of subculture are presented above. Error bars correspond to standard deviation of triplicates.

A5-3 TbMCP17 RNAi presents growth defect

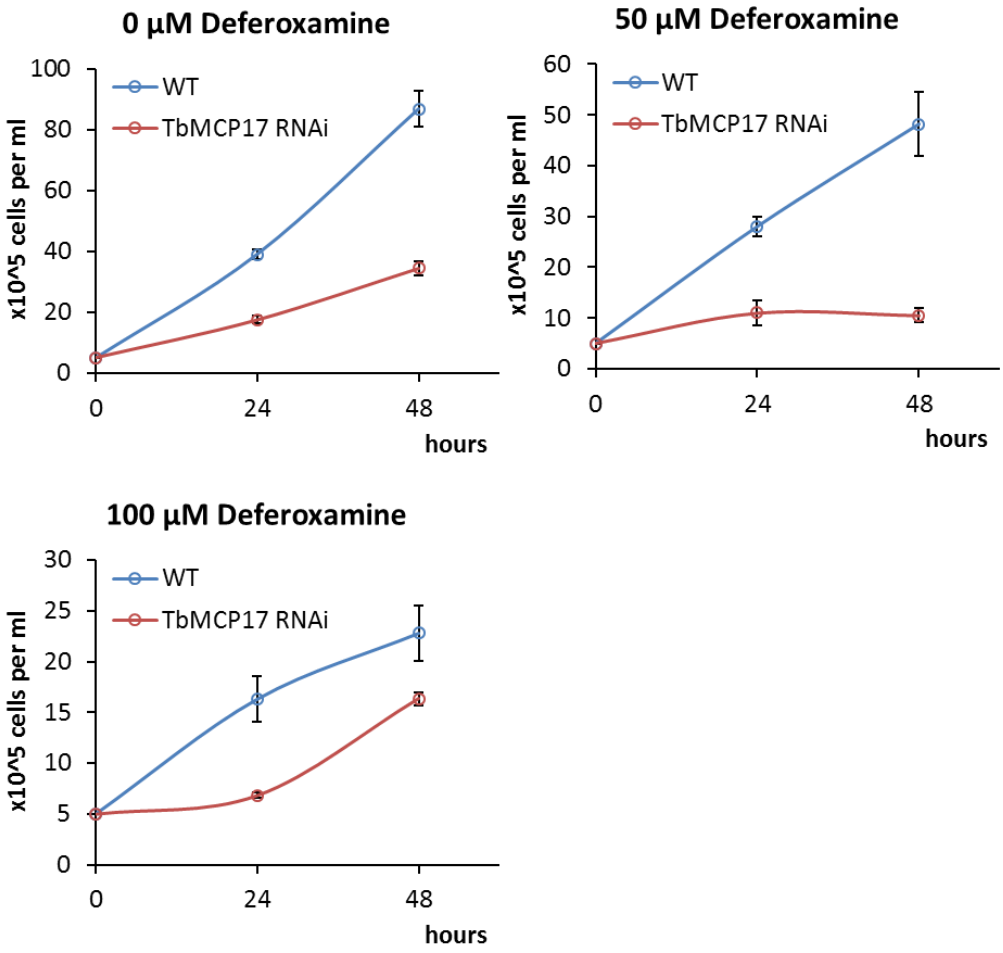

Figure A5-3 Cell densities of wild-type (WT) cells (blue) and TbMCP17 RNAi cells (red) treated with different concentrations of iron chelator deferoxamine measured every 24 hours of subculture are presented above. Error bars correspond to standard deviation of triplicates.